Optical Biosensing Using Localized Surface Plasmon Resonance of Gold Nanoparticles

by

Kanwarjeet Kaur

A thesis
presented to the University of Waterloo
in fulfillment of the
thesis requirement for the degree of
Doctor of Philosophy
in
Physics

Waterloo, Ontario, Canada, 2011

AUTHOR'S DECLARATION

I hereby declare that I am the sole author of this thesis. This is a true copy of the thesis, including any required final revisions, as accepted by my examiners.

I understand that my thesis may be made electronically available to the public.

Abstract

This thesis describes some experiments developed to probe the fundamental aspects of the interfacial behaviour of proteins. The contents of this thesis can be broadly divided into two parts.

In the first part, we studied how the size of the nanoparticles and other variables such as pH and bulk protein concentration affect the structure of the adsorbed protein layers. We also probed how these factors can influence the binding activity of adsorbed proteins. Study on the adsorption of IgG, Protein A and streptavidin on gold nanoparticles reveals that not all proteins are similarly affected by the size of the adsorbing surface. We found that though the optical properties of all the proteins vary with the size of the nanoparticle, their functionalities are not similarly affected by nanoparticle curvature. Protein A and streptavidin retain their binding capacity to IgG and biotin, respectively, irrespective of the size of the gold nanoparticle that they are attached to. On the other hand, a reduction/ loss in binding of adsorbed IgG to Protein A molecules is observed. The reduction in biological activity further depends on the radius of curvature of the adsorbing surface.

The second part of the thesis describes how nanoparticles can used as a probe to study the complex interfacial behaviour of proteins. We have utilized the extreme sensitivity of localized surface plasmon resonance (LSPR) of gold nanoparticles to local refractive index to determine the optical properties of BSA adsorbed on various polymer surfaces. The dielectric properties of the adsorbed protein depend on the nature of the substrate. Further, we have developed a model to determine the refractive index profile of adsorbed protein as a function of the distance from the substrate.

Acknowledgements

I would like to thank my supervisor Dr. James Forrest for supporting me and guiding me during the last five years. I would also like to thank Dr. Leonid Brown, Dr. Zoya Leonenko and Dr. Elizabeth Meiring for their support. I want to thank my coworkers, Johanthan Teichroeb, Dongping Qi, Chad Daley, James Chan, James Benson, Zahra Fakhraai, Mark Ilton, Katarina Illic. I would like to thank my husband, Palvinder, and my kids, Jasjeet and Jigarjeet for their endless love and support, without which this degree would not have been possible.

Table of Contents

List of Tables

List of Illustrations

List of abbreviations

AFM	atomic force microscopy
ALA	α-lactalbumin
Anti-IgG	anti immunoglobulin G
ATR-FTIR	attenuated total internal reflectance- Fourier transform infrared spectroscopy
BSA	bovine serum albumin
CD	circular dichorism
DSC	differential scanning calorimetry
HEMA	hydroxyethyl methacrylate
HPA	human plasma albumin
IgG	Immunoglobulin G
LSPR	localized surface plasmon resonance
LYZ	lysozyme
MAA	methacrylic acid
MGB	myoglobulin
NMR	nuclear magnetic resonance
PBS	phosphate buffer saline
PDMS	poly(dimethyl siloxane)
PEG	polyethylene glycol
pHEMA	poly(hydroxyethyl methacrylate)
pI	isoelectric point
PMMA	poly(methyl methacrylate)
Protein A	staphylococcal protein A
PS	polystyrene
QCM	quartz crystal microbalance
RNase	bovine pancreas ribonuclease
SAM	self assembled monolayer
SPR	surface plasmon resonance
STM	scanning tunneling microscopy
TIRF	total internal reflectance fluorescence
UV-Vis	ultraviolet/visible

CHAPTER 1

INTRODUCTION

1.1 Introduction to nanoparticles

Nanoparticles are defined as particles with one or more dimensions of the order of 1-100 nm. Nanoparticles evoke high scientific interest because they bridge the gap between bulk matter and the structural units - atoms and molecules [1]. As the size of the system decreases, many physical properties such as electrical, optical and mechanical properties may be altered as compared to those of macroscopic systems. Physical properties exhibited by a bulk material do not depend on its size but in the nanosized particles size-dependent properties are often observed. As the size of the particle decreases, the ratio of surface area to volume of the particle increases. As a consequence, the behavior of the particle is increasingly governed by the atoms at the surface of the particle at the expense of those in the interior. Surface plasmon Resonance (LSPR) in metallic nanoparticles, super paramagnetism in magnetic materials and quantum confinement in semiconductor particles are typical examples of size-dependent properties. As the size of the nanoparticle approaches the de Broglie wavelength of its charge carriers (electrons and holes), typically 1-5 nm depending on the material [2], the exciton (electron hole pair) is confined by the boundary of the particle. As a result, the energy levels available to the charge carriers are no longer continuous, but are rather split into discrete quantized energy levels. The spacing of electronic energy levels increases with decrease in the size of the particle. Therefore smaller nanoparticles emit shorter wavelength as compared to bigger nanoparticles.

1.1.1 History

Nanoparticles are not a wonder of modern technology but have been known to man for centuries. They have been used in various diverse fields ranging from pigments to paints, medicine, photography, agriculture. [3]. Lycurgus cup, one of the oldest artifacts containing nanoparticles, dates back to 4^{th} century [4]. The opaque green cup appears red in transmitted light due to the presence of gold and silver nanoparticles. Copper and silver pigments were used by artisans in 8^{th} and 9^{th} century on clear glass objects to generate a glittering effect [5]. Luster decorations were also applied on glazed pottery [6]. Luster originated from a thin film containing copper and silver nanoparticles with diameters ranging 5-50 nm, which was applied on the surface of the glazing. To generate the nanoparticles the artisans applied a mixture of copper and silver salts, oxides, ochre, vinegar and clay on the surface of previously glazed pottery. Heating these objects in a kiln caused the reduction of metal ions to metallic copper and silver.

The first samples of colloidal gold in scientific literature were reported by Michael Faraday in 1857 [7]. One of his original gold colloid samples is still on display at the British Museum in London. He believed that colloidal gold solution appeared red due to the presence of extremely small gold particles which interacted with light differently as compared to metallic gold.

In 1959, Richard Feyman predicted [8] that the properties of these small particles would not only be different from those of bulk matter but would also depend on the size, shape and the distance between the particles in his famous talk titled “There is plenty of room at the bottom”. He said that atoms on that scale would not behave like those on large scale, for they would obey the laws of quantum mechanics. He predicted the existence of electron beam lithography,

scanning tunneling microscope and building of small circuits on nanoscale for powerful computers. Gustav Mie [9] explained that the colour of the gold colloid suspension depended upon the size of the particles. Kawabata and Kubo [10] explained quantum confinement in small particles in 1966. They explained that in small nanoparticles the electronic states are quantized into discrete levels and the oscillations are damped due to transitions between these quantized electronic states. This causes a broadening of the plasmon peak with decrease in the nanoparticle size.

In 1974 Martin Fleishman and coworkers [11] observed an enhanced Raman scattering signal from pyridine molecules adsorbed on roughened silver surface. Although they were the first group to actually observe a large scattering signal from adsorbed molecules, they did not attribute it to SERS. They concluded that the high concentration of adsorbed molecules resulted in the large signal. In 1977 two independent groups gave explanation for the signal enhancement. Van Duyne's group explained the results on the basis of charge transfer effect [12], while Albrecht and Creighton [13] proposed that enhanced electromagnetic field was responsible for that signal enhancement.

In 1981, the scanning tunneling microscope (STM) was invented by Gerd Binning and Heinrich Rohrer (IBM Zurich) [14]. They were awarded Nobel Prize for this invention in 1986. STM made it possible to image individual atoms within a material not only in ultra high vacuum but even in air and liquids over a wide range of temperatures. Synthesis of single-walled carbon nanotubes (SWCNT) was first reported in 1993 by two independent groups, Ilijima and Ishihashi of NEC [15] and Bethune et. al. from IBM, California [16]. Semiconductor nanocrystals, quantum dots, were discovered by Brus at the Bell labs in 1983 [17].

1.1.2 Nanoparticle Synthesis

Methods for synthesis of nanoparticles can be divided into two categories: “bottom up” or “top down” techniques. The top-down method involves breaking down of the bulk material into smaller portions. This can be achieved by lithography [18] and mechanical techniques such as milling and attrition [19]. The bottom up technique involves nanoparticle fabrication from constituent atoms or molecules. Some examples of this approach are chemical synthesis [20], laser induced assembly [21], nanoparticle aggregation [22]. Top-down approach is used for mass production on industrial scale. However, to produce extremely small structures bottom up approach is better. Nanostructures can be generated using both approaches either in gas, liquid or solid states. Whatever technique may be chosen for nanoparticle synthesis control over particle size, shape, size distribution, composition and particle aggregation is extremely important.

1.1.3 Applications of Nanoparticles

Nanoparticles are being increasingly used in varied fields in science and engineering. Nanomaterials hold tremendous potential to not only improve existing medical diagnostic techniques but also provide novel means to treat human ailments. Magnetic nanoparticles have been used as contrast agents for magnetic resonance imaging [23]. Metallic and semiconductor nanoparticles have been used for cell labeling [24, 25], tracking cell migration [26], flow cytometry [27], fluorescence in situ hybridization [28], whole animal contrast agents [29], pathogenic detection [30], genomic and proteomic detection [31], fluorescence resonance energy

transfer (FRET) sensors [32], high throughput screening of biomolecules [33], specific DNA sequence detection [34] and photothermal therapy [35].

Silica nanoparticles have been utilized to create anti-reflective coatings for different materials [36]. By attaching nanoparticles to mesoporous materials, highly active and effective catalysts for a series of hydrogenation reactions have been generated. Due to the small size and low coordination numbers of the metal atoms involved, enhanced catalytic activity is exhibited by these systems [37].

Due to their high UV absorbance titanium dioxide and zinc oxide nanoparticles have also been used in sunscreens. Antibacterial properties of silver nanoparticles have led to their increased use in household items like refrigerator, air conditioners and washing machines. Nowadays, silver nanoparticles are being used in a wide variety of materials like toys, baby pacifiers, clothing, food storage containers, laundry detergents, face masks etc. [38].

1.2 Proteins

Proteins are natural polymer molecules. Proteins are a fundamental components of all human and animal cells. They perform various functions in the body such as reaction catalysis (enzymes), cell signaling, storage and transport of molecules such as oxygen, building and repairing body tissues, providing mechanical support, immune protection, generating movement and controlling cell growth. Thus, proteins are a very important class of biomolecules.

1.2.1 History

The term protein originated more than 170 years ago from the Latin word *primarius* or the Greek god *Proteus* [45]. Dutch chemist, Johannes Mulder gave the first description of proteins in 1839 when he studied the chemical composition of animal substances, mainly fibrin, albumin and gelatin. The elemental analysis of all these substances showed the presence of carbon, hydrogen, oxygen and nitrogen. In some cases he also discovered the presence of sulphur and phosphorus. He was the first to recognize that proteins were made up of large number of atoms. The term protein was coined in 1838 by his associate Jons Jakob Berzelius [46]. Circa 1873 Heinrich Hasiwetz and Josef Habermann found that hydrolysis of casein resulted in amino acids such as glutamic acid, aspartic acid, leucin, tyrosine, and ammonia. Thus, they discovered that proteins were composed of smaller units (called amino acids). Franz Hofmeister found that proteins were polypeptides in which individual amino acids were joined together through peptide bonds [45]. Urease was the first enzyme to be crystallized in 1926 [47]. In 1951, Linus Pauling predicted the secondary structure of proteins based on hydrogen bonding [48]. Study on the denaturation of ribonuclease by Kalman [49] and later some denaturation studies by Walter Kauzmann [50] established the role of various interactions - hydrophobic, electrostatic, Van der Waal's, hydrogen bonding in protein folding. Fredrick Sanger determined the complete sequence of amino acids of the protein, insulin. He concluded that the two polypeptide chains of insulin had a distinct sequence and thus concluded that every protein should have a definite sequence. In 1958 he was awarded Nobel Prize in Chemistry for this achievement. In 1958, the three-dimensional structures of two proteins, myoglobin and hemoglobin, were determined by Sir John Cowdery Kendrew [51] and Max Perutz [52], respectively, using X-ray diffraction analysis. They were awarded Nobel Prize in Chemistry in 1962 for their discoveries. Since then, there

have been major advancements in various fields in molecular biology that have increased our understanding of proteins.

1.2.2 The Structure of Protein

Proteins are linear polymers composed of amino acid residues. Proteins can be defined by four different levels of hierarchical structures - primary, secondary, tertiary and quaternary (shown in figure 1.1).

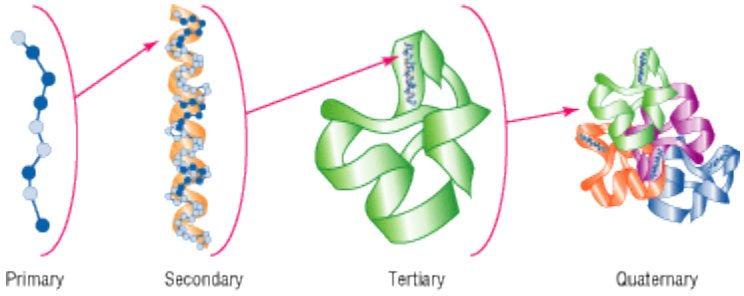

Figure 1.1 4 levels of protein structure (image taken from ref. 53)

1.2.2.1 Primary structure

Primary structure of a protein refers to the linear sequence of amino acids constituting the protein. Primary structure is formed by covalent bonds. Each protein has a unique sequence of amino acids that is determined by the genetic code and all higher hierarchical structures depend on the primary structure. All proteins are composed of 20 standard amino acids (listed in table

1.1). Not all amino acids occur with the same frequency in proteins. Alanine, glycine and leucine occur most frequently (7- 9%) whereas cysteine and tryptophan occur more rarely (~ 2%).

The general formula for an amino acid is shown below (figure 1.2). The central α carbon atom is attached to an amine group (NH_2), carboxyl group (COOH), a hydrogen atom (H) and a side chain group (R) which varies from one amino acid to another. The side chain R group is responsible for the different properties of individual amino acids. The charged amino and carboxyl groups present in the amino acids are responsible for their large dipole moment, high electrical conductivity and water solubility.

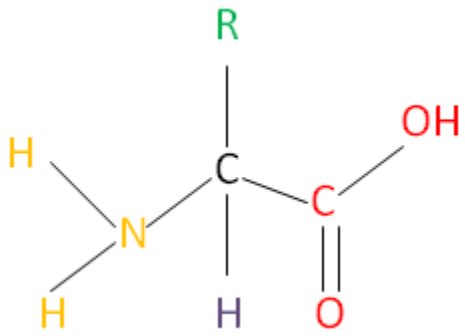

Figure 1.2 General structure of amino acid

Amino acids	**Short form**	**code**	**Polarity**	**Mass (g/mol)**	**Formula**
Alanine	Ala	A	NP	71.09	CH_3-CH(NH_2)-COOH
Arginine	Arg	R	P	156.19	H_2N-C(=NH)-NH-$[CH_2]_3$-CH(NH_2)-COOH
Asparagine	Asn	N	P	114.11	H_2N-CO-CH_2-CH(NH_2)-COOH
Aspartic acid	Asp	D	P	115.09	HOOC-CH_2-CH(NH_2)-COOH
Cysteine	Cys	C	NP	103.15	HS-CH_2-CH(NH_2)-COOH
Glutamine	Gln	Q	P	128.12	H_2N-CO-$[CH_2]_2$-CH(NH_2)-COOH
Glutamic acid	Glu	E	P	129.12	HOOC-$[CH_2]_2$-CH(NH_2)-COOH
Glycine	Gly	G	NP	57.05	H-CH(NH_2)-COOH
Histidine	His	H	P	137.14	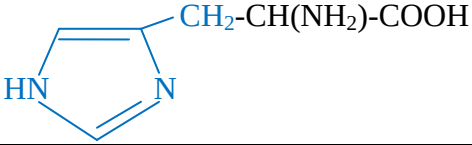
Isoleucine	Ile	I	NP	113.16	C_2H_5-CH(CH_3) -CH(NH_2)-COOH
Leucine	Leu	L	NP	113.16	(CH_3)CH-CH_2-CH(NH_2)-COOH
Lysine	Lys	K	P	128.17	H_2N-$[CH_2]_4$-CH(NH_2)-COOH
Methionine	Met	M	NP	131.19	CH_3-S-$[CH_2]_2$-CH(NH_2)-COOH
Phenylalanine	Phe	F	NP	147.18	C_6H_5-CH_2-CH(NH_2)-COOH
Proline	Pro	P	NP	97.12	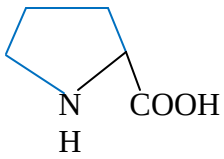
Serine	Ser	S	P	87.08	HO-CH_2-CH(NH_2)-COOH

Threonine	Thr	T	P	101.11	CH_3-CH(OH)-CH(NH_2)-COOH
Tryptophan	Trp	W	NP	186.21	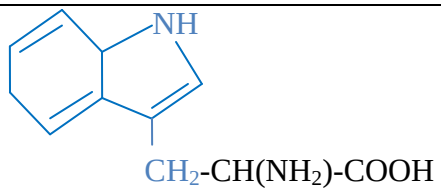
Tyrosine	Tyr	Y	P	163.18	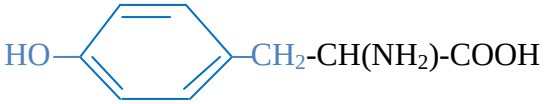
Valine	Val	V	NP	99.14	$(CH_3)_2$CH-CH(NH_2)-COOH

Table 1.1 List of major amino acids and their properties (P – Polar, NP- non polar)

Except for glycine all other amino acids have a chiral α-Carbon atom and can therefore exist as either of the two optical isomers - L or D (shown in fig. 1.3). All amino acids that occur in natural proteins have L form. Amino acid residues can be divided into three categories depending on the nature of the side chain. The first category contains hydrophobic groups in the side chain. Alanine, cysteine, valine, leucine, isoleucine, phenylalanine, proline and methionine belong to this group. The second group contains the four charged residues. Out of these aspartic acid and glutamic acid are negatively charged whereas lysine and arginine are positively charged. The charged groups mainly occur at the surface of the molecule. The third group comprises amino acids with polar side chains - serine, threonine, asparagine, glutamine, histidine, tyrosine and tryptophan. These polar groups are generally responsible for hydrogen bond formation. Glycine is the smallest of the amino acids as it has only a single hydrogen atom in its side chain. Since glycine does not have any bulky side chain groups it increases the flexibility of the main chain and can adopt unusual dihedral angles. Phenylalanine, tyrosine and

tryptophan have aromatic side groups and can therefore absorb ultraviolet light and are generally used for intrinsic protein fluorescence measurements.

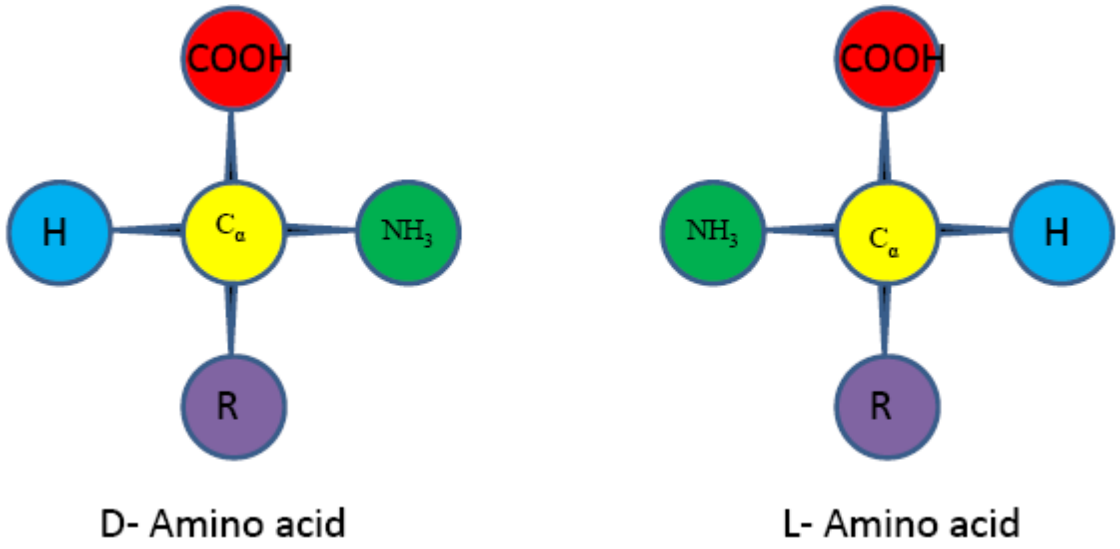

Fig.1.3 D and L stereo-isomers of amino acid

Amino acids are joined together by peptide bonds which are formed as a result of condensation reaction, i.e., when amino group of one molecule reacts with carboxyl group of second molecule to form a dipeptide by releasing water molecule. Further addition of more amino acid groups leads to the formation of polypeptides. The composition of the backbone is the same in every protein but it can differ in the number of residues. Due to the formation of the peptide bond, C-N bond acquires a partial double bond character (figure. 1.4). This partial double bond restricts motion about this bond. As a result all these atoms are confined in a plane. Due to this two isomers are possible - cis and trans. Trans configuration is preferred because it minimizes the steric repulsion between C_α atoms. For most peptide bonds, the cis form is 1000 times less stable than trans configuration. However, if the second residue is Proline, the cis is

only 4 times less stable than trans form. Although proline residues still occur mostly in trans form, some cis-prolines are found in tight bends of the polypeptide chains. The conformation of the main chain is governed by the two conformational angles φ and ψ (shown in figure 1.4). These angles can have only certain values due to steric hindrance between the backbone atoms and side-chain atoms.

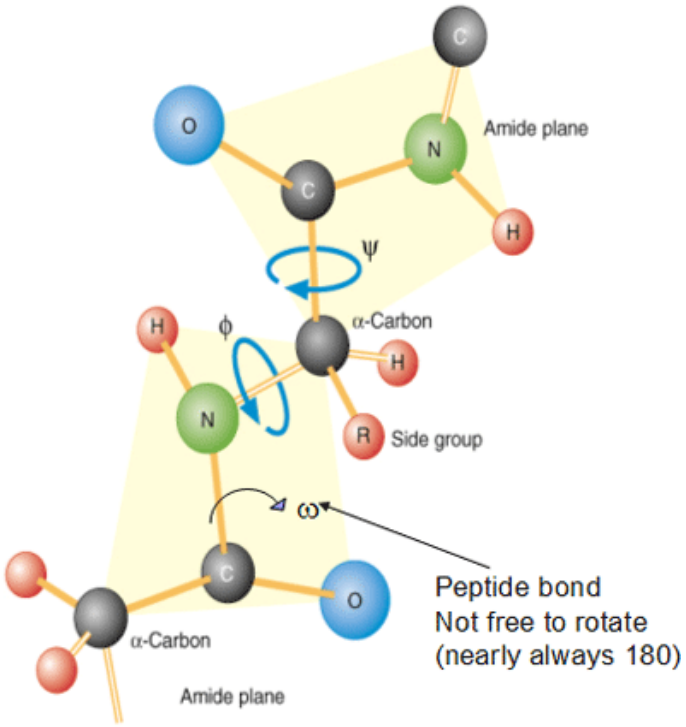

Figure 1.4 Planar peptide bonds due to partial double bond (shaded area) and rotating bonds (φ and ψ) [54]

1.2.2.2 Secondary structure

Secondary structure refers to local folding of the polypeptide chain. Three basic units of secondary structure are α-helix, β- sheets and random coils. Other secondary structure units are

an α-sheet, γ-helix, left-handed α-helix, 3_{10}-helix, π-helix, 2_7 ribbon, and polyproline helix. Spectroscopic techniques such as circular dichorism, FTIR and nuclear magnetic resonance are employed to detect the secondary structure of proteins.

α-helix has 3.6 residues per turn with hydrogen bonds between C=O group of nth residue and NH group of $n+4^{th}$ residue. Therefore, all C and N atoms in the helix are involved in hydrogen bonds except for the terminal C and N atoms. As a result, these polar terminal atoms usually occur at the surface of protein. An alpha helix can contain anywhere between 4 or 5 residues to over forty residues. Since all hydrogen bonds in a helix are aligned in the same direction, the dipole moments are also aligned. As a result, helices have a net dipole moment of magnitude 0.5-0.7 D with a partial positive charge at amino end and the negative charge at the C terminal. Some amino acids like Ala, Glu, Leu and Met have a weak preference for helices. On the other hand Pro, Gly, Tyr and Ser occur seldom in helices.

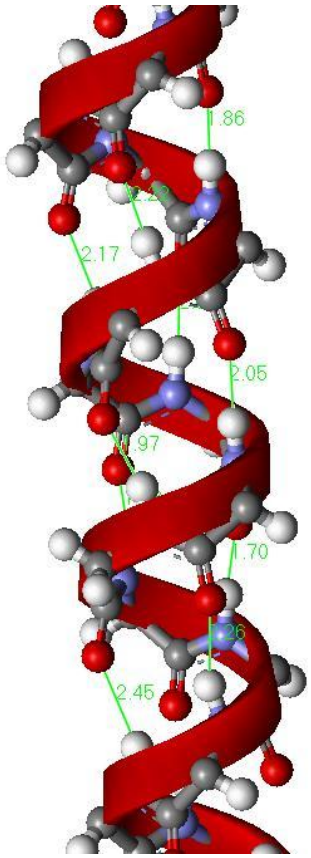

Figure 1.6 Alpha helix (image taken from ref. 55)

Variations of α-helix such as π-helix and 3_{10}- helix also exist. In π-helix hydrogen bonds exist between nth and n +5th residue whereas in 3_{10} helix hydrogen bonds occur between n and n + 3th residue. These helices are energetically unfavorable because the residues are either too loosely packed or too tightly packed. These helices usually occur at the end of α-helices.

β-strands have a more extended conformation as compared to α-helices. A single β-strand is not stable because there are not enough stabilizing interactions. When two or more β-strands interact to form hydrogen bonds, it can lead to the formation of very stable structures called β-sheets. β-sheets are formed from different regions of polypeptide as compared to α-helices which are formed from a continuous region of the polypeptide.

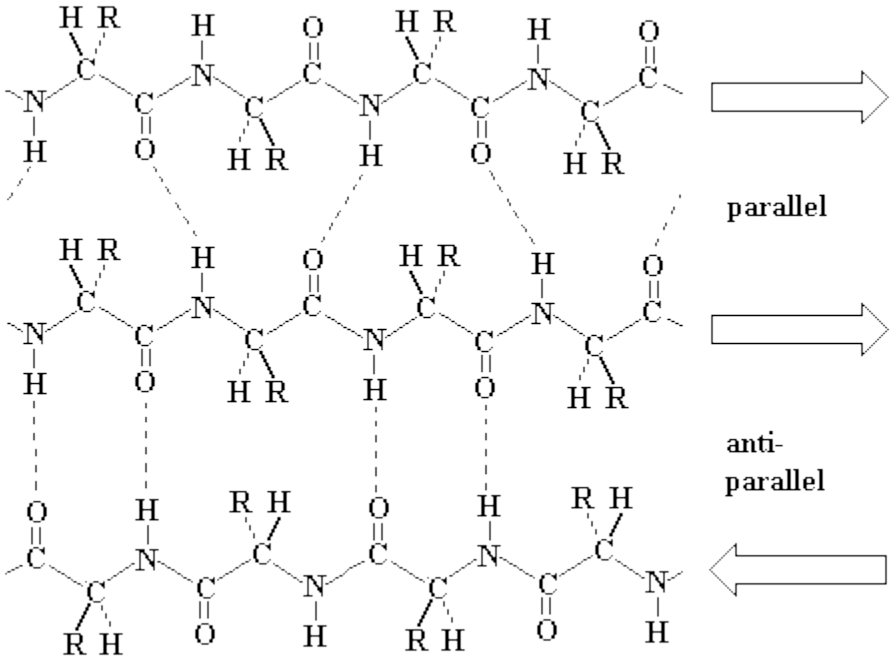

Figure 1.7 Beta sheet structure (image taken from ref. 56)

β-sheets can be both parallel and anti-parallel. In a parallel sheet all the β-strands are aligned in the same direction from N to C terminal. If adjacent strands are arranged in alternating directions then it is referred to as anti-parallel β-sheet. Hydrogen bonds are formed between C=O groups of one strand and NH groups of the adjacent strand. Side chains lie perpendicularly above and below the plane. Aromatic residues such as Tyr, Trp and Phe and branched amino acids, e.g., Thr, Val and Ile often occur in the middle of the β-sheets.

In proteins, α-helices and β-sheets are joined together by loop regions having irregular shapes. Loop regions generally occur at the surface of protein molecules. The solvent exposed parts of

these loops tend to contain charged and polar residues. Long loop regions are highly flexible and can adopt several different conformations.

Motifs or super secondary structures are formed from a simple combination of secondary structures, α-helices and β-sheets. Motifs can be formed from a combination of just α-helices such as helix-turn-helix motifs, two or more β-sheets such as hairpin motif and Greek key motif or a combination of both α-helix and β-sheet such as β-α-β motif.

1.2.2.3 Tertiary structure

Tertiary structure of protein refers to the compact three-dimensional structure of the protein. Domains are the structural units of protein tertiary structure. A domain is a part of the polypeptide chain that can independently fold to form a three-dimensional structure. Large proteins that contain more than 150 amino acid residues are often made of more than one domain. Domains of protein can have different tertiary structures and hence different functions. There are three main classes of domains - those containing only α helices, those containing β sheets, and others containing both α and β units. X-ray crystallography and NMR techniques are employed to obtain information about the three-dimensional structure of protein. Although X-ray crystallography can provide high resolution data, it cannot provide time-dependent information on the protein's conformational flexibility. NMR provides somewhat lower-resolution data and is limited to relatively small proteins, but it can provide information about both structure and dynamics of proteins. A domain with a particular structure and function may be part of the structure of several otherwise distinct proteins. Tertiary structure is mainly responsible for the function of the protein. Proteins having relatively different primary structure can still exhibit the same biological function if they have similar tertiary structure. Loop regions in a protein often

carry functional groups responsible for binding and enzymatic activity, e.g., antigen binding sites in immunoglobulins are made up of six loop regions. These loop regions in various antibodies differ both in the number and type of amino acid residues. Tertiary structure is not necessarily rigid and may change according to its surroundings. For example, the active site of an enzyme may have a specific shape under certain conditions that allows it to bind to the substrate (or ligand) prior to reaction catalysis. A conformational change during catalysis resulting in a change in the active site shape allows the reaction product to be released. Conditions such as high temperatures, or certain chemicals, can cause a protein to lose its tertiary structure and, thus, its function.

A number of interactions are responsible for the folding of proteins into compact three-dimensional structures and perform their biological functions. Tertiary structure is stabilized by disulphide bridges, hydrophobic interactions, electrostatic interactions, hydrogen bonding and van der Waals interactions.

Disulphide bridges are covalent bonds formed between two cysteine residues. Disulphide bonds cannot be formed between two consecutive cysteine residues. Usually, cysteine residues are separated by five or more residues in the amino acid sequence of a protein. Since these are covalent bonds they stabilize the protein structure. High temperatures, low pH and chemical reducing agents can break disulphide bonds.

Hydrogen bonds are formed between an electronegative donor atom and an acceptor atom. Hydrogen bonds between the main chain NH and CO groups stabilize the secondary structure of proteins. In addition to these hydrogen bonds between main chain atoms, other such bonds can also form between the main chain and the side chain atoms or between just side chain atoms.

Amino acids like tyrosine, serine, threonine, glutamine, asparagine, histidine, aspartic acid, glutamic acid, lysine and arginine are involved in hydrogen bond formation. Atoms in the side chain can also form hydrogen bonds with water molecules trapped inside the proteins. Sometimes, bifurcated hydrogen bonds, i.e., bonds between two donors and one acceptor, also occur.

Electrostatic interactions occur between oppositely charged residues in the side chain and the terminal amino and carboxyl groups of the main chain. Amino acids involved in these interactions are the positively charged lysine, arginine and histidine with the negatively charged aspartate and glutamate. The potential (V) between two charged groups (q_1 and q_2) can be described by Coulomb's law.

$$V = \frac{q_1 \ q_2}{\varepsilon 4\pi r} \tag{1.5}$$

These charge-charge interactions do not contribute much to the overall stability of proteins. Charged groups are usually present on the surface of proteins where they interact with water. Hydrogen bonding in α-helices induces a net negative charge on the C-terminal and a net positive charge on the N-terminal. As a result, positively charged residues more often occur at the carboxyl end and negatively charged residues occur at the amino end to neutralize the overall charge. Salt bridges also contribute to the stability of proteins. Salt bridges are strong hydrogen bonds formed between two oppositely charged species. In proteins salt bridges are formed between the negatively charged COO^- group of aspartic or glutamic acid and the positively charged ammonium group of lysine and guanidinium group of arginine. The distance between the charged residues should be less than 0.4 nm for salt bridges to be formed.

Hydrophobic interactions play an important role in the stability of the native state of a protein. Water is a poor solvent for non-polar compounds since they cannot form hydrogen bonds with water molecules. As a result, non-polar molecules tend to form aggregates when dissolved in water. There are many non-polar side-chains of proteins. These hydrophobic side chains avoid contact with water and approach other non-polar groups. This causes the polypeptide chain to collapse and form the hydrophobic core. This is especially evident for membrane proteins where the hydrophobic side chains are in contact with the membrane whereas more polar groups are present at the water interface.

Van der Waals interactions also play an important role in protein stability. Van der Waals interactions are attractive interactions and include interactions between permanent dipoles, permanent and induced dipoles and between induced dipoles. The interaction between permanent dipoles depends on relative orientation of the two dipoles and should average to zero for a freely rotating dipole. Most molecules are not free to rotate in every direction and thus have a preferred orientation. Thus, a net force exists between two permanent dipoles. This force is temperature dependent. The interaction between permanent and induced dipole does not depend on temperature. Also, a temporary dipole can induce a complementary dipole in the neighboring molecule. This results in a net attraction between the temporary and induced dipole. These dipoles are continuously shifting and depend on the polarizability of a molecule. At very small separation distances atoms repel each other due to overlap of electron clouds. The repulsive contribution dominates at small distances but drop as distance increases.

Although van der Waals forces are weak in nature, the net interaction is quite large due to the large number of residues present close to each other in a protein. Thus, van der Waals forces contribute significantly to the stabilization of protein structure.

1.2.2.4 Quaternary structure

If a protein contains more than one polypeptide then the global fold of all the chains together is referred to as quaternary structure. A multi-subunit protein may be composed of two or more identical polypeptides, or it may include different polypeptides. The quaternary structure is also stabilized by non covalent interactions. As an example the quaternary structure of immunoglobulin G (IgG) is shown in figure 1.8. IgG is composed of 4 polypeptide chains - two heavy chains and two light chains.

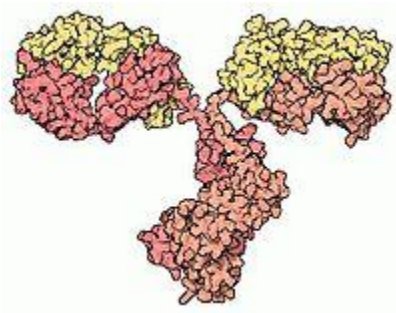

Figure 1.8 Quaternary structure of IgG. Two heavy chains are shown in red and two light chains are shown in yellow. (Figure is taken from ref. 57)

1.2.3 Protein folding and native state

The most typical conformation of a protein in its cellular environment is generally referred to as the native state or native conformation. According to Levinthal paradox [58], a protein does not sample all possible conformations; rather it folds through a series of meta-stable intermediate states. Molten globule is one such intermediate state which has native-like secondary structure, but lacks native three-dimensional tertiary structure. Folding of a protein to the native state can proceed through any of the large number of pathways and intermediates, rather than being

restricted to a single mechanism [59]. It is usually believed that the native state is thermodynamically the most stable state [60]. Some studies have suggested that the conformation assumed by the protein may not be the one with absolute lowest free energy. It may rather represent the lowest free energy state that is kinetically available to the protein. The native conformation could actually have higher free energy than some other states. However, these conformations might be unavailable to the protein due to large energy barriers. Whichever of these hypotheses is accepted, it can be concluded that protein will spontaneously assume the conformation with the lowest free energy in any given environment and under normal circumstances this conformation will be the native conformation.

The three-dimensional structure of the proteins is mainly stabilized by non-covalent interactions. It has been found that native state of a protein is only marginally stable. Protein conformation is affected by high temperature, acidic or alkaline pH, radiation and chemicals. A change in protein conformation from the native state is referred to as denaturation of protein. The difference in the free energy of a protein between folded and unfolded state is typically between 20 and 80 kJ/mol. A fully denatured protein lacks both tertiary and secondary structure, and exists as a random coil. The unfolded state retains the primary structure, i.e., peptide bonds linking the individual amino acid are still intact. Under certain conditions some proteins can refold; however, in many cases denaturation is irreversible.

CHAPTER 2

Protein adsorption onto solid surfaces

Proteins are highly surface active. Exposure of protein solutions to solid surface results in adsorption of proteins on interfaces. Protein adsorption to a surface is complex phenomenon. Adsorption of a homopolymer to a surface is driven mainly by enthalpic effects. Protein adsorption on the other hand, includes both enthalpic and entropic considerations. Protein adsorption on a surface will occur if there is a decrease in Gibbs free energy (G) of the system [61].

$$\Delta G_{ads} = \Delta H_{ads} - T\Delta S_{ads} < 0 \qquad (2.1)$$

where H, T and S are enthalpy, absolute temperature and entropy respectively. A single protein molecule may contain a large number of amino acid residues. Therefore, a small lowering of free energy for every residue lowers the free energy of the whole protein. Protein adsorption is a result of protein-protein interactions and protein-surface interactions. Solvent molecules (generally water) and other solutes such as low molecular weight ions also play an important role in adsorption process. Enthalpic interactions include van der Waal's forces, hydrogen bond forces and electrostatic interactions between oppositely charged surfaces and proteins or protein domains. Hydrophobic effects and internal packing restrictions contribute to entropic effects. Adsorption of proteins also involves release of solvation water/counter ions. In their native globular states, often proteins have a very compact structure. Their free volumes, compressibilities and conformational freedom are comparable to those of glasses [61]. As a

result, proteins have low entropies. Adsorption of protein molecules on a surface can lead to structural changes in the adsorbed protein, thereby increasing their entropy. All these factors are discussed in detail in the following sections. Further, adsorption can lead to changes in the functionality of the adsorbed protein. In this chapter, we briefly review some interesting findings on protein adsorption to surfaces.

2.1 Experimental Methods for Studying Protein-Surface Interactions

Many techniques are commonly employed to study protein adsorption. Some techniques are suitable for studying the adsorption process while others give information about the adsorbed layer. The amount of proteins adsorbed at an interface is of the order of several milligrams per square meter. Hence, the measurement of the adsorbed amount requires high precision. Depletion methods are often used to measure the adsorbed amounts. This method is based on determining the decrease in the concentration of protein solution after exposure to the surface [62-64]. However, these techniques require a large surface area to get accurate results [65]. Commonly employed substrates for this technique are latex beads and other small particles. Labeling of proteins with radioisotope such as ^{125}I or fluorescent molecules, e.g., fluorescein isothiocyanate (FITC), is commonly used to study protein adsorption [66-68]. These techniques can provide information about the adsorbed amount. With radiolabelling, there are no restrictions on the kind and the amount of the adsorbate. These labeling techniques can also be employed to study competitive adsorption from a multi-component protein solution [69, 70]. The fluorescence technique has been used to provide information about the structure of the adsorbed protein layer

[71]. However, labeling can affect the stability/structure of the protein and can hence influence the adsorption behaviour [72, 73]. The Quartz crystal microbalance (QCM) technique based on the change in the oscillating frequency of a piezoelectric crystal due to addition or removal of a small mass is often used for studying protein adsorption/desorption. QCM technique does not require protein labeling. It is a very fast technique and provides high sensitivity (ng/cm^2) [74]. In addition to the adsorbed amounts, this technique can provide information regarding the adsorption kinetics. It has been employed to study protein adsorption on various metallic and polymer surfaces [75-77].

Optical techniques, reflectometry and ellipsometry are routinely used to study protein adsorption on flat substrates [78, 79]. Ellipsometry is an optical technique that measures the changes in the polarization state of a beam upon reflection. These changes are modeled in terms of thickness and refractive index of the adsorbed protein layer. These parameters can provide information regarding the amount of the adsorbed protein and the structure of the protein layer [80]. Ellipsometry has also been used to study the binding between two proteins [81]. Neutron and X-ray reflectivity are relatively new techniques for studying physical parameters of adsorbed protein layers. These techniques provide information about thickness of the adsorbed layers. Neutron and X-ray reflectivity have been used to study albumin and β-casein adsorption on self assembled monolayers [82-84].

Protein adsorption on surfaces is also characterized by several techniques based on surface evanescent waves. If there are two transparent media with different refractive indices and light is incident on the interface at an angle greater than critical angle from the medium with higher refractive index, the light is totally reflected. The electric field is non zero in the medium with higher refractive index. Since the electric field cannot be discontinuous at the boundary, it

penetrates into the medium of lower refractive index and decays exponentially in that medium. Evanescent waves are generated on the surface. These waves propagate along the surface. Evanescent field can be used to excite other spectroscopic phenomenon. Total internal reflection fluorescence (TIRF) is one such technique in which fluorescence of the adsorbed species is excited by the evanescent field [85]. Tryptophan or tyrosine residues present in the adsorbed protein can be excited to give fluorescence spectra of the adsorbed species. Intrinsic fluorescence does not require any labeling and hence does not alter structure/ stability of protein molecules. It can be compared with the fluorescence of the protein in solution. It also has certain disadvantages. Some protein molecules show weak fluorescence due to low quantum yield, or may have few tryptophan residues or proteins may not be photostable [86]. Extrinsic fluorescence in protein molecules by labeling with a fluorescent dye can also be excited. The TIRF technique can provide information about competitive adsorption, conformational changes at the interface and the surface diffusion of the adsorbed protein molecules [87, 88].

Surface plasmon resonance (SPR) based biosensors utilize excitation of surface plasmons by the evanescent field generated on the metal/dielectric surface. Surface plasmon resonance (SPR) biosensor technique measures molecular binding events at a metal surface by detecting changes in the local refractive index. Since this method is based on measuring refractive index change, it requires no labeling. The depth probed at the metal-aqueous interface is typically 200 nm [89], making SPR a surface-sensitive technique ideal for studying interactions between immobilized biomolecules and a solution-phase analyte. SPR has been used to investigate protein–protein interactions [90], cellular ligation [91], protein–DNA interactions [92, 93], and DNA hybridization [94, 95].

Spectroscopic techniques such as infrared spectroscopy (IR), Raman spectroscopy, and circular dichorism (CD) spectroscopy are used to detect conformational changes in adsorbed proteins. IR spectroscopy can provide information about the secondary structure of the proteins [96]. Attenuated total reflection infra-red spectroscopy (ATR-IR) has previously been used to study protein adsorption from blood [97]. Protein adsorption kinetics has been studied by Fourier transform infrared spectroscopy (FTIR) in ATR configuration [98]. One disadvantage of IR spectroscopy is that water adsorbs strongly in this spectral region and it can dominate the obtained spectra. The disturbing effects from water can be avoided in ATR configuration. Raman spectroscopy can also give information about the secondary structure of proteins. However, most proteins have small Raman scattering cross-section. To enhance Raman scattering, evanescent wave propagation through polymer waveguides has been employed [99]. The total internal reflection technique has also been used to enhance Raman scattering of thin BSA layer adsorbed onto sapphire element [100]. Inducing resonance Raman scattering of proteins can also enhance signal [101]. Surface enhanced Raman scattering (SERS) can also be used to enhance Raman scattering of protein molecules adsorbed onto rough metallic films or metallic nanoparticles. SERS occurs due to enhanced local fields due to excitement of surface confined plasmons [102]. Circular Dichorism (CD) spectroscopy, generally used to study structure of proteins in solution, has also been applied to study structure of proteins adsorbed onto substrates. CD spectroscopy measures differences in the absorption of left-handed polarized light versus right-handed polarized light which arise due to structural asymmetry. CD spectroscopy has been used to study the conformation of α-amylase adsorbed onto silica particles [103] and albumin on SAM surfaces [104]. CD spectra give general information about the global secondary structure of the protein but cannot provide information about residue specific conformational change. Nuclear

magnetic resonance can be employed to obtain information about localized conformational changes [105, 106].

Atomic force microscopy (AFM) has been used to study protein deposits on various surfaces [107, 108]. AFM can image proteins on various surfaces under environmentally relevant conditions, e.g., in buffer liquids and can provide a three dimensional image of the adsorbed species. Tapping mode imaging has been used not only to image single protein molecules [109] but also to monitor changes in the three dimensional structure of adsorbed lysozyme molecules occurring during its enzymatic cleavage [110]. Even ligand-receptor forces can be measured using AFM [111]. Surface force apparatus (SFA) can be used to measure the interactions between adsorbed protein layers [112]. SFA can accurately determine the distance between two interacting surfaces.

Other techniques such as microcalorimetry can probe heats of adsorption [113]. X-ray Photoelectron spectroscopy (XPS) can determine protein amount deposited on nitrogen free polymer surfaces [114, 115]. XPS can also be employed to characterize the surface of the adsorbent.

2.2 Factors Influencing Protein Adsorption

The amount and the conformation of the adsorbed protein layer depends not only on the nature of the protein and the substrate but also on experimental variables such as temperature, pH of the solution, ionic strength etc. These factors are briefly discussed in the following sections.

Characteristics of protein surface such as effective surface area, charge and charge distribution, hydrophobicity and presence of any typical groups on the surface which bind specifically to some groups in the solvent or on the adsorbing surface influence the protein adsorption behaviour. Not only the surface properties of proteins but also the global characteristics of protein influence its adsorption behaviour. Some of these factors are the stability of the native structure, protein hydrophobicity and overall charge of the protein under experimental conditions.

2.2.1 Protein-Surface and Protein-Protein Interactions

2.2.1.1 Adsorption Irreversibility

Protein adsorption isotherms generally show saturation behaviour at higher concentrations. Therefore, Langmuir adsorption isotherm is sometimes adopted to explain the results. However, proteins generally adsorb irreversibly on to a surface [116]. Adsorption of small molecules such as monovalent ions onto solid surfaces is generally reversible [65]. Adsorption of random coil polymers on the other hand is rarely reversible. Polymers are large molecules with flexible chains. Hence they can form multiple contacts with the surface on adsorption [117]. Proteins being polymers can also form a number of contacts with a solid surface. Adsorption isotherms of most proteins are high affinity type. High affinity isotherms are typically found in systems where multiple contacts with surface are formed [118]. Experimental evidence of multiple bonding between proteins and surface was given by Morrissey and Stromberg [119]. They used IR spectroscopy to study adsorption of blood proteins on silica surface. They found that at pH 7.4

nearly 11% of backbone carbonyl groups in the polypeptide backbone in albumin were in contact with the surface. At more acidic pH values (<6), nearly 18% of carbonyl groups formed contact with the surface. For fibrinogen, almost 20% of carbonyl groups were in contact with the surface. Simultaneous dissociation of all contacts required for proteins to desorb from the surface, is an unlikely event. Therefore, protein adsorption is rarely reversible. Globular proteins have well defined secondary and tertiary structures. They have a very compact form in their native state. The polypeptide backbone has little rotational mobility. Adsorption on to a surface could lead to structural changes in the protein molecules and hence result in increased rotational mobility. Layer thicknesses of adsorbed protein are usually comparable to the size of the proteins in their native state [120]. This implies that even though adsorption could lead to structural changes in the protein, globular proteins do not completely lose their configuration.

2.2.1.2 Size of protein

As discussed in the previous section, proteins form multiple contacts with the adsorbent. Therefore, size of protein plays an important role in the adsorption process because larger protein molecules will have more contact points and hence be more surface active [121]. Such behaviour is indeed observed in case of homo and copolymers where the adsorbed amount increases with the molecular weight of the polymer [122]. Probing the effect of molecular weight in case of proteins is more complicated than in case of polymers because proteins with different molecular weights could also differ in stability or have different surface charges, e.g. hemoglobin with a molecular weight of 65 kD is about 1/5 the size of fibrinogen (M.W. 330 kD), but is much more surface active as compared to fibrinogen [119]. Hemoglobin is also more surface active than

albumin even though they are similar in size. Some investigators have studied the effect of protein self assembly on the adsorption behaviour. Although, self-assembly can induce some changes in the interaction, it is useful to study similar species differing in molecular weights. Okubo and coworkers studied the adsorption of monomers and dimers of BSA onto polymeric microspheres over a range of protein concentrations. They found that BSA dimer adsorbs preferentially over the monomer [123]. Similar behaviour in case of HSA adsorption has been reported by Lensen et. al. [124]. Preferential adsorptions of higher oligomers as compared to monomers have also been reported for lactoglobulin and insulin [125, 126].

2.2.1.3 Adsorption Behaviour of Small Peptides

Protein primary structure can also have an influence on its adsorption behaviour. It is possible that proteins have small peptide regions which directly interact with the surface and amino acid sequence of these regions could determine how the protein interacts with the surface. One way to study the effect of primary structure would be to synthesize peptides with varying amino acid sequence and compare their adsorption affinities [127, 128]. Whaley and coworkers [127] studied the adsorption of short peptides containing 12 amino acid residues to semiconductor surfaces and found that peptides that were rich in serine and threonine residues and also contained asparagine and glutamine residues adsorbed with high affinity. Small differences in amino acid sequence can influence protein/peptide interactions with a surface [129]. Read and Burkett monitored the adsorption of small polypeptides on both positively and negatively charged colloidal silica. Polypeptides were obtained by capping alanine with anionic aspartate on one end and cationic arginine on the other end. Adsorption is driven by electrostatic attraction

which results in orienting the charged peptide segment adjacent to the substrate of opposite charge. On adsorption α-helicity loss in the adsorbed peptide is observed on both anionic and cationic colloidal silica, despite inverse orientations. A single protein domain can dominate the adsorption of the protein molecule on a surface as shown in a study by Sakiyama et. al. [130] on the adsorption of peptide fragments of β-lactoglobulin (β-Lg) upon stainless steel surfaces. The authors found that peptides lacking acidic residues hardly adsorbed onto stainless steel surfaces. In contrast, peptides containing acidic residues adsorbed irreversibly at pH 3. This indicates that acidic residues play a major role in the adsorption process. The authors also found that β-Lg also showed similar adsorption behaviour. It is possible that these acidic residue peptides occurring at the surface of β-Lg are responsible for the adsorption of β-Lg. Thus, a small peptide region can determine the adsorption of protein.

The state of an amino acid can also depend on the surface to which it is attached as demonstrated by the following studies [130-132]. Liedberg et. al. [130] studied the adsorption of glycine on hydrophilic gold surface at pH 5.7 using IR spectroscopy and X-ray photoelectron spectroscopy. Glycine adsorbed onto the gold surface with NH_3^+ group close to the surface and COO^- group pointing away from the surface. However, glycine coordinates onto copper surfaces with both nitrogen as well as the oxygen atoms [131]. Alanine also adsorbed to copper with both oxygen and nitrogen atoms [132]. Adsorption of these amino acids also shows a pH-dependent behaviour. Depending on the pH of the solution these residues can exist in charged or neutral form [133, 134].

2.2.1.4 Protein Hydrophobicity

The surface of a protein contains both hydrophobic as well as hydrophilic residues. Since hydration of hydrophobic residues is entropically unfavourable, hydrophobic residues tend to stick together to minimize contact with polar water molecules in aqueous solution. Adsorption onto a non-aqueous surface leads to hydrophobic dehydration. Hence, presence of hydrophobic residues on the surface of protein can be a driving force for protein adsorption. Hydrophobic interaction chromatography studies have shown that surface hydrophobicity of protein influences protein adsorption behaviour [135]. Haynes and Norde compared the adsorption behaviour of proteins, α-Lactalbumin (αLA), lysozyme (LYS), bovine pancreas ribonuclease (RNase) and myoglobulin (MGB); with similar size but different surface hydrophobicities [65]. The study was conducted at the isoelectric point (i.e.p) of each protein, where the protein is electrically neutral. The authors found that in general adsorbed amount increases with the relative surface hydrophobicity of the protein molecule. However, plateau adsorption amount of αLA does not agree with this trend. αLA has very low structural stability as compared to the other proteins considered in this study. Structural rearrangements could be responsible for high adsorbed amounts (discussed in detail later).

An alternative approach to study the effect of hydrophobicity on protein-surface interaction is by mutating protein molecules. However, it is necessary to conduct control experiments as variation in the structure can stabilize/destabilize proteins. Malmsten and Veide [136] adopted a similar approach to study the effect of insertion of hydrophobic residues $(AlaTrpTrpPro)_n$ and $(AlaIleIlePro)_n$ on the adsorption of protein ZZ. They found that these hydrophobic tags did not change the adsorption behaviour of ZZ protein on hydrophilic surfaces. In contrast, adsorption

increased with the insertion of these hydrophobic stretches on hydrophobic surface. Further, extent of adsorption was found to be proportional to the length of these hydrophobic tags. These results indicate that hydrophobic interactions are the main driving force for protein adsorption in this system.

2.2.1.5 Electrostatic Effects

Protein adsorption on a charged surface involves overlap of the electrical double layers. There will be attraction if protein and the surface carry opposite charge and repulsion if both have same charge. Proteins are sometimes classified as 'soft' and 'hard' proteins. Soft proteins such as BSA, HSA, IgG, αLA, β-casein, hemoglobin etc. have low internal coherence and tend to adsorb on all surfaces even in case of electrostatic repulsion [116, 137]. The driving force in this case is gain in conformational entropy due to structural changes on adsorption.

In contrast, hard proteins are structurally more stable and undergo limited conformational changes on adsorption. The adsorption of such hard proteins is determined by electrostatic effect especially on hydrophilic surfaces as shown in a study by Barroug and coworkers [138], who studied adsorption of lysozyme (LYS), a hard protein, on hydroxyapatities and fluorapatite. They observed that LYS adsorbed onto these substrates only when it is electrostactically attracted towards the surface. Similar adsorption behaviour is also exhibited by other hard proteins such as RNase on hydrophilic substrates [139]. An alternate approach to study the effect of electrostatic interaction between proteins and solid surface is to vary the pH of the solution and thus vary the charge on the protein. If electrostatic attraction was the main driving force then as the charge on protein increases, the adsorbed amount should increase/decrease if there is electrostatic

attraction/repulsion. It is generally observed that the adsorbed amount is highest close to the i.e.p of protein [140]. This study shows that electrostatic effects are not the sole driving force in protein adsorption. One reason for this behaviour is that that the electrostatic repulsion between adsorbed protein molecules increases as the charge on the protein increases. Even though there is increasing attraction between protein and surface, repulsion between adsorbed protein molecules competes with this attractive force. Protein structural stability also varies with pH of the solution. Proteins have the highest stability close to their i.e.p and there are structural rearrangements on both sides of i.e.p as the charge on the molecule increases [141-143]. It is also known that solubility of a protein molecule in water increases as the charge on the molecule increases. As the solvency of polymers in a particular solvent decreases, adsorption of polymers at solvent adsorbate interface become more favourable. Similar behaviour can be expected in case of proteins which are copolymers. Experimental evidence has been provided by Asanov et. al. [144]. The authors used TIRF to study adsorption of BSA upon various surfaces and found that in thermodynamically good solvent conditions, a monolayer is formed on both hydrophobic and hydrophilic surfaces. On worsening the solvent conditions by addition of ammonium sulfate, a multi layer protein film is formed on surface.

2.2.1.6 Structural Stability of Protein in Native State

The effect of structural stability of protein molecule on its adsorption is clearly evident in the study by Norde and Lykelma [145-149]. The authors monitored the effect of temperature, pH and ionic strength on the adsorption of two proteins with different structural stability, human plasma albumin, HPA (a soft protein) and bovine pancreas ribonuclease, RNase (a hard protein)

on polystyrene lattices. The authors found that on changing the pH of the solution, adsorbed proteins molecules undergo rearrangements without desorbing from the surface. The steps observed in the adsorption isotherms of HPA also indicate reorientation or conformational change in the adsorbed HPA molecules. Similar kinks or inflection points have been reported for other proteins like BSA and ovalbumin [150]. The authors found that the plateau value of adsorption of HPA is largest at the i.e.p and falls symmetrically on both sides of i.e.p. The change in pH of the solution away from the i.e.p of protein results in increasing net charge on the protein molecules and therefore a more expanded conformation of the protein in solution. These structural changes in HPA with variation in pH of the solution are responsible for the observed decrease in the plateau value. The fact that plateau value falls continuously with change in pH indicates that there is a gradual change in the structure of the protein molecule. For HPA adsorption at pH 4.7, where protein molecules are uncharged, no change in the initial slope of the adsorption isotherm was found on varying the temperature from 5°C to 22°C. On further raising the temperature to 37°C, an increase in the slope is observed. HPA undergoes structural change at 37°C, but it retains its structure at lower temperatures. The lower adsorbed amount at 37°C also indicates more denaturation. The variation in the slopes of the initial isotherms on changing the temperature from 5°C to 22°C at all pH values other than 4.7 (i.e.p), points to different mode of adsorption at i.e.p as compared to other pH values. The data indicates that at same temperature, HPA is more denatured at higher pH as compared to i.e.p. At low surface coverage adsorption of HPA is an endothermic process. Adsorption isotherms of RNase do not vary much with pH, temperature or ionic concentration. This indicates that there is little variation in the mode of adsorption for RNase which is due to the high internal coherence of RNase. The authors suggest that hydrophobic interaction and increase in entropy due to structural rearrangements are

the major driving force for HPA adsorption. Hydrophobic effect plays a stronger role in the internal stabilization of HPA as compared to RNase. Hence, HPA unfolds to a greater extent on hydrophobic surface as compared to RNase. It is interesting that both proteins adsorb spontaneously even when they are electrostactically repelled by the surface and the adsorbed amount actually increases with increase in the surface charge. This indicates that electrostatic interactions are not the major driving force. Some of the positively charged groups of both HPA and RNase form ion pairs with the negatively charged sulphate groups on the surface. Such ion pairing reduces the charge in the dehydration layer. The results indicate that several carboxyl groups accumulate close to the negatively charged surface groups, which means that carboxyl groups prefer charged polystyrene surface as compared to water [148]. Carboxyl groups are bigger as compared to other cations, resulting in larger polarizability and weaker hydration of carboxyl groups.

Protein adsorption is accompanied not only by the coadsorption of protons [146] but also other low molecular weight ions. Norde and Lykelma [147] also studied electrophoretic mobility of all particles before and after adsorption to study which ions accompany HPA and RNase on polystyrene surface. They found that at low pH, when the protein is positively charged, anions are co-adsorbed to achieve charge neutrality. On the other hand, at high pH there is a net uptake of positively charged ions. Electrophoretic mobility studies show that mobility difference between dissolved and adsorbed HPA is smaller than that between RNase. This indicates that RNase layer incorporates more ions. Coadsorption of ions was further tested by using radiolabelled Na^{+}, Ba^{2+} and Mn^{2+} ions [151]. The authors found that the adsorption of ions does not depend on pH or ionic strength of the solution; it is affected by electrostatic considerations. Higher adsorption occurs in solution with divalent ions as compared to monovalent ions.

Energetically, insertion of larger and more polarizable Ba^{2+} is more favorable than Na^{+}. The authors developed a three layer model based on experimental results [152]. Region 1 contains the polystyrene surface charge, positively charged groups of protein that have formed ion pairs with surface charge and a fraction of carboxyl groups. Region 2 contains protein molecules. This region carries no net charge and oppositely charged ions occur in pairs. Region 3 contains protein surface charge and ions bound to proteins. Positive ions accumulate in region 1 and anions remain at the aqueous periphery. The authors also studied heats of adsorption using microcalorimetry [149]. On polystyrene surface with small negative charge, the driving forces for HPA adsorption at low pH values are increase in rotational freedom and hydrophobic dehydration. Hydrophobic dehydration is not so favourable on polystyrene surfaces with higher negative charge. Spontaneous adsorption occurs on this surface too. Driving forces on this highly charged surface are increased entropy due to structural change and co-adsorption of charged ions. Hydrophobic dehydration and structural rearrangements influence adsorption of RNase to a much smaller extent than HPA.

It is evident from the above mentioned studies that proteins like HPA with low internal coherence undergo structural change on adsorption. Changes in tertiary and secondary structures of other soft proteins such as α-Lactalbumin adsorbed on polystyrene surfaces have been reported [152].

Arai and coworkers [153] also studied some typical similarly sized proteins, RNase, lysozyme (LYS), myoglobin (MGB) and α-lactalbumin (α-LA) on various surfaces - polystyrene (PS), polyoxymethylene (POM) and hematite. Soft proteins α-LA and MGB adsorb on all surfaces irrespective of the hydrophobicity. The major driving force for adsorption of these soft proteins is structural rearrangements which counteracts the unfavourable contributions from hydrophilic

dehydration and electrostatic repulsion. Hard proteins, RNase and LYS, adsorb on hydrophobic PS surface irrespective of electrical attraction or repulsion. However, they adsorb on hydrophilic surfaces only when there is electrostatic attraction. Adsorption of proteins on surface leads to lowering of the charge of the system even in case of electrostatic repulsion between protein and surface. Coadsorption of small ions could be responsible for this. The authors also studied competitive and sequential adsorption of these proteins [154]. Adsorption on hydrophobic surface is generally irreversible. Sequential adsorptions of LYS, RNase and MGB are governed by electrostatic interactions. α-LA adsorbs on all surfaces with pre-adsorbed protein layers. High adsorbed amounts of α-LA are detected even in competitive adsorption experiments. Low structural stability of α-LA leads to its preferential adsorption. In general, greater the hydrophilicity of the surface, easier it is for the second protein to replace the already adsorbed protein.

2.2.1.7 Time effects: Kinetics and Conformational Change

The adsorption process can be divided into five steps: (1) transport to the surface, (2) actual attachment to the surface, (3) adsorption hindrance due to lateral repulsion between adsorbed proteins, (4) time dependent structural or orientational re-arrangements, (5) desorption or exchange and transport away from the surface [155]. Rate of adsorption is determined either by transport or the adsorption step itself.

Transport to the surface: For adsorption to occur, the protein has to be transported from the bulk phase to the adsorbent either by diffusion or convection. A stagnant layer exists close to the surface in all system, even well stirred ones. Protein has to diffuse to the surface through this

stagnant layer. Systems can be transport limited especially at low bulk concentration of protein [151].

Adsorption: On reaching the surface, protein could face an energy barrier. It could prevent some of the arriving protein molecules from adsorbing to the surface. The energy barrier could be caused by hydrodynamic effects or electrostatic repulsion [156, 157]. Teichroeb et. al. studied the adsorption kinetics of BSA, lactoferrin and LYS on p-HEMA [77]. The authors found that while adsorption of BSA is independent of the bulk concentration, lactoferrin and LYS adsorb in a concentration dependent manner. Adsorption occurs rapidly at first and then slowly for some time. Hence, there are two modes of adsorption. The first mode leads to a monolayer for lactoferrin and multilayer for LYS. Thus, adsorption is controlled by protein-surface interactions. Lin et. al [158] also studied protein deposition on commercial lenses and found deposits of albumin, IgG and other proteins after one minute exposure. The adsorbed amount of these proteins did not increase after 24 hours. On the other hand, LYS continued to be adsorbed for a week. As the surface becomes filled, the space available for adsorption becomes limited and the rate of adsorption falls below the diffusion rate. Hence, surface coverage becomes the rate determining step. Experimental evidence of this was given by Young and coworkers [159], who studied the adsorption of human serum albumin (HSA), transferrin (TF), α_2-microglobulin (α-MG), immunoglobulin (IgG) and fibrinogen (FGN) on polymer surfaces over a range of protein concentrations. At low bulk concentration adsorption was diffusion limited for HSA, FGN and IgG on silicone rubber and polyethylene. At long times as more surface fills up, adsorption rate falls below the diffusion limit. Fibrinogen adsorption is diffusion controlled for a longer time. Adsorption of TF onto silicone rubber is not controlled by diffusion. Rather, there exists an activation energy barrier for the actual attachment process. Similar results have been reported for

fibronectin adsorbed to silica surface [160]. Dass and others [160] employed a rotating disc to study the adsorption kinetics of BSA on ferric oxyhydroxide colloids. They found that at low concentration and low angular velocities, the adsorption was diffusion limited. At high angular velocities, adsorption was no longer limited by diffusion. Rather, attachment to the surface determined the adsorption rate.

Proteins can undergo structural rearrangements after adsorption. Higher degree of conformational changes occurs when surface coverage is low [104,139]. Soderquist and Walton reported that the adsorbed amount of protein is significantly reduced if the protein is adsorbed stepwise with repeated washings in the buffer as compared to adsorption in a single step [162]. This could also be due to the fact that rinsing with buffer leads to desorption of loosely attached protein, thereby leading to decrease in the adsorbed amount. Time dependent conformational change in albumin adsorbed on germanium and polyetherurethanes have been reported by Lenk et. al. [163]. Some studies have shown that protein adsorption occurs rapidly initially. The rapid uptake is subsequently followed by a decrease in the adsorbed amount. This decrease in the adsorbed amounts could be due to conformational changes in the adsorbed protein layer [159, 162]. Changes in the secondary structure of proteins on adsorption have been reported for various proteins [164-166]. Adsorption of fibrinogen onto Pyrex glass leads to 50% decrease in α-helical content [164]. Adsorption of IgG onto hydrophobic substrates results in a reduction in β-sheet content [165]. BSA adsorbed onto silica has lower helix content than the native BSA [166]. DSC studies of lysozyme, RNase, beta-lactoglobulin, alpha-lactoglobulin, cytochrome c, myoglobulin and hemoglobin adsorbed on chemically modified silica particles showed that adsorption resulted in decreasing the thermal stability of all proteins except cytochrome c [167].

Degree of conformational change further depends upon the nature of the surface. It has been generally observed that adsorption of proteins at water-solid interface leads to higher degree of denaturation on hydrophobic surfaces as compared to hydrophilic surfaces [168]. Wetrz and Santore used TIRF to study adsorption of albumin and fibrinogen on hydrophobic and hydrophilic SAM surfaces [169 - 171]. They found that for hydrophobic SAM's the adsorption rate as well as the final adsorbed amount is transport limited. Initially, the area occupied by each protein molecule (footprint) is comparable to its size in solution. With time the molecules spread on the surface. The relaxation rates are 0.12 and 0.15 nm^2 $molecule^{-1}$ s-1 for albumin and fibrinogen respectively. Relaxation rate is higher on hydrophobic SAM as compared to hydrophilic SAM [170]. Adsorbed protein molecules undergo denaturation on hydrophobic SAM. In contrast, no denaturation occurs on hydrophilic SAM; rather, the adsorbed protein molecules undergo reorientation. This indicates that denaturation occurs due to hydrophobic interactions. Due to denaturation, the amount of proteins adsorbed on hydrophobic surfaces is smaller than those on hydrophilic surfaces. The initial "footprint" is similar on all surfaces and lies in between that of side-on and end-on adsorbed molecules. It indicates that protein molecules are first randomly adsorbed and hydrophilic/hydrophobic interactions become important after protein adsorption. The authors found that relaxation rates are important even in competitive studies. If albumin is left on the surface for a longer time, the molecules have time to spread and it retards the adsorption of fibrinogen molecules. Due to faster spreading rate on hydrophobic SAM, shorter exposure times of albumin are required to retard subsequent fibrinogen adsorption. The authors also studied the adsorption of LYS on SAM's [172]. LYS is irreversibly bound to the surface and spreading indicates a transition from end-on to side-on adsorbed molecules. The

model calculations indicate that the adsorbed molecules change their orientation on the surface without desorbing.

The influence of the hydrophobicity of surface on the unfolding of adsorbed proteins can be obtained by using substrates with varying degrees of hydrophobicities [104, 167]. Steadman and Thompson [167] studied adsorption of lysozyme on surfaces with varying hydrophobicities using DSC, fluorescence and FTIR. They observed that an increase in the hydrophobicity of the adsorbing surface resulted in a decrease in the thermal stability of adsorbed protein with a simultaneous increase in conformational change. Also, adsorption resulted in heterogeneous conformational changes. Sivaraman and coworkers [104] used CD spectroscopy to study the adsorption of human fibrinogen and albumin on alkanethiol SAM's on gold with CH_3, OCH_2-CF_3, NH_2, COOH and OH terminal groups. They found that increase in the hydrophobicity of the surface resulted in the increase in the structural change as well as the amount of adsorbed protein. An increase in concentration of bulk solution resulted in the decrease of conformational change in the adsorbed proteins.

Desorption or Exchange: Protein adsorption is usually irreversible or partially reversible on dilution [116], though there are a few examples of reversible behaviour [138]. This indicates that some molecules are tightly bound to the surface while others are more loosely bound. Desorption of proteins is more probable on hydrophilic surfaces in comparison to hydrophobic surfaces [157]. On adsorption, protein molecules can undergo structural change. In such a case, the molecule has to overcome the sum of free energies of both adsorption and structural rearrangements in order to desorb from the surface. As a result, desorption process is slower and only a few molecules may desorb in the experimental timescales. Changes in pH and ionic strength of the solution can affect the interaction energy between protein and the surface, and

cause the protein molecules to desorb from the surface [66, 157]. Proteins, which bind with higher affinity, can also displace the adsorbed protein molecules.

Fluorescence photobleaching recovery technique has been used to study the exchange and desorption of labeled BSA [173]. Fluorescence recovery curves indicate that there is irreversibly bound state along with multiple reversibly bound states. Some of the reversibly bound molecules can diffuse along the surface. Surface diffusion of BSA has also been seen in the photobleaching and fluorescence recovery experiments of Tilton and coworkers [88]. They found that diffusion constant and the size of the mobile fraction depend on surface properties.

2.2.1.8 Organization of the Adsorbed Layer

Most proteins, being non-spherical, can bind to a substrate in two different ways: with their long axis parallel to the surface, referred to as side-on orientation or with their short axis parallel to the surface, referred to as end-on orientation. It has been hypothesized that at low bulk concentrations, the arrival of the protein molecules is slow and the incoming protein molecules have sufficient time to maximize their interactions with the surface and attach in side-on orientation [174]. As the bulk concentration increases, the number of molecules reaching the surface increases and at high concentrations protein molecules attach to the surface in end-on orientation. Steps observed in the adsorption isotherms of various proteins with increase in concentration are often attributed to change in orientation of proteins from side-on to end-on orientation [64, 145]. Calculations using ellipsometric and light scattering techniques have indicated a change in the thickness of the adsorbed protein layer with increase in the bulk protein

concentration [175, 176]. Other techniques such as microcalorimetry, CD and IR spectroscopy have also indicated that orientations adopted by adsorbed proteins depend on bulk concentration [149, 162, and 177].

The configuration of the adsorbed protein layers depend both on the nature of the protein and the substrate [178 - 180]. Hemoglobin forms a uniform layer on platinum [178]. Most of the protein molecules are specifically oriented such that nitrogen atoms are close to the platinum surface. On the other hand, the coverage on polytetrafluroethylene surface is non-uniform where hemoglobin is localized into islands. Similarly, insulin adopts different orientations on hydrophilic surfaces as compared to hydrophobic surfaces [179]. Higher adsorbed amounts of lysozyme, fibrinogen and BSA are found on hydrophobic polystyrene surface as compared to hydrophilic silica surface [180]. The adsorbed amount increases with increase in bulk concentration on both hydrophobic and hydrophilic surfaces. The orientations of adsorbed molecules depend on the hydrophobicity of the surface. Proteins are more randomly oriented on hydrophobic surface. With increase in bulk concentration, there is a change in the orientation of adsorbed BSA from side-on to end-on configuration. However, there is no detectable change in the orientation of adsorbed lysozyme. Rather, multilayers of lysozyme are obtained at high bulk concentration. Multilayer adsorption of lysozyme has also been indicated by AFM measurements, which show that at low bulk concentration, adsorbed lysozyme molecules diffuse along mica surface and form 5 molecule clusters [181]. At higher bulk concentrations, protein adsorbs uniformly and a monolayer is formed after nearly 2 hours. After this point adsorption in second layer also occurs. The authors suggest that on adsorption, hydrophobic residues are exposed and this could lead to protein aggregation on the surface.

Not only the equilibrium configuration, but also the buildup of protein layers on various surfaces proceeds differently, depending on the nature of both protein and surface [120, 182-184]. Ellipsometric studies have shown that for IgG, the refractive index of the adsorbed layer rises monotonically with increase in the adsorbed amount and finally levels off. The thickness of the adsorbed layer essentially remains constant throughout the adsorption process [182]. Formation of fibrinogen layers have been followed on various substrates. On methylated silica, fibrinogen layer buildup proceeds with an increase in both refractive index and thickness. After a certain concentration, the refractive index levels off and then gradually decreases. This decrease in the refractive index is accompanied with an increase in the thickness of the layer [182]. Qualitatively similar behaviour for fibrinogen adsorption is observed on silica surface [120]. Shaff et. al. [183] report a more pronounced decrease in the refractive index of fibrinogen layers adsorbed on silica surface. The authors found that fibrinogen adsorption initially proceeds with an increase in the layer refractive index to a maximum before falling off (shown in figure 2.1). Layer buildup of fibrinogen proceeds completely differently on hydrophobic chromium surfaces [184]. The thickness of the adsorbed layer rises rapidly at first and reaches a maximum. After that point, the thickness of the layer actually decreases before leveling off. According to ellipsometric measurements, initially the fibrinogen layers have high refractive index; which then falls to a minimum before rising again. Layer refractive index finally levels off. While on silica surfaces a maximum in refractive index is observed, a minimum in refractive index of fibrinogen occurs on chromium surfaces.

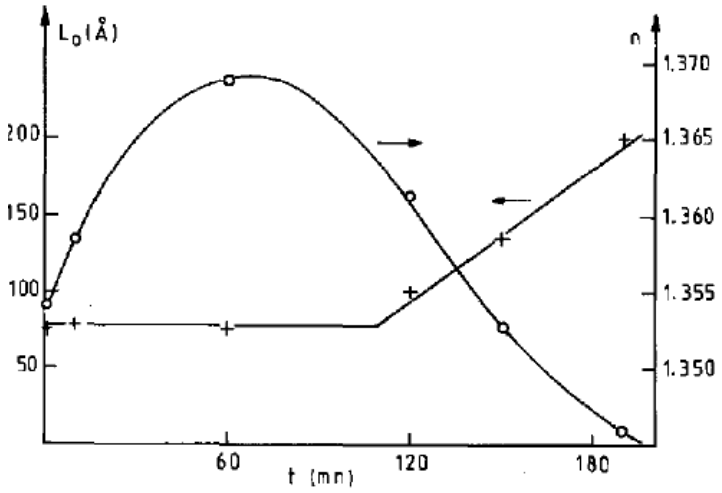

Figure 2.1 Variation of the optical layer thickness, L_0, (+) and mean refractive index, n, (0) in fibrinogen layer adsorbed on silica surface (Figure taken from ref. 183)

Most of the techniques used to study surface adsorbed protein layer such as ellipsometry assume that the adsorbed layers are homogeneous. There could be inhomogenity in the adsorbed protein layers. Young and coworkers showed that the binding affinity of the adsorbed protein layer decreases with distance away from the surface [185]. Techniques such as X-ray and neutron reflectivity can resolve the structure of adsorbed layer [186, 187]. Neutron reflectivity profiles of lysozyme adsorbed onto hydrophobic silicon showed that the adsorbed layer could be separated into two regions - a densely packed region close to the surface and a diffuse second region [186]. Further, the dimensions of the adsorbed layer indicate that adsorbed lysozyme denatures on the surface leading to exposure of hydrophobic fragments. The authors suggest that the dense layer contains peptide fragments with hydrophobic residues close to the surface and hydrophilic segments extending in the solution. Neutron reflectivity study of antibody (anti-β-hCG) on silicon oxide/water interface showed that at low concentration, the antibody forms a uniform 4 nm thick layer with molecules adopting a flat-on orientation [187]. At higher concentrations, there is a swelling of the adsorbed layer and the adsorbed protein layer could be

described by three sub-layers of 1, 3 and 2.5 nm with varying protein density. Due to twisting of the molecules, some fragments became loosely attached to the surface.

2.2.1.9 Effect of Adsorption on the Binding Activity of Adsorbed Proteins

Adsorption of proteins on solid surfaces can lead to a reduction in their binding activity [188-195]. This decrease in the binding activity could either be due to structural changes in the adsorbed proteins or due to unfavourable orientation of the adsorbed molecules [188 - 191]. Buijs et. al. [188] studied the effect of orientation of IgG adsorbed on silica surfaces on its antigen binding capacity. The authors found that adsorbed IgG exhibited higher antigen binding ratios at pH values where the Fab domains have low surface binding affinity. On the other hand, at pH values where Fab domains are electrostactically attracted towards the silica surface, adsorbed IgG molecules completely lose their antigen binding capacity. Reduction in antigen binding capacity due to restricted access to antigen binding sites has also been reported for other surfaces [189]. The enzymatic activity of RNase A adsorbed onto mica increases from 16% to 78% in a period of 24 h when compared to its activity in free solution [190]. Surface force measurements show that the thickness of the adsorbed RNase A layer changes from 2.8 nm one hour after adsorption to nearly 4.3 nm after 24 hours. Comparison with the tertiary structure of RNase indicates that initially RNase molecules lie flat on the surface of mica with their active site facing the surface. With time, the adsorbed molecules slowly reorient on the surface and finally adopt end-on after 24 hours with their active site partially exposed to the free solution. After 24 hours, there is no change in the orientation and hence the enzymatic activity of the

adsorbed molecules. Probe of secondary structure and activity of α-chymotrypsin attached to silicate surface revealed that although the enzyme undergoes structural change on adsorption, the inactivation of the enzyme in pH range 5-7 is due to unfavourable orientation of amino acids involved in catalytic activity towards the negatively charged silicate surface [191]. High surface concentration of the adsorbed antibody can also lead to restricted access to its antigen binding sites and hence a decrease in the antigen binding capacity [187].

The following studies demonstrate that conformational change on adsorption can also lead to reduction in the binding activity of adsorbed proteins [192-195]. Higher degree of enzyme inactivation occurs at low bulk concentrations [192]. This is due to the increased denaturation of adsorbed proteins at low surface coverage. The extent of deactivation depends on the nature of protein and the substrate [193-195]. Investigation of the adsorption of α-chymotrypsin and cutinase on hydrophobic Teflon and hydrophilic silica surface showed that both proteins had higher affinity for hydrophobic surface [193]. Although both proteins show a decrease in the α-helix content on adsorption to hydrophilic surface, they retain their biological activity. CD spectra show that while Teflon reduces the helix content in cutinase, it promotes the formation of helical structure in α-chymotrypsin. Hydrophobic Teflon induces higher deactivation of chymotrypsin as compared to hydrophilic silica. The increase in surface coverage of protein results in an increase of the fraction of the native-like conformation in the adsorbed layer.

The effect of native state stability of proteins on their binding activity in adsorbed state can be investigated by studying adsorption of protein mutants or proteins from different species [103, 194]. Kondo and Urabe [103] studied the adsorption of α-amylases with different thermal stabilities on silica particles. The authors found that the extent of deactivation of enzymes is closely related to the decrease in the α-helix content on adsorption. Enzymes with low structural

stability in their native state undergo higher degree of conformational change and reduction in their activity upon adsorption. Adsorption of T4 lysozyme variants on colloidal silica particles also showed that less stable variants exhibited lower biological activity due to more extensive structural change [194].

2.3 Protein-Nanoparticle Interactions

Nanoparticles are increasingly being used for various applications in science, technology and medicine. They are likely to be highly reactive, especially in biological medium and can accumulate in various organs of the body [195]. Nanoparticles have been shown to cross the blood brain barrier [196]. However, the mechanism of the transport is not clear. Although some risks associated with nanoparticles, such as cancer mesothelioma due to exposure to asbestos nanorods [197], are known; there is not much understanding about potential biological risks from nanoparticles [198, 199]. Over the past few decades there has been an increasing interest in developing nanoparticles as drug delivery agents [200, 201]. When nanoparticles enter body, they are coated with proteins [202, 203]. Adsorbed proteins can undergo conformational rearrangements. There is some agreement in the scientific community that the cellular response to materials in the biological medium is due to adsorbed biomolecule layer on the nanoparticle [204, 205]. Therefore, understanding the behaviour of proteins on nanoparticles is extremely important.

Several studies have been conducted to understand the fundamental properties governing protein nanoparticle interaction [206-209]. In general, higher amounts of protein are adsorbed onto hydrophobic particles as compared to hydrophilic particles [142, 206 - 208]. A study on the

adsorption of plasma proteins on particles with varying hydrophobicity showed a rise in adsorption of proteins with increase in the hydrophobicity of the particles [206]. A similar increase in the adsorbed amount with the degree of hydrophobicity of nanoparticle surface has also been reported in adsorption of HSA for nanoparticles of different sizes [208]. However, the nature of the surface group also influences the adsorption behaviour [206, 209 210]. Lundquist et. al. [209] studied the adsorption of blood plasma proteins on a range of labeled nanoparticles that differ in surface properties - plain polystyrene (PS), carboxyl-modified, and amine-modified PS of two sizes, 50 and 100 nm. They found that for nanoparticles of a particular size, the surface properties play a significant role in determining the kind and the amount of the adsorbed proteins. Brewer et. al. [210] studied the adsorption of BSA on gold surfaces using ξ-potential and quartz crystal microbalance. They found that the adsorbed amount of BSA on bare gold is higher as compared to citrate coated gold surface. Although the surface coverage is higher for BSA on bare gold, the Langmuir binding constant is lower. The authors suggest that electrostatic attraction between BSA and citrate groups present on gold surface are mainly responsible for binding of BSA. The role played by electrostatic interactions in binding of proteins to nanoparticles with different chemical compositions is also demonstrated by the following studies [211 -214]. BSA adsorbs preferentially to cerium oxide nanoparticles with positive zeta potential as compared to particles that have negative zeta potential [211]. Further, adsorption of protein increases with increase in the zeta potential of the nanoparticles. The uptake of nanoparticle also depends on the surface charge of the nanoparticles [211, 212]. Polystyrene nanoparticles with basic surface groups preferentially adsorb proteins that carry net positive charge and particles with acidic surface groups adsorbed proteins with net negative charge [213]. Kandori and coworkers studied the adsorption of BSA and lysozyme on colloidal calcium hydroxyapatitie

rods of varying lengths [214]. As the length of the rods is varied, the ratio of positively charged ions to neutral ions also varies with changing crystal sites. While BSA binds to positive sites, such behaviour is not seen for positively charged lysozyme as it faces electrostatic repulsion.

Study on kinetics of blood serum proteins on polystyrene nanoparticles [215] showed that proteins, albumin and fibrinogen, present in high concentration in plasma, are adsorbed from dilute plasma. On the other hand, adsorption from concentrated plasma results in displacement of these proteins within seconds by other proteins which are present in low concentration (the so called Vroman effect).

Nanoparticles have high surface to volume ratios. High local concentrations of proteins on nanoparticle surface can result in protein aggregation [119], reduction in protein activity and other structural changes. One example is that of enhanced fibrillation observed on range of nanoparticles – NIPAM/BAM copolymer, cerium oxide, gold nanoparticles, quantum dots and carbon nanotubes [216]. Though the nanoparticles lead to increase in fibril formation, they do not result in faster growth of the fibrils. The enhancement of fibril formation is due to the decrease in nucleation time. The nucleation phase depends on the amount and nature of nanoparticle surface. The authors suggest that high concentration of protein on the surface promotes fibril formation. Another possibility is that nanoparticle surface act as catalyst by reducing the energy barrier for fibril formation due to increased formation of prefibril aggregates [217]. Exchange of bound protein with free protein promotes oligomer formation. Similar enhancement in fibrillation of β-amyloid peptide due to shortening of nucleation phase in the presence of titanium dioxide nanoparticles was reported by Wu and coworkers [218]. Unlike Linse's group, these authors conducted the experiment in PBS at physiological pH. On the other hand, sterically stabilized phospholipid nanomicelles reduce fibril formation of β-amyloid [219].

This decrease in aggregation is due to 17 fold increase in α-helix and 10 fold reduction in β sheet content of the peptide. The nanomicelles under study not only reduce the rate of fibrillation but also the extent of fibril formation.

Protein adsorption onto nanoparticles can result in protein denaturation [220-223]. As demonstrated in the following studies, the native state stability of the proteins plays a key role in determining the extent of conformational change upon adsorption [221, 222]. Lundquist et. al. [221] studied the adsorption of two variants of human carbonic anhydrase, HCAI and HCAII, on silica nanoparticles. The authors found that soft protein HCAII lost its native structure on adsorption. The conformational rearrangements continued for days and adsorbed protein formed a molten globule structure. In contrast, hard protein HCAI did not undergo extensive conformational changes on adsorption. CD spectroscopy study of BSA and lysozyme shows that although adsorption leads to a decrease in the α-helix content of both proteins on adsorption, the extent of conformational change is higher at low surface coverage [222]. At high surface coverage, while there is no significant decrease in the helix content of lysozyme, secondary structure of BSA is strongly perturbed. On displacement under plateau conditions, lysozyme exhibits native like structure. However, desorbed BSA molecules do not retain their native state structure. Denaturation of adsorbed protein also depends on solution parameters such as pH and ionic strength [223, 224]. DSC measurements of lysozyme and RNase adsorbed on silica nanoparticles indicate that adsorption of these proteins induced structural alterations irrespective of the ionic strength of the solution [223]. However, the extent of denaturation is higher at low ionic strength. Increase in ionic strength also reduces the conformational heterogeneity of adsorbed proteins.

Unfolding on the surface can lead to decrease/loss of the biological activity of adsorbed protein [224, 225]. Adsorption of enzyme, α-chymotrypsin (CT), onto single walled carbon nanotubes leads to extensive change in the secondary structure of CT [225]. On adsorption CT only retains 1% of its native state activity. Although soybean peroxidase (SBP) retains its native three-dimensional shape (as seen from AFM images), SBP only exhibits 30 % of its activity in bulk. Therefore, reduction in the biological activity of adsorbed protein can occur even without extensive structural change.

2.3.1 Plasmonic nanobiosensors

Localized surface plasmon resonance (LSPR) of metallic nanoparticles is sensitive to changes in the local dielectric environment (refer to chapter 3 for details). UV-visible spectroscopy has been used to detect changes in the local refractive index by monitoring LSPR of metallic nanoparticles [226]. Other techniques that can be used for optical sensing using nanoparticles include nanoparticle aggregation [227, 228], resonant Rayleigh scattering of light [229], charge transfer reactions [230, 231] and optical imaging [232]. Nanoparticle aggregation leads to huge shifts in the plasmon peak positions and distinctive colour changes [227, 233]. Distance-dependent optical properties of gold nanoparticles have been exploited in the development of diagnostic method for DNA hybridization [234]. Resonant light scattering of gold nanoparticles has been utilized to study hybridization of DNA [229] and study binding between biotinylated BSA and streptavidin [235]. Gold nanoparticles labeled with anti-epidermal growth factor receptor protein (anti-EGFR) have been employed to target cancer cells that

overexpress EGFR [236]. Resonant light scattering of these labeled gold nanoparticles makes it possible to image these nanoparticles inside live cells.

The most common method for LSPR sensing is to measure the shift in the wavelength of the plasmon peak due to interaction of nanoparticle with adsorbed species [237- 240]. The first solution phase immunoassay using gold nanoparticles was developed by Englebienne [238, 241]. The author used 40 nm gold nanoparticles to monitor the binding kinetics of human chorionic gonadotropin (hCG) and anti hCG in real time. Adding of hCG to antibody coated gold nanoparticles resulted in a red shift of LSPR peak [241]. Since then, gold and silver nanoparticles have been increasingly employed for biosensing applications [242-245].

Natan and coworker showed that gold nanoparticles can be self-assembled onto polymer coated glass surfaces [246, 247]. Multiple contacts are formed between colloids and functional groups on the polymer such as cyanide (CN), amine (NH_2) and thiol (SH) [247]. Okamoto and coworkers followed this self-assembly method [248] to immobilize gold nanoparticles upon a glass slide using a coupling agent 3-aminopropyltrimethoxysilane. Immersion of these immobilized gold nanoparticles in solvents of varying refractive indices or coating gold nanoparticles with polymer film results in a change in both the position and intensity of LSPR peak. An increase in the resonance wavelength as well as absorbance can be observed with increasing thickness of the film (figure 2.2).

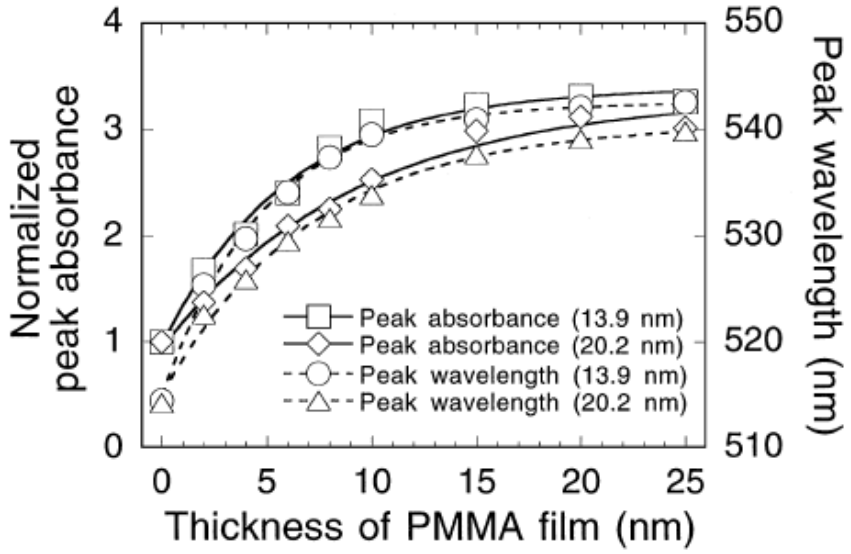

Figure 2.2 Peak absorbance and resonance wavelength of 13.9 and 20.2 nm gold colloid monolayer coated with PMMA film as a function of the thickness of PMMA film (taken from ref. 248)

Monolayer of immobilized gold nanoparticles prepared on glass by self-assembly has also been used as optical biosensors to monitor biotin streptavidin binding [249]. Self-assembly of gold nanoparticles on gold electrodes has been used to fabricate biosensors for glucose and hydrogen peroxide among others [250, 251].

Xu and Kaell used extended Mie theory to calculate extinction coefficients of gold nanospheres deposited on a transparent substrate in a non absorbing medium [252]. To estimate interparticle coupling effects, the authors assumed that the particles are distributed in a triangular two dimensional array. To calculate particle-substrate coupling, the authors considered a mirror charge located inside the substrate. Using this extended Mie theory, the authors calculated the shift in the peak positions due to coating of immobilized gold nanoparticles with PMMA film. The authors used the same nanoparticle coverage value as used by Okamoto and others [248]

(shown in fig 2.3). The calculated shifts agree well with the shifts observed experimentally by Okamoto et. al.

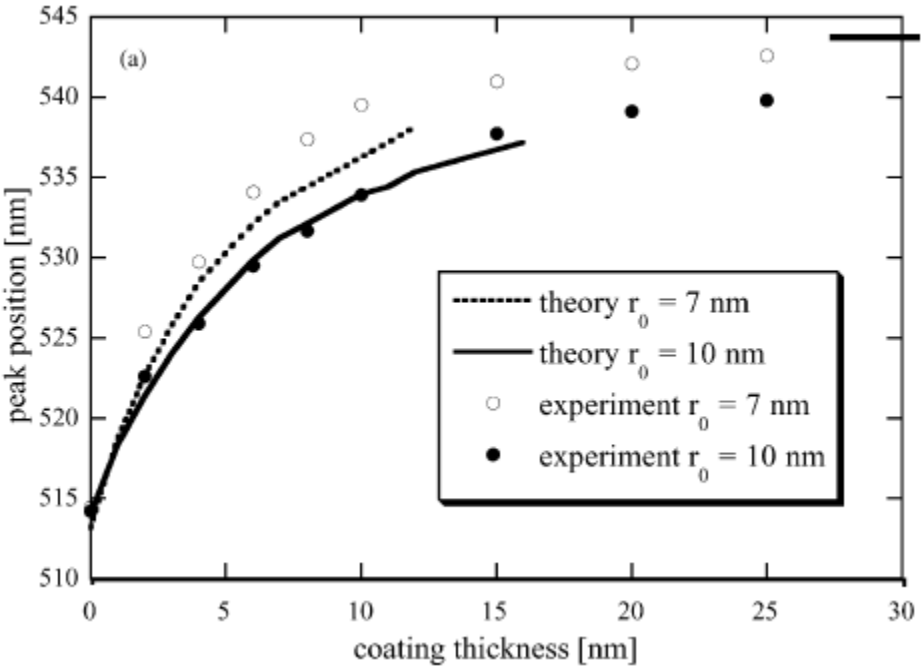

Figure 2.3 Comparison between experimental and calculated values of extinction peak positions vs. PMMA coating thickness for 20 and 14 nm Au particles. (Figure adapted from ref. 252)

2.3.2 Effect of the Size of the Nanoparticles

Nanoparticles are available in a range of sizes. As the size of the nanoparticle becomes smaller, it can approach the size of protein molecule or become even smaller than the protein molecule. Size limitations can induce packing constraints and lead to different structure on nanoparticles as

compared to flat substrates. The following studies indicate how the size of the nanoparticles can affect the conformation and stability of adsorbed protein layer.

Teichroeb and coworkers used LSPR to probe denaturation of BSA adsorbed onto gold nanoparticles [253-255]. The authors employed UV-visible extinction spectroscopy to monitor heat induced changes in BSA adsorbed on gold nanoparticles in the size range 5-60 nm [58]. The authors observed that thermal denaturation on smaller particles proceeded in a qualitatively different manner as compared to bigger spheres (fig. 2.4). As temperature is increased, the resonance peak shift to longer wavelengths for particles with diameter > 20 nm. This process continues till nearly 90°C. For smaller particles (5-20 nm) peak wavelength starts to blue shift at nearly 50°C. With further increase in temperature, a red shift in peak wavelength is observed. The magnitude of blue shift decreases as the size of the nanoparticle increases. Cooling down of the samples does not result in any change in the position of plasmon peak wavelength. This is due to the fact that adsorbed BSA has denatured and there is no change in the structure on cooling. As a control, bare spheres were also heated to a temperature of 90°C. Heating of bare spheres only resulted in reversible peak shifts of < 1 nm. Assuming that the adsorbed BSA layer is uniform and homogeneous, the authors used Mie theory to calculate the thickness of the adsorbed layer. A layer thickness value of 1.25 nm of BSA on 5 nm sphere indicates that BSA loses its tertiary structure on these small spheres. Thermal denaturing of BSA on 60 nm sphere occurs in two stages. A similar two step process is also observed in bulk denaturing studies of BSA.

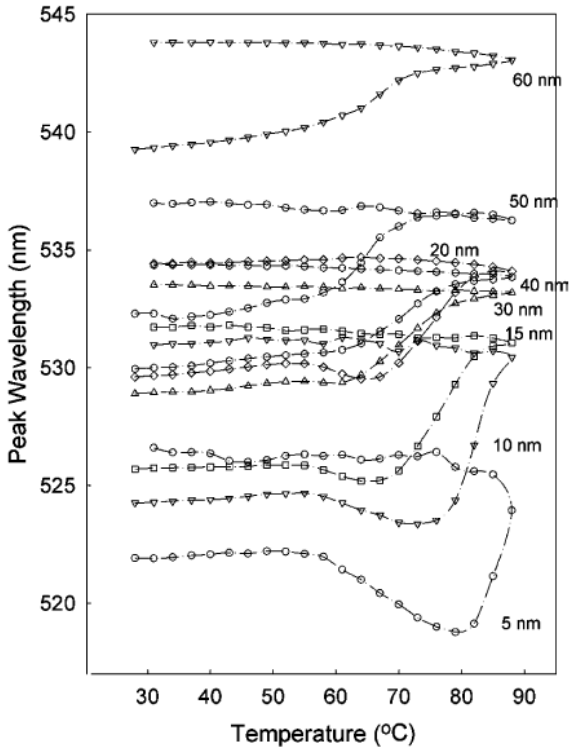

Figure 2.4 Peak wavelength values of BSA coated gold nanoparticles in the size range 5 to 60 nm as a function of temperature (fig. taken from ref. 253)

Teichroeb et. al. also studied kinetics of thermal denaturation of BSA adsorbed onto gold nanoparticles in the temperature range 60-70°C [254]. The lifetimes were used to calculate the activation energy barrier for thermal denaturing. The authors showed that the activation energy barrier for denaturation of BSA adsorbed onto gold nanoparticles is smaller than that in bulk solution; indicating that adsorption leads to protein destabilization. Further, activation barrier decreased with the size of the gold nanoparticles (figure 2.5). The activation energy for 100 nm particle is 25 times less than that for a 5 nm gold nanoparticle. The same group also investigated the effect of pH on the conformation of BSA adsorbed onto gold nanoparticles in the size range 5-30 nm [255]. The authors found an increase in the thickness in the adsorbed layer near pH 4 on spheres with diameter > 10 nm. Such extended state does not occur on 5 nm spheres. The authors

suggest that the absence of this pH induced conformational state on smaller spheres is due to the fact that adsorption on these small spheres results in the loss of tertiary structure.

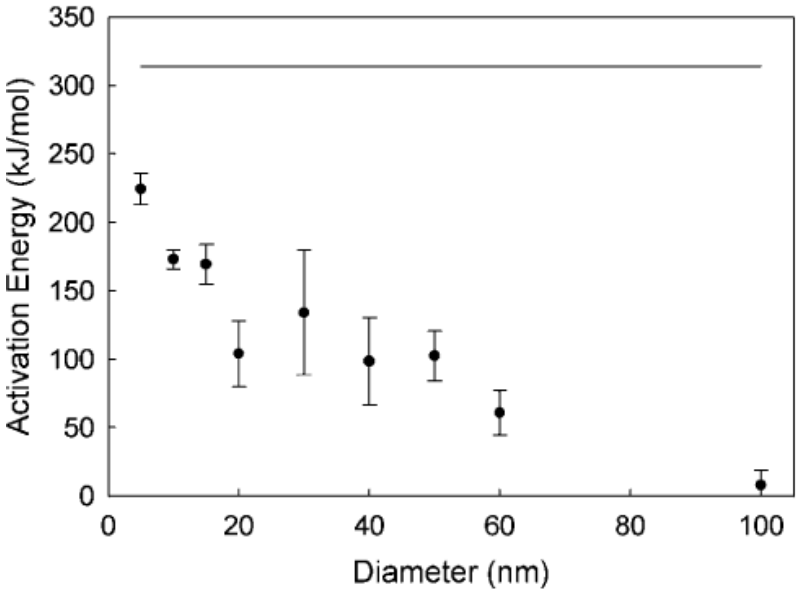

Figure 2.5 Activation energy for thermal denaturation of BSA as a function of size of gold nanoparticle (figure taken from ref. 254)

The above studies clearly indicate that the stability of adsorbed BSA layer depends on the size of gold nanoparticles. However, the extent to which surface curvature affects the structure and biological activity of the adsorbed proteins is not clear. Although there are studies available in the literature which deal with this subject, the studies have been conducted with a small number of proteins on nanoparticles in limited size range. The adsorption induced changes in protein conformation and activity depend on various factors such as nanoparticle chemistry, nature of protein (physical characteristics, stability etc.) and surface coverage [256-261]. As examples consider cytochrome c (cyt c) adsorbed onto gold and silica nanoparticles by two different groups [256, 257]. Adsorption of cyt c was studied on gold nanoparticles in two sizes, 2-4 nm and 16 nm [256], while that on silica nanoparticles of 4, 15 and 35 nm [257]. Although, both

studies conclude that the activity of the adsorbed cyt c depends on the size of the nanoparticles, it is observed that the activity of cyt c on 2-4 nm gold nanoparticles is higher than that on 16 nm gold nanoparticles. On the other hand, the activity of cyt c increases with the size of silica nanoparticles from 4 to 35 nm. CD studies indicate that while there is a decrease in the β sheet content on adsorption to 16 nm gold nanoparticles, adsorption on 2-4 nm gold nanoparticles results in increase in both α- helix and β-sheet content. The authors suggest that hydrophobic interactions are the main driving force for adsorption on 2-4 nm particles while electrostatic interactions are dominant on bigger particles. The size of the gold nanoparticles also affects the intramolecular hydrogen bonding. On the other hand, as the size of silica nanoparticle increases, there is an increasing degree of conformational change and change in the local heme environment [257]. Conformational changes induced by adsorption on silica nanoparticles are partially reversible.

Nanoparticle curvature can stabilize or destabilize the adsorbed protein as indicated by the following studies [224, 258-261]. A study on the adsorption of lysozyme onto silica nanoparticles of diameter of 4-100 nm shows that both the structure of the adsorbed layer and the activity of surface adsorbed lysozyme depend on the size of the nanoparticle [224]. While monolayer is formed on 20 nm particles, multilayers occur on 100 nm particles. Greater reduction in both helix content and activity of lysozyme occurs on bigger nanoparticles. Another study on the adsorption of human carbonic anhydrase I (HCAI) on silica nanoparticles with diameters of 6, 9 and 15 nm also shows a similar size-dependent behaviour [258]. Larger particles cause higher perturbation in the secondary structure of adsorbed protein. This could be due to increased protein surface interaction on bigger nanoparticles. Strangely, the authors do not observe any difference in tertiary structure of the adsorbed proteins. Perturbation in secondary

structure is related to tertiary structure. Roach and coworkers [259] studied the adsorption of BSA and fibrinogen on silica nanoparticles in the size range 15-165 nm. IR spectroscopy revealed that BSA denatures more on bigger spheres whereas fibrinogen lost more of its secondary structure on smaller nanoparticles. Both proteins denature more on hydrophobic spheres in comparison to hydrophilic spheres. The authors suggest that while fibrinogen adopts end-on orientation on bigger spheres, it adopts side-on orientation on smaller spheres. Due to the increase in protein-surface interaction, it denatures more on smaller nanoparticles. Asuri and coworkers [260] found that adsorption of enzyme soybean peroxidase on single walled carbon nanotubes resulted in increased stabilization of this enzyme at high temperatures as well as in the presence of organic solvents as compared to adsorption on flat substrates. The authors suggest that the curvature of these nanorods reduces lateral interactions between adsorbed proteins and results in their enhanced stabilization. In vivo protein binding studies exhibit additional complications as demonstrated by Jiang and coworkers [261]. The authors studied the binding of Herceptin-coated gold nanoparticles to its receptor ErbB2 in the size range 2-100 nm. The authors found that though all nanoparticles showed binding to the receptors and altered processes related to cell functioning, 40 and 50 nm particles showed highest binding ratios and cell death. Smaller nanoparticles have lower number of attached antibodies and possess lower binding avidity. On the other hand, greater membrane wrapping time is required for the internalization of large nanoparticles. Hence, extremely small and large particles do not yield high uptake.

The above studies show that protein nanoparticle interactions are not fully understood yet. A lot of contradictory findings regarding protein stability/instability on various protein nanoparticle combinations have been reported. Further studies need to be conducted to obtain complete characterization of protein nanoparticle system.

CHAPTER 3

Experimental Techniques

3.1 Synthesis of Gold Nanoparticles

For the synthesis of gold nanoparticles, we followed the method of Turkevich et.al. [262]. The materials required for the synthesis are as follows: Hydrogentetrachloroaurate (III) hydrate - ($HAuCl_4.xH_2O$, molecular weight 339.79), trisodium citrate dihydrate- ($Na_3C_6H_5O_7.2H_2O$, molecular weight 294.10), magnetic stir band, 250 ml Erlenmeyer flask, 50 ml glass beaker, 10 ml and 50 ml graduated cylinders, glass vials and glass pipettes. Both sodium citrate (Sigma Aldrich C-8532, purity ≥ 99%) and gold chloride (Sigma Aldrich 254169, purity 99.999%) were purchased from Sigma Aldrich and were used without further purification.

Procedure

(1) All glassware and magnetic stir bar are thoroughly washed with soap solution and water. Care should be taken that the glassware is thoroughly cleaned to remove traces of colloidal gold which can act as nucleating agents. The glassware are further rinsed with deionized water and dried.

(2) To prepare 1mM solution of gold salt, dissolve 0.03398 g of gold salt in 100 ml deionized water. Use of glass pipettes to scoop out gold salt is recommended as gold chloride car erode metal. Use electronic weighing balance (0.0001 g precision) to weigh the gold salt in a glass vial. Fill the glass vial with deionized water and then empty its contents into Erlenmeyer flask. Add more deionized water into the glass vial previously used to dissolve gold chloride

and again empty its contents into the flask. Repeat this procedure a couple of time to ensure that no gold chloride remains in the vial. Add the remaining amount of water to the flask.

(3) Place a magnetic stir bar in the flask and cover it with the precleaned beaker. Place the flask on a stirring hot plate. Turn the heat to maximum and adjust the stir speed to medium. Bring the solution to boil. It takes approximately 30 minutes. Control of temperature is required as lowering temperature by 10°C can increase the reaction time as well as reduce the particle size [262].

(4) In the meantime, calculate the amount of citrate solution required. The amount of citrate required depends on the size of the nanoparticles being produced. To prepare 30 nm gold colloids, a ratio of 15:1 gold chloride to citrate solution is required, i.e., for every 15 ml of 1mM gold chloride solution add 1 ml of 1 % solution of trisodium citrate (1 g of salt in 100 ml of deionized water). Add the desired amount of sodium citrate in a glass vial. Add deionized water to the vial to make 1% solution. Stir the solution to ensure that citrate dissolves completely. Different sizes of gold nanoparticles can be produced by varying the amount of citrate added. To obtain smaller gold nanoparticles add more citrate.

(5) Rapidly add citrate solution to the boiling gold salt solution and increase the stirring speed to maximum. Keep on heating for about 7 minutes. On addition of citrate, the colour of the solution changes from yellow to clear and then grey, then purple. Finally a deep red is obtained indicating the formation of colloidal nanoparticles.

(6) Switch off the hot plate and remove the flask containing gold nanoparticles. Let the suspension cool to room temperature and store it in glass vials. Seal the glass vials. The gold nanoparticles stored in these sealed glass vials are stable for about 2-3 months. After that

time the nanoparticles aggregate and settle at the bottom of the container. The nanoparticles synthesized in the lab are more concentrated than those commercially available.

There are two views regarding the mechanism of formation of gold nanoparticles. Turkevich [262], LaMer [263], Takiyama [264] and Frens [265] concluded from their research that nanoparticles are formed by nucleation followed by uniform growth. Chow and Zukoski [266] state that first large nanoparticles are formed which shrink over the course of reaction to result in smaller particles of uniform size.

In this recipe sodium citrate is used as a reducing agent. Citrate ions reduce Au (III) to Au (0) state. The reaction mechanism is given below [267].

Figure 3.1 Reduction of Au (III) to metallic gold by citrate ions.

Citrate ions act not only as reducing agents but also as stabilizing agents by capping gold nanoparticles. Electrostatic repulsion between citrate ions prevents nanoparticles aggregation. It has been theorized that there are some gold ions present on the surface of gold nanoparticles and citrate ions form complexes with these ions [267]. In the absence of some form of stabilization, e.g., charge or steric stabilization, these colloidal particles tend to aggregate. This phenomenon is

clearly seen in the presence of excess salt in these charge stabilized nanoparticles. The presence of ions screens the charge and thus leads to nanoparticle aggregation. On the other hand, polymer or protein coated gold nanoparticles are sterically stabilized and are therefore stable even in high ionic strength solutions.

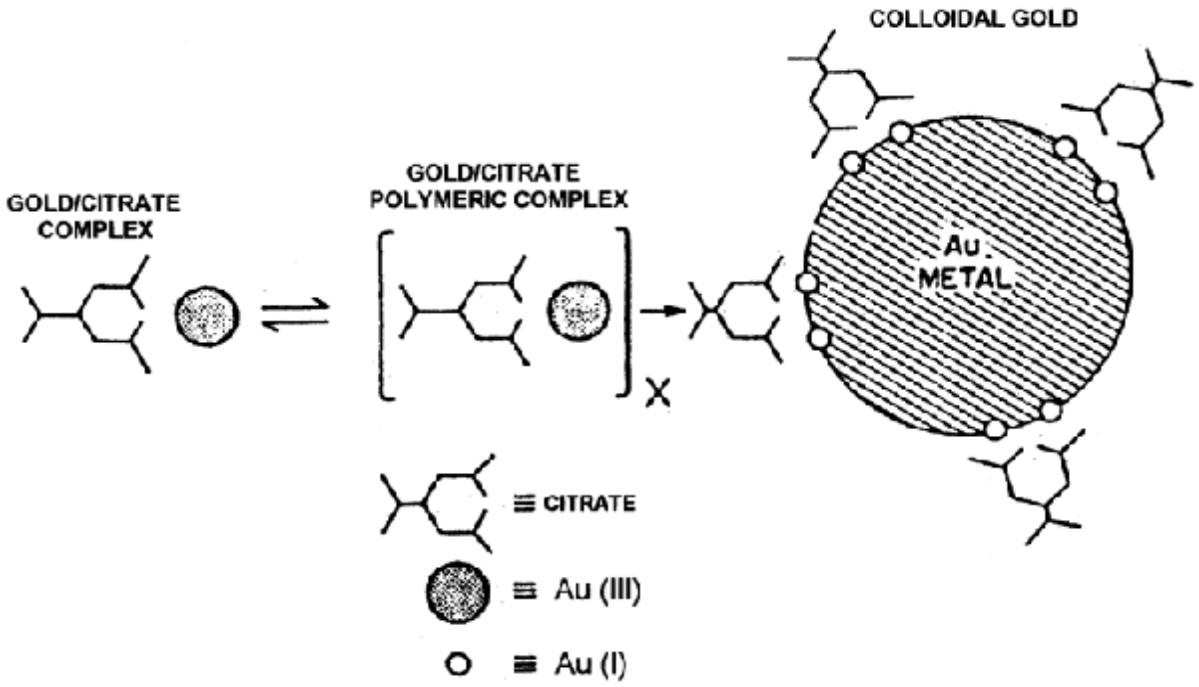

Figure 3.2 Complex formations of citrate ions on the surface of gold nanoparticles (taken from reference 267).

3.2 Substrate Preparation for Sizing Gold Nanoparticles

For sizing gold nanoparticles silicon wafers with crystal orientation (100) are used as substrates. These wafers were supplied by Silicon Quest International. The wafers were cut into 1cm x 1cm small squares with the help of silicon carbide pen. For cutting purposes they are laid on lens cleaning paper (Kodak) by placing the polished sides face down to avoid silicon dust contamination on that side. It is very hard to remove silicon dust particles once they settle on the surface. These wafers are scratched on the unpolished side with the help of a ruler. On bending these wafers lying face down, thin sections of wafers are produced. These thin sections are further divided into smaller squares (1 x 1 cm^2) using the same technique.

3.2.1 Thin film preparation

To prepare thin films atactic polystyrene with molecular weight 641000 was used. Materials required for making solution are polystyrene, toluene, tweezers, glass pipettes and glass vials. Polystyrene was purchased from Polymer source Inc. (P2767-S). Tweezers are cleaned first with water and then with the solvent toluene. Glassware required for this purpose, pipettes and vials are cleaned by blowing dry nitrogen gas. Polystyrene is placed in a cleaned glass vial using tweezers and then toluene is added to the vial to make 2% by weight polystyrene solution. The sample is left to sit at room temperature for ~ 3 days to ensure that polystyrene dissolves completely.

Thin films were prepared by spin coating polystyrene solution onto silicon substrates. For this purpose two glass pipettes are used. The glass pipettes are first cleaned by spraying them with

dry nitrogen. Silicon wafer is placed on the stage of the spin coater (shown in figure 3.3). To prepare films first the silicon wafers are cleaned with toluene. For cleaning 15-20 drops of toluene are dropped on the silicon wafer while it is spinning at a speed of 7500 rpm. After cleaning two drops of the PS solution are placed on the silicon wafer. After that the spin coater is set into spinning motion for about 10 seconds at a speed of 2500 rpm. Due to spinning the droplet spreads out on the substrate, whereas the solvent evaporates. After spin coating the PS films were kept at room temperature for ~ 4 hours to ensure that toluene evaporates completely. After that they were annealed at 120°C for nearly 20 hours in home built oven to remove any residual stress in the film due to spin coating. The annealing is done under nitrogen atmosphere to keep it free from any contaminants in air.

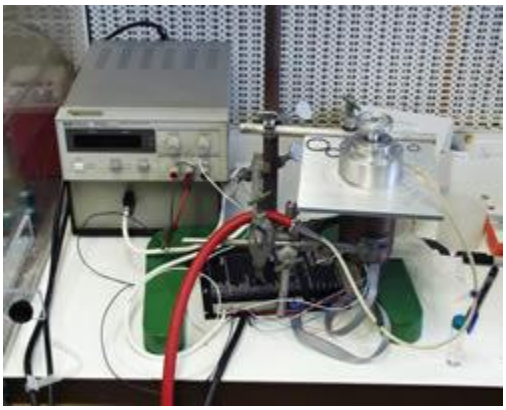

Figure 3.3 Spin coater apparatus (image taken from ref. 268)

3.2.2 Depositing Gold Nanoparticles on Polystyrene Films

Gold nanoparticles synthesized as described in section 3.1 were deposited on the polystyrene films using spin coater. The glassware used for depositing gold nanoparticles, pipettes and vials are cleaned by blowing nitrogen. Polystyrene coated silicon wafer is placed on the stage of the spin coater. Gold nanoparticles do not stick to the surface of PS films as they cannot wet the PS surface [269]. To increase surface wettability ethanol was added to the gold colloid. Using a pipette, 10 drops of gold colloid are introduced into a cleaned glass vial. 1 drop of ethanol is added to the vial. The solution is mixed with another pipette. Several drops of this solution are placed on the polystyrene film spinning at ~ 600 rpm resulting in the evaporation of solvent and hence deposition of gold nanoparticles on the PS films. Ethanol can lead to aggregation of nanoparticles. Therefore, nanoparticle-ethanol solution is prepared immediately prior to spin coating. It was observed that this procedure did not lead to high coverage of 30 nm gold nanoparticles on polystyrene films. So, gold colloid was placed on the centre of the polystyrene film and allowed to sit for 10 minutes. After 10 min the spin coater was set into motion. In this method gold nanoparticles have a longer time to adsorb on the surface and it leads to higher nanoparticle coverage.

3.3 Poly Dimethyl Siloxane Film Preparation

Poly dimethyl siloxane (PDMS) is silicon containing organic polymer. It has a wide range of applications. It is widely used in contact lenses, medical devices, shampoos, lubricating oils and

heat resistant tiles [270]. PDMS elastomer, Sylgard® 184 was obtained from Dow Corning ®. Sylgard comes in a two resin pack. Resin A contains vinyl groups and resin B contains hydrosiloxane groups (shown in fig. 3.4). A cross linked network of dimethyl siloxane groups is formed by mixing the two resins [271].

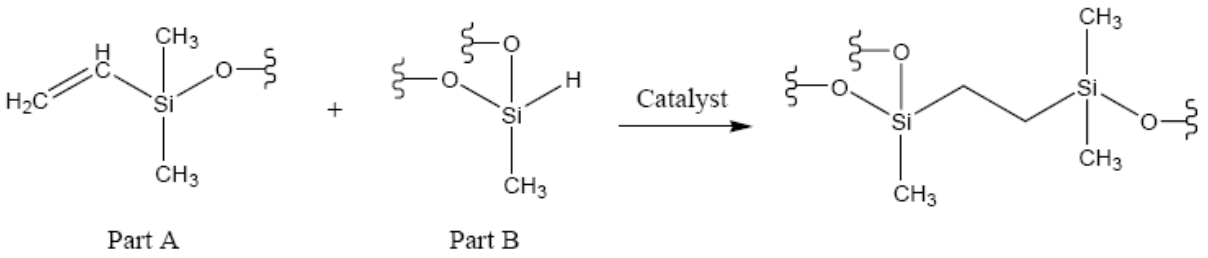

Figure 3.4 Scheme showing cross linking of PDMS (taken from reference 271)

The two resins are mixed in the ratio 10:1 in plastic cups. After adding the two resins in desired ratio, they are vigorously mixed with pipette tips to ensure uniform distribution of the curing agent. PDMS elastomer is used to obtain thin film on polystyrene cuvettes, purchased from VWR International (PS cuvettes, K1960 VWR, catalog number 58017-880). PDMS is gently lined inside the cuvette on all the four sides and the bottom with the help of spatula making sure that no air bubbles are formed in the PDMS lining. It is important that there is a uniform PDMS coating inside the cuvette and the protein solution placed inside the cuvette comes only in contact with PDMS and not polystyrene cuvette. Afterwards cuvettes are placed in the oven where the PDMS films are cured at 80° C for 24 hours in nitrogen environment. It was observed that the quality of PDMS films deteriorated with time. Therefore all films were freshly prepared and used within 24 hours after curing.

3.4 PolyHEMA Film Preparations

Linear Poly(HEMA) (Mw ~ 200,000) was purchased from Sigma Aldrich. A solution containing 5% water by weight in ethanol is prepared in a glass vial. PolyHEMA crystals are dissolved at 5% weight in the above mentioned solution in a glass vial. The vial is left to sit for 2 days. The supernatant containing dissolved polyHEMA is removed from the top of the vial after two days. Only the supernatant is used for film preparation. Dissolved polyHEMA is left to sit in a cuvette for several days. The solvent evaporates leaving polyHEMA sticking to the sides of the cuvette.

3.5 Protein Adsorption on Gold Nanoparticles

Five different proteins were used in this study – Rabbit Immunoglobulin G (IgG), Staphylococcal Protein A (Protein A), Goat anti-rabbit IgG (Anti-IgG), Bovine Serum Albumin (BSA) and Streptavidin. All proteins were purchased from Sigma Aldrich as essentially salt free lyophilized powders. The catalog numbers are given below.

IgG – I5006
Protein A – P3838
Anti-IgG – R2004
BSA – A0281
Streptavidin – S4762

Aqueous solutions of gold nanospheres of various sizes -5 nm (catalog number 15702-20), 10 nm (catalog number 15703-20), 15 nm (catalog number 15704-20), 20 nm (catalog number

15705-20), 30 nm (catalog number 15706-20), 40(catalog number 15707-20), 50 nm (catalog number 15708-20) and 60 nm (catalog number 15709-20) nm were purchased from Ted Pella Inc. (Redding, CA, USA). These commercial gold nanoparticles suspensions are citrate stabilized and hence carry a net negative charge. Two sizes of silver nanoparticles, 20 nm and 40 nm, were also used in this study. Aqueous solutions of silver nanoparticles were also purchased from Ted Pella Inc. Catalog numbers of these silver suspensions are 15705-20SC and 15707-20SC for 20 and 40 nm silver colloids respectively.

3.5.1 Conjugation with IgG, Protein A and Streptavidin

For conjugation procedure recipe from reference 272 was followed. Phosphate buffer solutions (PBS) of three different ionic strengths - regular, twice the regular and 25 the regular strength, are prepared. The materials required for preparation of PBS are sodium chloride (NaCl, EMD Chemicals Inc., catalog number SX0420-1), disodium hydrogen phosphate (Na_2HPO_4, Aldrich Chemical Company Inc., catalog number 21,988-6), sodium dihydrogen phosphate (NaH_2PO_4, Aldrich Chemical Company Inc., catalog number 33,198-8), 3 spatulas, glass bottles and plastic weighing cups. The spatulas are first scraped using paper towels. Next they are thoroughly rinsed with water and isopropanol to get rid of any impurities. After that they are dried in air. For regular strength PBS 6.4284 gm of NaCl, 2.6972 gm of Na_2HPO_4 and 0.5519 gm of NaH_2PO_4 (measured using plastic cups on electronic scale, 0.1 mg precision) are added to 1 liter of deionized water in glass bottle. PBS of different strengths is similarly prepared by adding these salts to different amounts of water.

IgG, Protein A and Streptavidin were conjugated to gold and silver nanoparticles bought from Ted Pella. For preparing conjugates of gold nanoparticles with proteins, first protein solutions are prepared in deionized water. Spatulas and glass vials required for preparation are cleaned as described previously.

Conjugation procedure for gold nanoparticles

(1) Protein powders are weighed in glass vials on electronic weighing balance. Deionized water is then added to the vials to make the concentration 1 mg/ml. These solutions are then gently mixed on a mixer (Vortex-Genie II, VWR International).

(2) Take 600 micro litres (µl) of gold colloid in a polystyrene cuvette. Add aqueous protein solution to the cuvette. Take care that no air bubbles are formed as protein can denature at air/water interface. For IgG add 10 µl, for Protein A add 40 µl and for Streptavidin add 70 µl of protein solution to 600 µl of gold colloid. Shake the cuvette gently for ~ 10 minutes. After that let the sample sit for an hour.

(3) Add 610 µl, 640 µl and 670 µl of 2x concentrated PBS to IgG coated, Protein A coated and Streptavidin coated gold colloid respectively to obtain a final solution of coated gold colloid in regular strength PBS to mimic physiological conditions. Shake the cuvette gently for 10 minutes.

Conjugation procedure for silver nanoparticles

In this study Protein A was adsorbed onto silver nanoparticles in a same way as gold. Take 600 micro litres (µl) of silver colloid in a polystyrene cuvette. Add 40 µl of 1mg/ml of aqueous Protein A solution to the cuvette carefully to avoid any air bubbles. Shake the cuvette gently for 10 minutes. Let the sample sit for an hour. Add 640 ml of 2x concentrated PBS to Protein A coated silver nanospheres. Shake the cuvette gently for 10 minutes.

3.5.2 Conjugation with BSA

BSA was adsorbed onto 30 nm gold nanoparticles synthesized in the lab because this experiment required a high concentration of nanoparticles.

Procedure

(1) BSA is weighed in glass vial on electronic weighing balance. Deionized water is then added to the vial to make the concentration 0.1 mg/ml. The sample is then gently mixed on a mixer (Vortex-Genie II, VWR International).

(2) Take 2.4 micro litres (µl) of gold colloid in a glass vial. Add 800 µl of BSA dissolved in deionized water to the cuvette. Take care that no air bubbles are formed as protein can denature at air/water interface. Shake the vial gently for ~ 10 minutes. After that let the sample sit for an hour.

(3) Add 128 µl of 25 x concentrated PBS to the cuvette. Shake the vial gently for 10 minutes.

(4) To remove free BSA, centrifuge the sample at 4° C. Divide the BSA nanoparticle solution into 4 centrifuge tubes and set the centrifuge into motion at 12000 rpm. Let it run for 20

minutes. BSA coated gold nanoparticles settle at the bottom of the tube while free BSA molecules remain suspended in the solution. Remove the supernatant with the help of syringe. Resuspend the conjugated gold colloid in regular strength PBS to obtain the same volume of the sample as before centrifugation.

3.6 Measurement Techniques

3.6.1 Atomic Force Microscopy

Atomic force Microscopy is a kind of scanning probe microscopy that can provide three-dimensional image of the surface. It has a very high resolution of the order of fractions of nanometer. A schematic diagram of AFM is shown in fig. 3.2 and the actual AFM device used in this work is shown in fig. 3.3. It consists of a sharp tip attached to a cantilever that is raster scanned along the surface. The cantilever oscillates at its resonance frequency. The laser bounces off from the back of the cantilever and is directed into a four quadrant photo diode through a mirror. The four quadrant photo detector can detect the motion of the tip both in horizontal and vertical direction. When the tip comes close to the surface, there is deflection in the cantilever due to interaction between the tip and the surface. The main forces of interaction are van der Waal's force, electrostatic interaction and Pauli's repulsion force. In the attractive regime van der Waal's forces are the most important. The difference between the actual deflection of the cantilever called setpoint and signal from the photodiode is referred to as error signal. A PID (proportional, integral and differential) circuit controls the force between the tip and the sample by adjusting the piezo voltage according to the error signal.

AFM can be operated in three modes - contact mode, non contact mode or tapping mode. During scanning in the contact mode the tip is in actual physical contact with the surface and thus experiences repulsion from the surface. In this mode a constant deflection of the cantilever is maintained. This mode is used for extremely flat surfaces. Any surface deformation can change the deflection of the cantilever; causing the z-piezo to adjust the height of the tip above the sample. Deflection of the cantilever gives information about the surface of the sample. This mode is not suitable for biological samples as it can damage the samples.

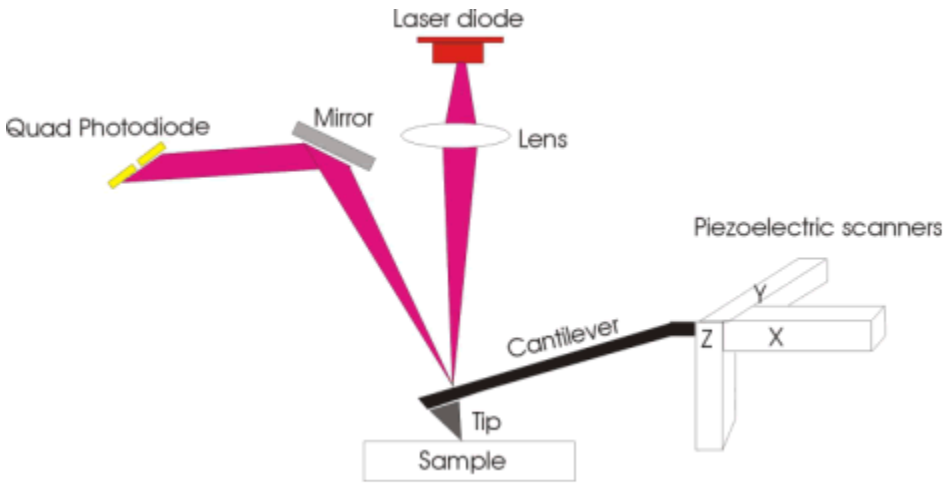

Figure 3.5 Schematics of atomic force microscopy [273]

In non contact mode the cantilever is oscillated at or close to its resonance frequency. The amplitude of the oscillations is small, typically < 10 nm. When the tip comes close to the surface the interaction between the tip and surface can damp the oscillations. Any protrusion on the surface will change the extent of damping; causing the z-piezo to adjust tip height to maintain the setpoint. In this mode the tip is not actually in physical contact with the sample and is therefore preferred for biological samples as it does not cause sample degradation.

Figure 3.6 AFM head mounted on the sample holder stage [273]

Tapping mode is similar to the non-contact mode, but the amplitude of oscillation is higher (100-200 nm) than in non-contact mode. Again, the cantilever is oscillated close to its resonance frequency. Close to the surface the interaction forces between tip and sample can cause the amplitude of the oscillation to decrease. In this mode the tip can occasionally come into contact with the surface or "tap" the surface. In this study only tapping mode was used.

The resolution of the AFM in the z direction is extremely high with sub nanometer resolution being possible. However, in lateral direction the resolution is limited by the radius of curvature of the tip which can be between 10 and 20 nm. The image of the sample that is obtained is actually a convolution of tip shape and the sample features.

3.6.2 UV-Visible Extinction Spectroscopy

Attenuation of an electromagnetic wave due to both absorption and scattering is referred to as extinction. Figure 3.7 shows the set-up for extinction measurement. The experimental set-up consists of a white light source fitted with optical fiber cable, collimating lens, sample holder and detector. The light source used in this study was a halogen lamp, HL 2000 purchased from Ocean Optics, Dunedin, Florida, USA. The light source should be switched on about 20 minutes before the start of the experiment to ensure it has stabilized. The detector was a hand held Ocean Optics USB 2000 spectrometer. The USB 2000 spectrometer takes the light energy transmitted by an optical fiber. This collected light is dispersed through a fixed grating across a linear CCD array detector. OOI Base 32 software was used to analyze the data. The spectra were recorded at room temperature.

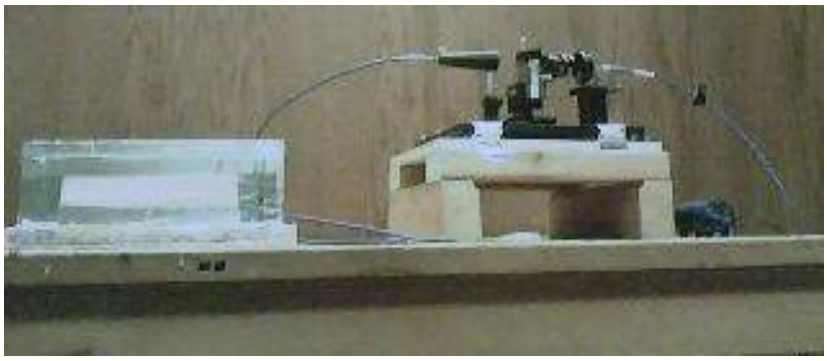

Figure 3.7 Extinction measurements set-up. The spectrometer is placed inside the pink temperature controlled box.

A collimated beam of white light passes through the sample. The light passing through the sample is collected by a second fiber optic cable and then directed to the spectrometer. The spectrometer measures the intensity of the light transmitted through the sample and compares it to the intensity of incident beam of light, i.e., the intensity of light before it hits the sample. To measure the intensity of incident light a non absorbing medium such as water is placed inside a cuvette and the light passing through the cuvette is measured by the spectrometer. This is then recorded as a reference spectrum. Light intensity spectra of both the incident light and light transmitted through 10 nm gold nanospheres are shown in figure 3.8. As is evident from the graph maximum attenuation occurs close to resonance (around 520 nm). The extinction spectrum of 10 nm gold nanoparticles obtained using Lambert-Beer law is shown on right in figure 3.8. In this extinction set-up, the transmitted light is detected. However, the beam would also contain light detected in the forward direction. For small nanoparticles used in this study, contribution of scattering to extinction is small and hence it is not as critical. As the size of the particle increases the light scattered also increases.

We use Lambert- Beer's law to calculate the extinction coefficient of gold nanoparticles. If I_o is the intensity of the incident light and I_t is the intensity of transmitted light, then absorbance A is given as

$$A = -Log\frac{I_t}{I_o}$$

Extinction spectrum of 10 nm gold nanospheres is shown in figure 3.8. Absorbance of a gold nanoparticles suspension is related to attenuation coefficient (α_{ext}) and path length i.e. the distance the light travels through the medium (l) and is given as

$$A = \alpha_{ext} l$$

Since extinction is the sum of absorption and scattering, extinction cross section (ε_{ext}) of a particle can be written as

$$\varepsilon_{ext} = \varepsilon_{abs} + \varepsilon_{sca}$$

Extinction cross section of a nanosphere can be calculated from attenuation coefficient (α_{ext}) and is given by

$$\varepsilon_{ext} = \frac{\alpha_{ext}}{C}$$

where C is the number of particles per unit volume. Extinction efficiency of a sphere is defined as the extinction cross section per unit area of the sphere and is given as

$$Q_{ext} = \frac{\varepsilon_{ext}}{\pi a^2}$$

where a is the radius of the nanosphere. Extinction cross section of a metallic nanosphere can be even greater than the geometric area of the sphere. Hence, extinction efficiency of a metallic nanosphere can be greater than 1.

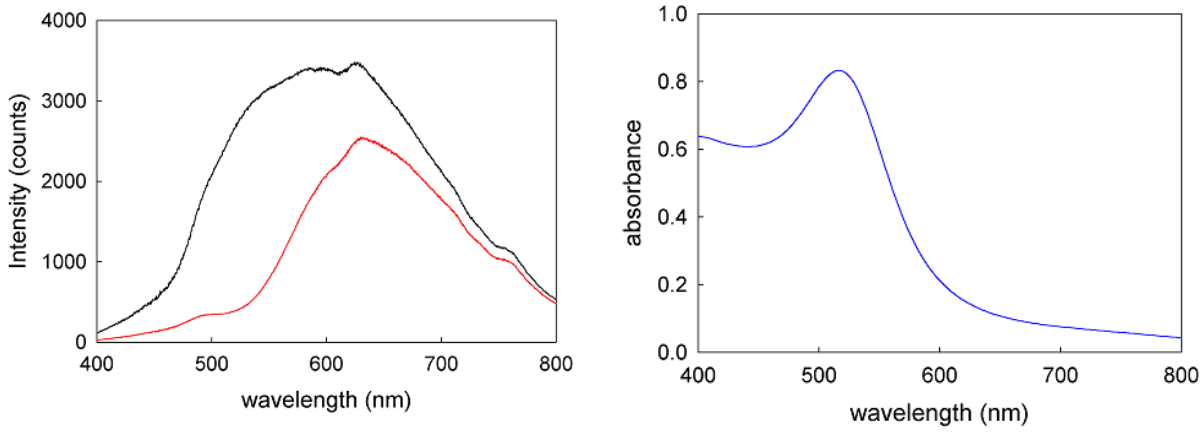

Figure 3.8 On the left, intensity of light passing through water (black line) and light passing through 10 nm spheres (red line) are shown as function of wavelength of light. On the right the absorbance, εcl, (containing contribution from both absorption and scattering), of 10 nm gold nanospheres calculated using Lambert-Beer's law is shown.

3.6.2.1 Temperature Controller for the Spectrometer

The variation of temperature of the spectrometer during the course of experiments can result in fluctuations in the recorded peak wavelength, especially in experiments which are carried out for long periods of time (10-20 hours). Therefore, the spectrometer was placed inside a home built temperature controlled box (see figure 3.9). The box was built out of Styrofoam. It was fitted with a resistive heater. The temperature was controlled with a PID based temperature controller (Micromega® CN77000 series controller) which was purchased from Omega engineering Inc. (Stanford, USA). With the help of this set-up the temperature was maintained to within ±0.3 K.

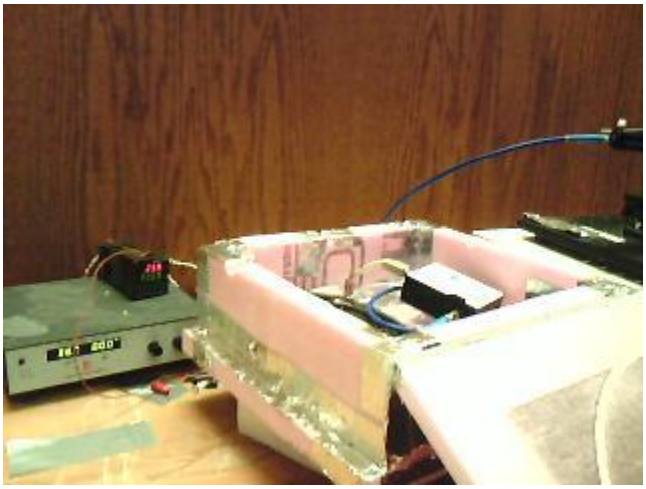

Figure 3.9 Temperature controlled box containing the USB 2000 spectrometer along with power supply and temperature controller.

3.7 Localized Surface Plasmon Resonance

Localized surface plasmon resonance (LSPR) refers to the collective oscillation of the conduction electrons in metallic nanoparticles such as gold, silver, platinum etc. This resonance occurs when the frequency of the incident radiation is in resonance with surface plasmons and metal nanoparticles exhibit this resonance in UV-visible spectral region. Surface plasmon resonance is only possible when these charge oscillations are confined and are therefore absent in bulk materials. LSPR results in strong absorption with extremely large molar extinction coefficients ~ 3 x 10^{11} M^{-1} cm^{-1} [274], resonant elastic scattering [275]. Another important aspect of LSPR is the enhancement of the local electromagnetic fields which is further responsible for effects such as surface enhanced Raman scattering.

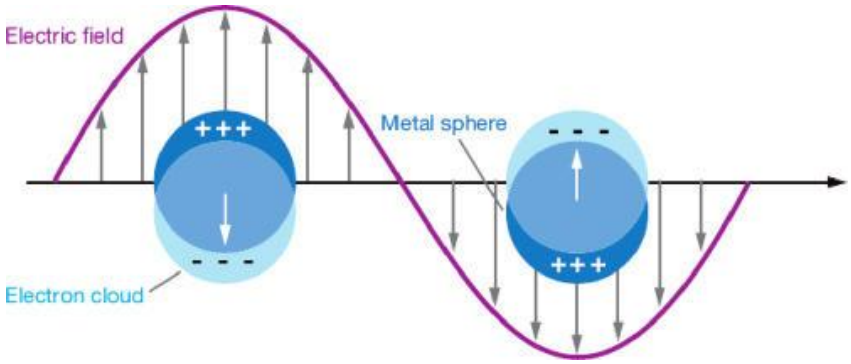

Fig. 3.10 Localized surface plasmon resonance (taken from ref. 276)

The position as well as magnitude of the plasmon resonance peak depends strongly on the shape, size, size distribution, as well as the dielectric properties of the surrounding environment (see figure 3.11 and 3.12).

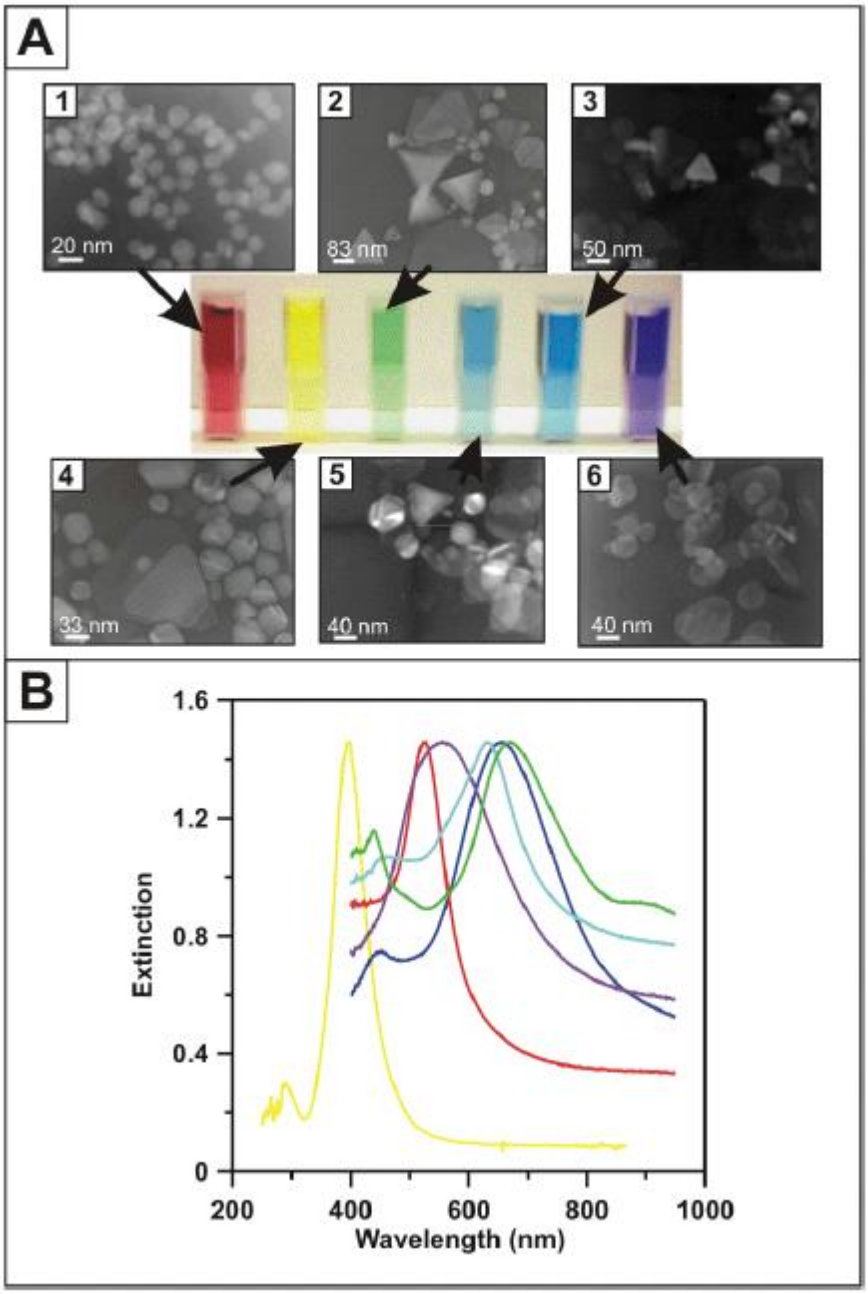

Figure 3.11 Gold and silver nanoparticles of various shapes and sizes. (A) Transmission electron micrograph images of various nanoparticles (1) Red solution contains 13 nm gold nanospheres. (2) Yellow solution contains a mixture of silver nanospheres, trigonal prisms and polygon platelets. (3) Green solution consists of silver nanoparticles of various shapes (spheres, trigonal prisms and polygon platelets). (4) Light blue solution contains silver trigonal nanoprisms and polygon nanoplatelets. (5) Dark blue solution contains silver nanoparticles (trigonal prisms with rounded tips and polygon platelets). (6) Purple solution contains inhomogeneous oblong silver

nanoparticles. (B) Extinction spectra of all the above solutions are shown (colour of the line corresponds to the colour of the solution). (Image taken from ref. 277)

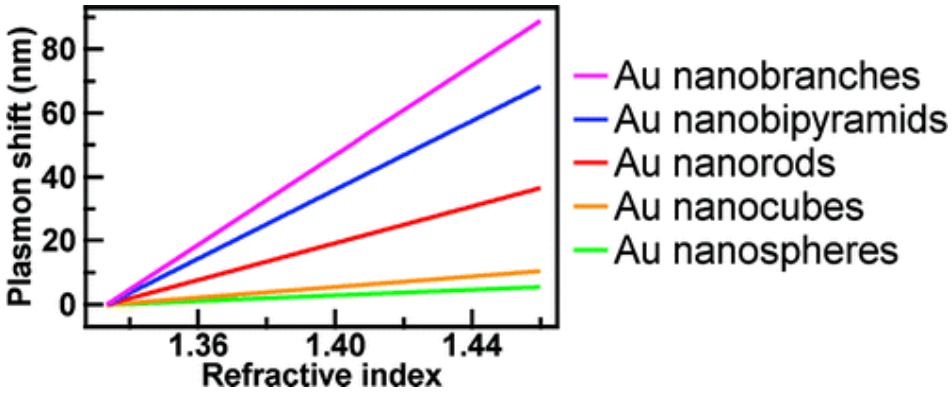

Figure 3.12 Shift in the position of plasmon resonance peak of gold nanoparticles as a function of refractive index of the surrounding medium for gold nanoparticles of different shapes (image taken from ref. 278).

3.7.1 Mie theory

Mie theory provides an exact solution to scattering of electromagnetic waves by particles. Mie theory has been described in detail in reference 279. To intuitively understand the behaviour of small spheres let us look at the first few terms in the expansion of extinction, absorption and scattering efficiencies of these small spheres.

By retaining only those terms with order x^4, we obtain the following expressions for extinction, scattering and absorption efficiencies. Here x (size parameter) = $ka = 2\pi Na/\lambda$, m is the relative refractive index, k and k_1 are the wave vectors in medium and inside the sphere, N and N_1 are the

refractive indices in the medium and inside the sphere and *a* is the radius of the sphere. Scattering efficiency (Q_{sca}), absorption efficiency (Q_{abs}) and extinction efficiency (Q_{ext}) are given as follows.

$$Q_{ext} = 4xIm\left\{\frac{m^2-1}{m^2+1}\left[1+\frac{x^2}{15}\left(\frac{m^2-1}{m^2+2}\right)\frac{m^4+27m^2+38}{2m^2+3}\right]\right\} + \frac{8}{3}\,x^4 Re\left\{\left(\frac{m^2-1}{m^2+2}\right)^2\right\} \; where\; m = \frac{k_1}{k} = \frac{N_1}{N} \quad (3.1)$$

$$Q_{sca} = \frac{8}{3}\,x^4\left|\frac{m^2-1}{m^2+2}\right|^2 \quad (3.2)$$

$$Q_{abs} = 4xIm\left\{\frac{m^2-1}{m^2+2}\right\}\left[1+\frac{4x^3}{3}Im\left\{\frac{m^2-1}{m^2+2}\right\}\right] \quad (3.3)$$

For extremely small spheres absorption cross section can be written as

$$Q_{abs} = 4xIm\left\{\frac{m^2-1}{m^2+2}\right\} \quad (3.4)$$

If $(m^2-1)/(m^2+2)$ is not a function of wavelength, the

$$Q_{abs} \propto \frac{1}{\lambda}\;,\; Q_{sca} \propto \frac{1}{\lambda^4},$$

$$Q_{abs} \propto a,\quad Q_{sca} \propto a^4 \quad (3.5)$$

Thus, extinction spectrum will vary as $1/\lambda$ if absorption is the main contributing factor towards extinction. On the other hand, if scattering is the major contributor, then extinction varies weakly with wavelength. Further, absorption is proportional to the radius of the sphere whereas

scattering is proportional to the fourth power of the radius. That is why absorption dominates over scattering for small colloids whereas scattering is dominant for bigger colloidal particles.

3.7.2 Optical Constants

Optical properties of a material are usually described by either refractive indices or dielectric functions [279]. Refractive index of a material $N = n + ik$ is related to dielectric function $\epsilon = \epsilon' + i\epsilon''$.

$$\epsilon' = \frac{\varepsilon'}{\varepsilon_0} = n^2 - k^2 ,$$

$$\epsilon'' = \frac{\varepsilon''}{\varepsilon_0} = 2nk,$$

$$n = \sqrt{\frac{\sqrt{\epsilon'^2 + \epsilon''^2} + \epsilon'}{2}},$$

$$k = \sqrt{\frac{\sqrt{\epsilon'^2 + \epsilon''^2} - \epsilon''}{2}} \qquad (3.6)$$

To find the optical constants we use Lorentz model in which electrons and ions are treated as simple harmonic oscillators. The driving force is provided by the applied electromagnetic fields. The equation of motion of such a system is

$$m\ddot{\vec{x}} + b\dot{\vec{x}} + K\vec{x} = e\vec{E} \qquad (3.7)$$

Where *m* is the mass of the oscillator, *e* is the charge of the oscillator, *E* is the applied field, b is the damping constant and *K* is the spring constant. This equation can be solved to give the dielectric function [279]

$$\epsilon = 1 + \frac{\omega_p^2}{\omega_o^2 - \omega^2 - i\gamma\omega} \qquad (3.8)$$

where $\gamma = b/m$, ω is the frequency of the applied field, $\omega_0^2 = K/m$ and ω_p^2 is the bulk plasmon frequency which is given as, $\omega_p^2 = \mathcal{N}e^2/m\varepsilon_o$, where *N* is the number of oscillators per unit volume. In metals, plasmon resonance is due to the collective oscillations of free electrons. In the classical model the nanoparticle can be considered as a network of periodic, immobile positive ions, where conduction electrons are free to move against those immobile ions. If at any instant electrons are not at equilibrium, this results in an electric field due to uneven distribution of charges. The system wants to return to equilibrium. However, the electrons overshoot the equilibrium position due to the momentum acquired from the field. This results in an oscillation. The free electron response can be calculated from Lorentz model by setting spring constant *K = 0*. In that case dielectric function is given as

$$\epsilon = 1 - \frac{\omega_p^2}{\omega^2 + i\gamma\omega}$$

$$\epsilon' = 1 - \frac{\omega_p^2}{\omega^2 + \gamma^2}$$

$$\epsilon'' = \frac{\omega_p^2\gamma}{\omega(\omega^2 + \gamma^2)} \qquad (3.9)$$

This is the Drude model for the optical properties of free electron metal. In this case, plasmon frequency is given as $\omega_p^2 = \mathcal{N}e^2/m\varepsilon_o$, where $\mathcal{N}$ is the density of free electrons, e and m are the

charge and effective mass of the free electrons. The damping is due to electron collisions and electro-phonon scattering. The above results for free and bound electrons can be combined to give the optical properties of the system.

$$\epsilon = 1 - \frac{\omega_{pe}^2}{\omega^2 + i\gamma_e\omega} + \sum_j \frac{\omega_{pj}^2}{\omega_j^2 - \omega^2 - i\gamma_j\omega} \qquad (3.10)$$

Where subscript *j* refers to the jth type of oscillator whereas subscript *e* refers to free electrons.

3.7.3 Surface Modes in Small Spheres

If we only consider the first term in the expansion of electric field (E_1) inside the sphere, $E_{1r} \propto r^{n-1}$ for $(x, |m|x \ll 1)$. The field increases with r and attains the maximum value at the r = a, i.e. at the surface of the sphere. As the normal mode (*n*) increases, the field is localized more near the surface of the spheres. Therefore, these modes are referred to as surface modes. If we consider vanishingly small spheres, i.e., $x \to 0$, then the condition for the scattering coefficients a_n to dominate is

$$m^2 = -\frac{n+1}{n}, \qquad n = 1,2 \ldots\ldots \qquad (3.11)$$

For b_n, there is no solution in this limit. For extremely small spheres, a_1 will be the dominant coefficient. Then, for mode for $n = 1$, the condition 3.11 is

$$m^2 = -2 \qquad (3.12)$$

The complex dielectric functions of the sphere are then related to the dielectric functions of the medium by

$$\epsilon = -2\epsilon_m,$$

$$\epsilon' = -2\epsilon_m, \qquad (3.13)$$

$$\epsilon'' = 0$$

The frequency at which the above conditions are met is referred to as Fröhlich frequency and the corresponding mode is called Fröhlich mode. The absorption efficiency is given as

$$Q_{abs} = 4xIm\left\{\frac{\epsilon - \epsilon_m}{\epsilon + 2\epsilon_m}\right\} \qquad (3.14)$$

The condition mentioned above is valid only for infinitesimally small *x*. If we consider more terms in the series expansion, then the dielectric function is given as

$$\epsilon = -\left(2 + \frac{12}{5}\, x^2\right)\epsilon_m \qquad (3.15)$$

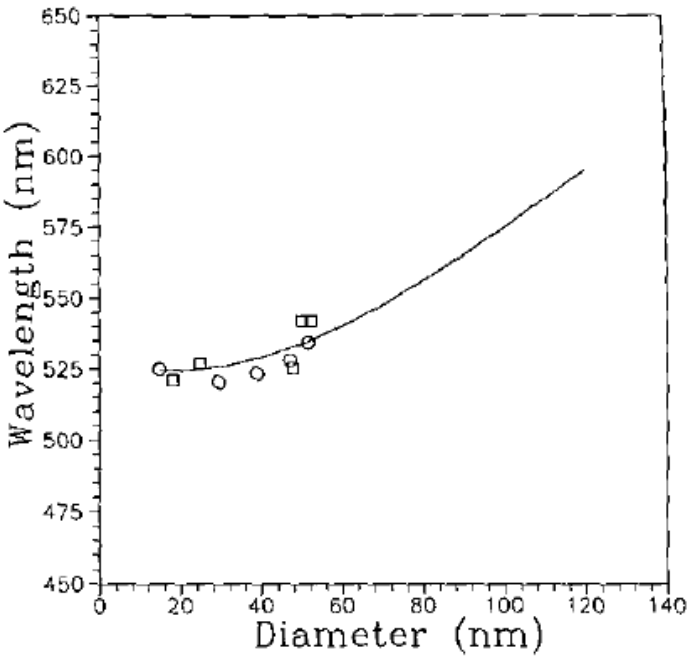

Figure 3.13 Shift in the plasmon resonance peak to longer wavelengths with increase in the size of the gold nanospheres based on Mie theory (solid line) and experimental data (symbols). (Image taken from ref. 266)

If ϵ' increases with frequency, then an increase in the size of the sphere ($x = 2\pi a/\lambda$) shifts the Fröhlich frequency to smaller values. Thus, resonance condition is met at lower frequencies or longer wavelengths (as shown in figure 3.13).

For coated spheres the condition for Fröhlich mode is given as [279]

$$\epsilon_1 = -2\epsilon_2 \left[\frac{\epsilon_2(1-f) + (2+f)}{\epsilon_2(2f+1) + 2(1-f)} \right] \quad (3.16)$$

Here ϵ_1 and ϵ_2 are the dielectric functions of the sphere core and the coating respectively and f is the fraction of volume occupied by the coating.

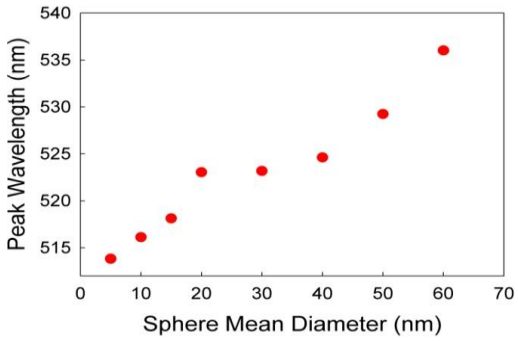

Figure 3.14 Position of the plasmon peak vs. diameter of gold nanospheres.

If the size of the particle becomes smaller than the mean free path of the electrons in the bulk matter, then condition 3.15 does not hold any longer (figure 3.14). In that case the mean free path of conduction electrons can be influenced by collisions with particle boundary. The dielectric function of the metal can be decomposed into two parts - one due to bound and the other due to free electrons. Only the free electron term is affected by the mean free path limitation. In case of free electrons, damping constant, inverse of the collision time (τ), increases due to collisions with the boundary of the particle.

$$\gamma = \gamma_{bulk} + \frac{v_f}{L} \quad (3.102)$$

Where γ_{bulk} is the bulk metal damping constant, v_f is the Fermi velocity and L is the effective mean free path for collisions with the boundary. For spheres L = 4a/3 was suggested by Kreibig [280]. Real part of the dielectric is not affected much by the mean free path limitation but the imaginary part of the dielectric function increases. It lowers the peak height and broadens the peak resonance.

Chapter 4

Protein Adsorption on Gold Nanoparticles: Influence of Gold Nanoparticle Size on the Optical Properties and Binding Activity of Immunoglobulin G, Staphylococcal Protein A and Streptavidin

4.1 Introduction

Nanoparticles are being increasingly used in varying fields such as medical diagnostics and biosensors, drug delivery, cosmetic products and cancer therapy [281-284]. In addition, the use of nanoparticles in non-medical applications (car wax, sunscreens, textiles etc.) increases the accidental exposure of humans to nanoparticles. These situations result in an need to characterize the interactions of nanoparticles with biological molecules. This is especially true for protein/nanoparticle combinations which have similar characteristic length scales. Today, nanoparticles of various chemical composition, sizes and shapes can be generated [285], and all of these properties have a strong influence on the structure and function of the absorbed protein. To successfully employ nanoparticle-based biosensors it is important that biomolecules such as proteins adsorbed on the nanoparticles retain their biological activity. Although several studies have focused on protein adsorption on nanoparticles [286-288], a detailed understanding of the actual state of the adsorbed protein or about the functional consequences of protein adsorption to nanoparticles still eludes us. Detailed studies are required to understand the effects of adsorption on protein structure, to determine orientation and to study the effect of orientation on protein activity. Such studies would not only help us in characterizing the protein nanoparticle system but also help in designing biosensors based on nanoparticles.

The study of the behavior of proteins on interfaces is the science that underpins the entire field of biomaterials, and has been a subject of fascination for the past century [289]. Adsorption of proteins on surfaces can lead to changes in the structure and hence biological activity of the adsorbed protein [290]. Changes in protein conformation due to adsorption depend on both the nature of the substrate and the protein [120, 225, 291, 292] (For details see chapter 2). In the case of protein adsorption onto nanoparticles an additional factor, i.e., the boundary of nanoparticles comes into play. The effect of the local curvature and the resulting steric effects on protein adsorption are not well understood. When the size of nanoparticles becomes comparable to the dimensions of the proteins it seems reasonable that this can affect (and perhaps dominate) the possible binding mechanisms through steric hindrance and hence influence their functionality. The effect of curvature on the structure and stability of adsorbed proteins is not properly understood. Some studies have shown that small globular proteins like BSA are increasingly destabilized by the curvature of nanoparticles with smaller nanoparticles inducing more destabilization [253, 254]. Other studies show that curvature of nanoparticles actually stabilizes the adsorbed protein as compared to protein adsorbed on flat or pseudo flat surfaces or even protein in solution [224, 256, 258, 260]. The degree of stabilization/destabilization of proteins by the size of nanoparticles further depends on the size, shape, orientation and nature of protein [259]. Therefore, the effect of nanoparticles curvature on the structure/function of protein cannot be generalized as results for one protein differ from those of other proteins. This is the first in vitro study to probe the effect of size on the binding activity of adsorbed immunoglobulin G (IgG), Staphylococcal protein A (Protein A) or Streptavidin on gold nanoparticles.

In this chapter the study on the optical extinction measurements of gold nanoparticles to probe the LSPR of the nanoparticle-protein systems is discussed. These extinction measurements

were made to determine the size dependent change in the binding activity of model proteins – IgG, Protein A and Streptavidin. Streptavidin is smaller in comparison to both Protein A and IgG. Further, all the proteins under study have different shapes. Protein A is a rod-shaped molecule whereas IgG is a Y-shaped molecule. On the other hand Streptavidin can be approximated as an elliptical molecule. Binding activity for Protein A and IgG was probed on gold nanoparticles in the size range 5-60 nm. This size range was chosen so that the diameter of the gold nanoparticles becomes comparable to the dimensions of the proteins. Specifically, 5-10 nm spheres have diameters smaller than the length scales of proteins under study. Spheres sized 15-20 nm have length scales comparable to those of IgG and Protein A, whereas spheres with diameter > 30nm are bigger than the proteins under study. Adsorption of Streptavidin was probed on gold nanoparticles with diameters ranging from 5 to 30 nm. Streptavidin did not form stable conjugates with gold nanoparticles in the size range 40 to 60 nm. The results indicate that IgG and Protein A adopt different orientations on bigger spheres (≥ 30nm) as compared to smaller nanoparticles. Interestingly, although optical properties of both the adsorbed proteins depend on the size of the nanoparticle, their binding activities are not similarly affected by the size of the gold nanosphere. The binding activity of Streptavidin was not affected by the size of the gold nanoparticles.

4.1.1 Experimental Details

Details regarding protein samples and unconjugated gold and silver nanoparticles are given in chapter 3. The concentrations and extinction coefficients of gold nanoparticles are given in table 4.1. Aqueous solutions of silver nanoparticles of sizes 20 and 40 nm had concentrations of 7 x 10^{10} and 9 x 10^{9} particles/ml.

Gold nanoparticle diameter (nm)	Concentration (particles/ml)	Extinction coefficient ($M^{-1}cm^{-1}$)
5	$5x10^{13}$	9.696×10^{6}
10	$5.7x10^{12}$	9.550×10^{7}
15	$1.4x10^{12}$	3.640×10^{8}
20	$7x10^{11}$	9.406×10^{8}
30	$2 x10^{11}$	3.583×10^{9}
40	$9x10^{10}$	9.246×10^{9}
50	$4.5x10^{10}$	1.935×10^{10}
60	$2.6 x10^{10}$	3.535×10^{10}

Table 4.1 Concentrations and extinction coefficients of gold nanoparticles (taken from ref 293)

Since polyclonal rabbit IgG has various sub classes, it does not have a single isoelectric point. The isoelectric point of rabbit IgG is found in the range 6.0-8.0. Therefore the pH of aqueous IgG solution was adjusted to slightly above 8.0 using 0.2 M NaOH before conjugation. Only a few drops of NaOH were added so that the concentration of IgG solution did not change. After conjugation the spectra were recorded as described in chapter 3 (see figure 3.7). For binding studies the second protein solution was added to the conjugated gold nanospheres and allowed to sit for 30 minutes following procedure described in references 294 and 295. The spectra were recorded 30 minutes after addition of the second protein solution. The spectra were again recorded 24 hours later and no change was observed.

Localized surface Plasmon resonance of gold nanoparticles has been previously established as a technique with a capability to monitor protein binding events [249, 296]. Details of LSPR technique have been described in chapter 3. Briefly, it refers to the collective oscillations of the conduction electrons in metallic colloids. The position and magnitude of the LSPR spectrum

depends not only on the size, shape and composition of the nanoparticles but also on the dielectric properties of the immediate surroundings of the nanoparticles. For bare particles, resonance depends on the optical properties of the medium. For coated particles it depends on the thickness and refractive index of the coating and the refractive index of the surrounding medium. Adsorption of protein onto the nanoparticles causes a shift in the peak position due to the change in the optical properties of the surrounding environment. Binding of ligands in solution with these surface adsorbed proteins results in additional changes in dielectric properties of the surrounding environment of metallic nanospheres. The changes in local environment due to molecular binding events can be followed by monitoring the small shifts in the peak position of the LSPR spectrum.

Surface Plasmon based techniques require no extrinsic labeling such as radioactive labeling or fluorescent dye. Another advantage of this technique is that only the protein attached to the nanoparticles is sensed. Unadsorbed protein (i.e. protein present in the bulk solution) has no effect on the LSPR of gold nanoparticles even when the concentration of the free protein is orders of magnitude greater than that of the adsorbed protein. In addition, the actual optical extinction measurements are straightforward to perform and do not require an elaborate set-up.

4.1.2 Data Analysis

The experimental spectra were automatically smoothed using a local negative exponential smoothing technique with second degree polynomial regression. The spectra were then normalized and differentiated. Comparison between differential of raw and smoothed data is shown in fig. 4.1. To find the extinction peak the numerical derivative was fitted to a linear

function to find zero crossing (shown in fig.4.2 for bare and coated 15 nm gold spheres). With this procedure the extinction peak position can be determined with an accuracy of 0.2 nm.

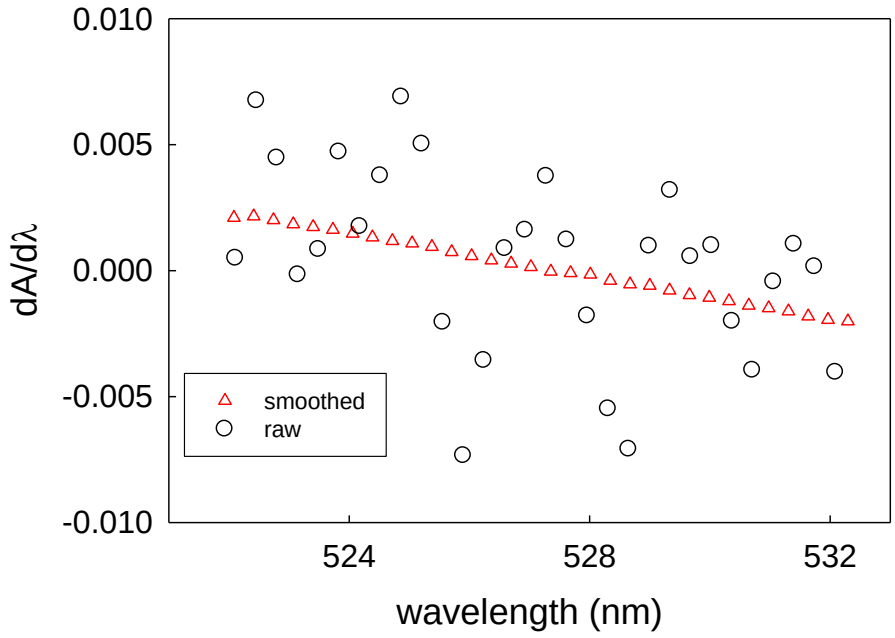

Figure 4.1 Comparison between differential of raw (circles) and smoothed data (triangles)

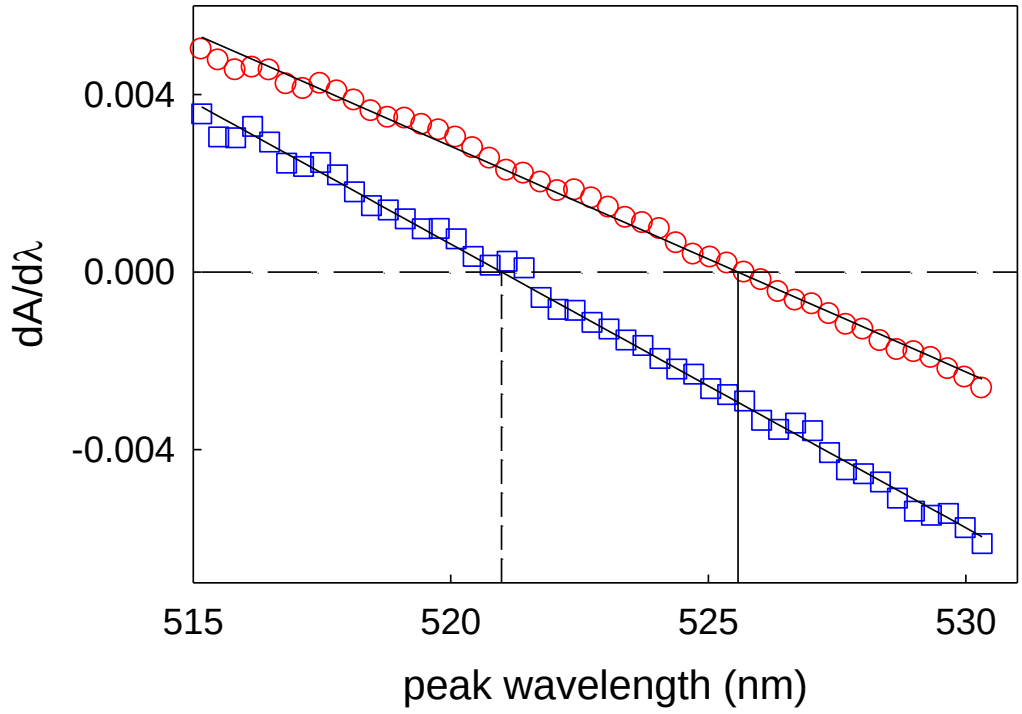

Figure 4.2. Numerical derivative (slope) of the extinction spectrum for bare (squares) and coated (circles) 15 nm gold spheres vs. wavelength. Lines show the linear fitting of the actual points of the slope to find the point of zero crossing.

Within the context of an approximation that protein adsorbed on the spheres forms a uniform and isotropic coating, we can theoretically calculate the extinction spectrum of the conjugated nanoparticles using Mie Theory as described in chapter 3. Using the routines described in reference 253, extinction spectra are generated for each sphere size over a range of refractive indices and coating thicknesses. We can then determine peak wavelength (λ_o) and the maximum extinction (ε_o) for each of the calculated extinction spectra. Using these values we can generate contour plots for peak wavelength (λ_o) and peak extinction (ε_o) value as a function of coating thickness and refractive index (as shown in figure 4.3 for 30 nm spheres). Using these contour

plots we can correlate the experimentally measured values of peak wavelength and peak extinction to the values of coating layer thickness (*h*) and refractive index (*n*) required to produce a theoretical spectrum with the same λ_o and ε_o within the spherical shell model of a protein. While we do not necessarily expect the number generated within the context of this simple model to be quantitatively precise, changes in the number, or comparisons between different nanosphere sizes, should be indicative of changes in the real physical system.

The amount of protein adsorbed per unit area of the spheres (Γ) can be determined from the thickness and the refractive index of the adsorbed protein layer and is given by [182].

$$\Gamma = \frac{d(n_p - n_s)}{(\frac{dn}{dc})} \qquad (4.1)$$

where d is average layer thickness, n_p is the refractive index of the protein layer, n_s is the refractive index of the buffer solution and (dn/dc) is the refractive index increment (specific refractivity) of the adsorbed protein layer. Specific refractivity (dn/dc) is equal to 0.212 cm^3/g for streptavidin [297] and 0.188 cm^3/g for Protein A and IgG [120].

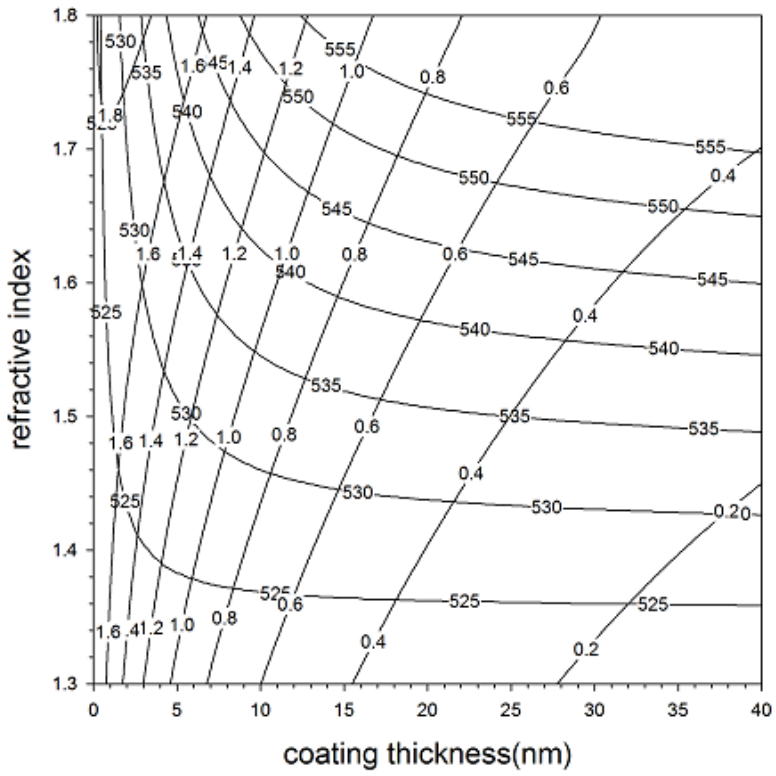

Figure 4.3 Contour plots showing the results of Mie scattering calculations for uniformly coated 30 nm gold nanospheres. Position and extinction efficiency of Plasmon peak is plotted against refractive index and thickness of the adsorbed protein layer.

4.2 Adsorption Studies

4.2.1 Introduction to Proteins - Protein A, IgG, and Streptavidin

IgG and Protein A have a strong mutual binding affinity. Protein A molecules are used for purification [298] and immobilization [299] of antibodies. Immunoglobulin's conjugated nanoparticles are used for biosensing [300] and drug delivery [301, 302]. Protein A is a 42 kDa protein built of a single polypeptide chain. Protein A has five homologous IgG binding units (E, D, A, B and C). Each domain contains 56-61 amino acid residues and is capable of binding to Fc

domain of IgG. The C-terminal region is referred to as part X and is responsible for attachment to the cell wall. It has a very elongated shape and does not bind to IgG [303, 304, 305]. The length of entire Protein A molecule is expected to be 20-30 nm [307]. Schematic of protein A molecule is shown in figure 4.4.

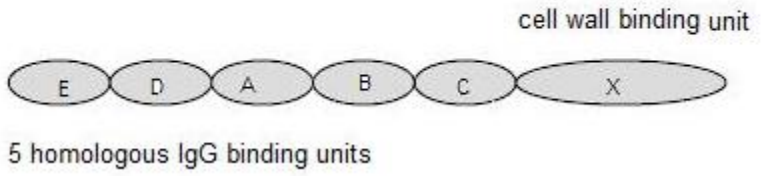

Figure 4.4 Schematic diagram of Protein A showing 5 IgG binding domains - E, D, A, B, C and the cell wall binding domain X.

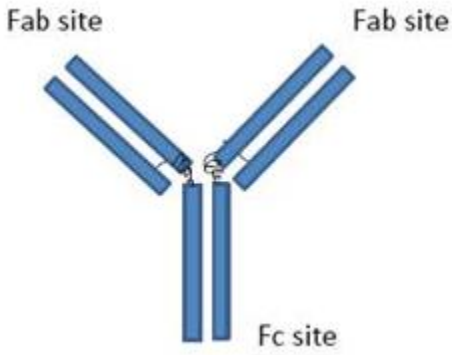

Figure 4.5 Schematic diagram of Immunoglobulin G showing binding sites for Protein A (Fc binding sites) and Anti-IgG (Fab binding sites).

IgG antibody is a large Y shaped molecule of about 150 kD. Schematic diagram of IgG is shown in figure 4.5. Each IgG molecule is composed of 4 peptide chains - 2 heavy chains of 50 kD each and 2 light chains of 25 kD each. Heavy chains are linked to each other by disulfide bonds (black curvy lines in fig. 4.5). The light chains are also attached to the heavy chains through disulfide linkages. Functionally, IgG consists of three domains: 2 Fab domains, each of

which contains an antigen binding site and an Fc region, responsible for binding to cells. Its dimensions are 7.0 nm x 6.3nm x 3.1 nm for Fab and 8.2 nm x 5.0 nm x 3.8 nm for Fc part [307].

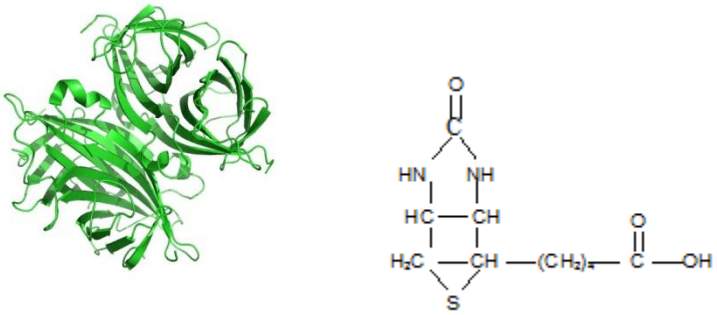

Figure 4.6 On the left Streptavidin tetramer (Figure taken from reference 308) and on the right biotin.

Streptavidin is 60 kD homo-tetrameric protein purified from bacterium *Streptomyces avidinii*. Streptavidin is composed of 159 residues per chain and has an isoelectric point of ~ 5. The dimensions of Streptavidin are 4.5 nm x 4.5 nm x 5.0 nm [297]. All four monomers are identical with a molecular weight of nearly 15 kD. Each monomer has a beta barrel structure containing eight beta strands arranged in anti-parallel fashion (fig. 4.6). To probe the functionality of adsorbed Streptavidin, its binding to vitamin biotin was utilized. 5-[(3a*S*,4*S*,6a*R*)-2-oxohexahydro-1*H*-thieno[3,4-*d*]imidazol-4-yl]pentanoic acid, commonly referred to as biotin or vitamin H or Vitamin B_{12} is a water soluble vitamin. Biotin consists of uriedo (tetrahydroimidizalone) ring fused with a tetrahydrothiophene ring. The molecular dimensions of biotin are 0.53 nm x 1.0 nm x 2.1 nm [309]. Biotin helps in metabolism and transportation of carbon dioxide. It also regulates blood sugar levels. Biotin- Streptavidin system was chosen because Biotin-Streptavidin linkage is the strongest non-covalent interaction with dissociation constant of the order of 10^{-14} mol/L [310]. Due to their high binding affinity and

easy availability Streptavidin and biotin are used in various biochemical assays, affinity chromatography, and as linkers for attachment of DNA, proteins, and other ligands [311 – 315]. Each of the four subunits of Streptavidin binds biotin with equally high affinity. The biotin binding site is located in the interior of each monomer (shown in figure 4.7). Each monomer binds to biotin with same binding affinity.

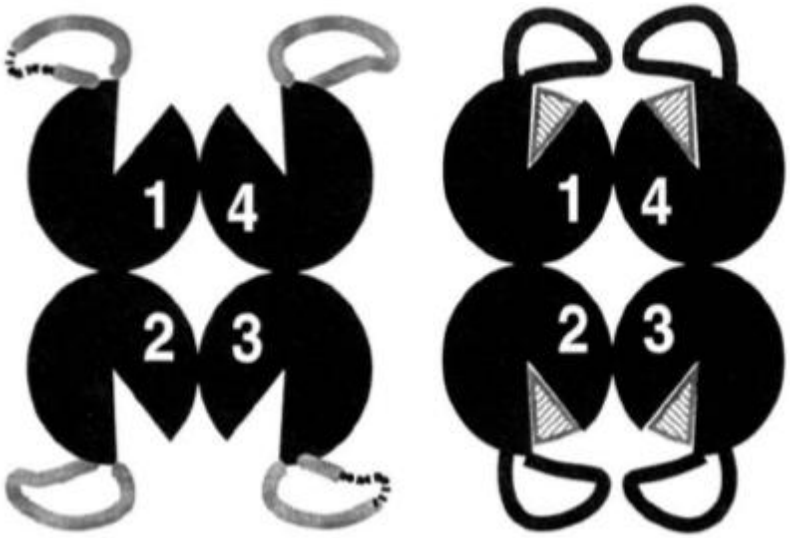

Figure 4.7 Schematic of streptavidin molecule in the unbound (left) and bound state (right) and the resulting ordering of the surface loops (Figure adapted from ref. 316)

This is first study to probe the effect of the size of the nanoparticle on the binding activity of adsorbed Streptavidin. Lea and Gross [317] used electron microscopy to study thickness of the adsorbed IgG and Protein A layers on gold nanoparticles with diameters ranging from 8 nm to 40 nm. To image protein conjugated gold nanoparticles with electron microscope, the samples had to be dried. In the present study we not only calculate the optical properties (effective layer

thickness and refractive index) of the adsorbed protein layers but also study their binding activities by looking at changes in the LSPR peak position upon exposure to other proteins. These studies are conducted over a wide range of gold nanoparticles size (5-60 nm) in aqueous solution to exclude drying effects.

4.2.2 Adsorption of IgG onto Gold Nanoparticles

The peak wavelength values for both bare and IgG coated gold nanospheres are shown in figure 4.8. The position of the Plasmon resonance peak of gold nanospheres in the size range 10-60 nm lies in the red region of the visible spectrum. The position of the Plasmon peak varies from 516 nm for 10 nm gold nanoparticles to 534 nm for 60 nm gold nanospheres. A shift in the position of plasmon peak on addition of IgG molecules clearly indicates that IgG has adsorbed onto gold nanoparticles.

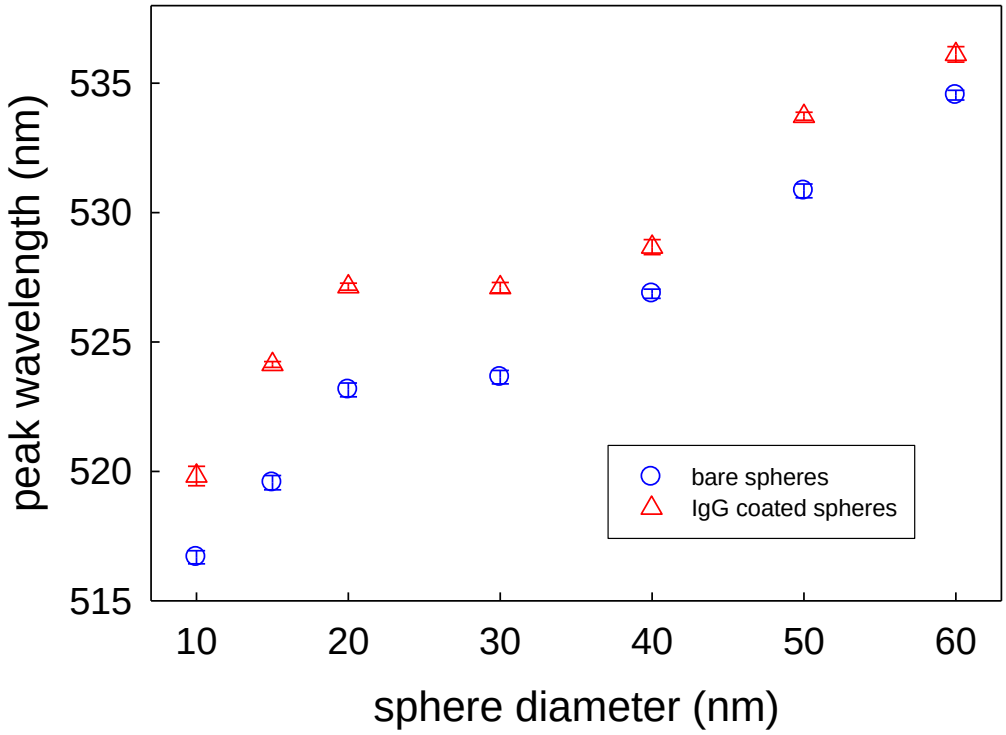

Figure 4.8 Plasmon peak position values for bare gold nanospheres (circles) and IgG coated gold nanospheres (triangles) vs. diameter of gold nanoparticles.

4.2.2.1 Optical Thickness and Refractive Index of Adsorbed IgG

Fig. 4.9 shows the optical thickness of the adsorbed IgG layer. The thickness of IgG coating layer varies with the size of the gold nanoparticle. The width of IgG layer on 10 nm gold nanospheres is 4 nm. Thickness of 4 nm roughly corresponds to the width of both Fab and Fc segments of IgG molecule. As the size of the gold sphere increases, the thickness of the adsorbed IgG layer also increases. The width of the layer varies from 13 to 17 nm on 30-60 nm spheres.

The calculated value of layer thickness on spheres with diameter ≥ 30 nm is roughly equal to the length of a single IgG molecule.

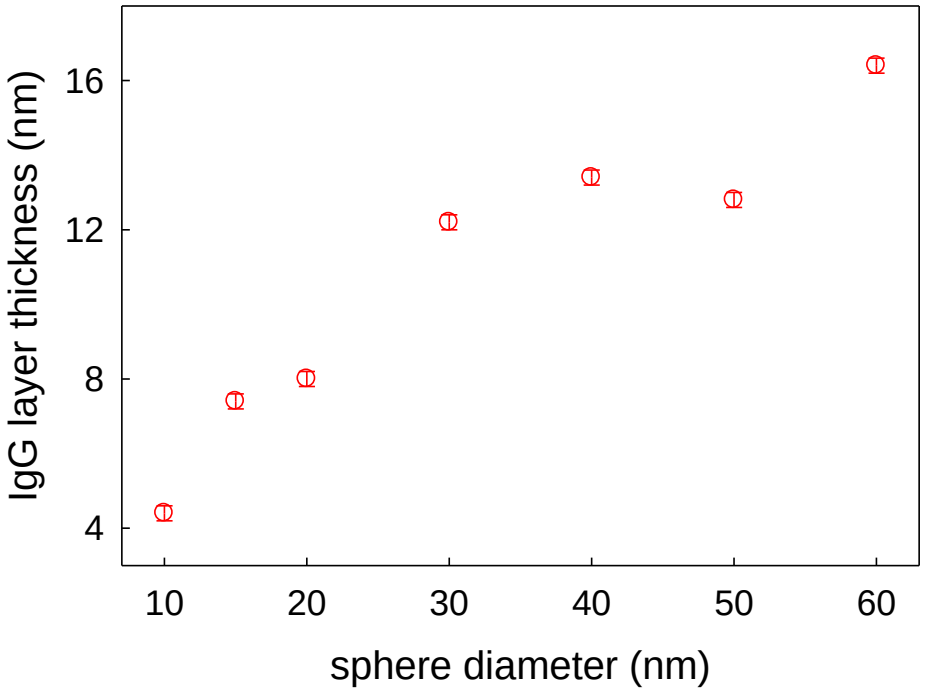

Figure 4.9 Optical thickness of adsorbed IgG layer as a function of diameter of gold nanoparticles

We also measured the thickness of the coating using AFM. For those measurements, first, bare 10 nm gold nanospheres were deposited on a silicon wafer and then imaged with AFM in tapping mode. Later, IgG coated 10 nm gold nanospheres were also deposited on a wafer and imaged. Average height of bare nanospheres was found to be 10 nm whereas the average height of IgG coated nanospheres came out to be 17 nm. This height is the sum of diameter of gold nanospheres and twice the width of coating. Thus, average width of IgG coating on 10 nm gold nanospheres is 3.5 nm. This result agrees reasonably with calculated value. It should be noted

that the protein thicknesses obtained using AFM are affected by drying of the protein layer, by the tip-sample interaction and also by water-protein interaction.

Calculated values of the effective refractive indices of IgG layer are plotted in figure 4.10. The refractive index of the adsorbed IgG layer also depends on the size of the nanoparticle.

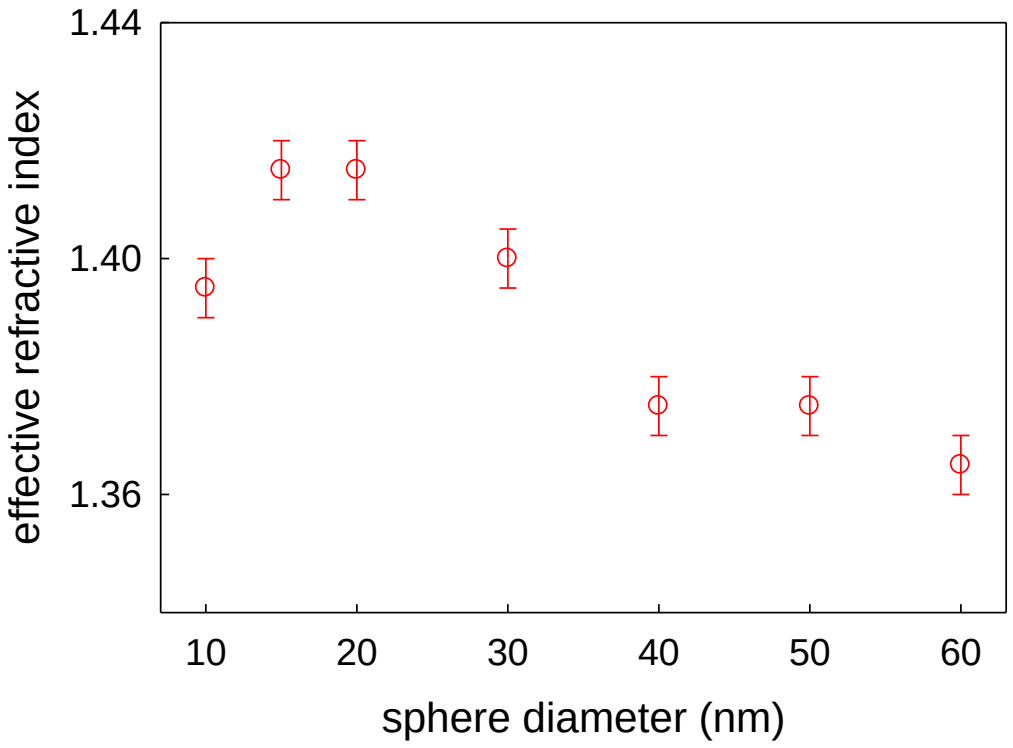

Figure 4.10 Apparent refractive indices of adsorbed IgG layer as a function of diameter of gold nanoparticles.

The apparent refractive index of the adsorbed protein layer increases from 1.39 on 10nm nanospheres to 1.42 on 15 nm nanospheres. For spheres with diameter ≥ 15 nm the refractive index of the adsorbed layer decreases as the size of the gold nanosphere increases. The apparent refractive indices of IgG layer on 40-60 nm spheres lie between 1.36-1.37. High value of refractive index on 15 nm spheres could be due to the high packing density of adsorbed IgG

layer on these spheres (see figure4.11). For sphere sizes between 40 and 60 nm there is relatively small change in the refractive index value. Smaller layer thickness and higher refractive index values on spheres with diameter < 20 nm indicate that the structure of adsorbed IgG layer is different from that of spheres with diameter > 20 nm. IgG absorbed on nanospheres with diameter ≥ 30 nm does not show any size dependence. It is interesting to compare the effective thickness (13-17 nm) and refractive indices (1.36-1.4) of adsorbed IgG layer on these sizes with those reported for flat surfaces. Malmsten reported values of ~18 nm and ~1.37 for thickness and refractive index, respectively, for IgG layers adsorbed onto flat methylated silica surfaces using ellipsometry [120]. Elwing and coworkers calculated the adsorbed IgG layer thickness and refractive index to be 17±5 nm, 1.39±0.02 on flat hydrophobic surfaces [318]. This comparison suggests that in the case of spheres with diameter ≥ 30 nm the radius of curvature is large enough that the protein adopts the same configuration as it does on a flat surface. Further, the thickness of IgG layer adsorbed on spheres ≥ 30 nm is comparable with the length of a single IgG molecule (~15 nm). It is possible that IgG adopts an end-on orientation on these spheres. End–on adsorption of IgG has previously been observed by Morrissey and Han on polystyrene [176] and by Bagchi and Birnbaum on poly (vinyl toluene) colloidal particles [319]. As compared to these big spheres (≥ 30 nm), calculated value of layer thickness 10nm sized spheres is only 4 nm. One possible scenario would be that IgG adopts side-on orientation on 10 nm spheres.

4.2.2.2 Calculations for Adsorbed Amount of IgG per Unit Area

Figure 4.11 shows the amount of IgG adsorbed per unit area on gold nanospheres of sizes 10-60 nm. Packing density of the adsorbed layer varies with the size of the nanoparticle. Specifically, coverage of adsorbed IgG layer increases from 1.52 mg/m^2 on 10 nm spheres to a maximum

value of 4.5 mg/m^2 on 30 nm spheres. 40 nm spheres actually have a lower surface coverage (2.8 mg/m^2) than 30 nm spheres. Further increase in the sphere size (50-60nm) does not result in changes in the adsorbed amount per unit area. Teichroeb and coworkers found a similar change in surface coverage of adsorbed BSA as a function of the size of the nanoparticles in their study on denaturation kinetics of BSA [254].

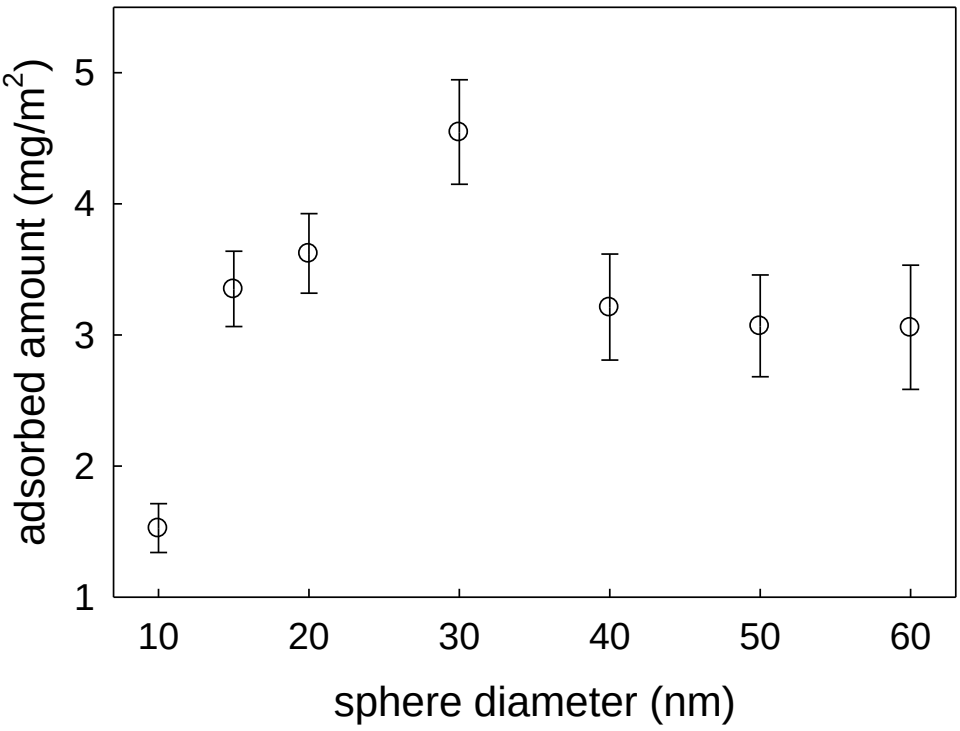

Figure 4.11 Amount of IgG adsorbed per unit area on gold nanospheres calculated using equation 4.1 vs. diameter of gold nanoparticle

A side-on monolayer packing of IgG would lead to coverage of 2.0 mg/m^2 whereas an end on adsorption would lead to coverage between 2.6 mg/m^2 and 5.5 mg/m^2 depending on the repulsion between the Fab arms [306]. The small amount of IgG adsorbed on 10 nm spheres might imply that close packed monolayer coverage is not realized for these small sized spheres. Due to their

compact three dimensional tertiary structures, protein molecules are not flexible like linear polymers. Therefore, it is possible that higher curvature of smaller nanoparticles constraint the way proteins pack onto these small structures. Hence, there might be relatively large areas on these small nanospheres with no protein coverage [320]. Amount of protein adsorbed per unit area for all sphere sizes ≥ 15nm is greater than 2.0 mg/m^2, i.e., it exceeds the amount per unit area for side-on monolayer coverage. Coating thickness values of 13 to 15 nm and adsorbed amounts between 2.7 and 4.5 mg/m^2 on spheres of diameter 30-60 nm agree with the end-on orientation of IgG on these spheres. Adsorbed IgG layer density of 3.5 and 3.9 mg/m^2 on 15 and 20 nm spheres, respectively, is greater than calculated layer density for side-on monolayer coverage. However, calculated coating thickness value of nearly 8 nm observed on these spheres does not agree with end-on orientation on these sizes. It could be possible that there is a transition from a side-on to a more end-on orientation on these sphere sizes (see figure 4.26) or both side-on and end-on orientations coexist on these spheres.

Further, we calculated the number of protein molecules attached to a single sphere by dividing the total adsorbed mass with the mass of a single protein molecule (figure 8). It is clearly evident from the figure that the number of attached IgG molecules does not increase linearly with the increase in the surface area of the sphere. The rate of increase of the number of attached molecules on spheres with diameter ≥ 30 nm is different from that of smaller nanoparticles (5-20 nm). This again shows that packing of IgG molecules on spheres > 30 nm proceeds in a different manner as compared to smaller spheres. This could be due to different orientations of IgG on these sphere sizes.

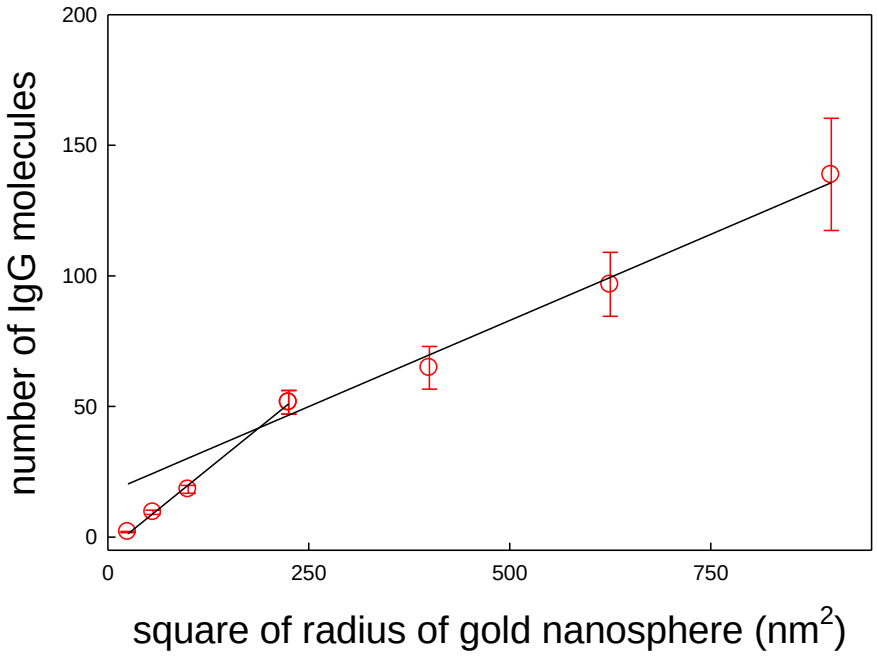

Figure 4.12 Number of IgG molecules attached to single gold nanosphere vs. square of the radius of the gold nanoparticle

4.2.2.4 Effect of Change in the Amount of IgG

We also probed if the thickness of adsorbed protein layer would depend upon the amount of protein added. These studies were conducted on 30 nm gold nanospheres. For these studies we added 10 ml, 100 ml and 150 ml of 1 mg/ml of IgG solution to 600 ml of gold nanosphere solution. We calculated the optical thickness values of the adsorbed IgG layer from the values of the position and extinction values of Plasmon peaks (shown in figure 4.13).

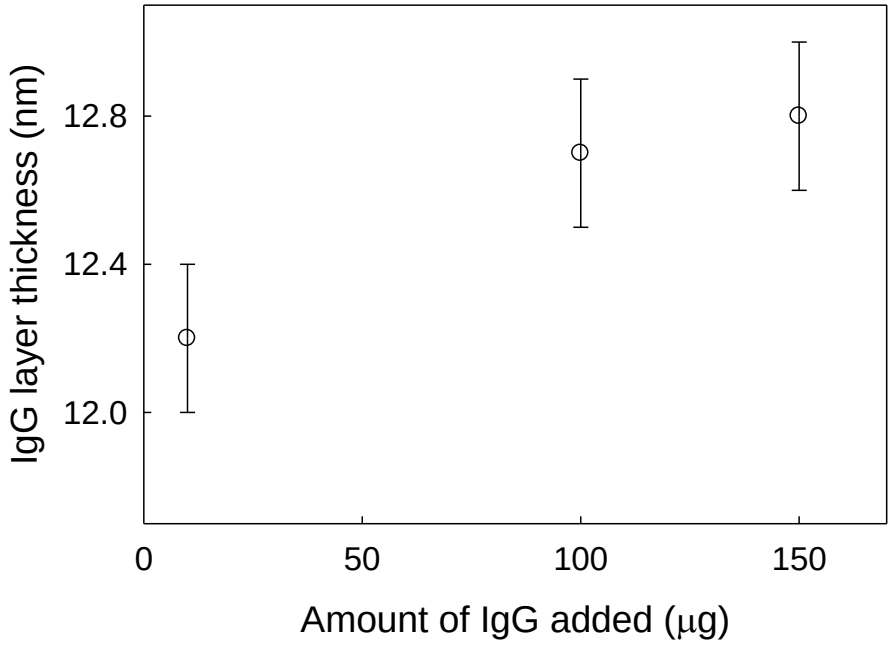

Figure 4.13 Optical thickness of adsorbed IgG on 30 nm spheres vs. the amount of IgG added to gold nanospheres.

There is little variation in the thickness of IgG layer. Even with a tenfold increase in the amount of IgG there is little increase in the coating thickness. Coating thickness values point towards end-on adsorption for different added amounts (10, 100 and 150 μg). The result is not surprising since even the smallest amount of added IgG (10 μg) exceeds the minimum amount of IgG required to stabilize the nanoparticles. Our results agree with the ellipsometric measurements of thickness of IgG layer adsorbed onto flat silicon surfaces [120]. In that study, it was also observed that thickness of the adsorbed IgG layer did not vary with bulk concentration.

4.2.3 Adsorption of Protein A on gold nanospheres

4.2.3.1 Optical Thickness and Refractive Index of Adsorbed Protein A

The results for effective coating thicknesses of Protein A layer adsorbed on gold nanospheres and modeled as above are shown in fig. 4.14. Just as is the case for IgG, the thickness of Protein A layer also depends upon the size of the nanoparticle. Calculated layer thickness value is the smallest (~ 2 nm) for 5 nm particles, the smallest sphere size under study. The width of the layer increases with size of the sphere to a maximum value of 20 nm on 60 nm spheres.

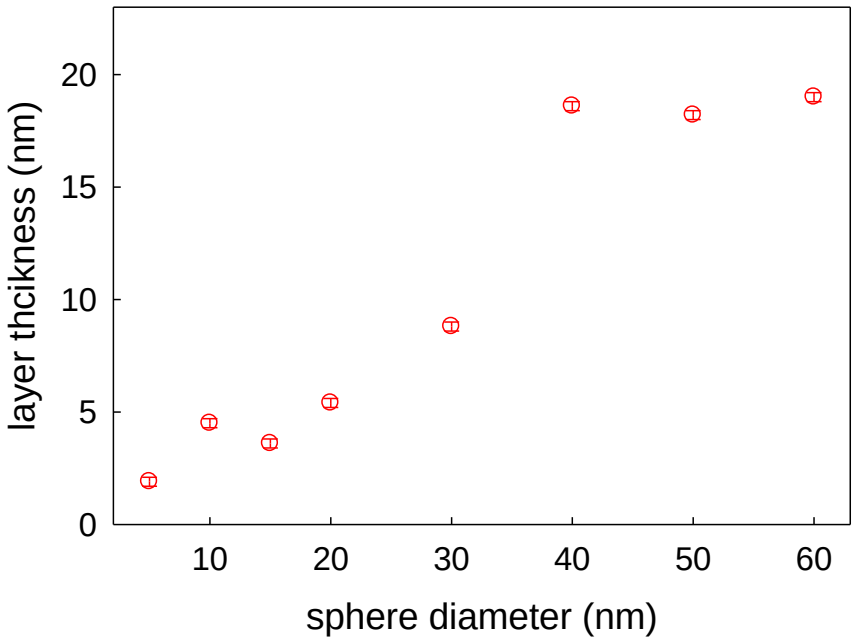

Figure 4.14 Optical thickness of Protein A layer vs. gold nanosphere diameter

The effective refractive index of the adsorbed layer also varies with the size of the spheres (see fig. 4.15). The refractive index of adsorbed Protein A layer varies from 1.48 to 1.36. In

general, the refractive index of the adsorbed Protein A layer decreases as the sphere size increases. Variation in the values of layer thickness and refractive indices as a function of sphere size could imply that the structure of the adsorbed protein layer varies with the size of the nanosphere. There is little variation in both layer thickness and refractive indices on spheres with diameters ≥ 40, i.e., there is no size dependence for these relatively big spheres. If we compare the observed layer thickness with the dimensions of Protein A molecule, thickness of 2 nm seen on 5 nm spheres is comparable to the width of a Protein A molecule whereas the width of 20 nm (on 60 nm spheres) is roughly equal to the length of Protein A molecule.

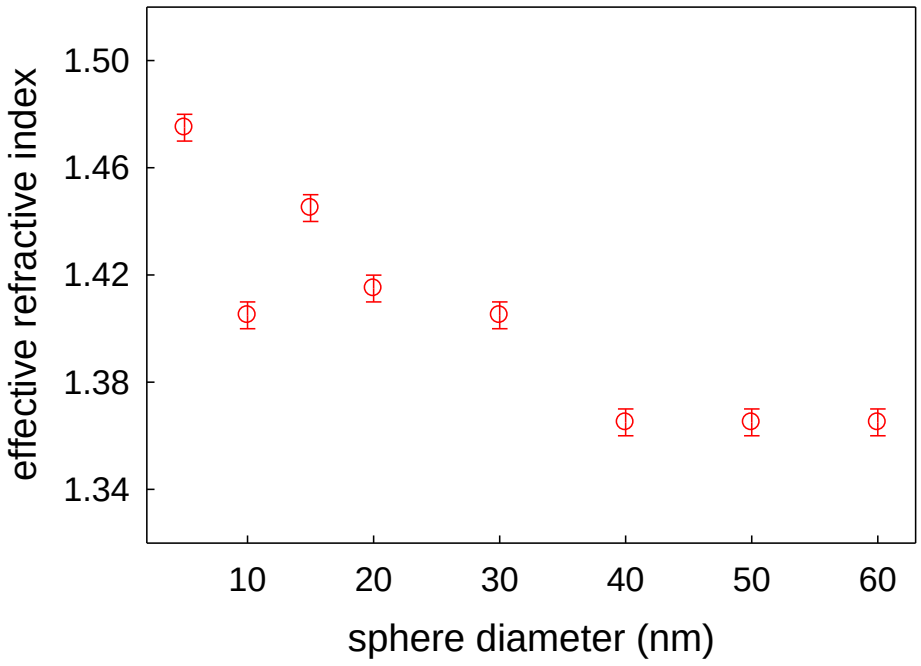

Figure 4.15 Apparent refractive indices of adsorbed Protein A layer vs. gold nanosphere diameter

Our results for layer thicknesses agree qualitatively with those of Lea and Gross [317] who used electron microscopy to monitor the width of Protein A and goat-anti rabbit IgG layers on gold nanoparticles of varying sizes (7-40 nm). These authors also observed that the thickness of the coating layer varied with the size of nanoparticles - the observed thickness of both Protein A and IgG varied from about 3nm to 8 nm depending on the size of the gold nanoparticle. In general, the thicknesses of protein layers reported by these authors are smaller than those found in this study. This is likely due to differences in the sample-preparation. Their method of ethanol dehydration - critical-point-drying for sample-preparation can cause shrinkage of samples, which may explain the smaller thickness values obtained in their study. The protein to gold ratio employed in their study also differs from the ratio in the current study. Protein concentration can affect the number of protein molecules binding to a gold nanosphere and hence the structure of the adsorbed layer [320]. Also, BSA and polyethylene glycol were used as stabilizing agents, which can further affect the adsorbed layer thickness.

4.2.3.2 Calculation for the Adsorbed Amount of Protein A per Unit Area

The packing density of Protein A also depends on the size of the gold nanoparticles. The amount of Protein A adsorbed per unit area increases from 1.5 mg/m^2 on 5 nm spheres to ~3 mg/m^2 on 30 nm spheres (data shown in figure 4.16). With further increase in the sphere size (40-50 nm) there is little variation in the packing density of adsorbed Protein A layer.

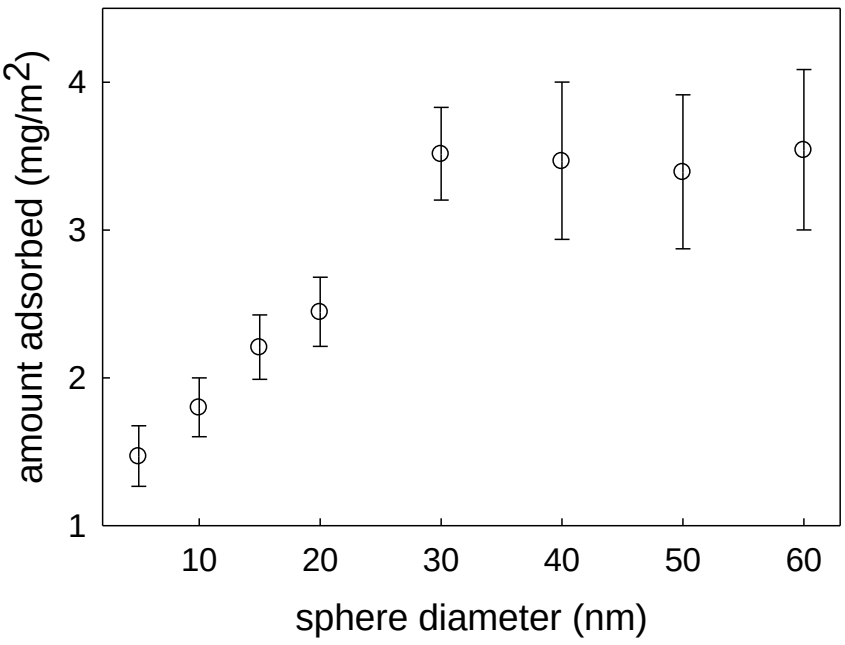

Figure 4.16 Amount of Protein A adsorbed per unit area vs. diameter of gold nanosphere

Packing of rod-shaped Protein A molecules is more efficient on nanoparticles with diameter ≥ 30 nm as compared to smaller nanoparticles. Higher curvature of smaller nanoparticles can restrict the way protein packs on it and hence result in lower packing density. The number of

Protein A molecules adsorbed on gold nanospheres is plotted in figure 4.17.

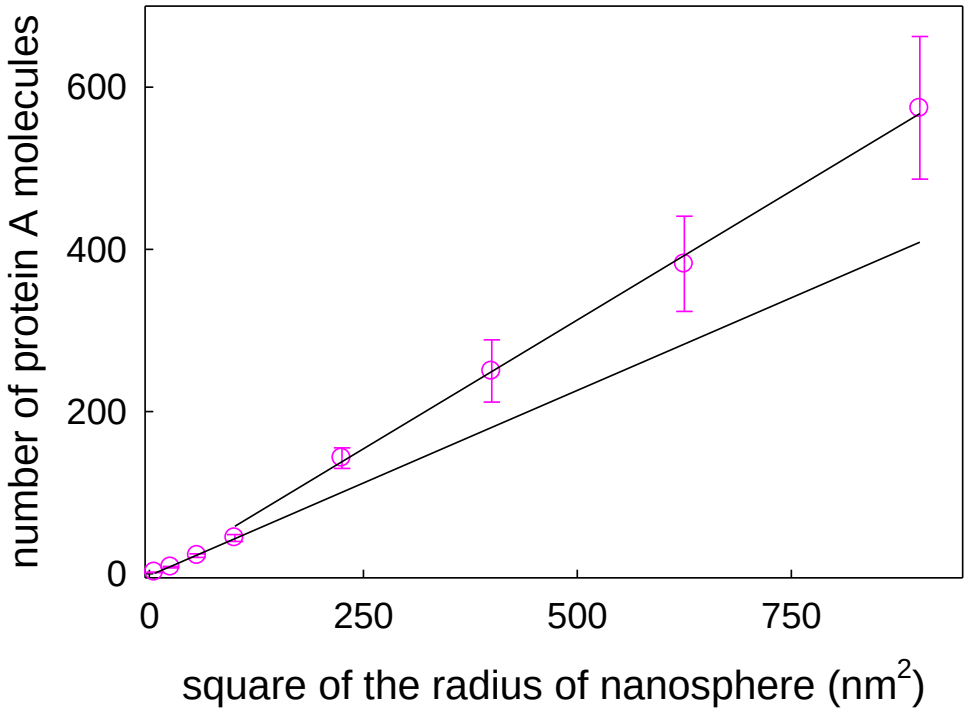

Figure 4.17 Number of Protein A molecules attached to a single nanosphere vs. square of the radius of the nanospheres

Just, as seen in the case of IgG conjugated gold nanoparticles, as the surface area of the nanospheres increases, more protein molecules are able to attach to the nanosphere. Again, the increase in the number of attached molecules is not linear with the increase in the surface area of the nanospheres. This could be possibly due to the different orientations adopted by Protein A molecules on bigger spheres (≥ 20 nm) as compared to smaller spheres. Interestingly, while in case of Protein A molecules, the transition occurs at 20 nm, for IgG coated nanospheres the change in the behaviour occurs at 30 nm. This could be due to the fact that these two proteins

have different sizes and shapes and hence their packing would be different on a nanosphere of same size.

Protein A is a rod shaped protein, ~2 nm in diameter and ~25 nm long. A layer thickness value of 20 nm on 60 nm spheres suggests an end-on orientation whereas a 2 nm thick protein layer on 5 nm spheres could imply a side-on orientation on these spheres. Calculated packing density of Protein A molecules on 5 nm spheres (2.1 x 10^{12} molecules/ cm^2) agrees well with the packing density of a closed packed side-on monolayer of Protein A molecules (2 x 10^{12} molecules/ cm^2) calculated by Onishi and coworkers from the dimensions of Protein A molecule [305].

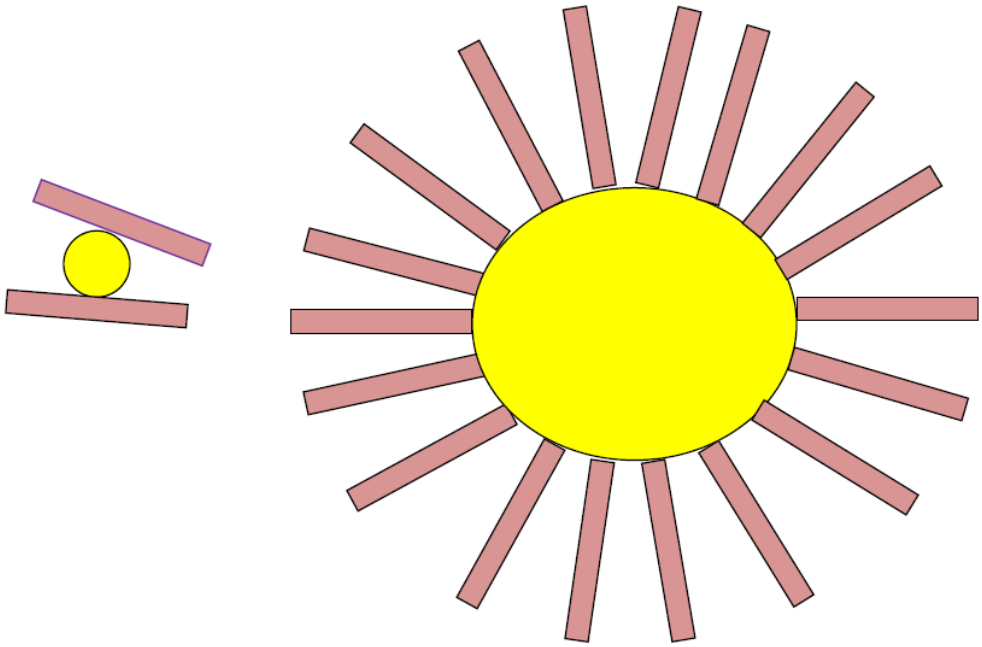

Figure 4.18 Possible orientations adopted by Protein A (pink rods) on 5 nm (left) gold nanoparticle (yellow circles) and 60 nm gold nanoparticle (right).

If rod shaped protein molecules were to adopt an end–on orientation on smaller spheres, the protein-protein interactions would be small as the protein backbones would be separated by a larger distance due to the curvature of the spheres. Also, there are relatively few molecules attached to small spheres. Hence, based on the observed layer thickness values, it can be speculated that Protein A adopts a side-on configuration on small spheres to maximize the protein-surface interactions. As the sphere size increases, a part of Protein A molecule might be attached to the spheres with their free ends suspended in the solution. On bigger spheres, with the radius of curvature being large, protein-protein interactions are maximized and hence an end-on orientation could be favored. Possible orientations adopted by Protein A on nanoparticles of two extreme sizes (5 and 60 nm) are shown in fig. 4.18. Similar transition from a side-on orientation on smaller spheres to an end on orientation on bigger spheres have been reported for another rod like molecule, fibrinogen adsorbed on silica nanoparticles [259].

4.2.4 Adsorption of Streptavidin on Gold Nanospheres

4.2.4.1 Optical Properties of Streptavidin Layer

Calculated optical thickness values of Streptavidin adsorbed on gold nanoparticles are plotted in figure 4.19.

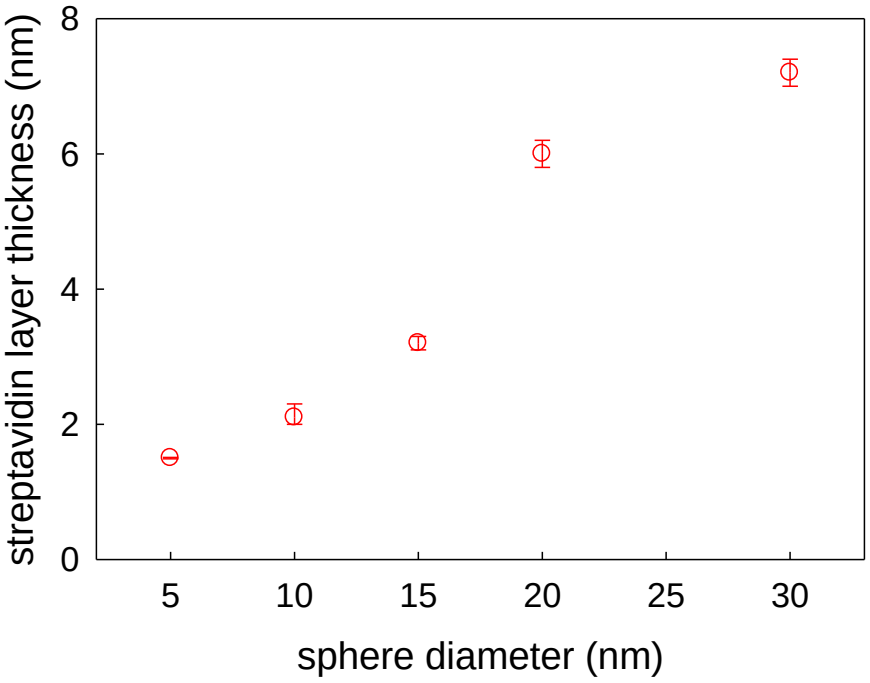

Figure 4.19 Optical thickness of Streptavidin layer on gold nanoparticles vs. diameter of gold nanoparticles.

Just as in the case of Protein A and IgG, the width of Streptavidin layer varies with the size of the gold nanoparticle. Specifically, the thickness of the coating increases from ~1.5 nm on 5 nm spheres to about 7 nm on spheres with diameter 30 nm. Coating thickness values between 4 and 7 nm observed on nanospheres in the size range 15-30 nm. This thickness value roughly

corresponds to the dimensions of a single Streptavidin molecule. A similar value of thickness (~ 6.3 nm) for Streptavidin adsorbed on biotin terminated flat surface has previously been reported by Touahir and co-workers [309]. Herron and coworkers calculated a thickness of 5 nm of Streptavidin layer on flat biotinylated surfaces assuming a refractive index of the layer as 1.46 [321]. Reiter and coworkers also studied the optical properties of Streptavidin binding to biotinylated lipids using ellipsometry [297]. They calculated that the average thickness of adsorbed Streptavidin layer was ~ 4.5 nm under assumption that the refractive index of the adsorbed layer was 1.47. Morgan et. al. used surface Plasmon resonance to calculate the thickness of adsorbed Streptavidin films [322]. They found that the thickness of the adsorbed Streptavidin layer varied from one sample to another. The width of Streptavidin layer varied from 2 nm to nearly 5 nm depending on the degree of coverage of the sample. The width of Streptavidin layer on 5 and 10 nm spheres are ~ 1.5 and 2 nm respectively. This layer thickness value is less than 4 nm, the smallest dimension of a Streptavidin molecule. Streptavidin layer of thickness less than 4 nm could imply that some of the tertiary structure has been lost on adsorption on spheres of sizes 5 and 10 nm. However, this is an average thickness value that has been calculated using the assumption that protein molecules form a uniform and homogeneous coating on the surface of gold nanoparticles. It is possible that these protein molecules do not pack efficiently on these small nanoparticles with high curvature. There could actually be some empty areas on these spheres. Such behavior for different proteins on small nanoparticles has been reported by others too [261, 320]. Further, if we calculate the volume of the adsorbed layer and compare it to the volume of a Streptavidin molecule from its native tertiary structure, then the volume of the adsorbed layer must be large enough to accommodate at least one Streptavidin

molecule. Volume of a Streptavidin molecule is 5.4 nm x 5.8 nm x 4.8 nm = 150 nm^3. The volume of the adsorbed layer can be calculated as

$$V = \frac{4\pi}{3}[(r+d)^3 - r^3] \qquad (4.2)$$

where r is the radius of the sphere and d is the thickness of the adsorbed layer. Volume of the layer calculated for 5 and 10 nm spheres comes out to be ~202 and 912 nm^3 respectively. These values are greater than the volume of a single Streptavidin molecule. Therefore, the volume of the adsorbed layer is large enough to pack at least one Streptavidin molecule.

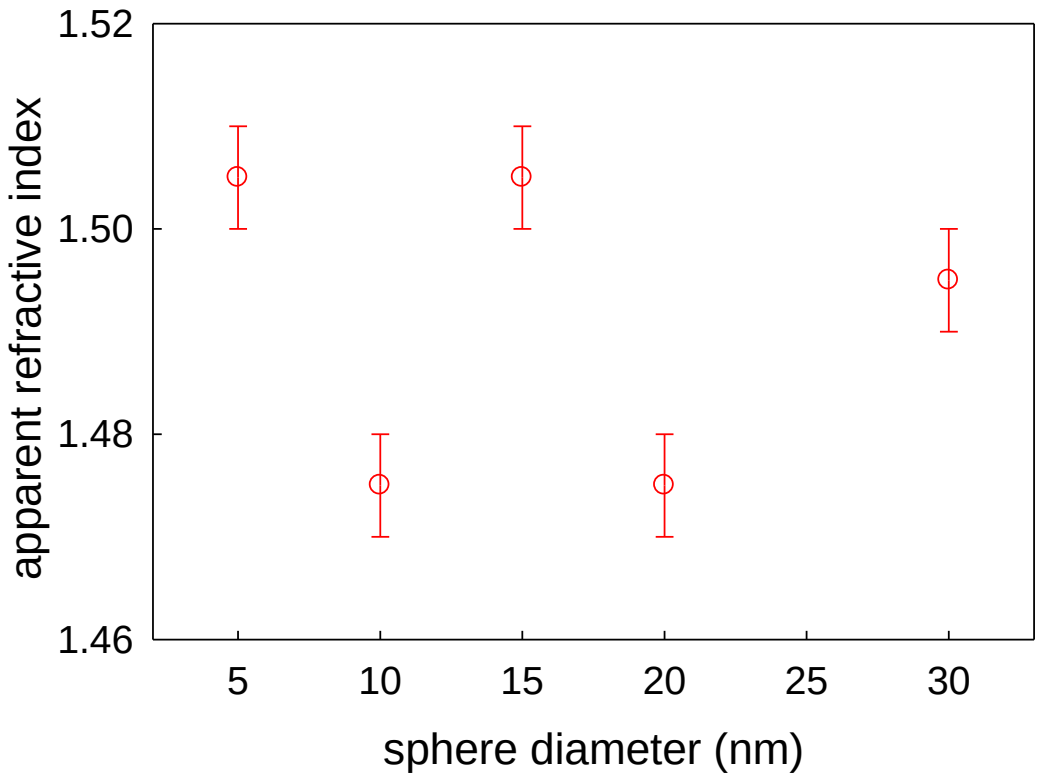

Figure 4.20 Apparent refractive index of adsorbed Streptavidin vs. gold nanosphere diameter

The effective refractive indices of the adsorbed Streptavidin layer on gold nanoparticles in the size range 5 -30 nm are shown in figure 4.20. The refractive index of the absorbed layer depends on the size of the nanoparticle. Specifically, it varies from 1.47 to 1.5 depending upon the size of the nanosphere.

All these calculated values agree with refractive index values usually reported for adsorbed proteins. Morgan and others calculated the relative permittivity and thickness of Streptavidin films on flat surface using surface Plasmon resonance [322]. They found that the value of ϵ' varied from 2.1 to 2.6. The value of ϵ'' lies in the range .0001 and .004. The corresponding value of n then varies from 1.45 to 1.61. The values of refractive indices calculated using Mie theory in this study lie in the same range. Thus, refractive index values of Streptavidin films on nanoparticles are similar to those seen on flat surfaces. Further, although the values of refractive index of adsorbed Streptavidin change with the size of the nanosphere, there is no clear trend in the values of refractive indices with the size of the nanoparticles. This size dependent variation in the values of coating thicknesses and refractive indices of Streptavidin on gold nanoparticles could be due to different packing arrangement or different structures of adsorbed Streptavidin on spheres of different sizes.

4.2.4.2 Surface Density of Adsorbed Streptavidin

Using the values of refractive index and layer thickness, packing density of the adsorbed protein layer can be calculated using equation 4.1.

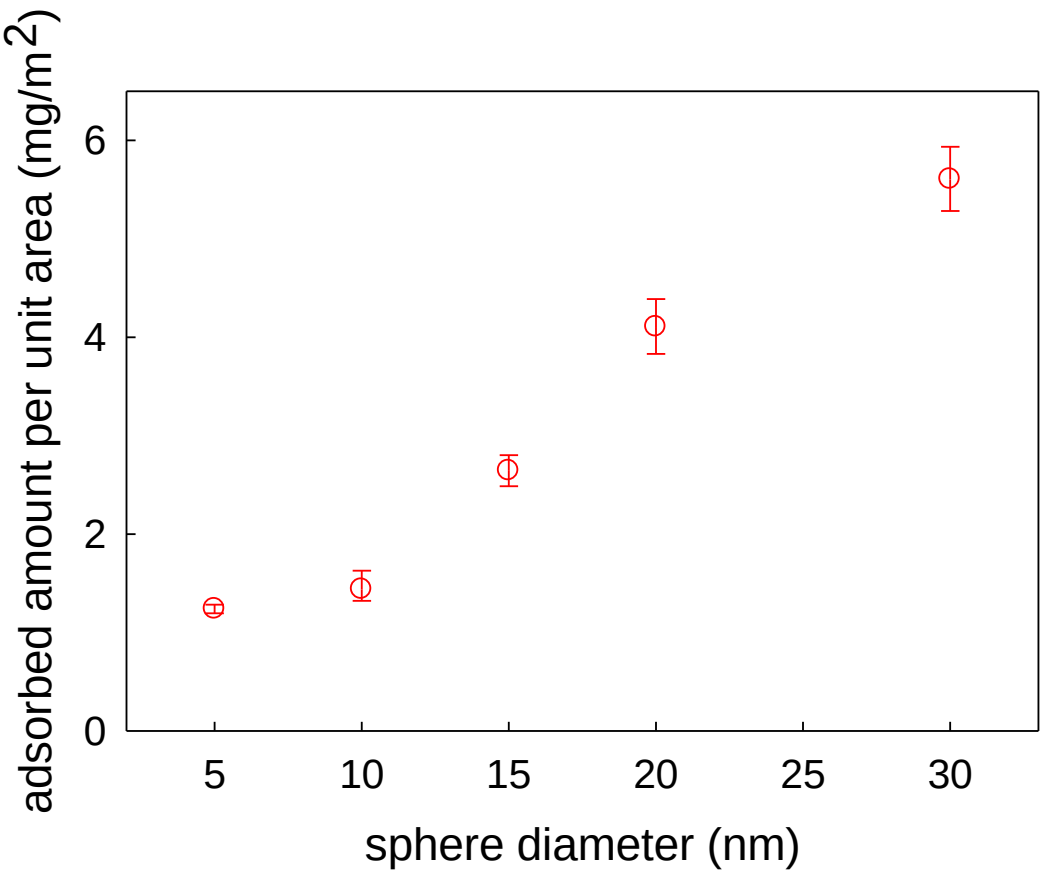

Figure 4.21 Surface density of the adsorbed Streptavidin as a function of the nanoparticle diameter

Amount of Streptavidin adsorbed per unit area on the surface of gold nanoparticles is shown in figure 4.21. Surface density of Streptavidin layers increases with the size of the gold nanoparticle. Specifically, it increases from nearly 1 mg/m^2 on 5 nm spheres to ~ 5.6 mg/m^2 on 30 nm spheres. Highest surface protein density is observed on 30nm spheres. The number of Streptavidin molecules attached per unit area varies from ~1 x 10^{12} /cm^2 on 5 nm particles to 5.6 x 10^{12} /cm^2 on 30 nm particles. For a closed packed monolayer of Streptavidin the surface density is ~5.2 x 10^{12} molecules/cm^2 [297, 323]. According to our calculations the surface density of Streptavidin layer on 30 nm gold nanoparticles is equal to the packing density of a

close packed monolayer. Surface density of Streptavidin on gold nanospheres with diameter < 30 nm is lower than that for a close packed monolayer. We also calculated the number of Streptavidin molecules attached to a single sphere (fig. 4.22). The number of Streptavidin molecules attached to a gold nanosphere increases with the corresponding increase in the surface area of the sphere from ~ 1 on 5 nm spheres to ~ 160 on 30 nm spheres.

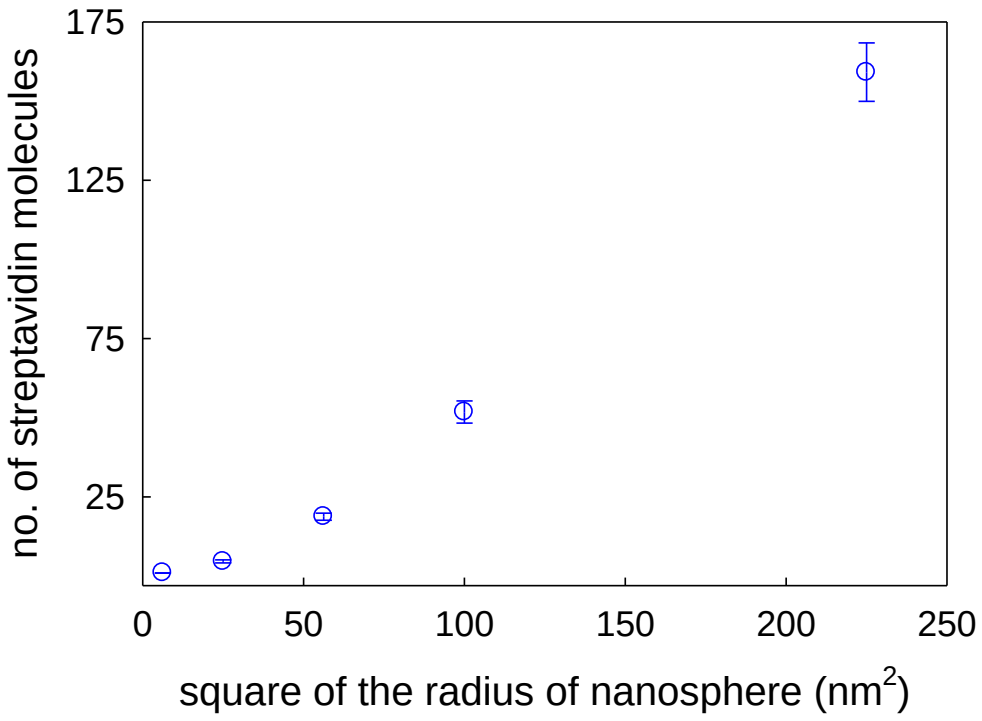

Figure 4.22 Number of Streptavidin molecules attached to gold nanospheres vs. diameter of the spheres

4.3 Protein Binding studies

4.3.1 Binding of IgG to Protein A Coated Gold Nanospheres

To test if the size of gold nanoparticle would affect the binding activity of the adsorbed Protein A molecules, aqueous IgG solution was added to the coated spheres solution. The results are shown in figure 4.23. There is a red shift in the plasmon peak for all sphere sizes on addition of IgG. When a protein molecule binds to the conjugated nanoparticles, there is a shift in the plasmon wavelength due to changes in the dielectric properties of the coating. The results indicate that Protein A adsorbed onto gold nanospheres on all sizes under study is able to bind to IgG.

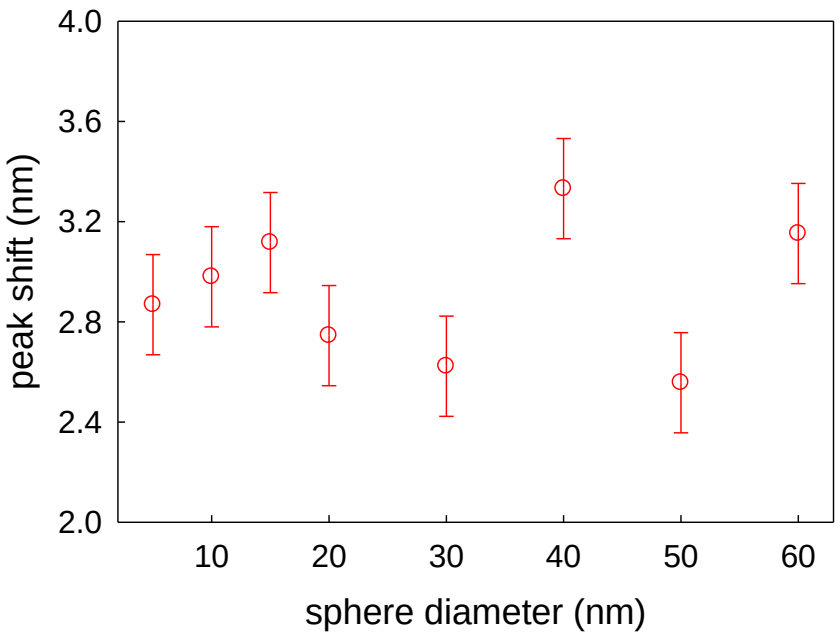

Figure 4.23 Shifts of the plasmon peak wavelength of Protein A coated gold nanospheres after addition of IgG

Although, the size of the spheres affects the orientation of the adsorbed Protein A layer (figure 4.18), it has no effect on the binding activity of adsorbed Protein A molecules. Protein A retains

its binding activity for IgG on all sizes of nanoparticles irrespective of the orientation that it adopts on spheres of different sizes. This result is not surprising since a single Protein A molecule has 5 IgG binding domains which should be accessible to the IgG molecules in solution, whether Protein A molecules are attached to the surface in side-on or end-on orientation (see figure 4.4).

4.3.2 Binding of IgG to Protein A Coated Silver Nanoparticles

We also monitored binding between IgG and Protein A coated on silver nanoparticles. For these binding studies silver nanospheres 20 and 40 nm were employed. Resonance peak position values for bare silver spheres, Protein A coated silver nanoparticles and those after binding to IgG are plotted in figure 4.23.

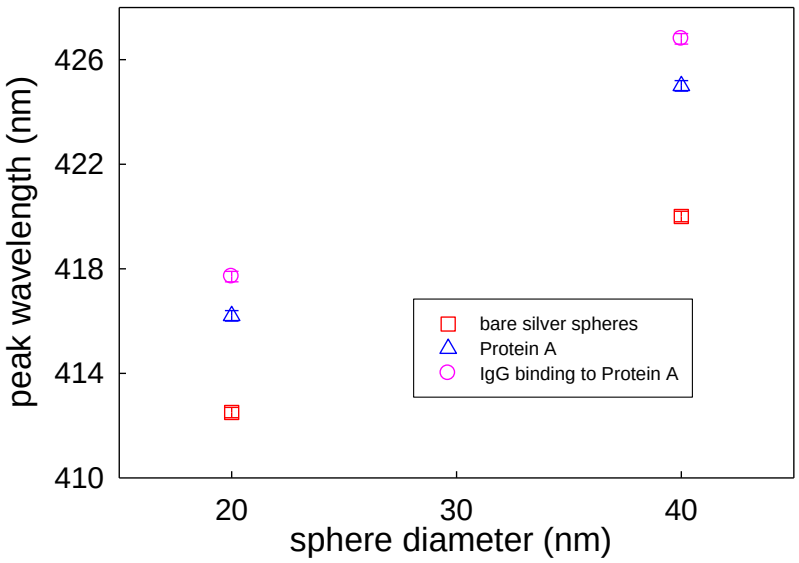

Figure 4.24 Position of the plasmon peaks for bare silver nanoparticles (squares), Protein A conjugated silver nanospheres (triangles) and on IgG binding to Protein A coated silver nanospheres (circles).

Localized surface plasmon resonance of silver nanoparticles occurs in the blue region of the visible spectrum as can be seen from the position of the Plasmon peaks. Since the resonance frequency of a metallic nanoparticle of specific size depends on its composition, the peak positions of similarly sized gold and silver nanoparticles lie in different region of the spectrum. On addition of Protein A molecules there is clear shift in position (≥ 4nm) of Plasmon peak to longer wavelengths indicating that Protein A had adsorbed onto silver nanoparticles. Extinction spectra of Protein A conjugated silver nanoparticles were again recorded after 24 hours and no shift in the plasmon peak position was observed. This indicates that Protein A forms stable conjugates with silver nanoparticles. On adding IgG solution there is a further shift in the position of the Plasmon peak for both 20 and 40 nm silver nanoparticles. The results indicate that IgG binds to Protein A adsorbed onto both 20 and 40 nm silver nanoparticles. Thus, Protein A retains its binding activity for IgG on metallic nanoparticles of different sizes irrespective of the nature of the nanoparticles. Unfortunately, we cannot quantify the binding activity of the adsorbed protein with LSPR. Curvature of nanoparticles in the size range 10 to 60 nm does not affect the functionality of Protein A.

4.3.3 Binding of Protein A and Anti-IgG to IgG coated Gold Nanospheres

To test if Protein A and Anti-IgG could bind to adsorbed IgG we first added Protein A solution to the IgG conjugated gold colloids and recorded the spectra. Later, we added Anti-IgG to IgG coated gold nanoparticle solution and recorded the spectra again. The results are shown in fig 4.25.

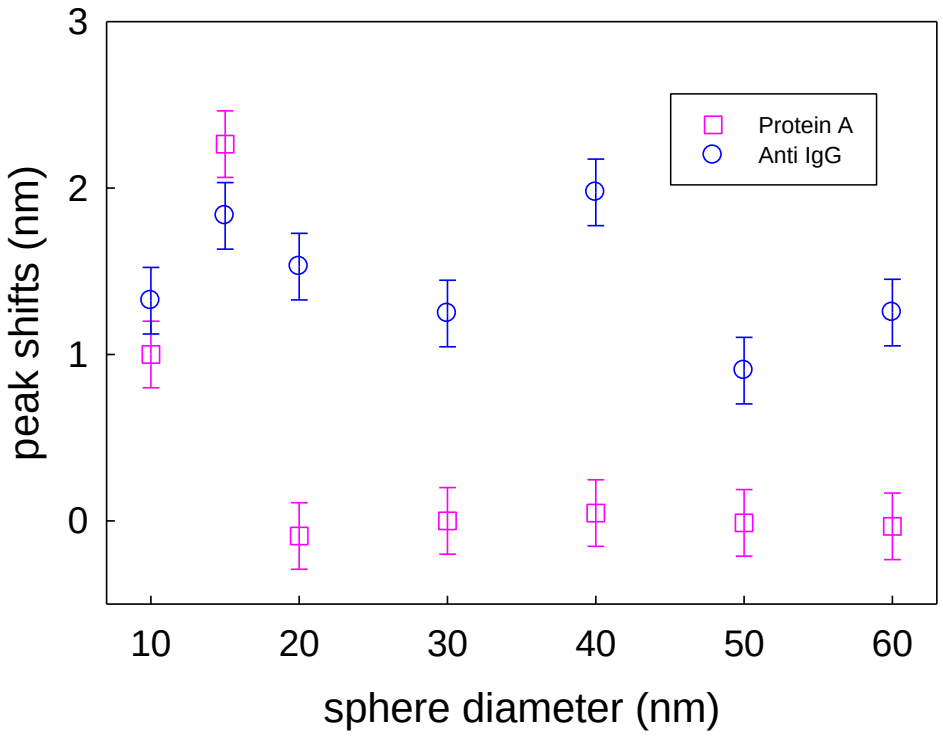

Figure 4.25 Peak shifts observed for Protein A- IgG binding (squares) and Anti IgG- IgG (circles) binding vs. diameter of gold nanoparticle

On addition of Protein A to IgG coated spheres, there is a shift in the plasmon peak towards longer wavelength for 10 and 15 nm spheres but no shift is observable for other sizes (20-60 nm). However, a clear red shift (≥ 1nm) is observable for all sphere sizes when Anti-IgG is added to the same solution. The results indicate that Anti-IgG is able to bind to IgG on all sphere sizes (10-60 nm) whereas Protein A binds only on small spheres (10-15 nm) for which there is an observable shift in resonance peak. The lack of shift on spheres with diameter ≥ 20 nm demonstrates that Protein A does not bind to IgG on these nanospheres. Although, the size of the nanoparticle does not affect binding between IgG and Anti-IgG, a clear size dependent variation in the binding between Protein A and IgG attached to gold nanoparticles is observed.

While Protein A binds to the Fc domain [324], anti-IgG does not a have a specific binding site on IgG molecule. The lack of binding on spheres with diameter ≥ 20 nm indicates that Protein A binding sites are not accessible. One possible scenario for the observed behavior is as follows: IgG adopts a side-on orientation on the small spheres (10 nm diameter). As the sphere size increases there is a transition from side-on to a more end-on orientation followed by a complete end-on orientation on the bigger spheres (40-60 nm diameters). End-on adsorption for IgG on flat surfaces has been reported previously [120, 176, 318, 319]. Roughly ,only one IgG molecule is attached to 5 nm gold sphere. It is possible that in order to maximize the protein-surface interaction IgG adopts a side-on orientation on these spheres.

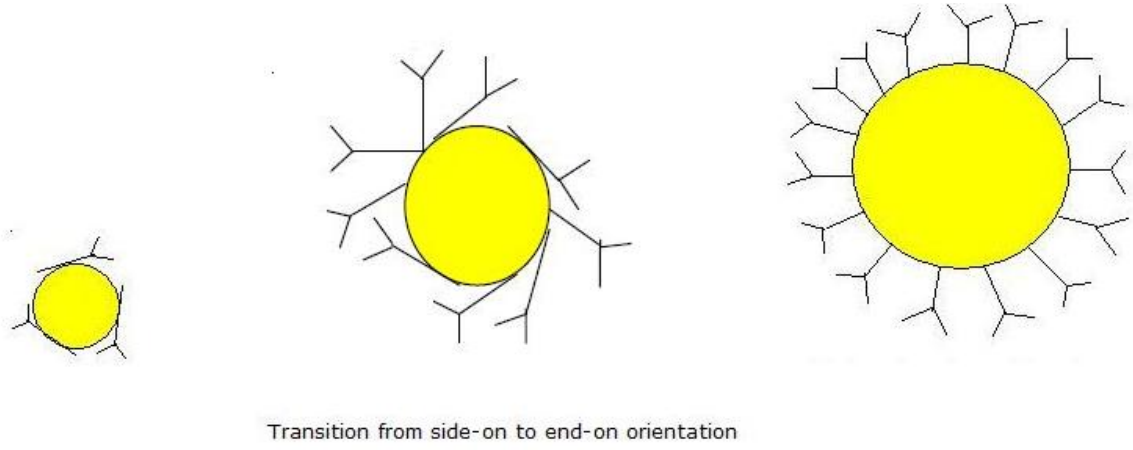

Figure 4.26 Schematic showing possible transition from side-on to end-on orientation for IgG due to change in size of gold nanospheres.

In a side-on orientation Fc binding sites should be accessible to the incoming molecules. Therefore, in this orientation both Protein A and Anti-IgG should be able to bind to adsorbed IgG. Such behavior is indeed observed on small spheres. Smaller layer thickness and adsorbed amount also agree with side-on orientation on 5 nm spheres. On spheres with diameter > 20 nm

if IgG were to adopt an end-on orientation with Fc domain directed towards the sphere and Fab domains pointing away from the spheres, then it is possible that the incoming Protein A molecules experience steric hindrance due to the bulky Fab domains and hence are not able to access the Fc binding sites. Anti-IgG would be able to bind to adsorbed IgG for all sphere sizes (fig.4.26).

4.3.4 Effect of pH on Binding of Protein A to IgG Coated Gold Nanospheres

This study was conducted on polyclonal rabbit IgG, whose isoelectric point ranged between 6 and 8. IgG is negatively charged above pH 8. The negative charge leads to repulsion between the Fab arms causing them to stretch out [319]. Adsorption of monoclonal IgG on latex microparticles carrying negative surface charge showed that adsorption of IgG through its Fab sites is supressed at alkaline pH values where IgG is negatively charged [325]. This leads to specific orientation of IgG molecules with their Fc site directed towards the latex spheres. The orientation can affect the binding activity of adsorbed IgG molecules [325, 326]. Although the effect of pH on the adsorption of IgG has been monitored on micro particles, no such study has been reported on nanoparticles. We probed how the pH of the adsorption would affect the binding activity of adsorbed IgG. The effect of pH of adsorption was probed on gold nanospheres of two sizes, 15 and 40 nm. The pH of adsorption was varied from 4 to 10 for 15 nm particles. Due to aggregation of 40 nm gold nanoparticles at pH 4, no measurement could be made at this pH value.

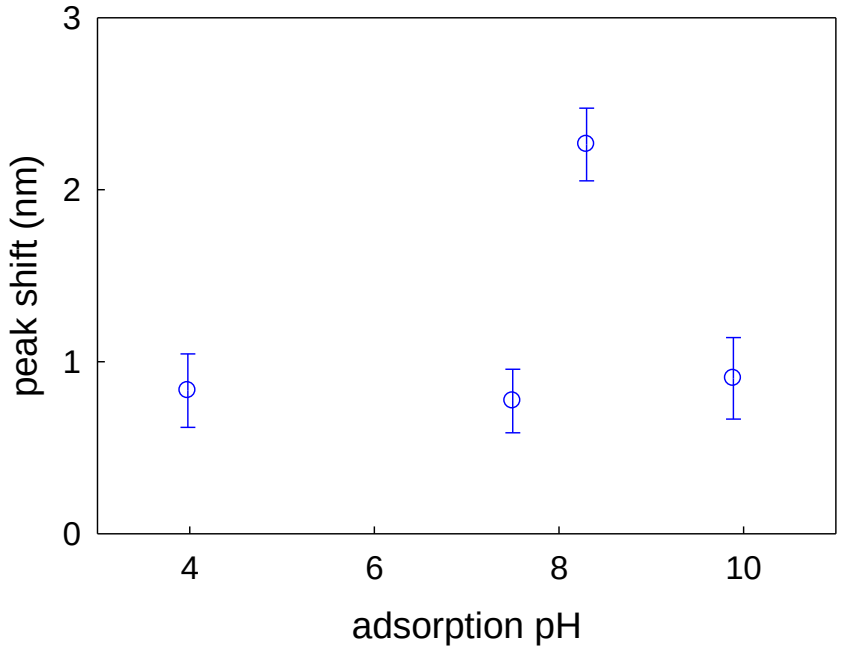

Figure 4.27 Shifts in the plasmon peak wavelengths of IgG coated spheres after addition of Protein A vs. adsorption pH.

There is spontaneous adsorption of IgG on gold nanospheres at all pH values, even when IgG molecules carry net negative charge and are electrostatically repelled by the surface charge on gold nanospheres. It is possible that low molecular weight cations present in the solution are coadsorbed with IgG to overcome the electrostatic repulsion. Figure 4.27 shows the shifts in LSPR peak wavelengths for IgG coated 15 nm gold nanospheres before and after addition of Protein A solution as a function of pH at which IgG was adsorbed onto gold nanospheres. On addition of Protein A solution to IgG coated 15 nm gold nanospheres, there is a shift in the resonance peak towards longer wavelengths at all pH values under study. The results indicate that irrespective of the pH of adsorption, Protein A is able to bind to IgG on 15 nm spheres. The magnitude of the shift in the peak at pH 8 is the highest. At this pH value, IgG molecules carry

little to no charge and thus have a compact structure. The adsorbed amount is the highest at this pH value. At pH values away from the pI, the charge on the molecule increases and it results in expansion of the molecule due to electrostatic repulsion. Hence, the amount of the adsorbed IgG decreases at pH values away from the i.e.p. Therefore, it can be expected that the highest number of Protein A molecules attach to IgG coated spheres at pH 8 and result in the biggest change in the dielectric properties of the coating layer. This change is reflected in the magnitude of the shift in the peak.

Shifts in plasmon peak wavelength values for IgG coated 40 nm gold nanospheres are plotted in figure 4.28. Adsorption pH was varied from 7 to 10. After addition of Protein A to IgG coated gold nanospheres, no shift in the position of the Plasmon peak is observable.

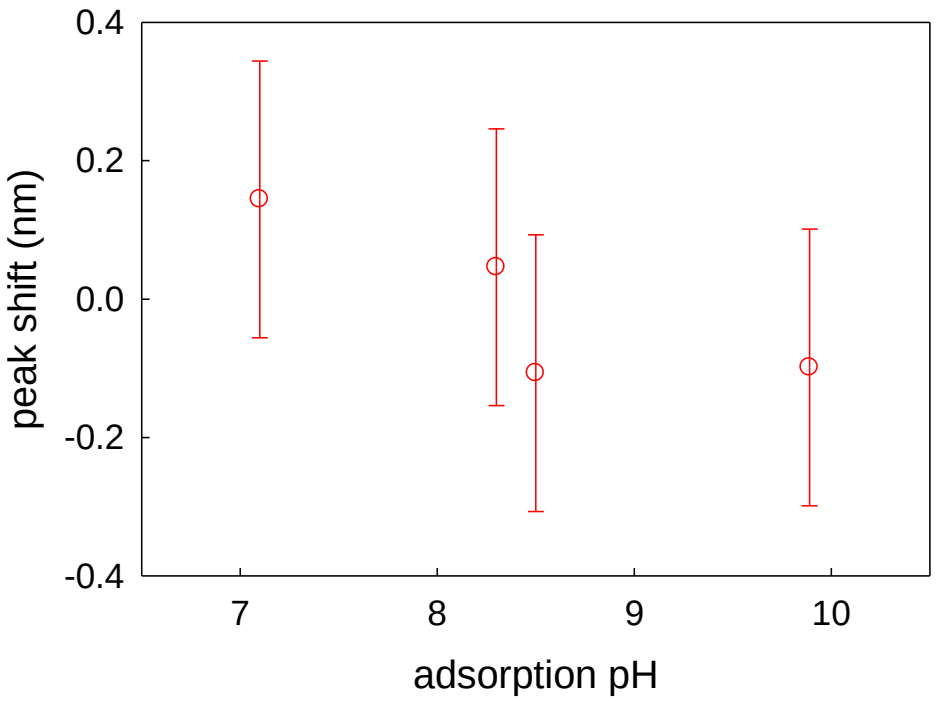

Figure 4.28 Shifts in the position of plasmon peak wavelengths for IgG coated spheres after addition of Protein A.

The results indicate that Protein A cannot bind to IgG coated spheres in the pH range under study. It is possible that IgG attaches to 40 nm gold nanospheres with Fc site and the bulky Fab arms provide steric hindrance to incoming Protein A molecules and restrict binding between IgG and Protein A. Others have reported adsorption of IgG through Fc site on various surfaces [327, 328]. At the pH values under study, both IgG and gold nanoparticles are negatively charged. Attachment of Fab site is governed mainly by electrostatic interactions. Therefore, attachment through Fab part is retarded at alkaline pH values whereas attachment through Fc sites is not affected [325]. Also, Fab part of IgG molecule is structurally more stable than Fc part. It has been previously reported that Fc part is more prone to acid denaturation as compared to Fab part [329, 330]. Therefore at alkaline pH values, attachment through Fc site is preferred. At pH values where IgG molecules neutral or carry negative charge, no binding occurs between IgG molecules adsorbed on 40 nm gold nanospheres and Protein A molecules. On the other hand, IgG molecules attached to 15 nm gold nanospheres retain their Protein A binding activity irrespective of the fact whether IgG molecules carry positive or negative charge.

4.3.5 Binding of Biotin to Streptavidin Conjugated Gold Nanospheres

Figure 4.29 displays the shifts in the position of plasmon peak of Streptavidin conjugated nanospheres after addition of biotin. We monitored the samples after addition of biotin for over a week. Samples were stable and we did not detect any change in the position of peak wavelength.

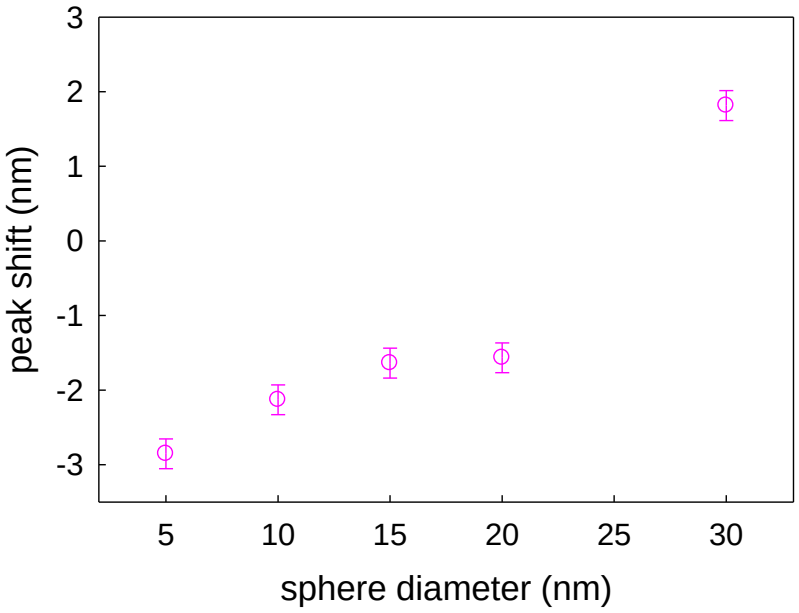

Figure 4.29 Shifts in Plasmon peak wavelengths for Streptavidin conjugated gold nanospheres after addition of biotin.

As evident from the figure there is a shift in the position of the peak for all the sphere sizes on addition of biotin indicating that there is a change in the dielectric environment of gold nanospheres. The results indicate that Streptavidin conjugated to gold nanoparticles in the size range 5 – 30 nm retains its biotin binding activity. However, the direction of the peak shift is puzzling. For sphere sizes 5 to 20 nm the peak shifts towards smaller wavelengths on addition of biotin. A shift to smaller wavelength of LSPR peak due to adsorption of molecules has previously been reported [326]. Biotin is small molecule and is hard to detect using optical techniques such as SPR and ellipsometry [321, 322]. Further, biotin binding sites are located in the interior of streptavidin molecules [316, 331, 332]. These binding sites are exposed to water molecules due to the open conformation of binding loops (shown in figure 4.7). Biotin binding to streptavidin involves displacement of the water molecules and ordering of loops into closed

conformation, thereby restricting the mobility of the loop in bound state. There is no change in the quaternary structure of streptavidin due to biotin binding [333]. In bound state the thickness of the streptavidin layer is estimated to be between 4.3 – 4.8 nm [297]. This might be the reason that biotin binding to streptavidin did not result in the shift of the peak towards longer wavelength. However, a shift of the peak towards longer wavelength is observed on addition of biotin to streptavidin conjugated 30 nm gold nanoparticles. The stability of streptavidin conjugates decreases with the size of the nanoparticle. Streptavidin does not form stable conjugates with 40 or 50 nm gold nanospheres and leads to aggregation of the nanoparticles. Streptavidin conjugated 30 nm nanospheres are not as stable as smaller spheres. The red shift could be a result of slow aggregation of these nanoparticles. Nath and Chilkoti [334] have previously studied chemisorption of gold nanoparticles of various sizes on glass substrate. The authors reported that while plasmon peak of gold nanoparticles with diameters ranging from 12 to 26 nm shifts to longer wavelength on adsorption, adsorption induces a blue shift in LSPR peak for gold nanoparticles in the size range 39 to 49 nm. However, it can be concluded that biotin binds to Streptavidin on all gold nanoparticles in the size range 5 to 30 nm as indicated by the shift in peak positions. Others have previously reported binding of streptavidin adsorbed on both planar gold surface and gold nanoparticles to biotinylated ligands [335, 336].

4.4 CONCLUSIONS

We used UV-visible extinction spectroscopy to study the binding activities of IgG, Protein-A and streptavidin molecules adsorbed onto gold nanospheres of various sizes (5-60 nm). By doing detailed calculations using Mie theory we can get information on the optical properties of the adsorbed proteins. Layer thickness values suggest that for both IgG and Protein A, the size of the gold nanoparticle can influence the orientation of adsorbed proteins. Optical properties of adsorbed IgG and Protein A layer showed no variation on gold nanospheres with diameters > 30 nm. The curvature of the nanoparticles has a strong influence on the binding activity of IgG, but it does not affect the binding activity of Streptavidin and Protein A molecules. Adsorbed IgG loses its ability to bind to Protein A on spheres with diameter ≥ 20 nm. On the other hand, Protein A adsorbed on all sphere sizes shows binding to IgG molecules. This behavior was observed for both gold and silver nanoparticles. Similarly, streptavidin molecules attached to gold nanospheres in the size range 5 to 30 nm retained their biotin binding. Thus, curvature of the nanoparticles can have different effect on the functionality of the adsorbed proteins depending on the shape and orientation of the adsorbed protein molecules. These results can have important implications in designing colloidal drug carriers.

CHAPTER 5

Depth Profiling of BSA Adsorbed onto Polymer Surfaces

5.1 Introduction

Adsorption of proteins at interfaces has been attracting scientific interest for many years [337, 338]. Biological processes such as blood coagulation involve proteins at interfaces [182]. Chromatography, generally used to purify proteins, involves protein interaction with solid surfaces. Understanding the interfacial behaviour of proteins is not only important to understand theses biological processes, but it is also relevant in diverse fields such as medical diagnostics, biosensors, contact lenses, pharmaceuticals, solid phase immunoassays and various other technologies [204, 339-342]. In the use of biosensors the adsorption conditions need to be optimized to get the maximum loading of proteins. On the other hand, it is important to inhibit protein adsorption in several processes such as fouling of heat exchangers, ultra filtration membranes and medical devices. Studies aimed at understanding the interfacial behaviour of proteins are essential for controlling protein adsorption to either optimize biosensors or prevent protein adsorption if it is undesired. Probing the behaviour of proteins on biomaterials is particularly important because proteins adsorb rapidly onto biomaterials when such materials are implanted in human bodies. The initially adsorbed protein layer dictates the behaviour of the implants because the cells interact with the adsorbed protein layers and not the implant material directly.

Protein adsorption on surfaces is driven by enthalpic contributions such as Van der Waal's forces, electrostatic and hydrophobic interactions, hydrogen bonding as well as entropic contributions [122]. Protein interaction with surface could also lead to protein unfolding on the surface. This could result in the loss of tertiary or even secondary structure of the adsorbed protein [343-345]. The degree of adsorption and the structure of the adsorbed layer depend on nature of both protein and the adsorbing surface [346, 347]. Other variables that affect the adsorption process are temperature, pH of the solution, ionic strength. Generally soft proteins with low structural stability undergo higher degree of structural change as compared to hard proteins. Further, the degree of protein unfolding depends on the charge and hydrophobicity of the substrate. Hence, it is interesting to study how different substrates can affect the adsorption of protein molecules.

In-situ study of the structure of the protein layers adsorbed at an interface is an essential prerequisite for resolving the mechanisms of protein adsorption. Ellipsometry is used to study protein layers adsorbed on flat surfaces. Ellipsometric parameters give information about the optical thickness and the refractive index of the adsorbed layer, but these two variables are strongly coupled and cannot be unambiguously resolved. Moreover, the structural analysis with ellipsometry is based on the assumption that the adsorbed layer is homogeneous. The structure of the adsorbed protein layer could vary with distance from the adsorbent surface. It has been previously shown that binding constants are smaller for protein layers farther away from the surface as compared to the layers closer to the surface [185]. Currently, only X-ray and neutron reflectivity techniques are available to observe the heterogeneity within the adsorbed layer [348, 349]. However, these techniques are highly labour and cost intensive. In this study, we

demonstrate similar study of the interfacial structure of the adsorbed protein using optical spectroscopy.

We describe a new technique based on optical spectroscopy to determine the refractive index profile of protein adsorbed onto various polymeric surfaces. LSPR of the gold nanoparticles was employed to probe the optical properties of the adsorbed protein layer. In this chapter, we describe the use of LSPR to probe the optical properties of protein adsorbed on a surface. Using this technique, we can also differentiate between the optical properties of the protein molecules close to the surface with the protein molecules farther away from the substrate. This is the first study that uses nanoparticle as reporters to determine changes in the protein layer as a function of distance from the substrate. This technique can be applied to study a wide range of protein on any material that is transparent to visible light.

In this study we use bovine serum albumin (BSA) as a model protein. Serum albumins are the most abundant blood proteins in humans and other mammals [350]. BSA is a well characterized protein and has been used as a model protein to study physical and biological aspects of protein adsorption [351, 352]. BSA can be approximated as prolate ellipsoid with dimensions 4 nm x 4 nm x 14 nm [253].

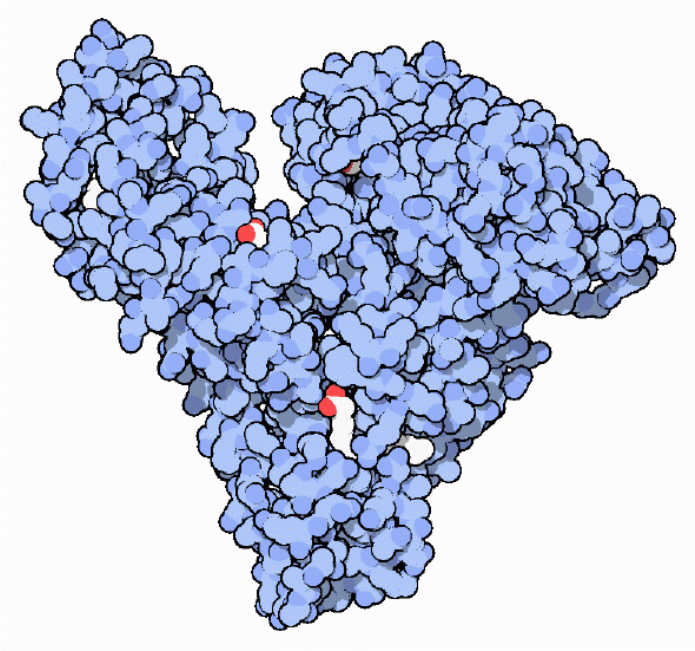

Figure 5.1 Structure of Bovine Serum Albumin (Image taken from ref. 353)

In the current study, we probed the interaction of BSA with four biomaterials - Polystyrene (PS), poly-(methyl methacrylate), PMMA, poly-dimethyl siloxane (PDMS) and poly-2-hydroxyethyl methacrylate (polyHEMA) with varying hydrophobicity. PolyHEMA is a soft, flexible, water-absorbing hydrophilic polymer. PolyHEMA is used to manufacture contact lenses and as drug delivery agent [354, 355]. It is a polymer of 2-hydroxyethyl methacrylate (HEMA). Polystyrene is an aromatic polymer with a chemical formula $(C_8H_8)_n$. Polystyrene has a wide range of applications. Polystyrene latex particles are used as drug carriers. Polystyrene plays an important role in biomedical research as it is employed to manufacture Petri dishes, test tubes and laboratory material. PDMS belongs to the family of organosilicon compounds referred to as silicones. The monomer occurring in PDMS is $[SiO(CH_3)_2]$. PDMS is inert and non-flammable. PDMS is used in contact lenses, medical devices, breast implants etc. The hydrophobicity of the materials decreases in order; PDMS > PS > PMMA > pHEMA.

5.2 Experimental Details

PS and PMMA cuvettes were used without further modification. Preparation of Poly (dimethyl siloxane), PDMS and polyHEMA substrates has been described in chapter 3. Method for synthesis of gold nanoparticles has previously been explained in chapter 3. The procedure for conjugating gold nanoparticles has also been previously described (Ch. 3).

To ensure that the cuvette stays in the same position, a piece of cardboard (packing carton) was used. A small hole was cut in the centre of the cardboard piece and the cuvette was placed inside that hole. After that the cardboard piece was taped to the sides of the cuvette. The cuvette was then placed inside the sample holder and the cardboard was then taped to the sides of the sample holder. PBS was introduced in the cuvette and a reference spectrum was recorded. Ocean optics USB 2000 spectrometer was used to measure the spectra. PBS was then removed with the help of a glass pipette. The protein/ nanoparticle solution obtained after centrifugation and resuspension in regular PBS was introduced into a cuvette and were left to sit for some 5 minutes. After that time the nanoparticle solution was removed from the cuvette and was replaced by PBS buffer solution. After introduction of the buffer, the extinction spectrum of the gold nanoparticles adsorbed on the sides of the cuvette was recorded. At this point the buffer was removed from the cuvette and the protein/nanoparticle solution was again added to the cuvette. This procedure of removing the protein/nanoparticle solution and replacing it with the buffer was repeated several times and the spectra were recorded each time after addition of buffer (fig. 5.2).

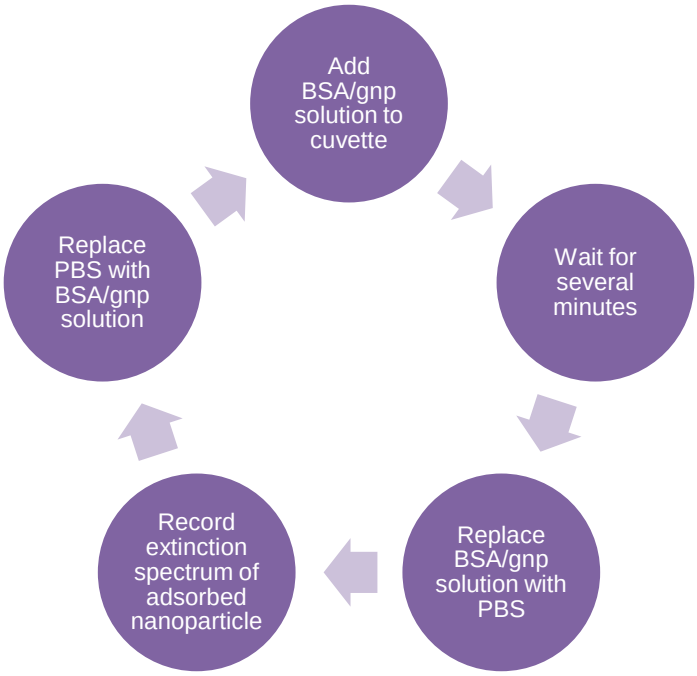

Figure 5.2 Repetitive steps to measure extinction spectra of BSA coated gold nanoparticles (gnp) adsorbed on a substrate

With time more BSA coated nanoparticles adsorbed on the sides of the cuvette. This also resulted in a visible change of colour on the sides of the cuvette to pale pink (see figure 5.3). At the same time the original nanoparticle solution was depleted of the nanoparticles. This resulted in the change of colour of the nanoparticle solution from red to pink. To calculate the number of gold nanoparticles removed from the solution the spectra of the solution was also recorded at regular time intervals.

Figure 5.3 On the left is shown the cuvette with PBS buffer solution used as reference. On the right is shown the same cuvette after exposure to gold nanoparticle solution.

Figure 5.4 BSA coated gold nanoparticle solution before the start of the experiment (shown on the left). On the right the same solution after exposure to PS cuvette is shown.

Since it was observed that BSA coated gold nanoparticles adsorbed onto the sides of the cuvette, these solutions were stored in glass vials during the course of the experiment. Also, as a control experiment uncoated gold nanoparticles were introduced into these cuvettes and were

stored in these cuvettes for more than 24 hours and the spectra were recorded. No change in the spectra was observed during that time. It was concluded that bare nanoparticles do not adsorb onto bare polystyrene or polymer coated polystyrene cuvettes. Only protein coated gold nanoparticles adsorb onto the sides of the cuvette.

Change in the temperature of the spectrometer can cause fluctuations in the position and the extinction of the resonance peak. To improve the sensitivity of the apparatus, the spectrometer was kept in a temperature controlled box (shown in figure 3.9). This kept the temperature of the spectrometer constant to within ±0.3 K. The temperature controller decreased the uncertainty of the measurement of peak position (λ_{max}) and absorbance (ϵcl) to ± 0.5 nm and ± 0.01 respectively (shown in figure 5.5).

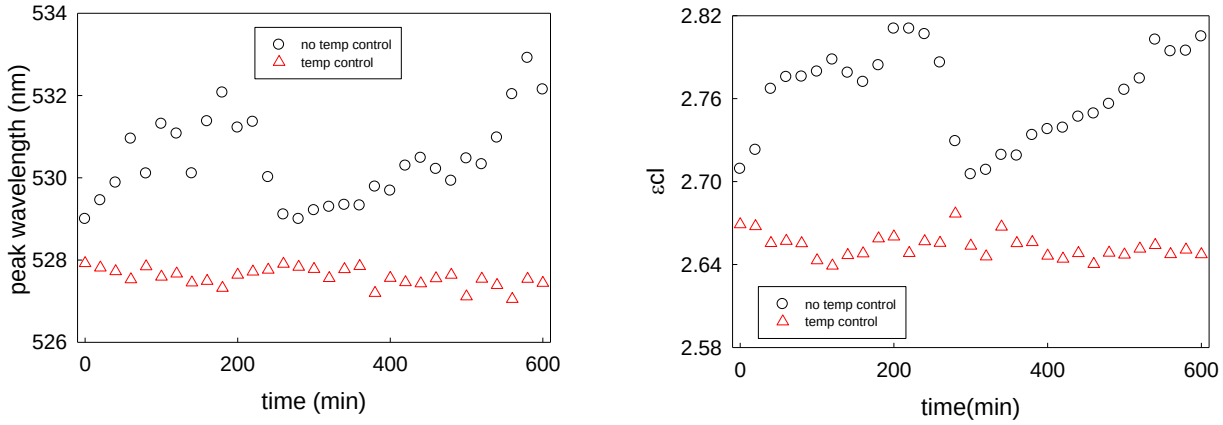

Figure 5.5 Reproducibility of the position and the extinction of the resonance peak with temperature control (triangles) and without temperature control (circles).

To characterize the gold nanoparticles, silicon wafers were coated with polystyrene films and then gold nanoparticles were deposited on those polymer coated wafers. These deposited nanoparticles were imaged with AFM in tapping mode. Tapping mode image of the gold

nanoparticles taken with AFM is shown in figure 5.6. The size of the nanoparticles was determined using Matlab program written by one of the group members, Mark Ilton [356]. To determine the size of nanoparticles the average was taken over 100 particles. The average size of the gold nanoparticles was 30 nm. For theoretical modeling, all simulations were run using Mathcad 14.

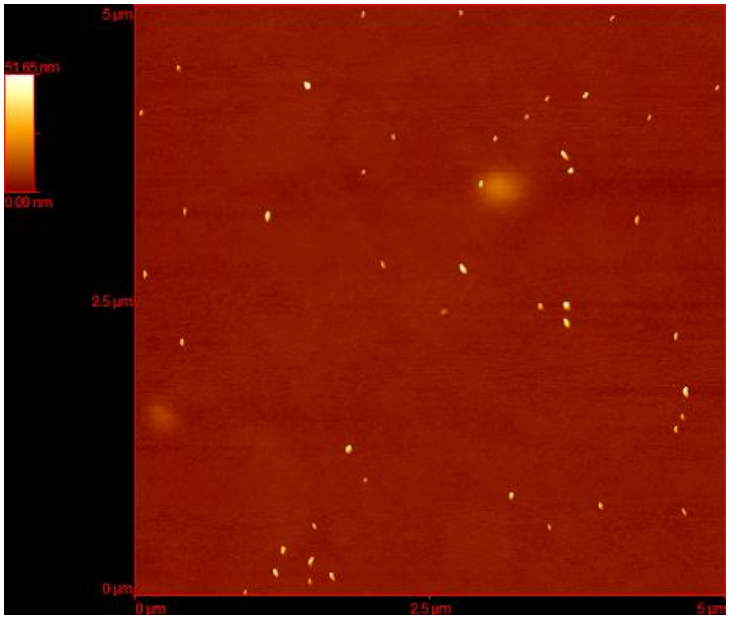

Figure 5.6 Tapping mode AFM image of gold nanoparticles

5.3 Results

5.3.1 Adsorption of BSA Coated Gold Nanoparticles on Substrates

The sample obtained after centrifugation contained both free BSA molecules (not attached to the spheres) and BSA molecules attached to the gold nanoparticles. Upon exposure to the cuvette both free BSA molecules and those attached to gold nanoparticles adsorb on the substrate. Bare gold nanoparticles do not attach to the substrate.

We monitored the change in the peak wavelength and absorbance when samples were introduced into the cuvettes. Figure 5.7 shows the change in the peak wavelength of gold nanoparticles that are adsorbed on various substrates. The spectrum at 0 minutes corresponds to the spectrum of the BSA coated gold solution. The solution was initially allowed to sit in the PDMS lined cuvette for 2 minutes. After removing the solution and replacing it with PBS the spectrum was first recorded. The solution was again introduced in the cuvette for several minutes. The spectra were recorded after every exposure. For PDMS, the spectra were recorded after an interval of 5 minutes and for other substrates, the spectra were recorded every 10 minutes. The value of peak wavelength of BSA coated particles in solution is 532 nm. In case of PDMS and pHEMA, the signal at 2 minutes was too low to be resolved. There is a huge shift (10-15 nm) in the position of plasmon peak wavelength of gold nanoparticles initially, when these nanoparticles adsorb onto the substrates. This is followed by comparatively small changes in the peak position after adsorption of more BSA and gold nanoparticles. These changes in the peak position vary with the nature of the polymer film.

After 7 minutes exposure to PDMS substrate, the peak wavelength shifts by nearly 11 nm to give a value of 543 nm. There is a rapid change in the peak wavelength for the first 30 minutes. After the first half an hour peak wavelength becomes nearly constant. The value of peak wavelength after 67 minutes is 555 nm.

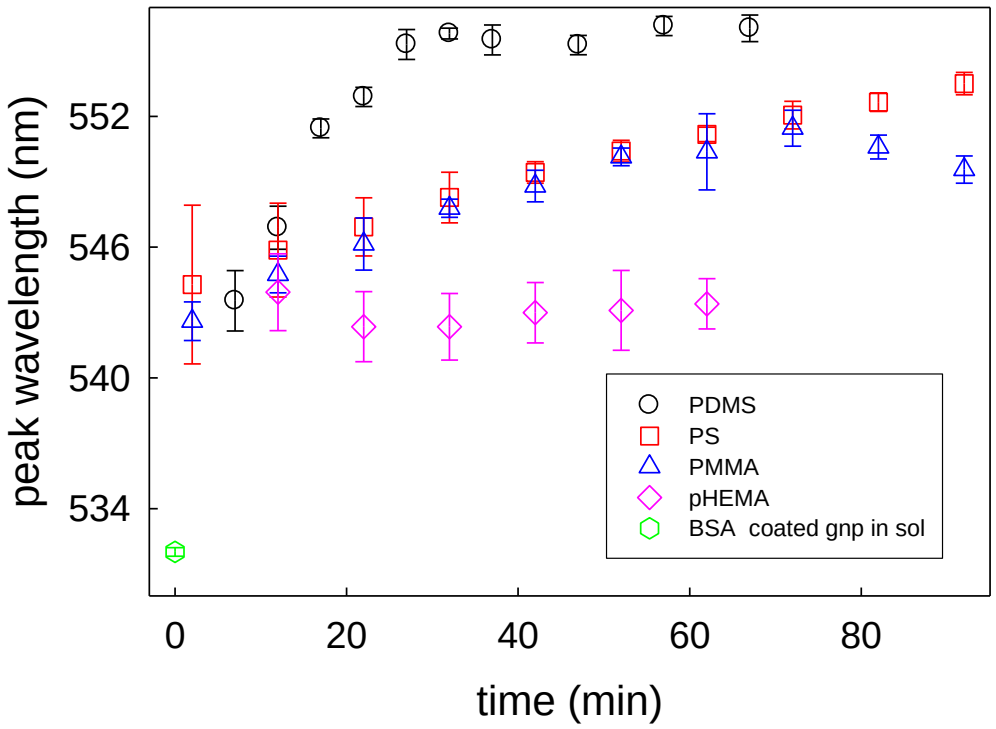

Figure 5.7 Variation of the peak wavelength of BSA coated gold nanoparticles on exposure to various polymer films vs. time.

On adsorption to PS surface, , the resonance peak shifts by 14 nm after 2 minutes exposure. With passage of time the peak shifts continuously. In contrast to the behaviour of BSA coated particles on PDMS, where the peak wavelength reaches a nearly constant value after 30 minutes, the peak wavelength continuously shifts to longer wavelengths even after 90 minutes. The value

of the resonance peak is 553 nm after 92 minutes. The total shift in the value of peak wavelength is about 21 nm which is smaller than the peak shift observed in case adsorption on PDMS (23 nm). The behaviour of BSA/gold nanoparticle system on PMMA is similar to that observed on PS. This is not surprising since both substrates are hydrophobic in nature. Although PDMS is also hydrophobic in nature, the shifts observed in case of BSA coated gold nanoparticle adsorption on PDMS are different from those observed for other hydrophobic substrates, PS and PMMA. The shifts in the peak positions on adsorption of BSA coated gold nanoparticles onto pHEMA surfaces are smaller than those observed for other surfaces. There is only a change of 13 nm from that of BSA coated gold nanoparticles in solution. After 10 minutes adsorption the peak wavelength shifts from 532 to 543 nm. After that initial increase, there is hardly any change in the position of plasmon peak. PHEMA is a hydrophilic substrate in contrast to other substrates. Hence, the results are not surprising since the structure of the adsorbed protein layer depends on the nature of the adsorbing surface.

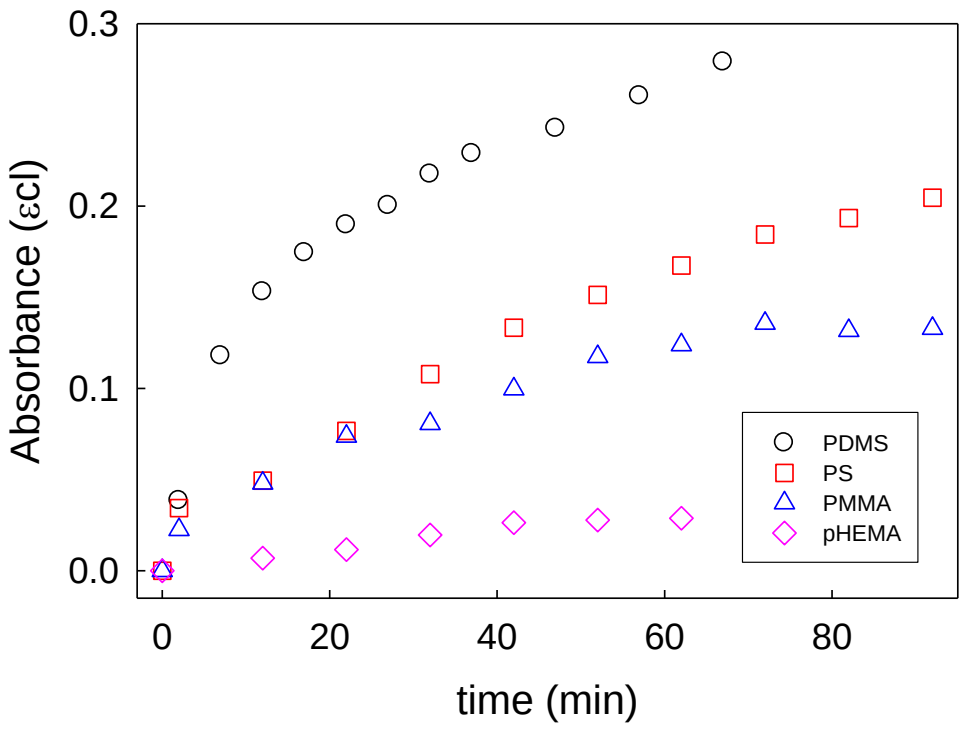

Figure 5.8 Variation in the absorbance (εcl) of BSA coated gold nanoparticles adsorbed onto polymer films vs. time. Error bars are smaller than symbols.

The change in the absorbance of BSA coated gold nanoparticles adsorbed on polymer films are shown in figure 5.8. Absorbance is the product of extinction (ε), concentration (c) and path length (l). Initially the absorbance is zero as no gold nanoparticles are attached to the polymer film. As BSA coated gold nanoparticles attach to the surface there is an increase in the absorbance value. Absorbance increases to about 0.3 after 67 minutes in case of PDMS. Even after 1 hour there is a rise in the absorbance value indicating that the surface is still not saturated.

For BSA/gnp adsorption onto PS, absorbance value changes from 0.03 at 2 minutes to nearly 0.24 after 92 minutes. The increase in absorbance indicates that an increasing number of BSA

coated gold nanoparticles attach to polystyrene surface as time progresses. Similar to the behaviour on PDMS surface, no saturation of adsorption occurs even after 90 minutes. The value of absorbance is lower on polystyrene surface (~0.16) as compared to PDMS surface (~0.26) after 60 minutes. This implies that more BSA coated gold nanoparticles attach to the PDMS surface as compared to polystyrene surface. The initial increase in absorbance value for BSA adsorption onto PMMA surface is the same as in the case of adsorption onto PS surface. After 20 minutes, differences begin to emerge. While the absorbance continues to rise at the same rate on PS, the rate of increase diminishes on PMMA as the surface begins to saturate. The rate of increase in the absorbance value is the slowest in case of adsorption on pHEMA indicating that extent of adsorption is the least in case of pHEMA . Our results agree with those reported by other authors that the extent of protein adsorption increases with the increase in hydrophobicity of the adsorbing surface.

5.3.2 Comparison of Adsorption Behaviour on PDMS, PS, PMMA and polyHEMA

The adsorption of BSA coated gold nanoparticles results in shifting of the resonance peak to increasingly longer wavelengths. This indicates that dielectric properties of the surrounding of the gold nanoparticles are changing. Although, attachment of nanoparticles to a surface also results in the shift of the resonance peak, this cannot alone explain the observed peak shifts. The observed peak shifts are related to the structure of the adsorbed protein layers. The values of peak wavelength and absorbance of BSA coated gold nanoparticles adsorbed on various surfaces

are listed in Table 5.1. The shift in the peak wavelength value of adsorbed BSA conjugated gold nanoparticles is smallest for polyHEMA surface followed by PS and the highest peak shift is observed for PDMS surfaces. Particle substrate coupling would bring about the same shift in the peak for all the polymer films. The fact that the observed shift in the peak is different for the three polymer shifts indicates that the adsorbed BSA film has different optical properties on the three films studied.

substrate	Shift in peak wavelength (nm)	absorbance
PDMS	23	0.2604
PS	19	0.1674
PMMA	17	0.1239
polyHEMA	11	0.0288

Table 5.1 Change in the position of plasmon peak and the absorbance of BSA coated gold nanoparticles adsorbed onto polymer films after 1 hour.

5.3.3 Difference absorption calculations

LSPR of nanoparticles is sensitive to the refractive index of the surrounding environment. The length scale of sensitivity of the nanoparticle to the surrounding environment is roughly equal to the dimensions of the nanoparticle. During the course of these experiments, more protein gets deposited over these immobilized nanoparticles. The extinction measured at a particular time is due to protein deposited at all times prior to that particular measurement. Extinction of each layer needs to be resolved for depth profiling measurements. This can be achieved if the

extinction of the adsorbed protein does not change appreciably over experimental time scales. For these measurements, we let BSA coated gold nanoparticles adsorb onto the polymer films and then replaced the gold nanoparticle/protein solution with PBS and let it sit for nearly 10 hours and recorded the absorption spectra every 20 minutes for those 10 hours. This study was conducted for adsorption times varying between 10 minutes and 2 hours.

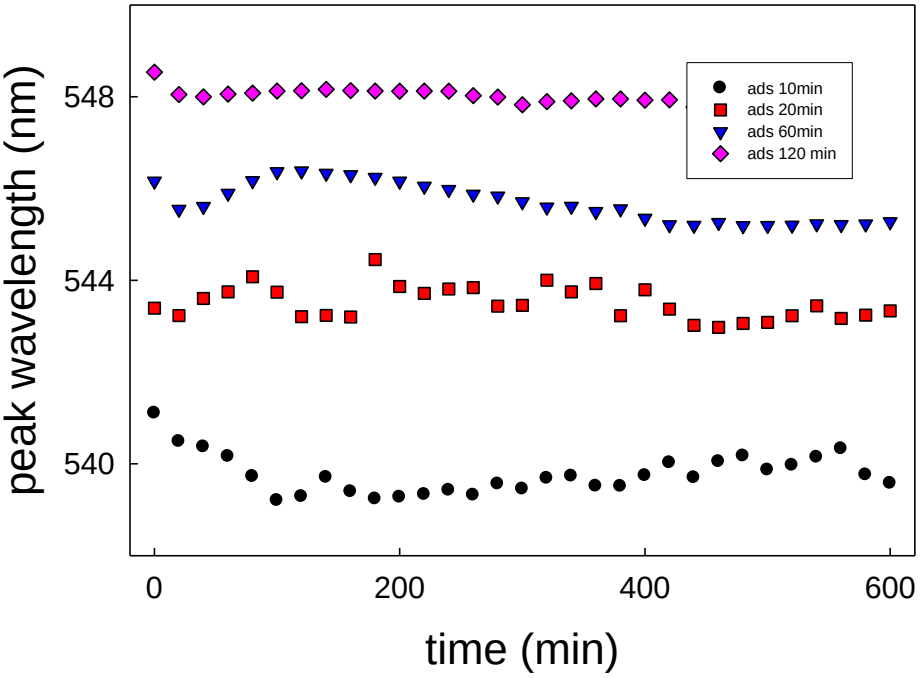

Figure 5.9 Variation in the peak wavelength of BSA coated gold nanoparticles adsorbed onto PDMS film in PBS vs. time

The variation in the peak wavelength for BSA coated gold nanoparticles adsorbed onto PDMS films are shown above. As is evident from the graph, peak wavelength value does not change

appreciably after adsorption. It is possible that every time PBS is added, it removes some loosely attached protein molecules.

Since there is no change in the adsorbed protein layer after adsorption, we can differentiate between extinction of each layer or each time interval. We can do this by calculating difference absorption spectra. Thus, if we have collected absorption spectra every 5 minutes, we take the absorption spectrum at one particular time interval (say at 10 min) and subtract the spectrum at time interval before it (i.e., at 5 min) to get the absorption spectrum for the time interval between 5 and 10 minutes. That can help us to calculate the optical properties of the molecules that adsorbed on the surface between 5 and 10 minutes. Extinction spectra of BSA coated gold nanoparticles adsorbed on polyHEMA surface after 10 and 20 minute exposures are shown in figure 5.14. The difference absorption spectrum obtained on subtracting the absorption spectrum at 10 minutes from that at 20 minutes is also shown in the same figure.

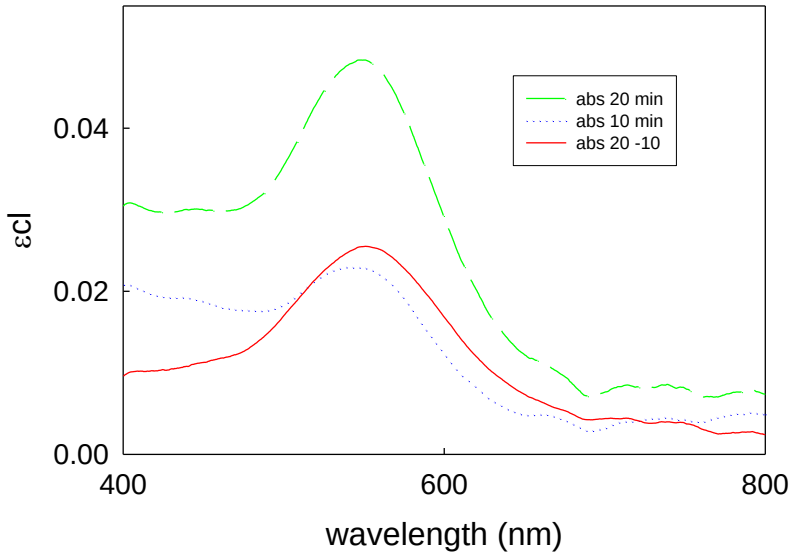

Figure 5.10 Absorption spectra of BSA coated gold nanoparticles adsorbed onto polyHEMA surface after 10 minutes (black short dash) and after 20 minutes (green long dash). Red solid line shows the difference absorption spectrum.

5.3.3.1 Difference absorption spectrum of BSA coated gold nanoparticles adsorbed on PDMS, PS, PMMA and polyHEMA

Peak wavelengths of difference absorption spectra of BSA coated gold nanoparticles absorbed onto PDMS, PS, PMMA and polyHEMA are shown in figures 5.11, 5.12, 5.13 and 5.14. With these spectra we can look at each individual layer. If we look at the trend in the peak wavelength values, the behaviour of each layer differs strikingly with substrate. On PDMS, the peak wavelength of the difference absorption spectra increases with time or the absorbed amount, reaches a peak value and then decreases again.

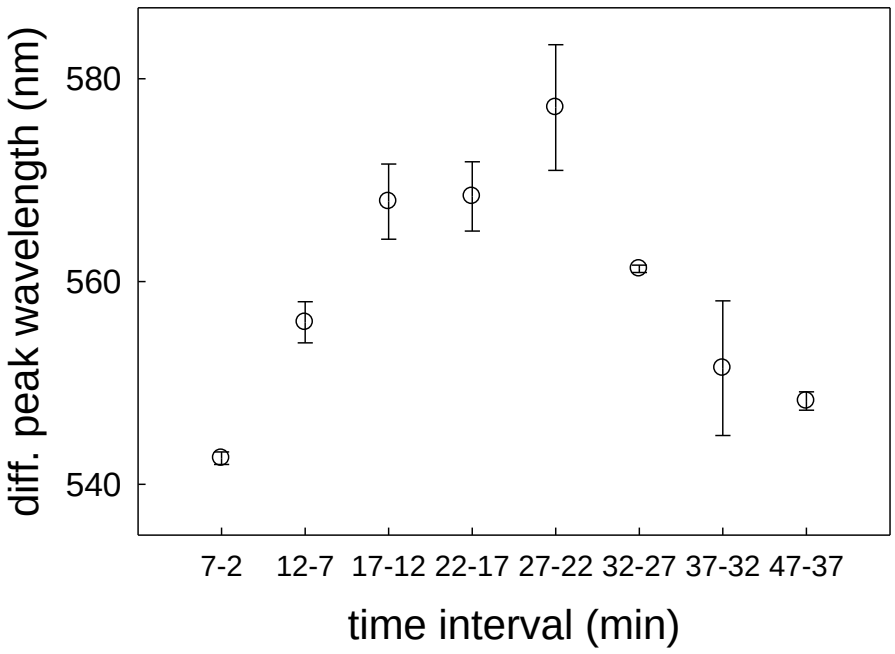

Figure 5.11 Peak wavelengths of difference absorption spectra of BSA coated gold nanoparticles adsorbed onto PDMS films vs. time interval.

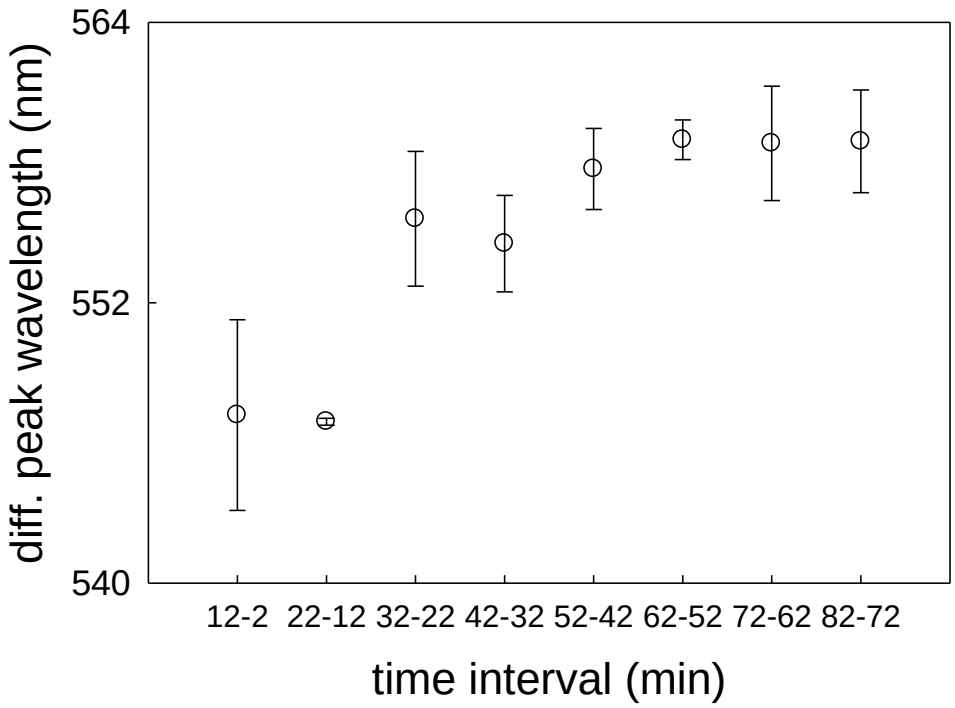

Figure 5.12 Peak wavelengths of difference absorption spectra of BSA coated gold nanoparticles adsorbed onto PS films as a function of time interval.

Peak wavelength of the difference absorption spectrum of BSA coated gold nanoparticles adsorbed on PS increases with time and finally attains an almost constant value (fig. 5.12). Peak wavelengths of difference absorption spectra of BSA coated gold nanoparticles adsorbed on PMMA increases with time and becomes nearly constant like in the case of PS. The behaviour of the protein on these substrates (PS and PMMA) is similar.

On polyHEMA the behaviour of gold nanoparticles is altogether different. The peak wavelength is first constant and then as the adsorbed amount increases peak wavelength value drops with time. Highest peak wavelengths are seen in case of adsorption on PDMS, followed by PS and the polyHEMA. This agrees with the data in table 5.1. It could be speculated that the

highest degree of structural change occurs in BSA on adsorption to PDMS, followed by PS and polyHEMA.

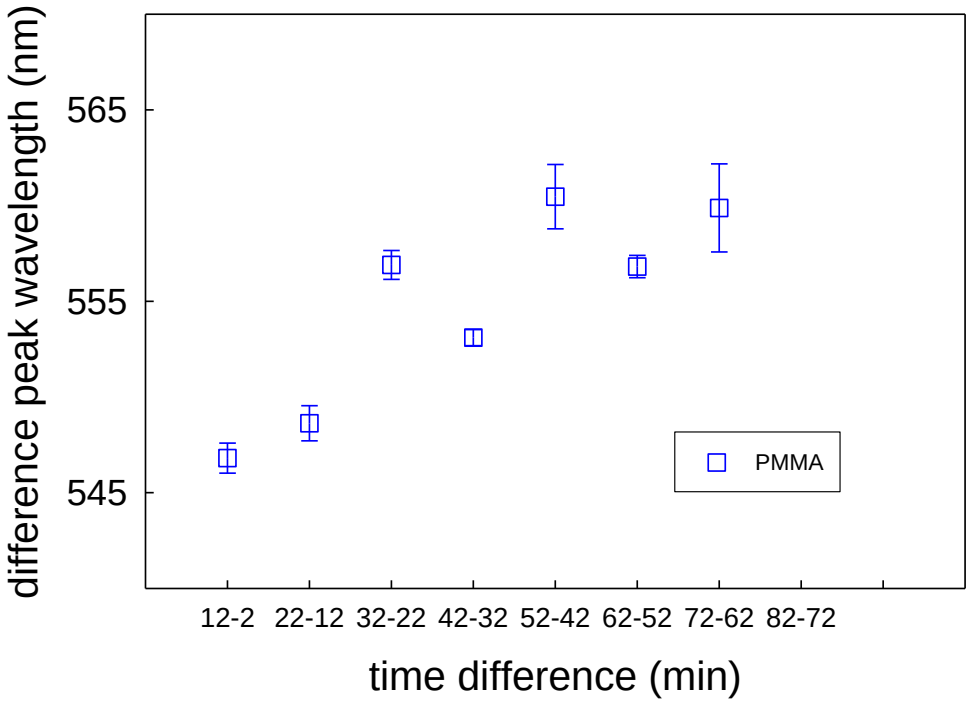

Figure 5.13 Peak wavelengths of difference absorption spectra of BSA coated gold nanoparticles adsorbed onto PMMA films vs. time interval

It is surprising that such variations are seen in the difference absorption peak positions due to absorption of the same protein. It is expected that adsorption of protein follows different patterns on hydrophilic and hydrophobic substrates. Such differences indeed emerge when we compare the trends in the diff. absorption spectra of BSA coated gold nanoparticles on pHEMA with other surfaces. However, other three surfaces PDMS, PS and PMMA are all hydrophobic. The trends observed in the position of difference absorption peaks for BSA coated gold nanoparticle adsorption on PDMS is vastly different from that observed on other hydrophobic substrates.

Unlike PS and PMMA, PDMS films not smooth. Roughness of the surface can also influence the adsorption of incoming protein molecules.

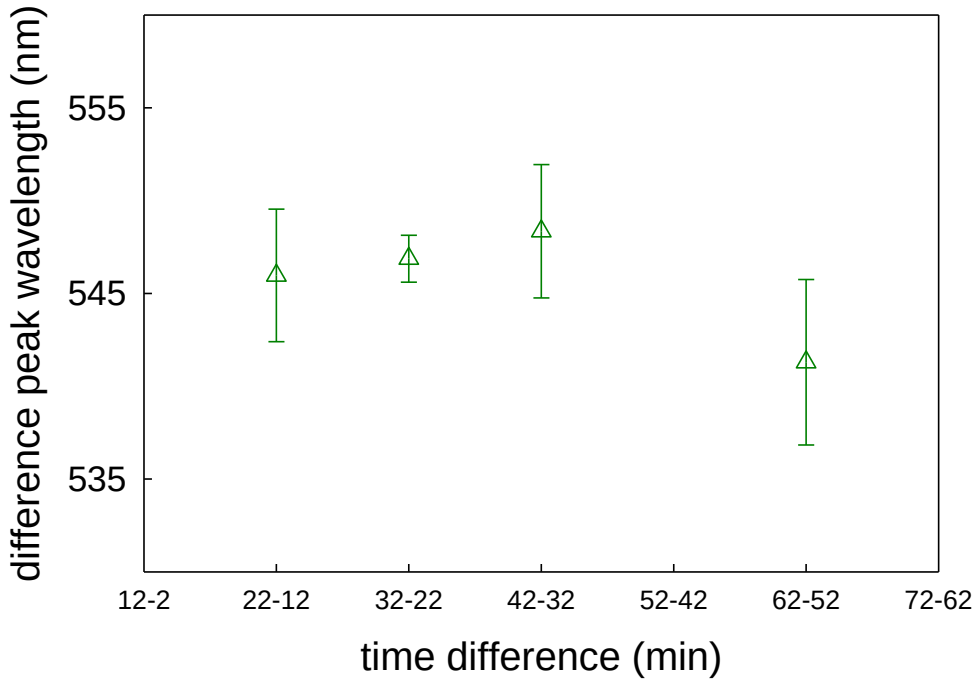

Figure 5.14 Peak wavelengths of difference absorption spectra of BSA coated gold nanoparticles adsorbed onto polyHEMA films vs. time interval.

5.3.3.2 Estimation of the thickness of the adsorbed layer

To evaluate the layer by layer adsorption behaviour of BSA adsorption on polymer, we calculated the thickness of the adsorbed BSA layer. For that purpose, we first calculated the concentration of gold nanoparticles. To calculate the concentration, we used optical density values of commercially available gold nanoparticles [357]. According to Ted Pella website, 30 nm gold nanoparticles having a concentration of 2 x 10^{11} particles/ml have an optical density (absorbance of the solution at wavelength value of 520 nm) of 1.0. Using that calibration, it was

found that gold nanoparticles used in this study had a concentration of 5.2 x 10^{11} particles/ml. We also know the number of BSA molecules present in the solution. The width of BSA layer adsorbed on gold nanoparticles calculated using contour plots for 30 nm gold particles (generated using Mie theory) as shown in figure 4.3 was 5 nm. The volume of that 5 nm thick layer is 19363 nm^3. On dividing the volume of this layer by the volume of a single BSA molecule (224 nm^3), we get that on average there are 86 BSA molecules on each nanosphere. Subtracting the number of BSA molecules attached to the gold nanospheres from the total number of BSA molecules in the solution gives us the number of free BSA molecules. Before centrifugation there are 6.2 free BSA molecules for every BSA molecule that is attached to the sphere. Upon centrifugation, nearly 90% of the free protein is removed. After centrifugation, for every BSA molecule attached to gold nanosphere, there are 0.6 free BSA molecules.

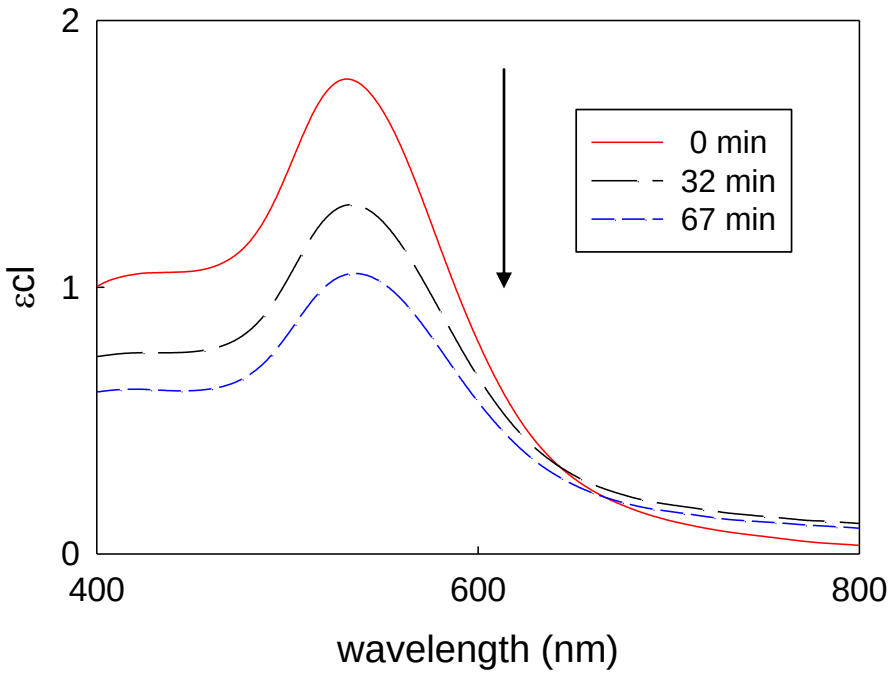

Figure 5.15 Absorption spectra of the gold nanoparticle solution. The arrow indicates increasing time.

During the course of the experiment we monitor the absorbance of the gold nanoparticle solution after exposure to the polymer films. Absorption spectra of gold nanoparticle solution after exposure to PDMS are shown in figure 5.15. We know the number of gold nanoparticles present initially in the sample. As time progresses, the number of gold nanoparticles left in the solution decreases. This is reflected in the decreasing extinction value (peak height) of the spectra. Since the decrease in the extinction corresponds to the decrease in the number of gold nanoparticles present in the solution, we can calculate the number of gold nanoparticles in the solution at successive time intervals from the absorbance value of the solution. The gold nanoparticles that are removed from the solution get attached to the polymer surface. Thus, we know the number of gold nanoparticles attached to the polymer surface. Figure 5.16 shows the absorbance of the solution and the calculated number of gold nanoparticles attached to the polymer surface.

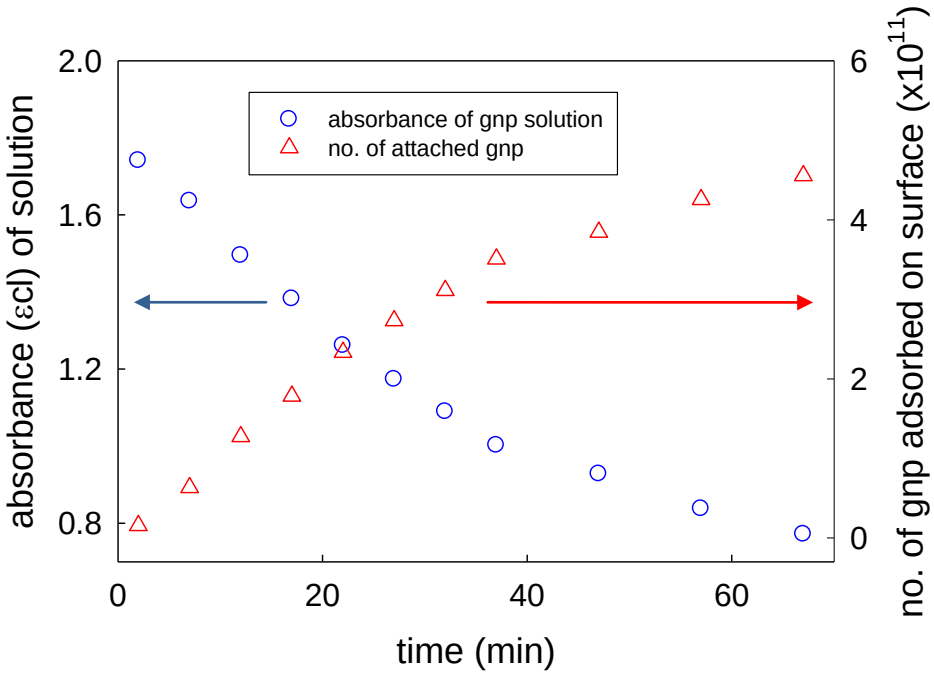

Figure 5.16 Axis on the left indicates the absorbance of the gold nanoparticle (gnp) solution (circles) vs. time. The right axis corresponds to the number of gold nanoparticles attached to the polymer surface (triangles) vs. time.

It is assumed that the change in extinction is only due to attachment of gold nanoparticles. Comparison of the change in extinction values due to adsorption of BSA with that of BSA/gold nanoparticle actually shows that the change in extinction due to gold nanoparticles is nearly 20 times that due to adsorption of BSA molecules (fig. 5.22). Since we know that for every BSA molecule attached to gold nanoparticle, there are 0.6 free BSA molecules, we can determine the number of free (not attached to the gold nanospheres) BSA molecules adsorbed on the polymer surface. Knowing the volume of single BSA molecule we can calculate the volume of adsorbed BSA layer (excluding gold nanoparticle). By dividing the volume of BSA layer by the total area on which the adsorption takes place, we can determine the thickness of the adsorbed BSA layer. Using the thickness of BSA layer at various times, we can plot the difference absorption curves

as function of layer thickness. Difference absorption plots for BSA adsorbed on PDMS and PS as function of layer thickness are plotted in figure 5.17 and 5.18.

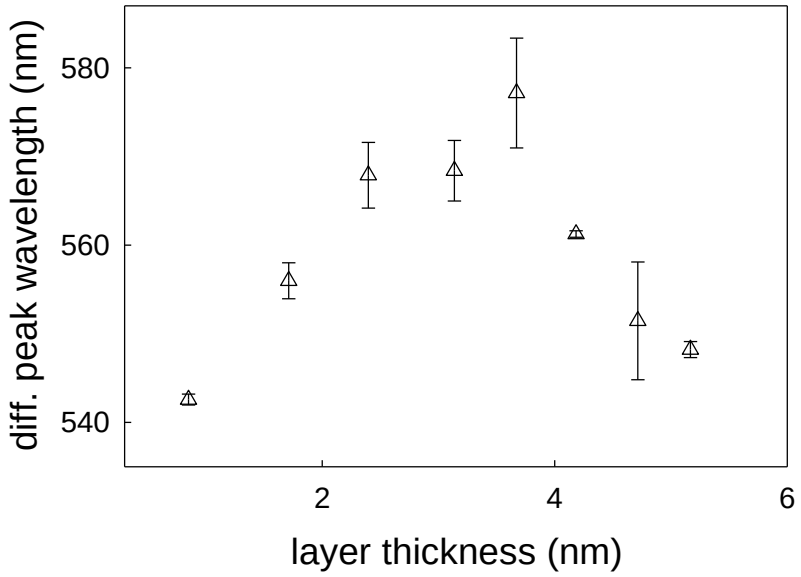

Figure 5.17 Peak wavelength values of difference absorption spectra as a function of thickness of BSA layer deposited on PDMS

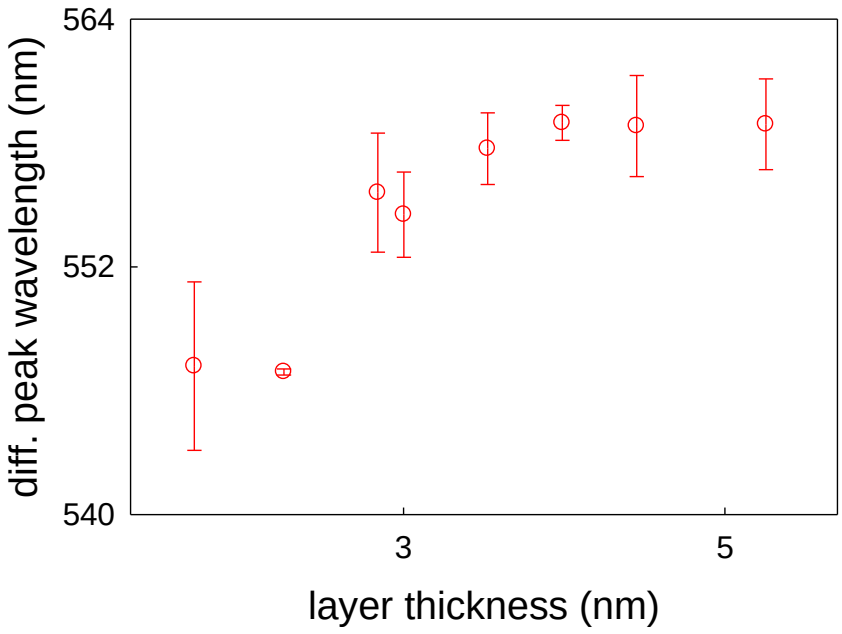

Figure 5.18 Peak wavelength values of difference absorption spectra as a function of thickness of BSA layer deposited on PS

Difference absorption curves represent the extinction spectrum of a particular layer. As is evident from the graphs, peak position of each layer varies with the distance from the substrate. For BSA adsorbed on PDMS, there occurs a maximum in the peak wavelength value at a distance of nearly 4 nm from the surface. For BSA adsorbed on PS, the peak wavelength value becomes nearly constant after 3 nm. Comparison of PDMS and PS surface indicates that the peak position of each layer depends on the nature of the substrate. Further, the values of the plasmon peak also vary from one substrate to another. Highest value for peak wavelength in case of PDMS is ~ 580, while that for PS is ~ 560. Thus, these curves qualitatively show that protein adsorbed close to the surface behaves differently as compared to protein molecules farther from the surface. Further, the behaviour of these different layers of the adsorbed system (free BSA and BSA coated gold nanoparticles) depends upon the nature of the substrate, but we cannot make

quantitative comparisons based on these curves. To obtain optical parameters such as refractive index, we have to look at some theoretical models.

5.4 Adsorption Kinetics

The kinetics of adsorption of BSA on PDMS, PS, PMMA and pHEMA are shown in figure 5.19. The final adsorbed amounts are the highest on PDMS, followed by PS, PMMA and pHEMA. This is in accordance with the hydrophobicity of the adsorbing surface. Not only does the final adsorbed amount depend on the nature of the adsorbent, even the rate of adsorption varies with the nature of the polymer surface.

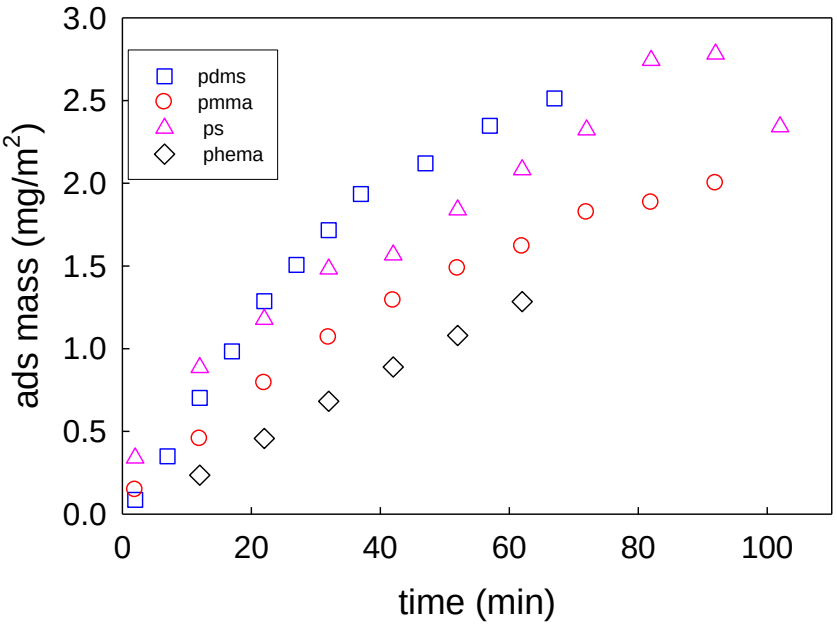

Figure 5.19 Variation in the surface density of BSA with time on PDMS, PS, PMMA and pHEMA.

5.5 Theoretical Analysis

The first model that we tried was that of a coated sphere embedded in a uniform medium used to calculate the thickness and refractive index of the protein layer adsorbed onto gold nanoparticles. However, this model cannot be used for coated gold nanospheres adsorbed on a substrate. The huge shifts (≥ 20 nm) observed on adsorption of gold nanoparticles on a surface are due to nanoparticle substrate coupling [358, 359], which are not taken into account in this model. Even heat denaturation of BSA adsorbed on gold nanoparticles causes shifts of about 3-4 nm [253].

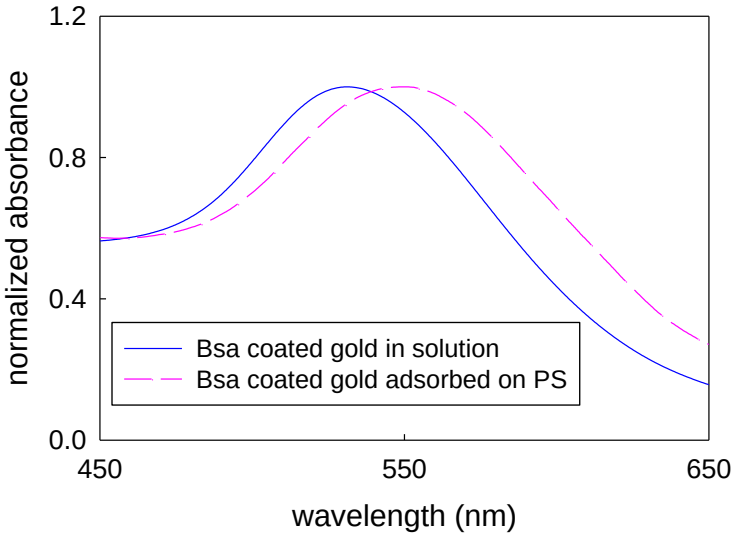

Figure 5.20 Absorption spectra of BSA coated gold nanoparticles in solution and those adsorbed onto Polystyrene surface.

Then, we looked at the experimental configuration of Okamoto and coworkers which is similar to ours [248]. The authors immobilized gold nanoparticles on a transparent substrate and monitored the extinction spectra of these immobilized gold nanoparticles after coating them with poly-(methyl methacrylate) (PMMA). Coating of these gold nanoparticles with PMMA film

causes a change in both the position and intensity of LSPR peak. An increase in the thickness of the PMMA film results in a corresponding increase in both wavelength as well as intensity of the resonance peak (fig. 2.2). Xu and Kaell developed a theoretical model based on extended Mie theory to calculate the optical response of gold nanoparticle deposited on a transparent substrate in a non absorbing medium [252]. The model took into account a coating layer, surrounding medium, interparticle coupling effects as well as particle-substrate coupling. Their theoretical predictions agree well with experimental results of Okamoto and Yamaguchi [248]. The electromagnetic field extending around a nanoparticle varies depending on the size of the particle [252]. For particles small compared to the wavelength of the light, i.e. in the Rayleigh limit the intensity of plasmon resonance I_{local} at distance r decays approximately as

$$I_{local} \propto (\,^{r_o}/_{r})^6 \qquad (5.1)$$

where r_o is the radius of the particle. Using this approximation the authors defined an effective refractive index (n_{eff}) of the medium surrounding the gold nanoparticle.

$$n_{eff} \equiv \frac{n_2 \int_{r_o}^{r_o+d} 4\pi r^2 \left({}^{r_o}/_{r}\right)^6 \partial r + n_1 \int_{r_o+d}^{\infty} 4\pi r^2 \left({}^{r_o}/_{r}\right)^6 \partial r}{\int_{r_o}^{\infty} 4\pi r^2 \left({}^{r_o}/_{r}\right)^6 \partial r} \qquad (5.2)$$

$$= n_2 - \frac{n_2 - n_1}{(1 + \left({}^{d}/_{r_o}\right))^3}$$

Here n_1 is the refractive index of the non absorbing medium, n_2 is the refractive index of the coating, d is the thickness of the coating. We know that the for small spherical metallic nanoparticles, condition for LSPR to occur is,

$$\varepsilon_r + 2\varepsilon_m = 0, where\ \varepsilon_m = n_{eff}^2 \qquad (5.3)$$

where ε_r is the real part of the metal dielectric function and ε_m is the dielectric constant of the medium.

Further, since the real part of the metal dielectric function varies slowly with wavelength, we can neglect the higher order terms in the expression, i.e. $\varepsilon_r \approx a - b\lambda$. Here a and b are constants depending on the nature of the material (gold in our case). Peak shift is calculated as

$$\Delta\lambda \approx c\left[n_2^2\left(1 - \frac{1 - \left({}^{n_1}/_{n_2}\right)}{\left(1 + \left({}^{d}/_{r_o}\right)\right)^3}\right)^2 - n_1^2\right] \qquad (5.4)$$

Here c = 2/b is the fitting parameter.

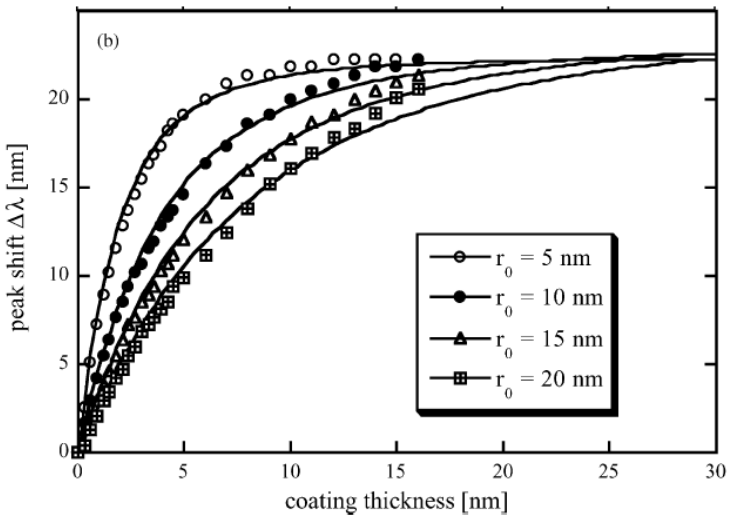

Fig 5.21 Comparison of the peak shifts obtained using full calculations (symbols) and single parameter fits using eq. 5.4 (lines) for gold nanoparticles with radius 5, 10, 15 and 20 nm vs. thickness of the coating. (Figure taken from ref. 252)

Figure 5.21 compares peak shifts obtained from full calculations using Mie theory and those obtained using equation 5.4 for gold nanospheres coated with PMMA films of varying thicknesses. It is evident from the figure above that there is an excellent agreement between the peak shifts calculated using a simple analytical model described by equation 5.4 and those using full calculations of extended Mie theory.

In our experiment BSA coated gold nanoparticles stick to polymer surfaces. As a first approximation to explain the results, we used the analysis of Xu and Kaell to develop a multilayer model of coated gold nanoparticles adsorbed on a substrate. In this model coated gold nanoparticles are attached to the substrate and are coated by a series of layers (see figure 5.22). In the figure n_p is the refractive index of the non absorbing medium, n_1, n_2, $n_{3\ldots}$ are the refractive indices of the adsorbed layers, d_1, d_2, d_3….. are the thicknesses of the adsorbed layers.

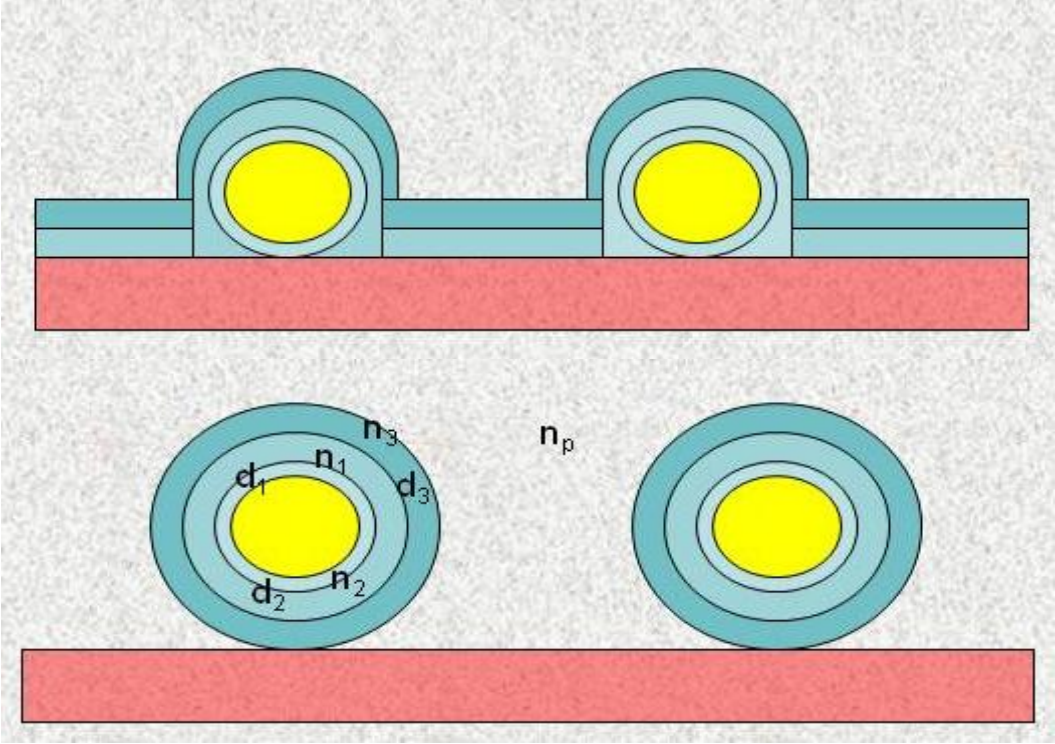

Figure 5.22 Schematic of the experimental configuration (top) and model of multilayer coated gold nanoparticle adsorbed on the substrate (bottom)

In our model the gold nanoparticles are immobilized on the substrate, while the protein layers build up one by one. In the experimental setup, protein coated gold nanoparticles are not all adsorbed to the surface in one step. Rather, the adsorption takes place in steps on successive exposure of the protein/nanoparticle solution to the polymer coated surfaces. As a control experiment, we actually ran a trial where BSA coated gold nanoparticles were initially adsorbed on PS biomaterial for 5 minutes and then this surface was exposed to BSA solution at a concentration of 2.0 μg/ml (the same concentration as that found in BSA/nanoparticle solution). The peak shifts and extinctions are plotted in figure 5.23. The peak shifts due to adsorption of BSA molecules and those due to BSA/gold nanoparticle solution are equal within experimental uncertainty. Therefore, the model developed to probe the changes in the peak positions of

immobilized gold nanoparticles due to deposition of protein layers was used to calculate peak shifts due to deposition of protein/gold nanoparticle layers. The change in extinction is almost entirely due to adsorption of gold nanoparticles (fig 5.23).

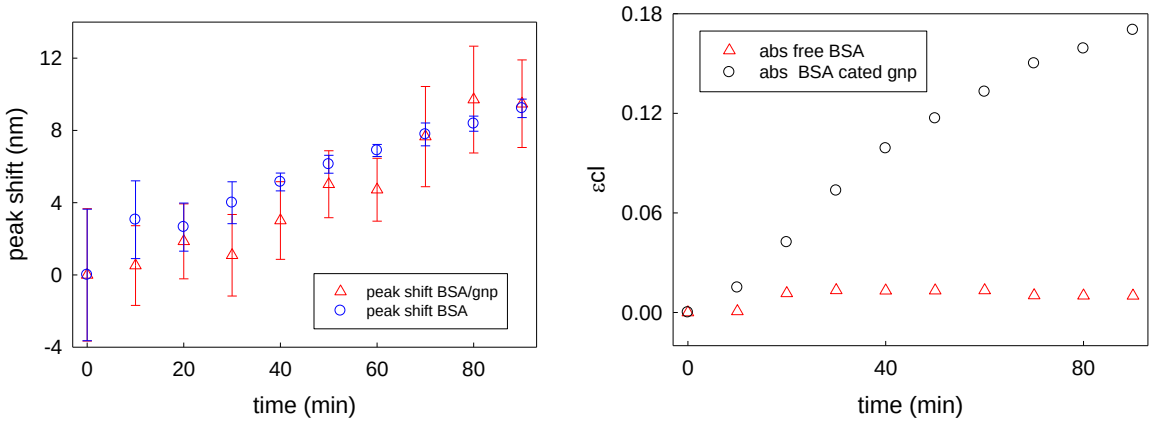

Figure 5.23 Comparison of peak shifts (left) and extinction (right) due to adsorption of BSA/gold nanoparticle solution (triangles) and BSA solution without gold nanoparticles (circles).

For the case of N layer coating, the effective refractive index of the medium is then given as

$$n_{eff} \equiv$$

$$\frac{n_1 \int_{r_o}^{r_o+d} 4\pi r^2 \left({}^{r_o}/_{r}\right)^6 \partial r + \sum_{i=2}^{N} n_i \int_{r_0+d_{i-1}}^{r_0+d_{i-1}+d_i} 4\pi r^2 \left({}^{r_o}/_{r}\right)^6 \partial r + n_p \int_{r_o+\sum_{i=1}^{N} d_i}^{\infty} 4\pi r^2 \left({}^{r_o}/_{r}\right)^6 \partial r}{\int_{r_o}^{\infty} 4\pi r^2 \left({}^{r_o}/_{r}\right)^6 \partial r} \quad (5.5)$$

The corresponding peak shift is given as

$$\Delta\lambda \approx$$

$$c\left[\left(n_1 - \frac{n_1 - n_2}{\left(1 + \left(\frac{d_1}{r_0}\right)\right)^3} - \frac{n_2 - n_3}{\left(1 + \left(\frac{d_1 + d_2}{r_0}\right)\right)^3} \ldots\ldots\ldots\ldots - \frac{n_N - n_p}{\left(1 + \left(\frac{\sum_{i=1}^{N} d_i}{r_0}\right)\right)^3}\right)^2 - n_p^2\right] \quad (5.6)$$

5.4.1 Simulation results

Using equation 5.2, we can calculate how the effective refractive index of the medium would vary as function of the layer thickness. Data for 30 nm (diameter) gold nanoparticles immobilized on a transparent substrate coated with layers of varying refractive indices is shown in figure 5.24. The refractive index of the medium is taken to be equal to 1.33. As is evident from the graph; as the thickness of the coating increases, the effective refractive index of the medium also increases. For the same layer thickness value, higher the refractive index of the coating layer, higher is the effective refractive index. Comparison of the initial slopes of the two extreme cases (1.4 and 1.7) shows that the effective refractive index rises more rapidly if the refractive index of the layer is 1.7 as compared to the case where the refractive index of the layer is 1.4.

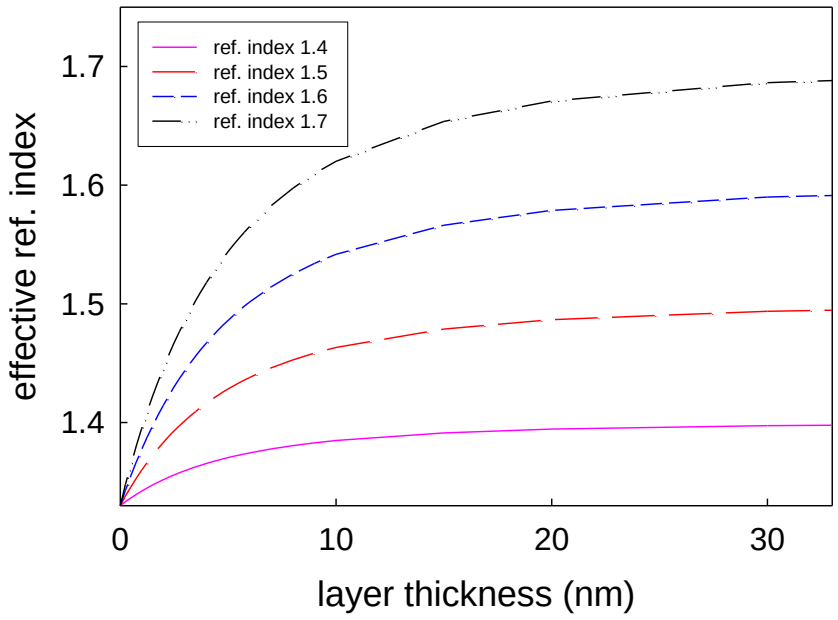

Figure 5.24 Effective refractive index of the medium surrounding 30 nm gold nanoparticles vs. thickness of the coating.

Figure 5.25 illustrates the effect of radius of the nanosphere on the effective refractive index. The refractive index of the coating is taken as 1.57. The effective refractive index rises more rapidly for smaller spheres as compared to larger spheres. At the same time, the coating thickness value for which no change in the effective refractive index is measureable increases with the increase in the radius of the sphere.

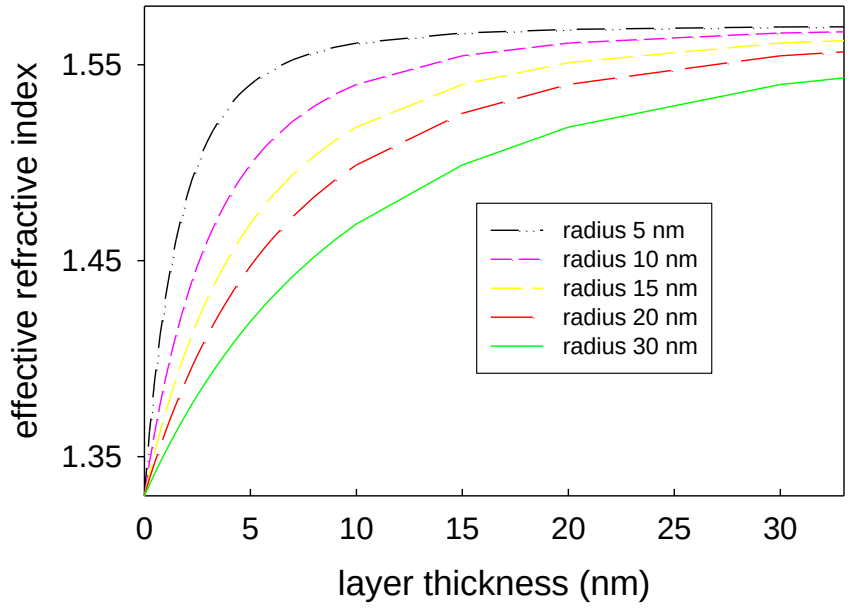

Figure 5.25 Effect of radius of the nanosphere on the effective refractive index

Using equation 5.4, we can calculate the peak shifts if thickness and refractive index of the coating are known. Variation of peak shift with the refractive index of a single layer is shown below in figure 5.26 for different c values. The value of this parameter can lead to different values of the peak shift even when all other variables are kept the same. It is clearly evident from the figure above that for a 10 nm thick layer; change in the value of c from 1 to 50 results in 25 fold increase in the peak shift. Henceforth, the value of c is taken to be 29 from the data of Johnson and Christy [360].

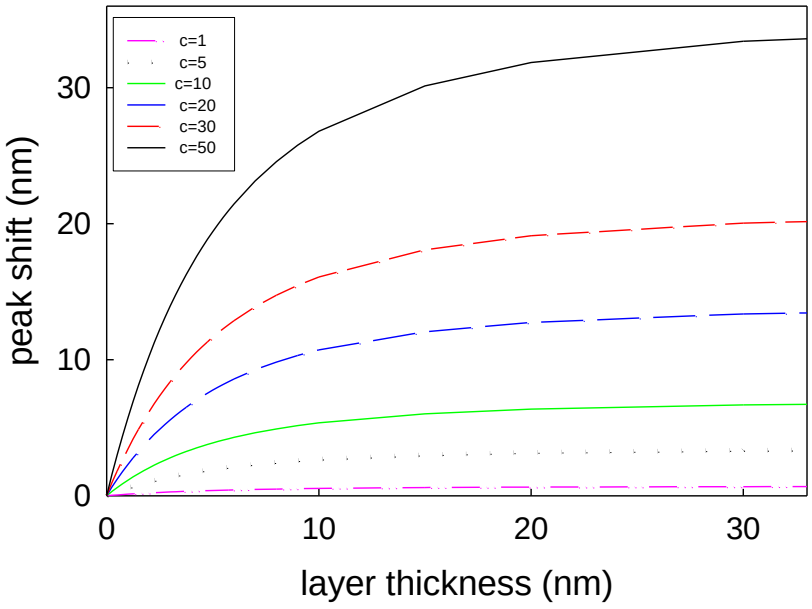

Figure 5.26 Peak shift for 30 nm gold nanoparticles vs. coating thickness for various c values.

The variation of peak shift for 30 nm gold nanoparticles coated with layers of varying thickness is shown in figure 5.27. For constant refractive index value, as the thickness of the layer increases, the magnitude of the peak shift also increases. For a particular thickness, an increase in the refractive index results in bigger peak shift. For a thicker layer, a similar change in the refractive index of the layer results in bigger shift in the peak value, There is sharp increase in peak shift when the coating thickness increases from 1 to 5 nm. Further increase to 10 nm results in a smaller change in peak width. As the width of the layer increases beyond 15 nm, there is relatively little change in the peak wavelength value.

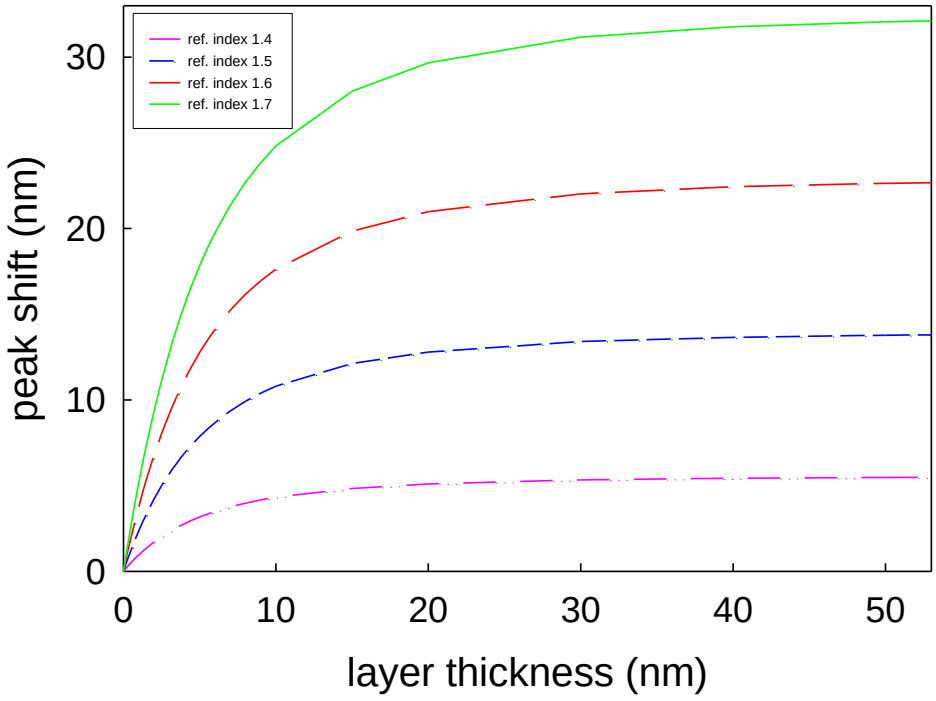

Figure 5.27 Variation of peak shift vs. thickness of the coating layer for various refractive index of the coating layer.

The sensitivity to peak shift also depends on the size of the gold nanoparticle. Variation in the peak shift with coating thickness for spheres of various radii is shown in figure 5.28. The refractive index of the layer is 1.57. For thin layers (< 5 nm) 5 nm spheres show the maximum value of peak shift. As the thickness of the coating increases, peak shift for 5 nm spheres reaches saturation while a shift in the peak is still observable for bigger nanoparticles. Smaller nanoparticles show higher sensitivity (peak shifts) for thinner coatings while bigger nanoparticles are more sensitive for thicker coatings. In other words, bigger nanoparticles can probe larger area as compared to smaller nanoparticles.

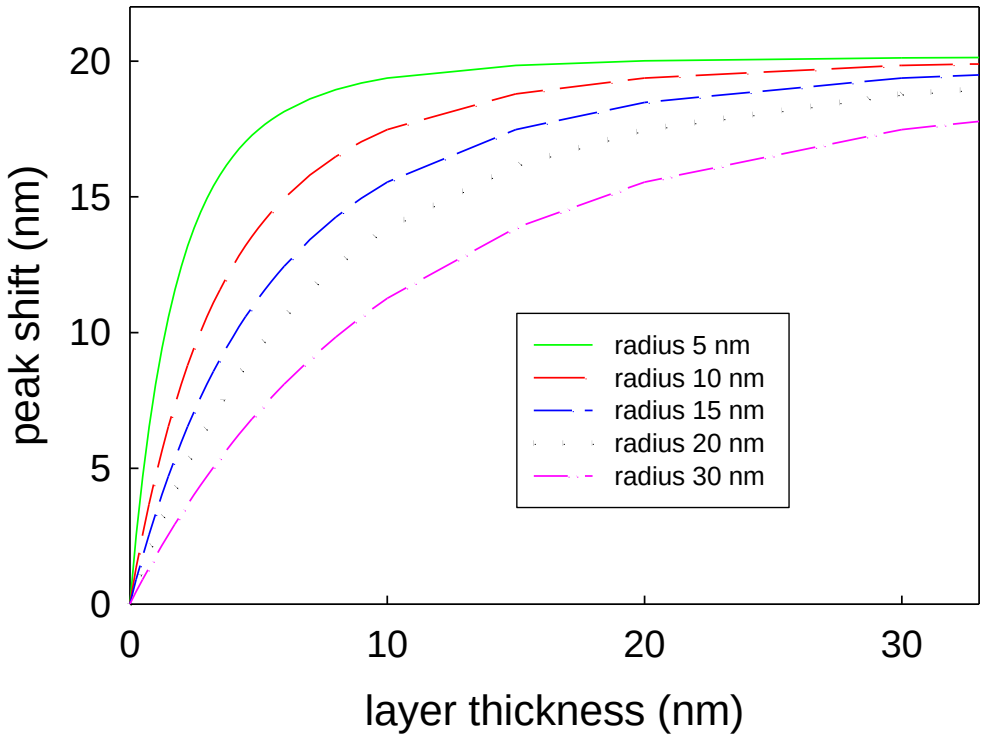

Figure 5.28 Variation in peak shift with the thickness of the coating layer for gold nanospheres of different radii.

Next, we considered how the variation in the refractive index of successive layers would change the position of the plasmon peak. We looked at the following scenarios: (a) layers of constant refractive indices, (b) layers of constantly increasing refractive index, (c) layers with first increasing and then decreasing refractive index, (d) layers of first increasing and then constant refractive index, (e) layers with stepwise decrease in refractive index. Similar trends of layer build up have actually been experimentally observed in ellipsometry studies [182]. We calculated peak shifts for all the above mentioned scenarios using equation 5.6. The refractive

indices and the corresponding peak shifts for all the above scenarios are presented below (figure 5.29 a-e).

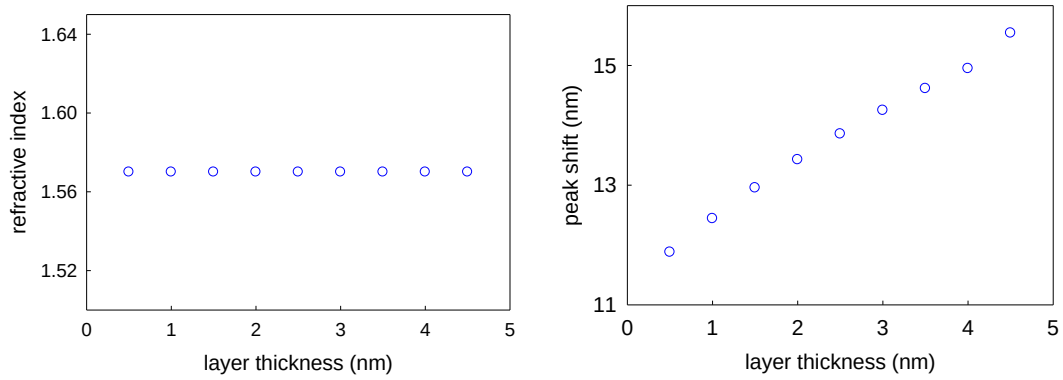

Figure 5.29 (a) Variation in refractive index of nanoparticle coating vs. distance from the nanoparticle surface (left). On right peak shifts vs. distance from nanoparticle surface corresponding to scenario b are plotted.

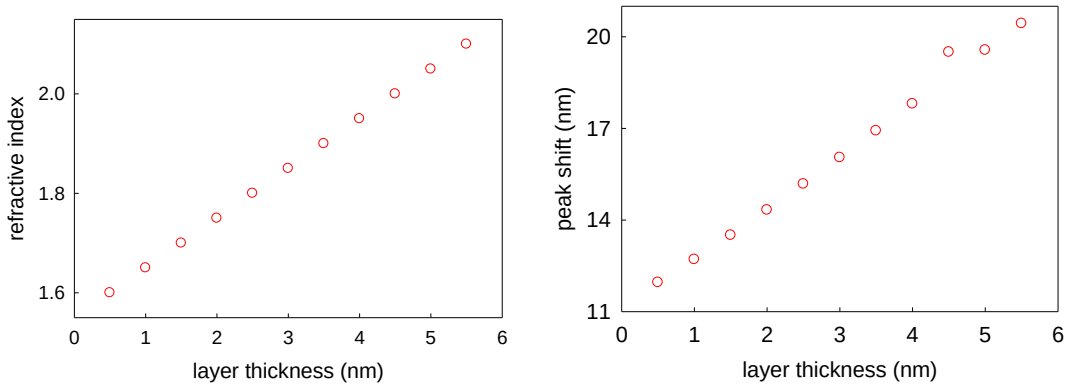

Figure 5.29(b) Variation in refractive index of nanoparticle coating vs. distance from the nanoparticle surface (left). On right peak shifts vs. distance from nanoparticle surface corresponding to scenario b are plotted.

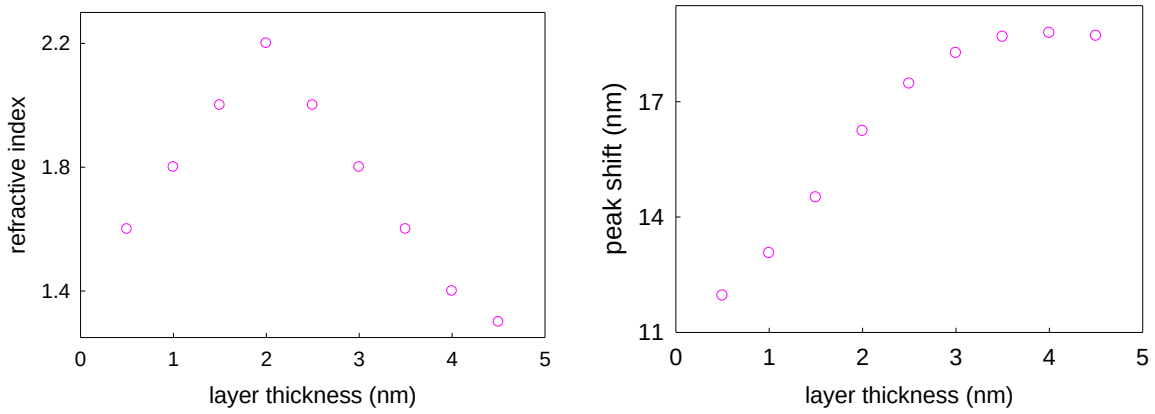

Figure 5.29 (c) Variation in refractive index of nanoparticle coating vs. distance from the nanoparticle surface (left). On right peak shifts vs. distance from nanoparticle surface corresponding to scenario b are plotted.

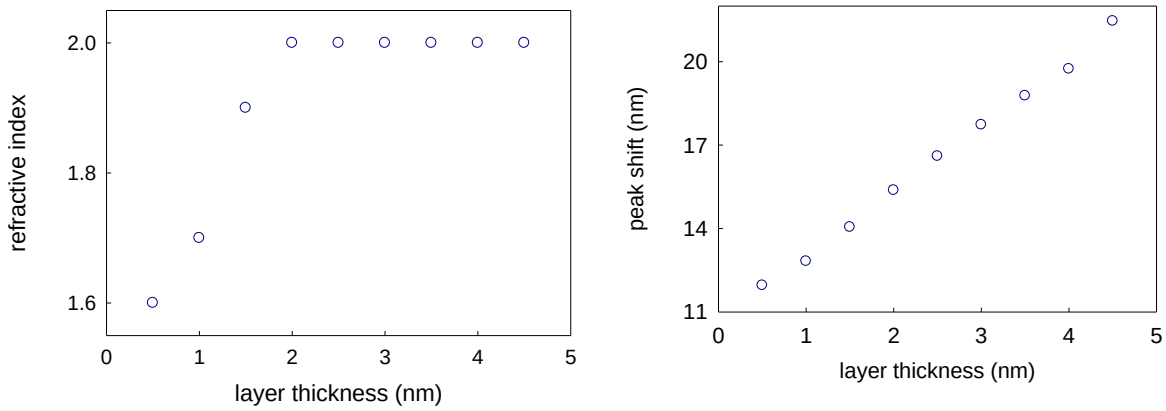

Figure 5.29 (d) Variation in refractive index of nanoparticle coating vs. distance from the nanoparticle surfaces (left). On right peak shifts vs. distance from nanoparticle surface corresponding to scenario d are plotted.

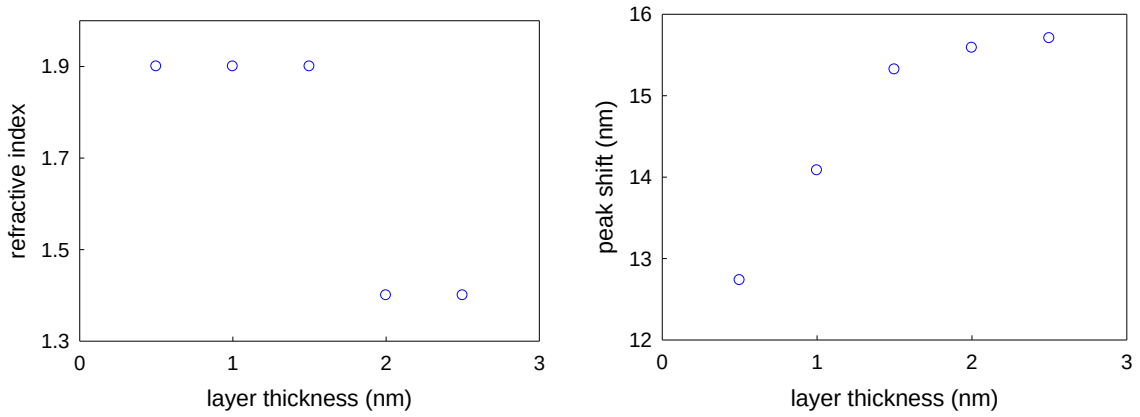

Figure 5.29 (e) Variation in refractive index of nanoparticle coating vs. distance from the nanoparticle surfaces (left). On right peak shifts vs. distance from nanoparticle surface corresponding to scenario d are plotted.

Figures 5.29 (a-e) demonstrate how this simple analysis can predict the peak wavelengths for various cases in which each successive layer s different refractive index value. A continuous increase in the peak shift is obtained in three cases (a) if the refractive index of the incoming layers is constant, (b) each successive layer has a higher refractive index than the one preceding it, (c) if the refractive index of the incoming layers first increases and then becomes constant. As long as the refractive indices of the successive layers increase or stay constant, a continuous shift in peak wavelength to higher values is observed. However, the magnitude of the total shift differs depending on the actual value of the refractive indices. If the refractive index of the adsorbing layers first increases and then decreases (fig. 5.29 c) or there is a step wise decrease in the refractive index of the following layers (fig. 5.29 e), the peak shifts first increase with increasing thickness and then becomes nearly constant.

5.4.2 Refractive Index Profile of BSA adsorbed on PS, PMMA, pHEMA and PDMS

There are some limitations of the model. First of all, we are using only an approximation and not the full Mie theory. As is evident from the graph 5.21, there is some deviation between calculations using Mie theory and the approximation as the coating thickness increases. Further, we also neglect the nanoparticles adsorbing at later stages. As the thickness of the layer increases, the nanoparticle effectively moves away from the substrate. Hence, the influence of the substrate decreases with increasing layer thickness. The sensitivity of the peak shift to the refractive index of the layer also decreases with increasing layer thickness (figure 5.30).

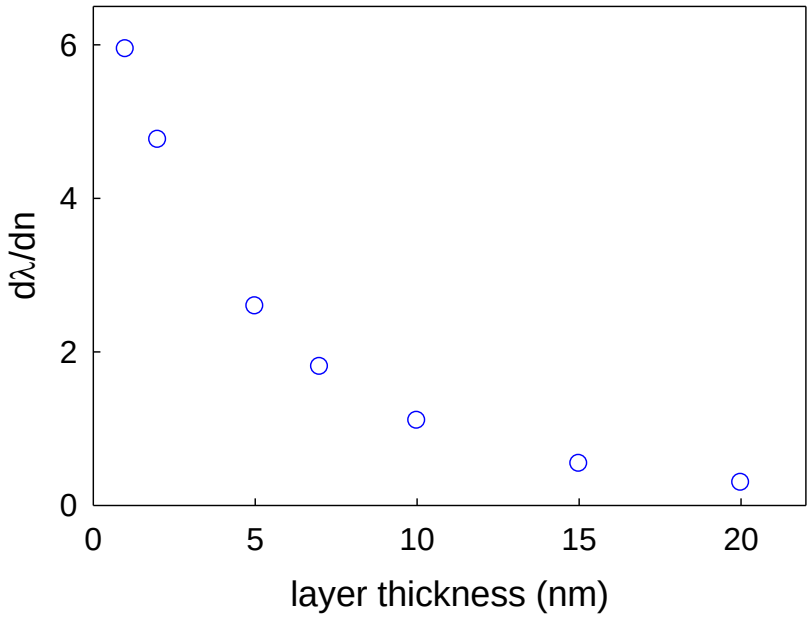

Figure 5.30 Variation in the sensitivity of shift in the peak to refractive index of the layer as a function of layer thickness

Therefore, although we cannot use the model to actually calculate the refractive index of the layers, we can use the model to compare the refractive indices of BSA adsorbed on various polymers. The refractive index values for BSA adsorbed on various polymers (PS, PMMA and pHEMA) are shown in figure 5.31.

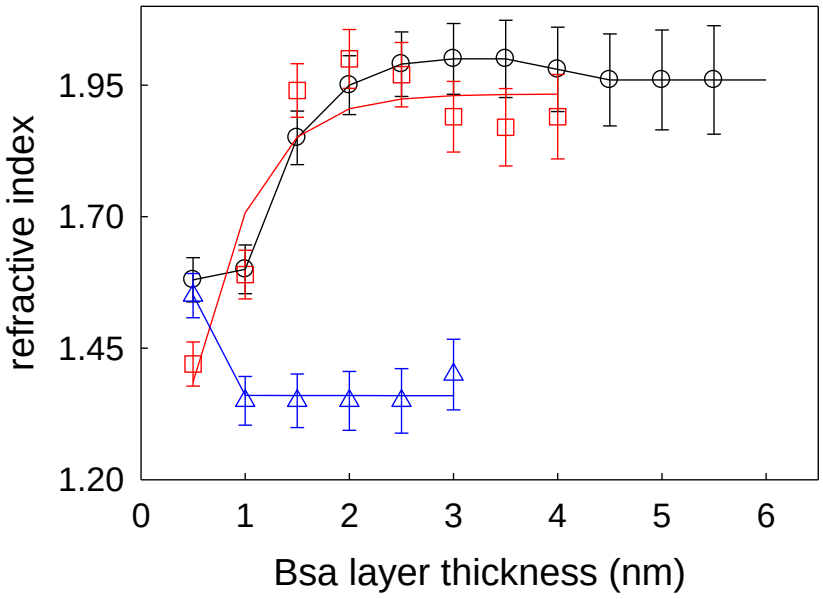

Figure 5.31 Refractive index profile of BSA adsorbed on PS (circles), PMMA (squares) and pHEMA.

Clearly the refractive index profile of BSA is different on hydrophobic substrates (PS and PMMA) as compared to hydrophilic substrates (pHEMA). Initially BSA has similar values of refractive index on these substrates. However, as the layer builds up, while the refractive index of BSA on pHEMA decreases, the incoming layers on hydrophobic substrates increases and finally attains a constant value. The refractive index profile of BSA on PDMS is shown below.

Although PDMS is also hydrophobic, the refractive index profile of BSA on PDMS does not resemble the profile on other hydrophobic substrates. PDMS is not only more hydrophobic, it is also rough as compared to PS and PMMA. The effect of surface roughness is explained in the following section.

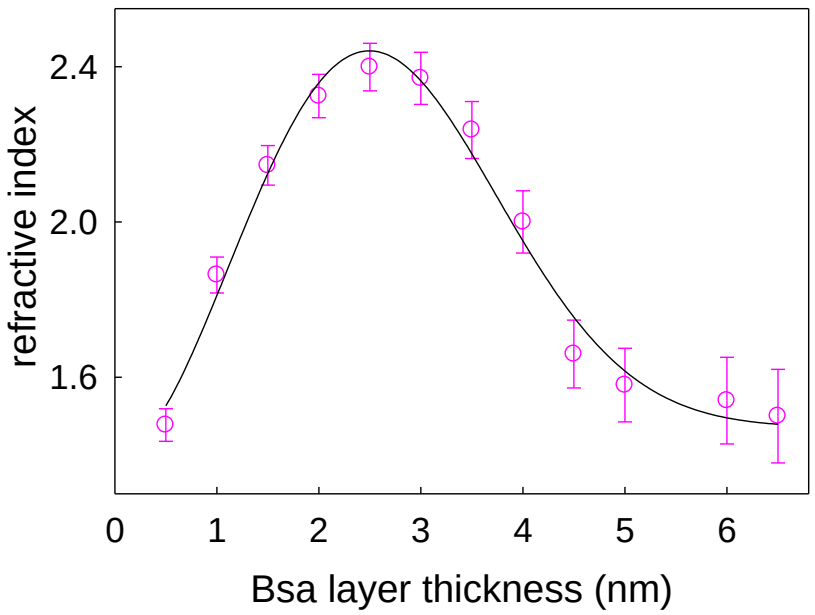

Figure 5.31 Refractive index profile of BSA adsorbed on PDMS

5.5 Effect of Surface Roughness

To monitor the influence of surface roughness, we artificially roughened the sides of PS cuvette by swiping the sides with Kim wipe dipped in toluene. The kinetics of adsorption of BSA on smooth and roughened PS surface are shown in figure 5.32. Adsorption of BSA on rough PS

surface was performed four time. Data for all four runs is shown in figure 5.32. Initially, the rate of adsorption is higher on smooth PS surface as compared to rough surface. Roughness of the surface seems to provide a barrier to adsorption in the initial stages. The refractive index profile of BSA adsorbed on rough and smooth PS surface is shown in 5.33.

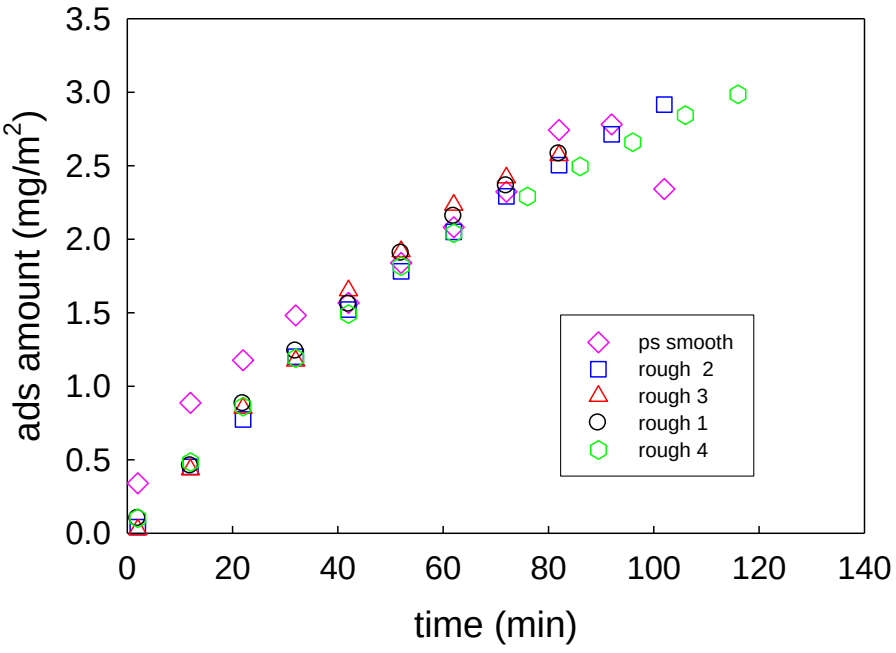

Figure 5.32 Variation in the surface density of BSA adsorbed on smooth (diamonds) and rough PS surfaces

The refractive index profile of BSA adsorbed on roughened PS surface is similar to the refractive index profile of BSA on PDMS surface. Hence, it is the surface roughness of PDMS which causes BSA to behave differently on PDMS as compared to PS and PMMA.

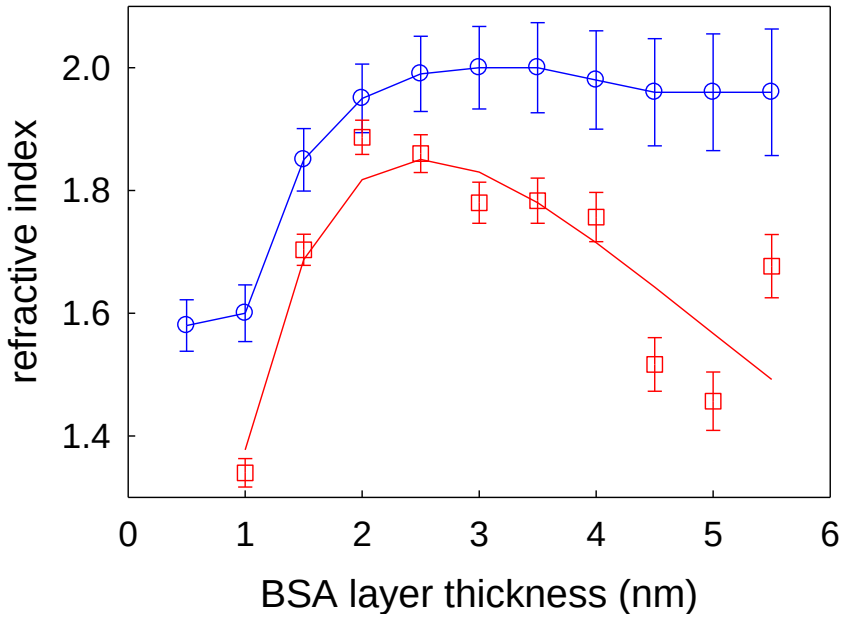

Figure 5.33 Comparison of refractive index profile of BSA on rough (square) and smooth (circle) PS surface.

5.6 Adsorption of denatured BSA

To evaluate the difference in the refractive index profile of BSA in native state and denatured state, we heated BSA coated gold nanoparticles at 95°C for 20 hours and studied the adsorption of denatured BSA on smooth PS surface. Adsorption kinetics of native state and denatured BSA adsorption on PS surface is shown below (figure 5.34). Rate of adsorption of denatured BSA is much higher than that of native state BSA. In the same time the surface density of denatured BSA is 3 times that of native state BSA. The refractive index profiles of denatured and native

state BSA are shown in figure 5.35. Whereas, adsorption of native state BSA results in layer thickness of 5 nm, adsorption of denatured BSA leads to a layer thickness of 14 nm (figure 5.35).

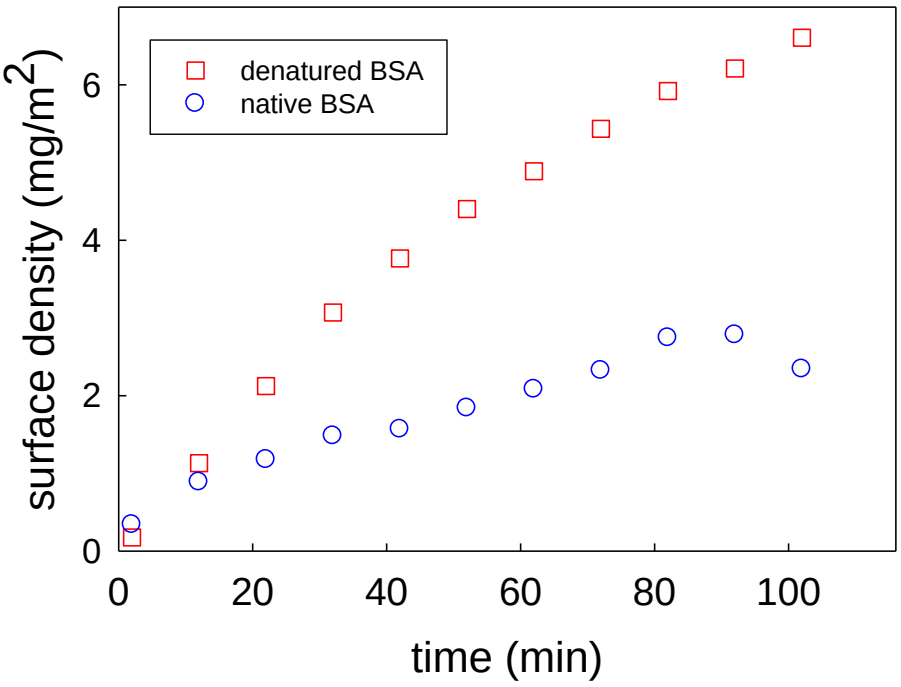

Figure 5.34 Comparison of the change in surface density of denatured (square) and native state (circle) BSA with time on PS surface

As is evident from the graph, the refractive index profile of denatured BSA differs significantly from that of native state BSA. Thus, the model can differentiate native state protein from denatured protein.

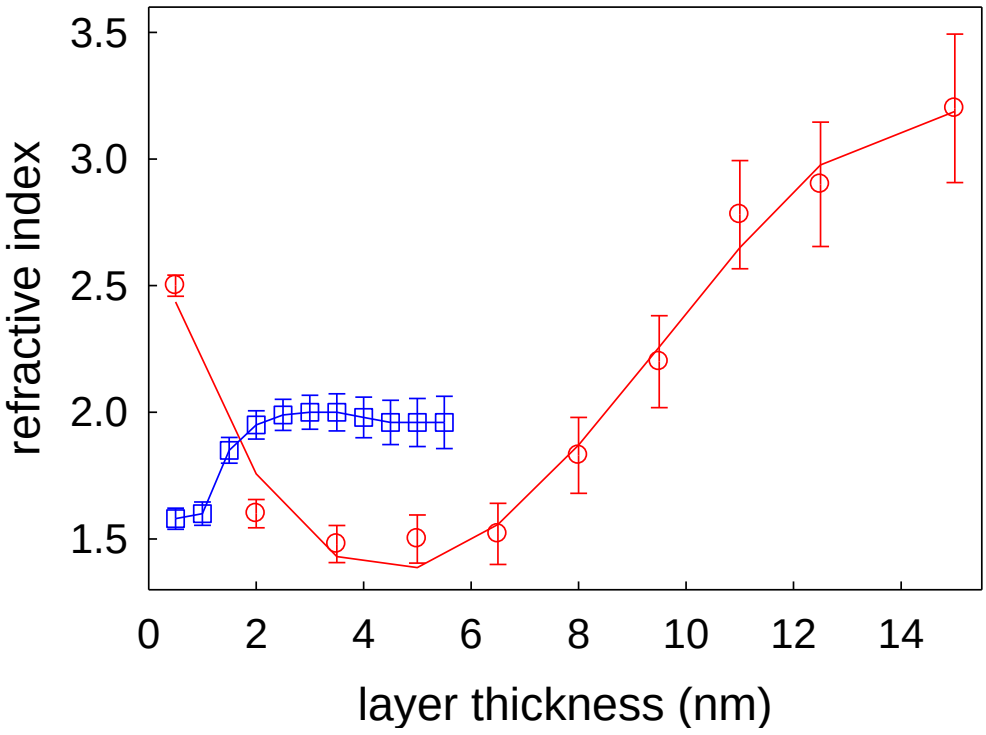

Figure 5.34 Comparison of the refractive index profile of denatured BSA (circle) and native state BSA adsorbed on PS surface.

5.7 Conclusions

In this study we have employed gold nanoparticles to obtain the refractive index profile of proteins adsorbed on various substrates. We have used optical extinction spectroscopy to study the dielectric properties of adsorbed protein. This is the first study to use LSPR of gold nanoparticles to probe the optical properties of the adsorbed protein layers a a function of distance from the substrate. The results indicate that the structure of surface adsorbed protein depends on the nature of the substrate. Further, the dielectric properties of the adsorbed protein vary with distance from the surface. We have developed a simple analytical model to calculate

the refractive index profile of the adsorbed protein. Though the model cannot predict the actual values of the refractive indicies, it can differentiate between the refractive index profiles of protein adsorbed on hydrophilic substrtes as compared to hydrophobic substrates. The model can also be used to study the effect of surface roughnesson protein adsorption. Using this technique, we can easily distinguish beween structurally stable and denatured protein. This technique is suitable to study adsorption of a wide range of proteins on any transparent substrate. We have shown that a simple extinction setup can provide similar information as that obtained from labour and money intensive techniques like neutron reflectivity.

CHAPTER 6

Concluding remarks

Today, nanoparticles are increasingly being used as drug delivery agents. When these nanoparticles come into contact with living systems, they invariably interact with proteins. The adsorbed protein layer actually determines the behaviour of these nanoparticles. It has been shown that adsorption of proteins onto flat substrates can lead to conformational changes in the adsorbed protein layer. It can be expected that as the size of the nanoparticles becomes smaller and approaches the size of the protein, the structure of the adsorbed layer can be significantly different from that on flat substrates. High curvature of small nanoparticles can retard protein adsorption [361].

This thesis describes experiments developed to probe the fundamental aspects of protein nanoparticle interactions such as dependence of protein functionality on the curvature of nanoparticles. We also developed a novel experiment to utilize gold nanoparticles as tools to study the complex interfacial behaviour of proteins. We have shown how we can utilize the extreme sensitivity of LSPR of gold nanoparticles to local refractive index to determine the structure of adsorbed protein and probe protein ligand binding. Therefore, we have made noteworthy contributions in promoting the use of nanoparticles as means for studying protein adsorption at solid/liquid interface. This work sheds some light on the complicated interfacial behaviour of proteins. The structure of a protein adsorbed on any substrate depends on the nature of the substrate itself as seen in the behaviour of BSA adsorbed on polymer surfaces. For surfaces with similar surface chemistries, the structure of the adsorbed protein layer can depend on the surface curvature. Study on the adsorption of IgG, Protein A and streptavidin on gold

nanoparticles reveals that not all proteins are similarly affected by the size of the adsorbing surface. It depends on the shape, size and nature of protein. For some proteins adsorption on a surface can lead to reduction/ loss of its biological activity. The reduction in biological activity can further depend on the radius of curvature of the adsorbing surface.

This work can be broadly divided into two parts. In the first part, we studied how the curvature of the nanoparticles and other variables such as pH and bulk protein concentration influence the structure and functionality of adsorbed proteins. For these studies we chose three proteins IgG, Protein A and Streptavidin. Whereas Streptavidin is small molecule (5 x 5.2 x 4.8 nm^3), IgG and Protein A are long molecules approximately 15 and 25 nm long respectively. IgG has different binding sites for Protein A and Anti-IgG. Protein A binds to Fc site on IgG and Anti-IgG binds to Fab sites. Binding between streptavidin conjugated gold nanoparticles and biotin was probed and it was found that the size of the gold nanoparticle does not affect binding. Streptavidin has 4 biotin binding sites, one on each side. So it is not surprising that it retains its biotin binding activity. Protein A, which has 5 IgG binding sites, also retains its IgG binding activity on all nanospheres from 5 to 60 nm. The size of the nanoparticle significantly affects the functionality of adsorbed IgG. While IgG retains its binding activity for Anti-IgG on all spheres (10-60nm), IgG attached to spheres with diameters $\geq$ 20nm is not able to bind to Protein A. The restricted access of Protein A to Fc site of IgG adsorbed on gold nanospheres with diameter suggest that IgG adopts an end-on orientation with Fc site attached to the spheres and Fab parts extended in the solution. In such a scenario, bulky Fab groups would sterically hinder Protein A and thus prevent Protein A from binding to adsorbed IgG. We also used Mie scattering theory to generate theoretical extinction spectra for gold nanoparticles over a range of thicknesses and refractive indices of the coating layer. We then compared the experimentally obtained peak

position and extinction with those obtained using Mie theory. This helps us in obtaining the optical thickness and refractive index of the adsorbed protein layer. The analysis shows that orientation of small, symmetrical Streptavidin is not affected by the size of gold nanoparticles. On the other hand, the thicknesses of IgG and Protein A suggest that these proteins adopt different orientation on spheres with diameter ≥ 30 nm as compared to smaller spheres. Packing density of the proteins also varies with the size of the nanosphere. In particular, there is little variation in the optical properties and surface density of adsorbed proteins for nanoparticles with diameter ≥ 30 nm.

The effect of bulk concentration of IgG was probed on 30 nm gold nanospheres. It was found that the width of IgG layer does not change appreciably with the bulk protein concentration. The layer thickness suggests that IgG adopts end-on orientation for all values of concentration examined. The effect of pH on IgG adsorption was probed on two sphere sizes; 15 nm, comparable to the length of IgG molecule and 40 nm. The layer thickness values indicate that IgG adopts end-on orientation on 40 nm spheres close to its i.e.p and at higher pH values where it is negatively charged. Layer thickness value on 15 nm spheres is smaller than that expected for end-on adsorption. Adsorption of IgG to 40 nm spheres at pH values where IgG is neutral or carries negative charge, leads to retardation/ loss of its Protein A binding activity. On the other hand, pH of adsorption has no influence on the binding activity of IgG attached to 15 nm spheres. Thus, IgG adsorbed onto 15 nm spheres retains its Protein A binding activity, irrespective of the fact whether it carries positive or negative charge or it electrically neutral. These results again point to different orientations of IgG on 15 nm spheres as compared to 40 nm spheres.

Thus, it can be concluded that high curvature of small nanoparticles (≤ 15 nm) can constraint the way protein packs on to the sphere. This effect is more prominent for bigger proteins such as IgG and Protein A as compared to smaller proteins such as streptavidin. The behaviour of proteins on spheres with diameter ≥ 30 nm is actually comparable to their behaviour on flat substrates. Adsorption of protein on surfaces can lead to reduction/ loss of its functionality due to restricted access to its binding site. The functionality of the adsorbed protein can also depend on the size of the gold nanoparticle that it is attached to. The effect of nanoparticle size on the binding activity of the adsorbed protein varies from one protein to another.

In the second part of my research, we developed a new technique to study the optical properties of the adsorbed protein as a function of distance from the substrate. In this study we employed gold nanoparticles as reporters to study refractive index profile of a model protein, BSA. We used UV-Visible extinction spectroscopy to study free BSA and BSA coated gold nanoparticles on three substrates- PDMS, PS and pHEMA. The sensitivity of peak position and extinction of LSPR peak was used to determine the optical properties of adsorbed protein layer. The extinction spectra of protein coated gold nanoparticles were monitored at regular intervals of time. By subtracting the extinction spectrum obtained at a particular time from the one preceding it, we obtained extinction spectra at of each layer. To obtain refractive index of each layer, we developed a simple analytical model of coated gold nanoparticles adsorbed on a substrate. Comparison of experimental results with model showed that the optical properties of adsorbed layers varied from one substrate to another. We found that the adsorbed layer is not homogeneous. On PDMS and PS, the refractive index of the adsorbed layer initially increases with distance from the surface. Differences begin to emerge at a distance of nearly 3 nm from the surface. On PDMS surface there is a peak in the refractive index value at this point. There is a

decrease in the refractive index value farther away from the surface. On PS on the other hand the refractive index of the adsorbed BSA layer becomes nearly constant after a distance of about 3 nm. BSA layers adsorbed on polyHEMA have a high refractive index close to the surface. As the distance from the surface increases, the refractive index drops down.

In this study we have shown that LSPR of gold nanoparticles can be used to obtain optical properties of the adsorbed protein layer. We found that the adsorbed layer is not uniform and the refractive index of the adsorbed layer varies with the distance from the surface. Further, the optical properties of the adsorbed layer depend on the nature of the substrate. The simple model developed by us can be used to calculate the optical properties of the adsorbed layer. This is the first time that technique has been developed to use optical extinction measurements to obtain depth dependent refractive index profile of an adsorbed protein. This technique is not just valid for one protein and can be used to study a wide range of proteins adsorbed on any transparent substrate.

There are still some aspects of protein-nanoparticle interaction that are not fully understood. There are few reports on the detailed structure of protein adsorbed onto nanoparticles. By utilizing Raman spectroscopy in combination with LSPR, secondary structure of the adsorbed proteins can be probed. Raman scattering from molecules, which are either adsorbed onto or in close proximity of plasmonic nanostructures, is enhanced due to large electromagnetic fields around the nanostructure. This phenomenon referred to as surface enhanced Raman scattering (SERS) can be used to gain insight into the secondary structure of the adsorbed species. LSPR cannot be utilized to identify molecular species. However, SERS is a useful tool and can be applied for molecular recognition.

Most studies involving nanoparticles utilize a large number of particles. Instead a single nanoparticle can be used as a probe. More studies employing individual nanoparticles are required as single nanoparticles are especially useful for imaging inside cells and tissues. However, such studies are limited by low signal to noise ratio. Dark field microscopy can be utilized to observe scattering from individual nanoparticles. However, care should be taken to select a particular size of the nanoparticle because absorption and scattering depend strongly on the size of the nanoparticle. While nanoparticle absorbance scales as the volume, scattering scales as the square of the volume of the particle. Scattering and absorption cross-section become comparable for 80 nm silver nanoparticle and 60 nm gold nanoparticle. Development of this technique could help in the detection of molecular binding events and conformational changes by monitoring shifts in the peak.

Adsorption of proteins from multi-component solutions onto flat surfaces showed different behaviour as compared to adsorption from single component solution [77]. Similar studies need to be conducted on nanoparticles to explore competitive adsorption of proteins onto nanoparticle surface. Such competitive binding conditions are experienced by nanoparticles on contact with living systems. Our studies have shown that proteins can adopt specific orientations depending on the size of a nanoparticle. Similar studies on nanoparticles with varying chemistries, shapes and sizes can help in optimizing nanoparticles for biosensing applications as a particular protein-nanoparticle combination could result in increased stability/functionality of the adsorbed protein. Such studies can also help in developing therapies against various amyloidogenic diseases as nanoparticles have been shown to affect rate of protein fibrillation. Kinetics of protein association/dissociation from nanoparticles is another critical parameter that has not been

explored yet. Collecting the findings from various techniques may result in a unified theory to fully explain protein nanoparticle interactions.

References

[1] G. Schmid, Nanoparticles: From theory to application, Wiley-VCH verlag, Weinhein, **2004**.

[2] W. Chan and S. Nie, "Quantum dot bioconjugates for ultrasensitive nonisotopic detection," Sci, **1998**. 281; p. 2016-2018.

[3] D.B. Harden, "Glass of Ceasers," **1988**, Exh, cat., The British Museum Press, London.

[4] F. Caruso and G. Sukhorukov, " Coated colloids: preparation, characterization assembly and utilization," edited by G. Decher and J.B. Schlenoff, Wiley-VCH verlag, **2002**.

[5] T. Pradell et. al., "The invention of luster: Iraq 9th and 10th centuries AD," J. Arche. Sci., **2008**. 35; p. 1201-1215.

[6] S. Padovani, "Copper in glazes of Renaissance luster pottery: nanoparticles, ions and local environment," J. Appl. Phys., **2003**, 93(12); p. 10058-10063.

[7] M. Faraday, "Experimental relations of gold (and other metals) to light," Phil. Trans. Roy. Soc. London., **1957**, 147; p. 145-181.

[8] http://www.zyvex.com/nanotech/feynman.html

[9] G. Mie, "Beitrage zur Optik teuber Madien, speziell kolloidaler metalleosungen," Annalen der Physik, **1908**, 4(25); p. 377-445.

[10] A. Kawabata and R. Kubo, " Electronic Properties of fine metallic particles.II. Plasma resonance absorption," J. Phys. Soc. Jap., **1966**. 21; 1765-1772.

[11] M. Fleishman, P.J. Hendra and A.J. McQuillan, "Raman spectra of pyridine adsorbed at a silver electrode", Chem. Phys. Lett., **1974**, 26(2); p.163-166.

[12] D.L. Jeanmaire, R.P. van Duyne, "Surface Raman electrochemistry part I. Heterocyclic, aromatic and aliphatic amines adsorbed on the anodized silver electrode", J. Electroanaly. Chem., **1977**, 84; p.1-20.

[13] M.G. Albrecht, J. A. Creighton, "Anomalously intense Raman spectra of Pyridine at a silver electrode", J. Am. Chem. Soc., **1977**, 99; p.5215-5219.

[14] G. Binning. H Rohrer," Scanning tunneling microscopy", IBM J. Res. And Devel., **1986**, 30(4).

[15] S. Ilijima, T. Ichihashi, "Single-shell carbon nanotubes of 1-nm diameter", Nature, **1993**, 363; p. 603-605.

[16] D.S. Bethune, C.H. Kiang, M.S. De Vries, G. Groman and R. Savoy, "Cobalt catalyzed growth of carbon nanotubes with single atomic layer walls, Nature, **1993**, 363; p. 605-607.

[17] R. Rosetti, S. Nakahara and L.E. Brus, "Quantum size effects in the redox potentials, resonance Raman spectra, and electronic spectra of CdS crystallites in aqueous solution", J. Chem. Phys.,**1983**, 79(2); p.1086-1088.

[18] Y.N. Xia, J.A. Rogers, K.E. Paul and G.M. Whitesides, "Unconventional methods for fabricating and patterning nanostructures", Chem. Rev.,**1999**, 99(7); p.1823.

[19] T. Tsuzuki and P.G. McCormik, "Mechanochemical synthesis of nanoparticles", J. Mat. Sci., **2004**, 39 (16-17); p. 5143-5146.

[20] S. O'Brien, L. Brus, C.B. Murray, "Synthesis of nanoparticles of Barium Titanante: towards a generalized strategy of oxide nanoparticle synthesis", J. Am. Chem. Soc., **2001**, 123; 12085-12086.

[21] S. Sun, "Recent advances in chemical synthesis, self assembly and applications of FePt nanoparticles", Adv. Mat, **2006**, 18, 393-403.

[22] M. Li, H. Schnablegger and S. Mann, "Coupled synthesis and self assembly of nanoparticles to give structures with controlled organization", Nature, **1999**, 402; 393-395.

[23] S. Mornet et. al., "Magnetic nanoparticle design for medical diagnosis and therapy", J. Mat. Chem., **2004**, 14; p. 2161-2175.

[24] X. Wu et. al., "Immuno fluorescent labelling of cancer marker Her2 and other cellular targets with semiconductor quantum dots", Nature Biotech., **2003**, 21(1); p.41-46.

[25] J.K. Jaiswal et. al., "Potentials and pitfalls of fluorescent quantum dots for biological imaging", Nature Biotech., **2004**, 14(9); p.497-504.

[26] S. Pathak et.al., "Hydroxylated quantum dots as luminescent probes for in situ hybridization", J. Am. Chem. Soc., **2001**, 123(17); 4103-4104.

[27] X. Gao and S. Nie, "Quantum dot-encoded mesoporous beads with high brightness and uniformity: Rapid readout using flow cytometry",Anal. Chem., **2004**, 76; p.2406-2410.

[28] Y. Xiao and P.E. Barker, "Semiconductor nanocrystal probes for human metaphase chromosomes", Nucl. Acid Res., **2004**, 32, e28.

[29] R.K. Jain and M. Stroh, "Zooming in and out with quantum dots"' Nature Biotech., **2004**, 22; p.959-960.

[30] R. Edgar et. al., "High sensitivity bacterial detection using biotin tagged phage and quantum dot nanocomplexes", **2003**, 103(13); p. 4841-4845.

[31] E.R. Goldman et. al., "Multiplexed toxin analysis using four colours of quantum dots flouroreagents", Anal. Chem.,**2004**, 76(3); p. 684-688.

[32] I.L. Medinitz et. al., "Self assembled nanoscale sensors based on quantum dot FRET donors", Nat. Mats. , **2003**, 2(9); p.630-638.

[33] X. Gao, W.C.W. Chan and S. Nie, "Quantum dot nanocrystals for ultrasensitive biological labelling and multicolour optical coding", J. Biomed. Opt., **2002**, 7(4); p. 532-537.

[34] P. Eaton et. al., "Imaging gold nanoparticles for DNA sequence recognition in biomedical applications", IEEE Trans Nanobioscience, **2007**,6; p.282-288.

[35] I.L. Maskimova et. al., "Near infrared laser photothermal therapy by using gold nanoparticles: computer simulations and experiment, Med. Laser Appl.,**2007,** (22); p.199-206.

[36] S. E. Yancey et. al., "The influence of void space on antireflection coatings of silica nanoparticle self assembled films", J. Appl. Phys., **2006**, 99; p.03413-1 – 03413-10.

[37] B.F.G. Johnson, "Nanoparticles in catalysis", Topics Catalysis, **2004**, 24(1-4); p.147-159.

[38] http://www.azonano.com/Details.asp?ArticleID=1695

[39] Nel et.al., "Toxic potential of materials at nanolevel", Science, **2006**, 3; p. 622-627.

[40] A. Isakovic, Z. Markovic, N. Nikolic, B. Todorovic-Markovic et. al., "Inactivation of nanocrystalline C_{60} cytoxicity by gamma irradiation", Biomat., **2006**, 27(29); p. 5049-5058.

[41] S.M. Hussain et. al., "Invitro toxicity of nanoparticles in BRL 3A rat liver cells", Toxicology in Vitro, **2005**, 19; p.975-983.

[42] E. E. Connor, J. Mwamuka, A. Gole, C. J. Murphy, et. al., "Gold nanoparticles are taken up by human cells but do not cause acute cytotoxicity", Small, **2005**, 1(3); p. 325-327.

[43] E. Oberdorster, "Maufactured nanomaterials (fullerenes C60) induce oxidative stress in the brain of juvenile largemouth bass, Environ. Health Perspectives, **2004**, 112; p. 1058-1062.

[44] T.C. King-Heiden et.al., "Quantum dot nanotoxicity assessment using the zebrafish embryo", Environ. Sci. Technol., **2009**, 43(5); p. 1605-1611.

[45] D. Whitford, Proteins: structure and function, John Wiley and sons Ltd., 2005.

[46] D.P. David, "From proteins to the beginnings of clinical proteomics", Proteomics- Clinical Appl., 2007, **1(8)**; p. 720-738.

[47] J. B. Sumner, “The isolation and crystalization of the enzyme urease”, J. Bio. Chem., 1926, 69; p. 435–441.

[48] L. Pauling, R.B. Corey and H.R. Branson, “The structure of proteins: two hydrogen bonded helical configurations of the polypeptide chain”, Proc. Natl. Acad. Sci., 1951, **37**; p. 237-240.

[49] S.M. Kalman, K. Linderstorm-Lang, M. Ottesen and F.M. Richards, “Degradation of ribonuclease by subtilisin”, Biochimica Biophy. Acta, 1955, **16 (9)** ; p. 297-299.

[50] W. Kauzmann, Some factors in the interpretation of protein denaturation”, Adv. Prot. Chem., 1959, **14**; 1-63.

[51] J. Kendrew, G. Bodo, H. Dintzis, R. Parrish, H. Wyckoff, D. Phillips, (1958). "A three-dimensional model of the myoglobin molecule obtained by x-ray analysis", 1958, *Nature* 181 (4610); p. 662–666.

[52] H. Muirhead, M. Perutz,1963). "Structure of hemoglobin. A three-dimensional fourier synthesis of reduced human hemoglobin at 5.5 Å resolution", 1963, *Nature* 199(4894); p.633–638.

[53] http://www.piercenet.com/media/ProStructureFig1.gif

[54] http://www.molecularsciences.org/structural_bioinformatics/protein_structures

[55] http://designmatrix.wordpress.com/2009/01/28/the-rational-essence-of-proteins-and-dna/

[56] http://www.chemistry.uoguelph.ca/educmat/phy456/456lec01.htm

[57] http://pharm1.pharmazie.uni-greifswald.de/bednarski_web/web/data/personen/Lectures/PMC/Wechselwirkungen/Alpha-helix.jpg

[58] C. Levinthal, “Are there pathways for protein folding”, J. Chim. Phys., **1968**, 65(1); p. 44-45.

[59] P.E. Leopold, M. Montal and J.N. Onuchic, “Protein folding funnels: a kinetic approach to the sequence structure relationship”, Proc. Natl. Acad. Sci., **1992**, 89(18); p. 8721-8725.

[60] C.M. Dobson and M. Kaplaus, “The fundamentals of protein folding: bringing together theory and experiment”, Current Opinion Structural Bio., **1999**, 9(1); p. 92-101.

[61] C.A. Haynes and W. Norde, “Globular proteins at solid/liquid interfaces”, Colloid Surfaces: B Biointerfaces, **1994**, 2; p.517-566.

[62] J.C. Kim and D.B. Lund, “Adsorption of β-lactoglobulin onto stainless steel surfaces”, in H.G. Kessler and D. B. Lund (ed.), Fouling and cleaning in food processing, **1989**; p. 187-199.

[63] H. Itoh, A. Nagata, T. Toyomasu, T. Nagai et. al., "Adsorption of β-lactoglobulin onto the surface of stainless steel particles", Biosci. Biotech. Biochem., **1995**, 59; p.1648-1651.

[64] B.D. Fair and A.M. Jamieson, "Studies of protein adsorption on polystyrene latex particles", J. Colloid Interface Sci., **1980**, 77; p. 525-534.

[65] C.A. Haynes and W. Norde, "Globular proteins at solid/liquid interfaces", Colloids Surfaces B. Biointerfaces, **1994**, 2; p. 517-566.

[66] B.M.C. Chan and J.L. Brash, "Adsorption of fibrinogen on glass: reversibility aspects", J. Colloid Interface Sci., **1981**, 82; p. 217-225.

[67] H.J. van Enkevort, D.V. Dass and A.G. Landgon, "The adsorption of bovine serum albumin at the stainless steel/aqueous solution interface", J. Colloid Interface Sci., **1984**, 98; p. 138-145.

[68] K. Anikin, C. Röcker, A. Wittemann, J. Wiedenmann, "Polyelectrolyte-Mediated Protein Adsorption: Fluorescent Protein Binding to Individual Polyelectrolyte Nanospheres, J. Phys. Chem. B, **2005**, *109* (12); p. 5418–5420.

[69] T. Arnebrant and T. Nylander, "Sequential and competitive adsorption of β-lactoglobulin and k-casein on metal surfaces", J. Colloid Interface Sci., **1986**, 111; p. 529-533.

[70] C. F. Wertz and M. M. Santore, "Adsorption and Relaxation Kinetics of Albumin and Fibrinogen on Hydrophobic Surfaces: Single-Species and Competitive Behavior", Langmuir, **1999**, 15 (26); p. 8884–8894.

[71] P. J. Wilde, D. C. Clark, D. Marion, "Influence of competitive adsorption of a lysopalmitoylphosphatidylcholine on the functional properties of puroindoline, a lipid-binding protein isolated from wheat flour, J. Agric. Food Chem., **1993**, 41 (10); p. 1570–1576

[72] H.G.W. Lensen, D. Bargeman, P. Bergveld, C.A. Smolders, "High performance liquid chromatography as a technique to measure competitive adsorption of plasma proteins onto lattices", J. Colloid Interface Sci., **1984**, 99(1); p. 1-8.

[73] E. Dickinson, "Mixed proteinaceous emulsifiers: review of competitive protein adsorption and the relationship to food colloid stabilization", Food Hydrocolloids, 1986,1(1); p. 3-23

[74] J. Teichroeb, "Selected experiments with proteins at solid-liquid interfaces", thesis, **2008**.

[75] F. Caruso, E. Rodda and D.N. Furlong, "Orientational aspects of antibody immobilization and immunological activity on quartz crystal microbalance electrodes", J. Colloid Interface Sci., **1996**, 178; p. 104-115.

[76] B.S. Murray and C. Deshaires, "Monitoring protein fouling of metal surfaces via a quartz crystal microbalance", J. Colloid Interface Sci., **2000**, 227; p. 32-41.

[77] J.H. Teichroeb, J.A. Forrest, L.W. Jones, J. Chan et. al., "Quartz crystal microbalance study of protein adsorption kinetics on poly(2-hydroxyethyl methacrylate)", J. Colloid Interface Sci., **2008**, 325(1); p. 157-164.

[78] P. Tengvall, I. Lundström and B. Liedberg, "Protein adsorption studies on model organic surfaces: an ellipsometric and infrared spectroscopic approach", Biomat**., 1998**, 19(4-5); p. 407-422.

[79] J.C. Djit, M.A. Cohen, K.M. Stuart and G.J. Fleer, "Reflectometry as atool for adsorption studies", Adv. Colloid Interface Sci., **1994**, 50; p. 79-101.

[80] H. Arwin, "Optical properties of thin layers of bovine serum albumin, γ-globulin and hemoglobin", Appl. Spec., **1986**, 40(3); p. 313-318.

[81] H. Elwing, "Protein adsorption and ellipsometry in biomaterial research", Biomat., **1998**, 19(4-5); p.397-406.

[82] S. Petrash, A. Liebmann-Vinson, M.D. Foster, L.M. Lander et. al., "Neutron and X-ray reflectivity studies of Human serum albumin adsorption onto functionalized surfaces of self-assembled monolayers", Biotechnol. Prog., **1997**, 13; p. 635-639.

[83] N.B. Sheller, S. Petrash and M.D. Foster, "Atomic force microscopy and X-ray reflectivity studies of albumin adsorbed onto self-assembled monolayers of hexadecyltrichlorosilane", Langmuir, **1998**, 14; p. 4535-4544.

[84] G.Fragneto, R.K. Thomas, A.R. Rennie and J. Penfold, "Neutron reflection study of bovine β-casein adsorbed on OTS self-assembled monolayers", Science, **1995**, 267; p. 657-660.

[85] B.K. Lok, Y.L. Cheung and C.R. Robertson, "Total internal reflection fluorescence: a technique for examining interactions of macromolecules with solid surfaces", J. Colloid Interface Sci., **1983**, 91; p. 87-103.

[86] J.D. Andrade and V. Hlady, "Protein adsorption and materials biocompatibility: a tutorial review and suggested hypotheses", Adv. Polymer Sci., **1986**, 79; p. 1-63.

[87] B. Lassen and M. Malmsten, "Structure of protein layers during competitive adsorption", J. Colloid Interface Sci., **1996**, 180; p. 339-349.

[88] R.D. Tilton, C.R. Robertson and A.P. Gast, "Lateral diffusion of bovine serum albumin adsorbed at the solid-liquid interface", J. Colloid Interface Sci., **1989**, 137; p. 192-203.

[89] J. Homola, S.S. Yee and G. Gauglitz, Surface plasmon resonance sensors: review, Sens Actuators B Chem, **1999**, 54; p. 3–15.

[90] O. Shliom, M. Huang, B. Sachais, A. Kuo, J.W. Weisel, C. Nagaswami, T. Nassar, K. Bdeir, E. Hiss and S. Gawlak, "Novel interactions between urokinase and its receptor", J Biol. Chem., **2000**, 275; p. 24304–24312.

[91] J.G. Quinn, S. O'Neill, A. Doyle, C. McAtamney, D. Diamond, B.D. MacCraith and R. O'Kennedy, "Development and application of surface plasmon resonance-based biosensors for the detection of cell-ligand interactions", Anal Biochem., **2000**, 281; p. 135–143.

[92] J.S. Shumaker-Parry, R. Aebersold and C.T. Campbell, "Parallel, quantitative measurement of protein binding to a 120-element double-stranded DNA array in real time using surface plasmon resonance microscopy", Anal Chem, **2004,** 76; p. 2071–2082.

[93] C. Mischiati, M. Borgatti, N. Bianchi, C. Rutigliano, M. Tomassetti, G. Feriotto and R. Gambari, "Interaction of the human NF-kappa B p52 transcription factor with DNA-PNA hybrids mimicking the NF-kappa B binding sites of the human immunodeficiency virus type 1 promoter", J Biol Chem, **1999,** 274, p. 33114–33122.

[94] K.A. Peterlinz and R.M. Georgiadis, "Observation of hybridization and dehybridization of thiol-tethered DNA using two-color surface plasmon resonance spectroscopy", J Am Chem Soc 119 **1997**, p. 3401–3402.

[95]A.W. Peterson, L.K. Wolf and R.M. Georgiadis, "Hybridization of mismatched or partially matched DNA at surfaces", J Am Chem Soc 124 **(2002**), pp. 14601–14607.

[96] W. K. Surewicz, H. H. Mantsch, D. Chapman "Determination of protein secondary structure by Fourier transform infrared spectroscopy: A critical assessment", Biochem., **1993**, 32 (2); p. 389–394.
[97] R. M. Gendreau, S. Winters, R. I. Leininger, D. Fink, C. R. Hassler, and R. J. Jakobsen, "Fourier transform infrared spectroscopy of protein adsorption from whole blood: ex vivo dog studies", App. Spectroscopy, **1981**, 35(4); p. 353-357.

[98] J.A. Bellisimo and S.L. Cooper, "Fourier Transform Infrared Spectroscopic Studies of Plasma Protein Adsorption under Well Defined Flow Conditions", Trans. Am. Soc. Artif. Int. Organs, **1984** , 30; p. 359-363.
[99] W.M. Reichert and J.D. Andrade, Surface Raman Spectroscopy in Surface and interfacial aspects of biomedical polymers, Vol.1, Surface chemistry and physics, Plenum Press **1985**; p. 421-442.

[100] R. Iwamoto, K. Ohta, M. Miya and S. Mima, "Total Internal Reflection Raman Spectroscopy at the Critical Angle for Raman Measurements of Thin Films", Appl. Spectroscopy, 1981, 35(6); p. 584-587.

[101] T.G. Spiro, T.C. Strekas, "Resonance Raman spectra of heme proteins. Effects of oxidation and spin state", J. Am. Chem. Soc., **1974**, 96 (2); p. 338–345.

[102] D. A. Weitz, S. Garoff, J. I. Gersten, and Abraham Nitzan , "The enhancement of Raman scattering, resonance Raman scattering, and fluorescence from molecules adsorbed on a rough silver surface", J. Chem. Phys., **1983,** 78; p. 5324-5339.

[103] A.Kondo and T. Traube, "Temperature dependence of activity and conformational changes in α-amylase with different thermostability upon adsorption on ultrafine silica particles", J. Colloid Interface Sci., **1995**, 174; p. 191-198.

[104] B. Sivaraman, K.P. Fears and R.A. Latour, "Investigation of the effects of surface chemistry and solution concentration on the conformation of adsorbed proteins using an improved circular dicohrism method", Langmuir, **2009**, 25; p. 3050-3056.

[105] W. J. Shaw, J. R. Long, J. L. Dindot, A. A. Campbell et. al., "Determination of Statherin N-Terminal Peptide Conformation on Hydroxyapatite Crystals", J. Am. Chem. Soc., **2000**, 122 (8); p. 1709–1716

[106] J.R. Long, W. J. Shaw, P. S. Stayton and G. P. Drobny, "Structure and Dynamics of Hydrated Statherin on Hydroxyapatite As Determined by Solid-State NMR", Biochemistry, **2001**, 40 (51), p. 15451–15455.

[107] E. Droz, M. Taborelli, P. Descouts and T.N.C. Wells, "Influence of surface and protein modification on immunoglobulin G adsorption observed by scanning force microscopy", Biophys., **1994**, 67; p. 1316-1323.

[108] D.C. Cullen and C.R. Lowe, "AFM studies of protein adsorption. I. Time resolved protein adsorption to highly oriented pyrolytic graphite", J. Colloid Interface Sci., **1994**, 166; p. 102-108.

[109] A.P. Quist, L.P. Bjorck, C.T. Reimann, S.O. Oscarsson et. al., Ascanning force microscopy study of human serum albumin and porcine pancreas trypsin adsorption on mica surfaces", Surface Sci., **1995**, 325:L; p. 406-417.

[110] M. Radmacher, M. Fritz, H.G. Hansma and P.K. Hansma, "Direct observation of enzymatic activity with atomic force microscope", Science, **1994**, 265; p. 1577-1579.

[111] E.L.Florin, V.T. Moy and H.E. Gaub, "Adhesion forces between individual ligand-receptor pairs", Science, **1994**, 264; p. 415-417.

[112] D. Leckband, "The surface force apparatus- a tool for probing molecular protein interactions", Nature, **1995**, 376; p. 617-618.

[113] W. Norde and J. Lyklema, "The adsorption of human plasma albumin and bovine pancreas ribonuclease at negatively charged polystyrene surfaces, V. Microcalorimetry", J. colloid Interface Sci., **1978**, 66(2); p. 295-302.

[114] S.L. McArthur, K.M. Mclean, H.A.W.S. John and H.J. Griesser, "XPS and surface-MALDI-MS characterization of worn HEMA-based contact lenses", BioMaterials, **2001**, 22; p. 3295-3304.

[115] H. Ichijima, T. Kawai, K. Yamamoto and H.D. Cavanagh, "Contact lenses- determination of protein deposits on RGP lenses by X-ray photoelectron spectroscopy", Clao. J., **2000**, 26; p. 18-20.

[116] T. Sakiyama, K. Tanino, M. Urawaka, K. Imamura et. al., "Characteristics of trypsin fragments of bovine β-lactagolbulin on a stainless steel surface", J. Biosci.Bioeng., **1999**, 88; p. 536-541.

[117] J. M. H. M. Scheutjens, G. J. Fleer, "Statistical theory of the adsorption of interacting chain molecules. 1. Partition function, segment density distribution, and adsorption isotherms", J. Phys. Chem., **1979**, 83 (12), pp 1619–1635.

[118] G.J. Fleer and J. Lyklema, in "Adsorption from solution at the solid-liquid interface", G. D. Parfitt and C.H. Rochester (eds.), Academic press, New York, **1983**, p. 153-167.

[119] B.W. Morrissey and R.R. Stromberg, "The conformation of adsorbed blood proteins by infrared bound fraction measurements", J. Colloid Interface Sci., **1974**, 46(1); p. 152-164.

[120] M. Malmsten, "Ellipsometry studies of the effects of surface hydrophobicity on protein adsorption", Colloids Surf. B: Biointerfaces, **1995**, 3; p. 297-308.

[121] T.A. Horbett and J.L. Brash, "Proteins at interfaces: current issues and future prospects", in Proteins at interfaces, physiochemical and biochemical studies, ed. T.A. Horbett and J.L. Brash, ACS symposium series, 343, **1986**.

[122] M. Malmsten, "Formation of adsorbed protein layers", J. Colloid Interface Sci., **1998**, 207; p. 186-199.

[123] M. Okubo, I. Azume and Y. Yamamoto, "Preferential adsorption of bovine serum albumin dimer onto polymer microspheres having a heterogeneous surface consisting of hydrophobic and hydrophilic parts", Colloid poly. Sci., **1990**, 268(7); p. 598-603.

[124] H. G. W. Lensen, D. Bargeman, P. Bergveld, C. A. Smolders and J. Feijen, "High-performance liquid chromatography as a technique to measure the competitive adsorption of plasma proteins onto lattices", J. Colloid Interface Sci., **1984**, 99(1); p. 1-8.

[125] U. M. Elofsson, M. A. Paulsson, and T. Arnebrant, "Adsorption of β-Lactoglobulin A and B in Relation to Self-Association: Effect of Concentration and pH", Langmuir, **1997**, 13 (6); p. 1695–1700.

[126] P. Nilsson, T. Nylander, and S. Havelund, "Adsorption of insulin on solid surfaces in relation to the surface properties of the monomeric and oligomeric forms", J. Colloid Interface Sci., **1991**, 144(1); p. 145-152.

[127] S.R. Whaley, D.S. English, E.L. Hu, P.F. Barbara et. al., "Selection of peptides with semiconductor binding specificity for directed nanocrystal assembly", Nature, **2000**, 405; p. 665-668.

[128] M. J. Read and S. L. Burkett, "Asymmetric α-helicity loss within a peptide adsorbed onto charged colloidal substrates", J. Colloid Interface Sci., **2003**, 261; p.255-163.

[129] T. Sakiyama, K. Tanino, M. Urakawa, K. Imamura et. al., "Adsorption characteristics of trpytic fragments of bovine β-lactoglobulin on a stainless steel surface", J. Biosci. Bioeng., **1999**, 88; p. 536-541.

[130] B. Liedberg, I. Lundstrom, C.R. Wu and W.R. Salaneck, "Adsorption of glycine on hydrophilic gold", J. Colloid Interface Sci., **1985**, 108; p. 123-132.

[131] K. Uvdal, P. Bodo, A. His, B. Liedberg and W.R. Salaneck, "X-ray photoelectron and infrared spectroscopy of glycine adsorbed upon copper", J. Colloid Interface Sci., **1990**, 140; p. 207-216.

[132] A. His, B. Liedberg, K. Uvdal, P. Bodo and I. Lundstrom, "Infrared and photoelectron spectroscopy of amino acids on copper", J. Colloid Interface Sci., **1990**, 140; p. 192-206.

[133] G.M. S. El. Shafei and C. Philip, "Interactions at an alumina aqueous glycine interface: characterization of glycine modified boehmite", J. Colloid Interface Sci., **1995**, 176; p. 55-62.

[134] G.M.S. El Shafei and C. Philip, "Adsorption of α-alanine on boehmite", J. Colloid Interface Sci., **1997**, 185; p. 140-146.

[135] FE Regnier, "The role of protein structure in chromatographic behavior", Science, **1987**, 238 (4825); p. 319-323.

[136] M. Malmsten and A. Veide, "Effects of Amino Acid Composition on Protein Adsorption", J. Colloid Interface Sci., **1996**, 178(1); p. 160-167.

[137] M.A. Bos, Z. Shervani, A.C.I. Anusiem, M. Giebsers et. al., "Influence of the electric potential of the interface on the adsorption of proteins", Colloids Surfaces B, **1994**, 3; p. 91-100.

[138] A. Barroug, J. Lemaitre and P.G. Rouxhet, "Lysozyme on Apatites: a model of protein adsorption controlled by electrostatic interactions**",** Colloids Surf**., 1989**, 37; p. 339-355.

[139] P.G.Koutsoukos, W. Norde and J. Lyklema, "Protein adsorption on hematite (alpha-Fe2O3) surfaces", J. Colloid Interface Sci., **1983**, 95(2); p. 385-397.

[140] H.B. Bull, "Adsorption of bovine serum albumin on glass", Biochim. Biophys. Acta,**1956**, 19; p. 464-471.

[141] D.E. Armstrong and G. Chesters, "Properties of Protein-Bentonite Complexes As Influenced By Equilibration Conditions", Soil Sci., **1964**, 98; p. 39-52.

[142] F. MacRitchie, "The adsorption of proteins at solid/liquid interface", J. Colloid Interface Sci., **1972**, 38; p. 484-488.

[143] A. S. Yang and B. Honig, "On the pH dependence of protein stability", J. Molecular Bio., **1993**, 231(2); p. 459-474.

[144] A.N. Asanov, L.J. Deucas, P.B. Oldham and W.W. Wilson, "Interfacial aggregation of bovine serum albumin related to crystallization conditions studied by total internal reflection fluorescence", J. Colloid Interface Sci., **1997**, 196(1); p. 62-73.

[145] W. Norde and J. Lyklema, "The adsorption of human plasma albumin and bovine pancreas Ribonuclease at negatively charged polystyrene surfaces, I. Adsorption isotherms, effects of charge, ionic strength and temperature", J. Colloid Interface Sci., **1978**, 66(2); p; 257-265.

[146] W. Norde and J. Lyklema, "The adsorption of human plasma albumin and bovine pancreas Ribonuclease at negatively charged polystyrene surfaces, II.Hydrogen ion tirations", J. Colloid Interface Sci., **1978**, 66(2); p; 266-276.

[147] W. Norde and J. Lyklema, "The adsorption of human plasma albumin and bovine pancreas Ribonuclease at negatively charged polystyrene surfaces, III. Electrophoresis", J. Colloid Interface Sci., **1978**, 66(2); p; 277-284.

[148] W. Norde and J. Lyklema, "The adsorption of human plasma albumin and bovine pancreas Ribonuclease at negatively charged polystyrene surfaces, IV. The charge distribution in the adsorbed state", J. Colloid Interface Sci., **1978**, 66(2); p; 285-294.

[149] W. Norde and J. Lyklema, "The adsorption of human plasma albumin and bovine pancreas Ribonuclease at negatively charged polystyrene surfaces, V. Microcalorimetry", J. Colloid Interface Sci., **1978**, 66(2); p; 295-302.

[150] D. K. Chattoraj, H. B. Bull, "Electrophoresis of Adsorbed Protein", J. Am. Chem. Soc., **1959**, 81 (19); p. 5128–5133.
[151] P. van Dulm, W. Norde and J. Lyklema, "Ion participation in protein adsorption at solid surfaces", J. Colloid Interface Sci., **1983**, 95(2); p. 385-397.
[152] C.A. Haynes, E. Swilinsky and W. Norde, "Structural and electrostatic properties of globular proteins at a polystyrene-water interface", J. Colloid Interface Sci., **1994**, 164(2); p. 394-409.
[153] T. Arai and W. Norde, "The behaviour of some model proteins at solid-liquid interfaces I. Adsorption from single protein solutions", Colloids Surfaces, **1990**, 51; p.1-15.
[154] T. Arai and W. Norde, "The behaviour of some model proteins at solid-liquid interfaces II. Sequential and competitive adsorption", Colloids Surfaces, **1990**, 51; p.17-28.
[155] J. Buijs, P.A.W. van den Berg, J.W. T. Lichtenberg, W. Norde et.al. , "Adsorption dynamics of IgG and its F(ab)2 and Fc fragments studied by reflectometry", J. Colloid Interface Sci., **1996**, 178; p.594-605.

[156] D. Brune and S. Kim, "Predicting protein diffusion coefficients" Proc. Natl. Acad. Sci., **1994**, 90(9); p. 3835-3839.

[157] W. Norde, F. Macritchie, G. Nowicka and J. Lyklema, "Protein adsorption at solid-liquid interfaces: reversibility and conformation aspects", J. Colloid Interface Sci., **1986**, 112; p. 447-456.

[158] S. Lin, "protein accumulation on disposable extended wear lenses", Clao J., **1991**, 17-18; p. 44-50.

[159] B.R. Young, W.G. Pitt and S.L. Cooper, "Protein adsorption on polymeric biomaterials II. Adsorption kinetics", J. Colloid Interface Sci., **1988**, 125; p. 246-260.

[160] G.K. Iwamoto, L.C. Winterton, R.S. Stoker, R.A. Van Wagenen et. al., "Fibronectin adsorption detected by interfacial fluorescence" J. Colloid Interface Sci., **1985**, 106; p. 459-466.

[161] D. V. Dass, H. J. van Enckevort and A. G. Langdon, "Protein adsorption by colloidal particles: I. The adsorption of bovine serum albumin by immobilized colloidal β-ferric oxyhydroxide", J. Colloid Interface Sci., **1987**, 116(2); p. 523-531.

[162] M. E. Soderquist and A. G. Walton**,** "Structural changes in proteins adsorbed on polymer surfaces", J. Colloid Interface Sci., **1980**, 75(2); p. 386-397.

[163] T. J. Lenk, B.D. Ratner, R. M. Gendreau, K. K. Chittur, "IR spectral changes of bovine serum albumin upon surface adsorption", J. Biomed. Mater. Res., **1989**, 23; p. 549-569.

[164] B.M. C. Chan and J.L. Brash, "Conformational change in fibrinogen desorbed from glass surface", J. Colloid Interface Sci., **1981**, 84(1); p. 263-265.

[165] C.E. Giacomelli, M. Bremer and W. Norde, "ATR-FTIR study of IgG adsorbed on different silica surfaces", J. Colloid Interface Sci., **1999**, 220; p.13-23.

[166] C.E. Giacomelli and W. Norde, "The adsorption desorption cycle reversibility of the BSA silica system", J. Colloid Interface Sci., **2001**, 233; p. 234-240.

[167] B.L. Steadman, K.C. Thompson, C.R. Middaugh, K. Matsuno, "The effects of surface adsorption on the thermal stability of proteins", Biotech. Bioeng., **1992**, 40(1); p. 8-15.

[168] R. Hopkins and R. Jones, "Unfolding and intermolecular association in globular proteins adsorbed at interfaces", Langmuir, **1999**, 15; p. 5102-5110.

[169] C.F. Wertz and M.M. Santore, "Adsorption and relaxation kinetics of albumin and fibrinogen on hydrophobic surfaces: single species and competitive behaviour", Langmuir, **1999**, 15; p. 8884-8894.

[170] C.R. Wertz and M.M. Santore, "Effect of surface hydrophobicity on adsorption and relaxation kinetics of albumin and fibrinogen: single species and competitive behaviour", Langmuir, **2001**, 17; p. 3006-30016.

[171] C.R. Wertz and M.M. Santore, "Fibrinogen adsorption on hydrophilic and hydrophobic surfaces: geometrical and energetic aspects of interfacial relaxations", Langmuir, **2002**, 18; p. 706-715.

[172] C.R. Wertz and M.M. Santore, "Adsorption and reorientation kinetics of lysozyme on hydrophobic surfaces", Langmuir, **2002**, 18; p. 1190-1199.

[173] T.P. Burghardt and D. Axelrod, "Total internal reflection/fluorescence photobleaching recovery study of serum albumin adsorption dynamics", Biophys. J., **1981**, 33(3); p. 455-467.

[174] I. Oreskes and J.M. Singer, "The mechanism of particulate carrier reactions. I. Adsorption of human γ-globulin to polystyrene latex particles", J. Immunol., **1986**, 86 (3); p. 338-344.

[175] B.W. Morrissey and C.A. Fenstermaker, "Conformation of adsorbed gamma-globulin and beta-lactoglobulin. Effect of surface concentration" Trans. Am. Soc. Artif. Int. Organs, **1976**, 22; p. 278-284.

[176] B.W. Morrissey and C.C. Han, "The conformation of γ-globulin adsorbed on polystyrene latices determined by quasielastic light scattering", J. Colloid Interface Sci., **1978**, 65(3); p. 423-431.

[177] J.L. Brash and D.J. Lyman, "Adsorption of plasma proteins in solution to uncharged, hydrophobic polymer surfaces", J. Biomed. Mat. Res., **1969**, 3(1); p. 175-189.

[178] B. D. Ratner, T. A. Horbett, D. Shuttleworth and H. R. Thomas, "Analysis of the organization of protein films on solid surfaces by ESCA", J. Colloid Interface Sci., **1981**, 83(2); p.630-642.

[179] T. Nylander, P. Kekicheff and B.W. Ninham, "Adsorption of insulin on metal surfaces in relation to association behavior", J. Colloid Interface Sci., **1988**, 122 (2); p. 557-566.

[180] J. Kim and G. A. Somorjai, "Molecular Packing of Lysozyme, Fibrinogen, and Bovine Serum Albumin on Hydrophilic and Hydrophobic Surfaces Studied by Infrared−Visible Sum Frequency Generation and Fluorescence Microscopy", J. Am. Chem. Soc., **2003**, 125(10); p. 3150-3158.

[181] D. Kim, H. Blanch and C. Radke, "Direct imaging of lysozyme adsorption onto mica by atomic force microscopy", Langmuir, **2002**, 18; p. 5841-5840.

[182] M. Malmsten, "Ellipsometry studies of protein layers adsorbed at hydrophobic surfaces", J. Colloid Interface Sci., **1994**, 166; p. 333-342.

[183] P. Schaaf and P. Dejardin, " Structural changes within an adsorbed fibrinogen layer during the adsorption process: a study by scanning angle reflectometry", Colloids Surf., **1988**, 31; p. 89-103.

[184] P. A. Cuypers, W. Hermens and H.C. Hemker, " Ellipsometry as a tool to study protein films at liquid-solid interfaces", Anal. Chem. , **1978**, 84; p. 56-67.

[185] B.R. Young, W.G. Pitt and S.L. Cooper, "Protein adsorption on polymeric biomaterials I. Adsorption isotherms" J. Colloid Interface Sci., **1988**, 124(1); p. 28-43.

[186] J. R. Lu**,** T. J. Su, P. N. Thirtle, R. K. Thomas, A. R. Rennie and R. Cubitt, **"**The Denaturation of Lysozyme Layers Adsorbed at the Hydrophobic Solid/Liquid Surface Studied by Neutron Reflection", J. Colloid Interface Sci., **1998**, 206(1); p. 212-223.

[187]H. Xu, X. Zhao,C. Grant, J.R. Lu, D.E. Williams and J. Penfold, "Orientation of a monoclonal antibody at the solid/solution interface: A combined study using atomic force microscopy and neutron reflectivity", Langmuir, **2006**, 22; p. 6313-6320.

[188] J. Buijs, D.D. White and W. Norde, "The effect of adsorption on the antigen binding by IgG and its $F(ab`)_2$ fragments", Colloids Surf. B: Biointerfaces, **1997**, 8; p. 239-249.

[189] H. Xu, X. Zhao, J.R. Lu and D.E. Williams, "Relationship between structural conformation of monoclonal antibody layers and antigen binding capacity", Biomacromol., **2007**, 8, p. 2422-2428.

[190] C. S. Lee and G. Belfort, "Changing activity of ribonuclease A during adsorption: a molecular explanation", Pro. Natl. Acad. Sci. USA, **1989**, 86; p. 8392-8396.

[191] M.H. Baron, M. Revault, S.S. Moinville, J. Abadie and H. Quiquqmpoix, "Chymotrypsin adsorption on montmorillonite: enzymatic activity and kinetic FTIR structural analysis", J. Colloid Interface Sci., **1999**, 214; p. 319-332.

[192] R.K. Sandwick and K.J. Schray, "The inactivation of enzymes upon interaction with a hydrophobic latex surface", J. Colloid Interface Sci., **1987**, 115; p. 130- 138.

[193] T. Zoungrana, G.H. Findenegg and W. Norde, " Structure, stability and activity of adsorbed enzyme", J. Colloid Interface Sci., **1997**, 190; p. 437-448.

[194] C.K. Bower and Q.X.J. Mcguire, "Activity losses among T4 lysozyme variants after adsorption to colloidal silica", Biotechnol. Bioeng., **1998**, 58; p. 658-662.

[195] G. Dansher, "Light and electron microscopic localization of silver in biological tissue", Histochem. Cell Bio., **1981**, 71(2); p.177-186.

[196] J.M. Koziara, P.R. Lockman, D.D. Allen and R.J. Mumper,"In situ blood barrier transport of nanoparticles", Pharm. Res., **2003**, 20; p.1772-1778.

[197] M. E. Ramos-Nino, L. Scapoli, M. Martinelli and B.T. Mossman, "Mesothelial Cell Transformation Requires Increased AP-1 Binding Activity and ERK-dependent Fra-1 Expression", Cancer Res., **2003**, 63; p. 3539-3545.

[198] D.B. Warheit, "Nanoparticles health impact?", Materials today, **2004**, 7(2); p.32-35.

[199] R.D. Handy and B.J. Shaw, "Toxic effects of nanoparticles and Nanomaterials: implications for public health, risk assessment and the public perception of nanotechnology", **2007**, Routledge; p.125-144.

[200] K.S. Soppimath, T. M. Aminabhavi, A. R. Kulkarni and W.E. Rudzinski, "Biodegradable polymeric nanoparticles as drug delivery devices", J. Controlled Release, **2001**, 70(1); p.1-20.

[201] R. H. Müller, K. Mäder and S. Gohla, "Solid lipid nanoparticles (SLN) for controlled drug delivery – a review of the state of the art", Eur. J. Pharamaceuticals Biopharmaceuticals, **2000**, 50(1); 161-177.

[202] T. Blunk, D. F. Hochstrasser, J.C. Sanchez, B.W. Müller, R. H. Müller, "Colloidal carriers for intravenous drug targeting: Plasma protein adsorption patterns on surface-modified latex particles evaluated by two-dimensional polyacrylamide gel electrophoresis", Electrophoresis, **1993**, 14; p. 1382-1387.

[203] T. Cedervall, I. Lynch, S. Lindman, T. Berggård et. al., "Understanding the nanoparticle–protein corona using methods to quantify exchange rates and affinities of proteins for nanoparticles", Proc. Natl. Acad. Sci., **2007,** 104 (7); p. 2050-2055.

[204] J.J. Gray, "The interaction of proteins with solid surfaces", Curr. Opin. Stru. Bio., **2004**, 14; p. 110-115.

[205] I. Lynch and K.A. Dawson, "Protein nanoparticles interaction", Nanotoday, **2008**, 3(1-2); p. 40-47.

[206] A. Gessner, R. Waicz, A. Lieske, B. R. Paulke, K. Mäder, et. al., "Nanoparticles with decreasing surface hydrophobicities: influence on plasma protein adsorption", Int. J. Pharmaceuticals, **2000**, 196(2); p.245-249.

[207] M. Luck, K.F. Pistel, Y. Li, R.H. Blunk, et. al., "Plasma protein adsorption on biodegradable microspheres consisting of poly(D,L-lactide-co-glycolide), poly(L-lactide) or

ABA triblock copolymers containing poly(oxy-ethylene)", J. Control. Res., **1998**, 55; p. 107-120.

[208] S. Lindman, I. Lynch, Eva Thulin, Hanna Nilsson et. al., "Systematic Investigation of the Thermodynamics of HSA Adsorption to *N-iso*-Propylacrylamide/*N-tert*-Butylacrylamide Copolymer Nanoparticles. Effects of Particle Size and Hydrophobicity", Nano Lett., **2007**, 7 (4); p. 914–920.

[209] M. Lundqvist, J. Stigler, G. Elia, I. Lynch, "Nanoparticle size and surface properties determine the protein corona with possible implications for biological impact", Proc. Natl. Acad. Sci. **, 2008**, 105 (38); p. 14265-14270.

[210] S.H. Brewster, W.R. Glomm, M.C. Johnson, M.K. Knag, "Probing BSA binding to citrate coated gold nanoparticles and surfaces", Langmuir, **2005**, 21(20); p. 9303-9307.

[211] S. Patil, A. Sandberg, E. Heckert, W. Self et. al., "Potential adsorption and cellular uptake of cerium oxide nanoparticles as a function of zeta potential", Biomat., **2007**, 28(1); p. 4600-4607.

[212] C. Wilhelm, C. Billotey, J. Rogers, J.N. Pons et. al., "Intracellular uptake of anionic superparamagnetic nanoparticles as a function of their surface coating", Biomat., **2003**, 24(6); p. 1001-1011.

[213] A. Gessner, A. Lieske, B. R. Paulke and R. H. Müller, "Functional groups on polystyrene model nanoparticles: Influence on protein adsorption", J. Biomed. Mater. Res. Part A, **2003**, 65A, 3; p.319-326.

[214] K. Kandori, A. Fudo and T. Ishikawa, "Study on the particle texture dependence of protein adsorption by using synthetic micrometer sized calcium hydroxyapatitie particles", Colloids Surfaces B: Biointerfaces, **2002**, 12 (3); 145-153.

[215] T. Blunk, M. Luck, A. Calvoer, D.F. Hochstrasser et. al., "Kinetics of plasma protein adsorption on model particles for controlled drug delivery and drug targeting", Eur. J. Pharm. Biopharm., **1996**, 42; p. 262-268.

[216] S. Linse, C. cabaalerio-Lago, W. Xue, I. Lynch, "Nucleation of protein fibrillation by nanoparticles", Proc. Natl. Acad. Sci., 2007, 104(21); p. 8691-8696.

[217] V.L. Colvin and K.M. Kulinowski, "Nanoparticles as catalyst for protein fibrilation", Proc. Natl. Acad. Sci., 2007, 104(21); p. 8679-8690.

[218]W. Wu, X. Sun, Y. Yu, J. Hu, et. al., "TiO2 nanoparticles promote β-amyloid fibrillation in vitro", Biochem. Biophys. Res. Comm., **2008**, 373; p. 315-318.

[219] A.S. Pai, I. Rubinsten and H. Onyuksel, "PEGylated phospholipid nanomicelles interact with β- amyloid(1-42) and mitigate its β sheet formation, aggregation and neurotoxicity in vitro", Peptides, **2006**, 27; p. 2858-2866.

[220] I. lynch, K.A. Dawson and S. Linse, “Detecting cryptic epitopes created by nanoparticles”, Sci., **2006**, 337; p. 14-18.

[221] M. Lundqvist, I. Sethson and B. Jonsson, “High resolution 2D ^{1}H-^{15}N NMR characterization of persistent structural alterations of proteins induced by interactions with silica nanoparticles”, Langmuir, **2005**, 21; p. 5974-5979.

[222] W. Norde and J.P. Favier, “Structure of adsorbed and desorbed proteins”, Colloids Surfaces, **1992**, 64(1); p. 87-93.

[223] H.S. Larsericsdotter, S. Oscarsson and J. Buijs, “Thermodynamic analysis of proteins adsorbed on silica nanoparticles: electrostatic effects”, J. Colloid Interface Sci., **2001**, 237; p. 98-103.

[224] A.A. Vertegel, R.W. Siegel and J.S. Dordick, “Silica nanoparticles size influences the structure and enzymatic activity of adsorbed lysozyme”, Langmuir, **2004**, 20; p. 6800-6807.

[225] S.S. Karajanagi, A.A. Vertegel, R.S. Kane and J.S. Dordick, “Structure and function of enzymes adsorbed onto single-walled carbon nanotubes”, Langmuir, **2004**, 20; p. 11594-11599.

[226] A.J. Haes, R.P. van Duyne, “Nanosensors enable portable detectors for environmental and medical applications”, Laser Focus World, **2003**, 39; p. 153-156.

[227] J. J. Storhoff, A. A. Lazarides, R. C. Mucic, C. A. Mirkin, et. al., “What Controls the Optical Properties of DNA-Linked Gold Nanoparticle Assemblies?”, J. Am. Chem. Soc., **2000**, 122 (19); p. 4640–4650.

[228] C.A. Mirkin, R.L. Letsinger, R.C. Mucic and J.J. Storhoff, “A DNA based method for rationally assembling nanoparticles into macroscopic materials”, Nature, **1996**, 382; p. 607-609.

[229] P. Bao, A. G. Frutos, C. Greef, J. Lahiri, U. Muller, et. al., “High-Sensitivity Detection of DNA Hybridization on Microarrays Using Resonance Light Scattering”, Anal. Chem., **2002**, 74 (8); p. 1792–1797.

[230] A. Henglein and D. Meisel, “Spectrophotometric Observations of the Adsorption of Organosulfur Compounds on Colloidal Silver Nanoparticles”, J. Phys. Chem. B, **1998**, 102 (43); p. 8364–8366.

[231] T. Linnert, P. Mulvaney and A. Henglein, “Surface chemistry of colloidal silver: surface plasmon damping by chemisorbed iodide, hydrosulfide (SH-), and phenylthiolate” , J. Phys. Chem. **1993**, 97; p. 679-682.

[232] L. Cognet, C. Tardin, D. Boyer, D. Choquet,“Single metallic nanoparticle imaging for protein detection in cells” Proc. Natl. Acad. Sci., **2003** , 100 (20); p. 11350-11355.

[233] J. Liu and Y. Lu, “A colorimetric lead biosensor using DNAzyme directed assembly of gold nanoparticles”, J. Am. Chem. Soc., **2003**, 125; p. 6642-6643.

[234] J. J. Storhoff, R. Elghanian, R. C. Mucic, C. A. Mirkin, et. al.,"One-pot colorimetric differentiation of polynucleotides with single base imperfections using gold nanoparticle probes", J. Am. Chem. Soc., **1998**, 120 (9); p. 1959–1964.

[235] G. Raschke, S. Kowarik, T. Franzl, C. Sönnichsen, et. al., "Biomolecular Recognition Based on Single Gold Nanoparticle Light Scattering", Nano Letters, **2003**, 3 (7); p. 935–938

[236] A.C. Curry, M. Crow and A. Wax, "Molecular imaging of epidermal growth factor receptor in live cells with refractive index sensitivity using dark field microscopy and immunotargeted nanoparticles", J. Biomed. Optics, **2008**, 13(1); p.014022-1- 014022-7.

[237] J.J. Mock, D.R. Smith and S. Schultz, "Local refractive index dependence of plasmon resonance spectra from individual nanoparticles", Nano Lett., **2003**, 3; p. 485-491.

[238] P. Englebienne, "Use of colloidal gold surface plasmon resonance peak shift to infer affinity constants from the interactions between protein antigens and antibodies specific foe single or multiple epitopes", Analyst, **1998**, 123; p. 1599- 1603.

[239] T.R. Jensen, M.L. Duvall, L. Kelly, A. Lazarides, "Nanosphere lithography: effect of the external dielectric medium on the surface plasmon resonance spectrum of a periodic array of silver nanoparticles", J. Phys. Chem. B, **1999**, 103; p. 9846-9853.

[240] E. M. Hicks, X.Y. Zhang, S.L. Zou, O. Lyandres, "Plasmonic properties of film over nanowell surface fabricated by nanosphere lithography", J. phys. Chem. B., **2005**, 109; p. 22351-22358.

[241] P. Englebienne , A. van Hoonacker and Joseph Valsamis, "Rapid Homogeneous Immunoassay for Human Ferritin in the Cobas Mira Using Colloidal Gold as the Reporter Reagent", Clinical Chem., **2000**, 46; p. 2000-2003.

[242] X. Luoa, J. Xua, Y. Dua and H.Chen, "A glucose biosensor based on chitosan–glucose oxidase–gold nanoparticles biocomposite formed by one-step electrodeposition" Anal. Biochem., **2004**, 34(2); p. 284-289.

[243] Juewen Liu and Yi Lu, "Adenosine dependent assembly of aptazyme functionalized gold nanoparticles and its application as a colorimetric biosensor", Anal. Chem., **2004**, 76 (6); p. 1627–1632.

[244] P. Baptista, E. Pereira, P. Eaton, G. Doria, et. al., "Gold nanoparticles for the development of clinical diagnosis methods", Anal. Bioanal. Chem. , **2007**, 391(3); p. 943-950.

[245] K. K. Jain, "Nanotechnology in clinical laboratory diagnostics", Clinica Chimica Acta, **2005**, 358(1-2); p. 37-54.

[246] K. C. Grabar , R. G. Freeman, M. B. Hommer and M. J. Natan, "Preparation and Characterization of Au Colloid Monolayers", Anal. Chem., **1995**, 67 (4); p. 735–743

[247] R. G. Freeman, K. C. Grabar, K. J. Allison, R. M. Bright, et. al., "Self assembled metal colloid monolayers: an approach to SERS substrates", Sci., **1995**, 267(5204); p. 1629-1632.

[248] T. Okamoto, I. Yamaguchi, T. Kobayashi, "Local plasmon sensor with gold colloid monolayers deposited upon glass substrates", Opt. Lett., **2000**, 25; p. 372-374.

[249] N. Nath and A. Chilkoti, "A colorimetric gold nanoparticle sensor to interrogate biomolecular interactions in real time on a surface", Anal. Chem., **2002**, 74 (3); p. 504–509.

[250] S. Zhanga, N. Wanga, Y. Niua and C. Sun, "Immobilization of glucose oxidase on gold nanoparticles modified Au electrode for the construction of biosensor", Sensors and Actuators B: Chemical, **2005**, 109(2); p. 367-374.

[251] J. Jia, B. Wang, A. Wu, G. Cheng, et. al., "A method to construct a third generation horseradish peroxidase biosensor: self-assembling gold nanoparticles to three-dimensional sol−gel network", Anal. Chem., **2002**, 74 (9); p. 2217–2223.

[252] H. Xu and M. Kall, "Modelling the optical response of nanoparticle based surface plasmon resonance sensors", Sens. Actuators B, **2002**, 87; p. 244-249.

[253] J.H. Teichroeb, J.A. Forrest, V. Ngai and L.W. Jones, "Anomalous thermal denaturing of proteins adsorbed to nanoparticles", Eur. Phys. J. E, **2006**, 21, p. 19-24.

[254] J.H. Teichroeb, J.A. Forrest and L.W. Jones, "Size dependent denaturing kinetics of bovine serum albumin adsorbed onto gold nanospheres", Eur. Phys. J. E, **2008**, 26; p. 411-415.

[255] J.H. Teichroeb, P.Z. McVeigh and J.A. Forrest, "Influence of nanoparticle size on the pH dependent structure of adsorbed proteins studied with quantitative localized surface plasmon spectroscopy", Eur. Phys. J. E, **2009**, 30; p. 157-164.

[256] X. Jiang, J. Jiang, Y. Jin, E. Wang, "Effect of colloidal gold size on the conformational changes of adsorbed cytochrome c: probing by circular dichorism, UV- Visible and Infrared spectroscopy", Biomacromolecules, **2005**, 6(1); p. 46-53.

[257] W. Shang, J.H. Nuffer, V.A. Muniz-Papandrea, W. Colon, et.al., "Cytochrome c on silica nanoparticles: influence of nanoparticle size on protein structure, stability and activity", Small, **2009**, 5(4); p. 470-476.

[258] M. Lundqvist, I. Sethson and B. Jonsson, "Protein adsorption onto silica nanoparticles: conformational changes depend on the particles curvature and protein stability", Langmuir, **2004**, 20; p.10639-10647.

[259] P. Roach, D. Farrar and C.C. Perry, "Surface tailoring for controlled protein adsorption: effect of topography at the nanometer scale and chemistry", J. Am. Chem. Soc., **2006**, 128; p. 3939-3945.

[260] P. Asuri, S.S. Karajanagi, H. Yang, T. Yim, R.S. Kane and J.S. Dordick, "Increasing protein stability through control of the nanoscale environment", Langmuir, **2006**, 22; p. 5833-5836.

[261] W. Jiang, B. Y.S. Kim, J.T. Rutka and W.C.W. Chan, "Nanoparticle mediated cellular response is size dependent", Nature Nanotech., **2008**, 3; 145-150.

[262] J. Turkevich, P.C. Stevenson and J. Hillier, "A study of the nucleation and growth processes in the synthesis of colloidal gold", Discuss. Faraday Soc., 11, **1951**; p.55-75.

[263] V. K. LaMer, R. H. Dinegar, "Theory, Production and Mechanism of Formation of Monodispersed Hydrosols, J. Am. Chem. Soc., **1950**, 72 (11); p. 4847–4854.

[264] K. Takiyama, "Formation and aging of precipitates. VIII. Formation of monodisperse particles (1) gold sol particles by sodium citrate method", Bull. Chem. Soc. Jpn., **1958**, 31(8); p. 944-950.

[265] G. Frens, "Controlled nucleation for the regulation of the particle size in monodisperse gold suspensions", Nature Phys. Sci., **1973**, 241; p. 20- 22.

[266] M.K. Chow and C.F. Zukoski, "Gold sol formation mechanisms: role of colloidal stability", J. Colloid Interface Sci., **1994**, 165; p. 97-109.

[267] http://www.rice.edu

[268] http://www.polymer-physics.uwaterloo.ca/equipment/spincoater.htm

[269] Z. Fakhraai, "Dynamics of polymer thin films and surfaces", Ph.D. thesis, 2007.

[270] http://polydimethylsiloxane.co.tv/

[271] http://www.biomemsrc.org/biomems/documents/Lab_module_1_PDMS.pdf

[272] M.A. Hayat (Editor), Colloidal Gold: Principles, Methods and Applications (Academic press, 1989).

[273] http://www.polymer-physics.uwaterloo.ca/equipment/afm.htm

[274] T. R. Jensen, M. D. Malinsky, C. L. Haynes, and R. P. Van Duyne, "Nanosphere Lithography: Tunable Localized Surface Plasmon Resonance Spectra of Silver Nanoparticles, J. Phys. Chem. *B*, **2000**, 104 (45); p. 10549–10556.

[275] J. Yguerabide and E. E. Yguerabide, "Light-Scattering Submicroscopic Particles as Highly Fluorescent Analogs and Their Use as Tracer Labels in Clinical and Biological Applications: I. Theory", Anal. Biochem., **1998**, 262; p. 157-176.

[276] http://www.ebookee.com/-request_ebook-Optical-Properties-of-Metal-Clusters_360255.html

[277] A.J. Haes, "Localized surface plasmon resonance spectroscopy for fundamental studies of nanoparticle optics and applications to biosensors" Ph.D. thesis 2004.

[278] H. Chen, X. Kou, Z. Yang, W. Ni, "Shape and size dependent refractive index senstivity of gold nanoparticles", Langmuir, **2008**, 24(10); p. 5233-5237.

[279] C.F. Bohren and D.R. Huffman, Absorption and Scattering of Light by Small Particles, (John Wiley and sons, 1983).

[280] U. Kreibig, "Electronic properties of small silver particles: the optical constants and their temperature dependence", J. Phys. F: Metal Phys, **1974**, **4;** p. 999-1014.

[281] IH El-Sayed, X Huang and MA El-Sayed, "Surface plasmon resonance scattering and absorption of anti-EGFR antibody conjugated gold nanoparticles in cancer diagnostics: applications in oral cancer", Nano Lett.,**2005**, 5; p. 829-834.

[282] A. Dingler,R.P. Blum,H. Niehus, R.H. Muller ands. Gohla, "Solid lipid nanoparticles (SLNTM/LipopearlsTM) a pharmaceutical and cosmetic carrier for the application of vitamin E in dermal products" J Microencapsulation, **1999**, 16(6); p.751-767.

[283] A.J. Haes and R.P. van Duyne, "A nanoscale optical biosensor: sensitivity and selectivity of an approach based on the localized surface plasmon resonance spectroscopy of triangular silver nanoparticles", J. Am. Chem. Soc., **2002**, 124; p.10596 -10604.

[284] M. Arruebo, R Fernandez, M.R. Ibarra and Jesus Santamaria, "Magnetic nanoparticles for drug delivery", Nanotoday, **2007**, 2(3); p. 22-32.

[285] M.A. Hayat (Editor), Colloidal Gold: Principles, Methods and Applications (Academic press, **1989**).

[286] Z. Ma, Y. Guan and H. Liu, "Superparamagnetic silica nanoparticles with immobilized metal affinity ligands for protein adsorption", J. Magn. Magn. Mater, **2006,** 301(2); p.469-477.

[287] A. Gessner, R. Waicz, A. Lieske, B.R. Paulke, K. Mader and R. H. Muller, "Nanoparticles with decreasing surface hydrophobicities: influence on plasma protein adsorption", Inter. J. Pharma, **2000** , 196(2); p.245-249.

[288] S. Patil, A. Sandberg, E. Heckert, W. Self and S. Seal, "Protein adsorption and cellular uptake of cerium oxide nanoparticles as a function of zeta potential", Biomater. , **2007** , 28(31); p. 4600-4607.

[289] D.D. van Slyke and G.M. Meyer, " The fate of protein digestion products in the body", J. Bio. Chem.,**1913** ,6; p.197-212.

[290] J.D. Anrade, *Protein adsorption, Vol. 2*, (Plenum, New York, 1985).

[291] W. Norde, "Adsorption of proteins from solution at the solid-liquid interface", Adv. Colloid Interface Sci., **1986** , 25; p. 267-340.

[292] Q. Garrett, B. Laycock and R. W. Garret, "Hydrogel Lens Monomer Constituents Modulate Protein Sorption", Invest. Opthal. Vis. Sci., **2000** , 47; p. 1687-1695.

[293] http://www.tedpella.com/gold_html/gold-tec.htm

[294] T. Endo, K. Kerman, N. Nagatani, H.M. Hiepa, D. Kim, Y. Yonezawa, K. Nakano and E. Tamiya, Anal. Chem., **2006**, 78, 6465.

[295] S.W. Kessler, "Cell membrane antigen isolation with the staphylococcal protein A-antibody adsorbent", J. Immunology, **1976**, 117 (5); p. 1482-1490.

[296] P. Englebienne A. V. Hoonecker and M. Verhas , " Surface plasmon resonance: principles, methods and applications in biomedical sciences", Spectroscopy , **2003** ,17; p. 225-273.

[297] R. Reiter, H. Motschmann and W. Knoll, "Ellipsometric characterization of Streptavidin binding to biotin functionalized lipid monolayers at the water/air interface", Langmuir, 1993, **9**; p. 2430-2435.

[298] K.C. Hou, R. Zaniewski and S. Roy, "Protein A immobilized affinity cartridge for immunoglobulin purification", Biotech. Appl. Biochem., **1991**, 13(2); p. 257-268.

[299] T. Endo, K. Kerman, N. Nagatani, H.M. Hiepa, D. Kim, Y. Yonezawa, K. Nakano and E. Tamiya, " Multiple label free detection of antigen antibody reaction using localized surface plasmon resonance based core shell structured nanoparticle layer chip", Anal. Chem., **2006**, 78(18); p. 6465-6475.

[300] K.Y. Chumbimuni-Torres, Z. Dai, N. Rubinova, Y. Xiang, E. Pretsch, J. Wang and E. Baker, " Potentiomatric biosensing of proteins with ultrasensitive ion selective microelectrodes and nanoparticle labels", J. Am. Chem. Soc., **2006**, 128(42); p. 13676-13677.

[301] J. Huwyler, D. Wu and W.M. Pardridge, " Brain drug delivery of small molecules using immunoliposomes", Pro. Natl. Acad. Sci., **1996**, 93(24); 14164-14169.

[302] S.J. Son, J. Reichel, B. He, M. Schuchman and S.B. Lee, "Magnetic nanotubes for magnetic field assisted bioseperation, biointeraction and rug delivery", J. Am. Chem. Soc., **2005**, 127(20); p. 7316-7317.

[303] J. Sjodahl, "Repetitive sequences in Protein A from Staphylococcus aureus", Eur. J. Biochem., **1977**, 73(2); p: 343-351.

[304] J. Sjodahl, "Structural studies on the four repetitive Fc binding regions in Protein A from Staphylococcus aureus", Eur. J. Biochem., **1977**, 78; p: 471-490.

[305] D. Colbert, A. Anilionis, P. Gelep, J. Farley and R. Breyer, "Molecular organization of the Protein A gene and its expression in recombinant host organisms", J. Biol. Response. Modif., **1984**, 3(3); p: 255-259.

[306] S. Ohnishi , M. Murata and M. Hato, " Correlation between surface morphology and surface forces of Protein A adsorbed on mica", Biophys. J., **1998**, 74; p. 455-465.

[307] J.Buijs, J. W. Lichtenberg, W. Norde and J. Lyklema, “Adsorption of monoclonal IgGs and their F(ab)2 fragments onto polymeric surfaces”, Colloids and Surfaces B: Biointerfaces , **1995** , 5(1-2); p. 11-23.

[308] http://www.cytodiagnostics.com/streptavidin_and_biotin_products.html

[309] L. Touahir, J. Niedziolka-Jonsson, E. galopin. R. Bourkherroub et. al., “Surface Plasmon resonance on gold and silver films coated with thin layers of amorphous silicon-carbon alloys”, Langmuir, 2010, **26(8);** p. 6058-6065.

[310] A. Holmberg, A. Blomstergren, O. Nord, M. Lukas, J. Lindenberg and M. Uhlen, “The biotin-streptavidin interaction can be reversibly broken using water at elevated temperatures”, Electrophoresis, 2005, **26(3)** ; p. 501-510.

[311] E.A. Bayer and M. Wilchek, “Avidin-biotin technology: preparation of biotynlated probes”, Methods in Molecular Bio., 1992, **10**; p. 137-142.

[312] J.R. Wayment and J.M. Harris, “Biotin-Avidin binding kinetics measured by single molecule imaging”, Anal. Chem., 2009, **81**; p. 336-342.

[313] L. Haeussling, H. Ringsdorf, F.J. Schmitt and W. Knoll, “Biotin-functionalized self assembled monolayers on gold: surface Plasmon optical studies of specific recognition reactions”, Langmuir, 1991, **7(9)**; p. 1837-1840.

[314] J. Spinke, M. Liley, H.J. Guder, L. Angermaier and W. Knoll, “Molecular recoginition at self assembled monolayers: the construction of multicomponent multilayers”, Langmuir, 1993, **9(7)**; p. 1821-1825.

[315] R. Wacker, H. Schroeder and C.M. Niemeyer, “Performance of antibody microarrays fabricated by either DNA directed immobilization, direct spotting or Streptavidin biotin attachment: a comparative study”, Anal. Biochem., 2004, **330(2)**; p. 281-287.

[316] S.Freitag, I. Le Trong, L. Klumb, P.S. Stayton and R. E. Stenkamp, “Structural studies of the streptavidin binding loop”, Protein Sci., 1997, **6**; p. 1157-1166.

[317] P. Lea. and D.K. Gross, “Effective diameters of Protein A gold and gold anti-rabbit gold conjugates visualized by field emission scanning electron microscopy”, J. Histochem. Cytochem., **1992** , 40(6); p.751-758.

[318] H. Elwing, B. Ivarsson and I. Lundstrom, “Comlement deposition from human sera on silicon surfaces studied in situ by ellipsometry”, Eur. J. Biochem., **1986 ,** 156(2); p. 359-365.

[319] P. Bagchi and S.M. Birnbaum, “Effect of pH on the adsorption of immunoglobulin G on anionic poly(vinyltoluene) model latex particles”, J. Colloid Interface Sci.,**1981,** 83(2); p: 460-478.

[320] L. Ghitescu and M Bendayan, “Immunolabeling efficiency of Protein A-gold complexes”, J. Histochem. Cytochem., **1990 ,** 38(11); p.1523-1530.

[321] J. N. Herron, W. Muller, M. Paudler, H. Riegler, H. Ringdorf and P.A. Suci, "Specific recognition-induced self-assembly of a biotin lipid/Streptavidin/Fab fragment triple layer at the air/water interface: ellipsometric and fluorescence microscopy investigations", Langmuir, 1992, **8**; p. 1413-1416.

[322] H. Morgan, D.M. Taylor and C. D'Silva, "Surface Plasmon resonance studies of chemisorbed biotin streptavidin multilayers", Thin Solid Films, 1992, **209**; p. 122-126.

[323] M. Kajiura, T. Nannishi, H. Iida, H. Takada and T. Osaka, "Biosensing by optical waveguide spectroscopy based on localized surface Plasmon resonance of gold nanoparticles used as a probe or as a label", J. Colloid Interface Sci., 2009, **335**; p. 140-145.

[324] J. Deisenhofer, "Crystallographic refinement and atomic models of a human Fc fragment and its complex with fragment B of protein A from Staphylococcus aureus at 2.9- and 2.8-.ANG. resolution", Biochem. , **1981,** 20(9); p.2361-2370.

[325] H. Kawaguchi, K. Sakamato, Y. Ohtsuka, T. Ohtake, H. Sekiguchi and H. Iri, "Fundamental study on latex reagents for agglutination tests", Biomat. , **1989** , 10; p. 225-229.

[326] L. Davalos Pantoja, J.L. Ortega Vinuesa, D. Bastos Gonzalez and R. Hidalgo Alvarez, "Colloidal stability of IgG and IgY coated latex microspheres", Colloids Surf. B: Biointerfaces, **2001**, 20; p. 165-175.

[327] I. Vickholm and O. Teleman, "Adsorption of antibodies to a langmuir layer of octadecylamine and the interaction with antigen", J. Colloid Interface Sci., **1994** ,168(1), 125-129.

[328] J. Serra, J. Puig, A. Martin, F. Galisteo, M. J. Galvez and R. H. Alvarez, "On the adsorption of IgG onto polystyrene particles: electrophoretic mobility and critical coagulation concentration", Colloid Polym Sci., **1992** , 270, 574-583.

[329] E. Doi, B. Jirgensons, "Circular dichroism studies on the acid denaturation of γ-immunoglobulin G and its fragments", Biochemistry, **1970**, 9 (5); p. 1066–1073.

[330] L.V. Abatruov, R.S. Nezlin, R.S. Vengerova and J. A. Varshavsky, "Conformational studies of immunoglobulin G and its subunits by the methods of hydrogen deuterium exchange and infrared spectroscopy", Biochim. Biophys. Acta, **1969**, 9(2); p. 386-396.

[331] P.C. Weber, D.H. Ohlendorf, J.J. Wendoloski and F.R. Salemme, "Structural origins of high affinity biotin binding to streptavidin", Science, 1989, **243(4887)**; p.85-88.

[332] G.U. Lee, D.A. Kidwell and R.J. Colton, "Sensing discrete streptavidin biotin interactions with atomic force microscopy", Langmuir, 1994, **10**; p. 354-357.

[333] J. Carlsson, F. Winquist, B. Danielsson and I. Lundstrom, "Biosensing discrimination of meat juice from various animals using a lectin panel and ellipsometry", Anal. Chimica Acta, **2005**, 547; p. 229-236.

[334] N. Nath and A. Chilkoti, "Label-Free Biosensing by Surface Plasmon Resonance of Nanoparticles on Glass: Optimization of Nanoparticle Size", Anal. Chem., 2004, 76 (18); p. 5370–5378.

[335] P.M. Wolny, J.P. Spatz and R.P. Richter, "On the adsorption behavior of biotin binding proteins on gold and silica", Langmuir, 2010, **26(2)**; p. 1029-1034.

[336] S.P. Radko, S.A. Varonina, A.V. Gromov, O.V. Gnnedko, N.V. Bodoev, A.S. Ivanov and K.N. Yarygin, "Use of oligonucleotides conjugated to gold nanoparticles and streptavidin for amplification of optical biosensor signal during detection of telomeric repeats", Buletin Expt. Bio. Medicine, 2009, **147(6)**; p. 746-749.

[337] J.D. Andrade (Ed.), "Surface and Interfacial Aspects of Biomedical Polymers. Vol. 1. Surface Chemistry and Physics", Plenum Press: p. 470.

[338] V. Hlady, D. R. Reinecke and J. D. Andrade, "Fluorescence of adsorbed protein layers: I. Quantitation of total internal reflection fluorescence", J. Colloid Interface Sci., **1986**, 111(2); p. 555-569.

[339] B. Kasemo, "Biological surface science", Surf. Sci., **2002**, 500(1); p. 656-677.

[340] Texter, J. and Tirell, M., "Chemical processing by self-assembly", *AIChE J.*, **2001**, 47(8); p.1706– 1710.

[341] Castner, D. G. and Ratner, B. D. *Surf. Sci.,* Biomedical surface science: Foundations to frontiers, **2002**, 500 (1); p. 28– 50.

[342**]** E.J. Castillo, J.L. Koenig, J.M. Andersen and J. Lo, "Characterization of protein adsorption on soft contact lenses: I. Conformational changes of adsorbed human serum albumin", Biomat., **1984**, 5(6); p. 319-324.

[343] E. Dickinson, **"**Adsorbed protein layers at fluid interfaces: interactions, structure and surface rheology", Colloids and surfaces B: Biointerfaces, **1999**, 15(2); p. 161-176.

[344] N. Weber, D. Bolikal, S L. Bourke and J Kohn, **"**Small changes in the polymer structure influence the adsorption behavior of fibrinogen on polymer surfaces: Validation of a new rapid screening technique", J. Biomed. Mater. Res., **2004**, 67A(3); p.496-503.

[345] K.K. Chitur, "FTIR/ATR for protein adsorption to biomaterial surfaces", Biomat., **1998**, 19(4); p. 357- 369.

[346] M. Rodahl, F. Hook, C. Fredriksson, C.A. Keller, A. Krozer, P. Brzezinski, M. Voinova and B. Kasemo, "Simultaneous frequency and dissipation factor QCM measurements of biomolecular adsorption and cell adhesion", Faraday Discuss., **1997**, 107; p. 229-246.

[347] K. Ishihara, H. Nomura, T. Mihara, K. Kurita, Y. Iwasaki, N. Nakabayashi, "Why do phospholipid polymers reduce protein adsorption?, "J. Biomed. Res., **1998**, 39(2); p. 323-330.

[348] G. Jackler, R. Sreitz and C. Czeslik, "Effect of temperature on the adsorption of lysozyme at the silica/water interface studied by optical and neutron reflectometry", Langmuir, **2002**, 18, 6565-6570.

[349] F. Evers, K. Shokuie, M. Paulus, S. Tiemeyer, Ch. Sternemann and C. Czeslik, "Charaterizing the structure of protein layers adsorbed onto functionalized surfaces by means of in-situ X-ray reflectivity", Eur. Phys. J. Special Topics, **2009**, 167; p. 185-189.

[350] D. Voet and J.G. Voet, Biochemistry (3rd edn.), **2004**, Wiley and Sons, New York.

[351] T. J. Su, J.R. Lu, R.K. Thomas, Z.F. Cui and J. Penfold, "The conformational structure of bovine serum albumin layers adsorbed at the silica-water interface", J. Phys. Chem., **1998**, 102(41); p. 8100-8108.

[352] R. Kurrat, J.E. Prenosil and J.J. Ramsden, "Kinetics of human and bovine serum albumin adsorption at silica-titania surfaces", J. Colloid Interface Sci., **1997**, 185(1); p. 1-8.

[353] http://www.pdb.org/pdb/static.do?p=education_discussion/molecule_of_the_month/pdb37_1.html

[354] A. J. Cadotte, and T. B**.** DeMarse, Poly-HEMA as a drug delivery device for in vitro neural networks on micro electrode arrays, *J. Neural Eng*, **2005**, 2(4); p. 114-122.

[355**]** A. Kidane, J.M. Szabocsik and K. Park, "Accelerated study on lysozyme deposition on poly(HEMA) contact lenses", Biomat., **1998**, 19(22); p. 2051-2055.

[356] M.Ilton, "Viscoelastic embedding of gold nanoparticles" thesis, 2009.

[357] http://www.tedpella.com/gold_html/gold-tec.htm

[358] G. Videen, "Light scattering from a sphere on or near a surface", J. Opt. Soc. Am., **1991**, A 8; p. 483-489.

[359] G. Videen, "Light scattering from a sphere on or near a surface: errata", J. Opt. Soc. Am., **1992**, A 9; p. 844-845.

[360] P.B. Johnson and R.W. Christy, "Optical constants of the noble metals", Phys. Rev. B, **1972**, 6; p. 4370-4379.

[361] J. Klein, "Probing the interactions of proteins and nanoparticles", Proc. Natl. Acad. Sci., **2007**, 104(7); p. 2029-2030.